Applications of Geographic Information Systems in Landscape Ecotoxicology

by

Kristin M. Eccles

Thesis submitted to the University of Ottawa

in partial fulfillment of the requirements for the degree

Doctorate of Philosophy in

Biology with a specialization in Chemical and Environmental Toxicology

Ottawa-Carleton Institue of Biology

Faculty of Science

University of Ottawa

Abstract

Landscape ecotoxicology is the study of dose-response relationships to toxicants and integrating environmental factors across a defined landscape. In this thesis, I contributed new knowledge to the field of landscape ecotoxicology by adapting analytical methods to assess spatial patterns of chemical exposure among different wildlife keystone species, quantify the relationships between contaminant sources and exposures, and quantify dose-response relationships across large landscapes.

Currently, there are few landscape ecotoxicology tools available for quantifying geospatial patterns of environmental toxicology data. To address this gap, I adapted spatial and statistical methods and demonstrated how they can be used to 1) integrate data and assess spatial patterns of contaminant exposure; 2) assess spatial patterns of exposure to complex mixtures; and 3) examine dose-response patterns across landscapes.

I developed fur Hg as a biomarker medium as a non-invasive biomonitoring tool in river otter (*Lontra canadensis*) and mink (*Neovison vison*) by developing conversion factors that can be used to estimate internal organ Hg from fur Hg, using a meta-regression approach. Based on these results, I suggest that the fur Hg screening guideline be reduced from 20 μg/g to 15 μg/g to be more conservative. I also quantified how the distribution of fur Hg changes across the pelt of river otters. Results from this study indicate that topcoat should be used for biomonitoring as it is less variable than the undercoat and samples should be taken from the forebody (head and legs) for the most accurate organ Hg estimation.

Using biomarkers of exposure, I quantified the relationship between sources of Hg and factors that promote Hg bioaccumulation with dietary Hg from stomach contents and fur

Hg to establish fur as a proxy for bioavailability of environmental Hg. I also assessed spatial dose-response patterns between fur Hg and fur cortisol using a geographically weighted regression (GWR). Based on these results I use my proposed fur screening guideline of 15 μg/g to categorize fur Hg exposures and demonstrate that at low exposures (<15 μg/g) in fur, Hg has a positive relationship with cortisol. Conversely, at high exposures (>15 μg/g) in fur, Hg has a negative relationship with cortisol. This research provides a field example of heterogeneous dose-response relationships. Finally, I assessed spatial patterns of complex metal exposures in a variety of biomonitoring datasets. I used normalization and transformation techniques to effectively combine datasets comprised of different species and life stages. I then used a spatial principal components analysis (sPCA) to exemplify clusters of complex exposures associated with oil and gas development in regions of Alberta, Canada.

These advancements in the field of landscape ecotoxicology will help advance evidence-based long-term ecological monitoring programs.

Résumé

L'écotoxicologie du paysage est l'étude des relations entre la relation dose-réponse et l'intégration des facteurs environnementaux dans un paysage défini. Dans cette thèse, j'ai apporté de nouvelles connaissances dans le domaine de l'écotoxicologie du paysage en adaptant des méthodes analytiques pour évaluer les patrons spatiaux d'exposition aux produits chimiques entre différentes espèces fauniques clés, pour évaluer les relations entre les sources et les expositions et pour évaluer les relations dose-réponses sur de grandes paysages.

Actuellement, il existe peu d'outils d'écotoxicologie du paysage pour évaluer les modèles géospatiaux de données toxicologiques environnementales. Pour combler cette lacune, j'ai adapté les méthodes spatiales et statistiques et montré comment elles peuvent être utilisées pour 1) intégrer les données et évaluer les schémas spatiaux d'exposition aux contaminants; 2) évaluer les schémas spatiaux d'exposition à des mélanges complexes; et 3) examiner les schémas de réponse aux doses d'un paysage à l'autre.

J'ai développé la fourrure Hg comme outil de biosurveillance chez la loutre de rivière (*Lontra canadensis*) et le vison (*Neovison vison*) en développant des facteurs de conversion pouvant être utilisés pour estimer le Hg d'un organe interne provenant de la fourrure Hg, en utilisant une approche de méta-régression. En tenant compte de ces résultats, je suggère que la recommandation concernant le dépistage du Hg de fourrure soit réduite de 20 μg/g à 15 μg/g pour être plus conservatrice. J'ai également quantifié la manière dont la répartition de la fourrure de mercure se modifie dans la robe des loutres de rivière. Les résultats de cette étude indiquent que le poil doit être utilisée pour la biosurveillance, car elle est moins

variable que le sous-poil et que des échantillons doivent être prélevés à l'avant du corps (tête et jambes) pour une estimation plus précise du niveau de Hg dans les organes.

À l'aide de biomarqueurs d'exposition, j'ai quantifié la relation entre les sources de mercure et les facteurs favorisant la bioaccumulation de mercure avec le mercure alimentaire contenu dans l'estomac et la fourrure de Hg afin d'établir la fourrure comme indicateur de la biodisponibilité du mercure dans l'environnement. J'ai également évalué les schémas de relation dose-réponse entre le Hg de fourrure et le cortisol pilaire à l'aide d'une régression géographiquement pondérée (GWR). Sur la base de ces résultats, j'utilise la recommandation de 15 μg/g proposée pour le dépistage du pelage des fourrures afin de catégoriser les expositions au Hg de fourrure et de démontrer qu'à des expositions faibles (<15 μg/g), le mercure avait une relation positive avec le cortisol. À l'inverse, lors d'expositions élevées (>15 μg/g), le mercure a une relation négative avec le cortisol. Cette recherche fournit un exemple de terrain de relations dose-réponse hétérogènes. Enfin, j'ai évalué les patrons spatiaux d'exposition à des métaux complexes dans divers jeux de données de biosurveillance. J'ai utilisé des techniques de normalisation et de transformation pour combiner efficacement des ensembles de données composés d'espèces et de stades de vie différents. Ensuite, j'utilise une analyse en composantes principales spatiales (ACPs) pour illustrer les grappes d'expositions complexes associées au pétrole et au gaz se développant dans les régions de l'Alberta, Canada.

Ces progrès dans le domaine de l'écotoxicologie du paysage aideront à faire progresser les programmes de surveillance écologique à long terme fondés sur des preuves.

Acknowledgements

I must thank with my deepest gratitude everyone who has helped me to get to this point. I could not have accomplished what I have today without the never-wavering support from my family, friends, and the teachers who I have had throughout my education. These people have played an integral role in fostering my inquisitive nature and my love of learning. And a special thank you to my parents for supporting me in every way imaginable, even in my 11th year of post-secondary education. Your sacrifices have gotten me to where I am today, and for that, I am so very grateful.

To my supervisor, Laurie Chan, I am deeply grateful for the mentorship you have provided me over the course of my Ph.D. Your hard work has provided me opportunities that I would have otherwise not had. Thank you for the freedom to follow my passion. I am also grateful to my thesis committee for their thoughtful comments and suggestions throughout the course of this thesis.

I am very lucky to have been a part of the NSERC CREATE-REACT training program and the Chemical and Environmental Toxicology specialization. Thank you to members of the Chan Lab, Blais Lab, and Poulain Lab and Emmanuel for taking the time to discuss my research, help me with lab work, and provide feedback on my papers and presentations. And thank you to Dr. Alex Poulain for being a mentor and a friend and for most importantly showing me that being a scientist and being fun are not mutually exclusive.

To Bruce Pauli, I was very lucky to have crossed paths with you. Thank you for accepting me as part of your team, for being my advocate, and my cheerleader. You have expanded my network and my experiences outside the realm of academia. Thank you to everyone at Environment and Climate Change Canada who has graciously and without restriction provided me data. It is because of this data that I was able to turn my ideas of integrated spatial analyses into a reality.

To Phil Thomas, this thesis truly would not have been possible without you. Thank you for supporting all of my big ideas and providing me what seems like a never-ending supply of samples and data to bring those ideas to life. It has truly been a joy working with you over the course of my Ph.D. Your dedication to wildlife, conservation, community engagement, and science inspires me to be a better researcher. I look forward to a lifetime of collaborations with you.

To Dr. David Janz, and Dr. Stephane Dray, thank you for welcoming me into your labs and providing me with the opportunity to learn new analytical and methodological techniques that have played a critical role in the development of this thesis. It is also important to recognize and thank the open source and online community including (but not limited to) Stack Exchange, Stack Overflow, and R-Bloggers. It is because of this rich and decided online community that I have been able to develop my computational skills. I would also like to thank Dr. Wail Gueaieb for making this thesis template publicly available. You made it possible for me to push myself a little further and compile this thesis in LaTeX.

Dedication

This PhD was completed during an era of muzzled scientists, women's marches, and fake news. I dedicated this thesis to women;

To little girls, may you never let anyone or anything hold you back from achieving your dreams. To my peers, may we develop and foster relationships that support each other and encourage each other to be the best version of ourselves. And finally, to my female role models, may I do you proud in my pursuit of science, leadership, and community service.

Table of Contents

List of Tables

List of Figures

List of Abbreviations

ATCH	Adrenocorticotropin hormone
ACC	Animal Care Committee
AEP	Adverse Exposure Pathway
AIC	Akaike Information Criterion
AIHTS	Agreement on International Human Trapping Standards
ANOVA	Analysis of variance
AOP	Adverse outcome pathway
ASOR	Athabasca Oil Sands Region
BAF	Bioaccumulation factor
BCA	Between components analysis
CEEEM	Cumulative effects monitoring program
CRA	Cumulative risk assessment
CV	Coefficient of variation
DCM	Dichloromethane
DIW	Deionized water
DOC	Dissolved organic carbon
DPSEEA	Driving Force-Pressure-State-Exposure-Effect-Action
DPSIR	Driving Forces-Pressure-State-Impacts-Response
ERBC	Energy Resource Conservation Board
GIS	Geographic information systems
GWR	Geographically weighted regression
Hg	Mercury
HPA	Hypothalamic-pituitary-adrenal
IHg	Inorganic mercury
ICP-MS	Inductively coupled plasma mass spectrometry
IDW	Inverse distance weighting
JOSM	Joint Oil Sands Monitoring Program
LUR	Land use regression
LISA	Local indicators of spatial association
mACH	Muscarinic acetylcholine
MAUP	Modifiable areal unit problem
MeHg	Methylmercury
MEM	Moran Eigenvector Maps
NOx	Nitrogen oxides
NRMSE	Normalize root mean square error

OC	Organic carbon
OLS	Ordinary least squares
PAC	Polycyclic aromatic compounds
PAH	Polycyclic aromatic hydrocarbons
PCA	Principal components analysis
PCB	Polychlorinated biphenyls
PM	Particulate matter
POP	Persistent organic pollutants
QA/QC	Quality assurance/quality control
RMSE	Root mean square error
SAR	Spatial autoregression
SD	Standard deviation
SE	Standard error
SGAR	Second-generation anticoagulant rodenticides
SOx	Sulphur oxides
sPCA	Spatial principal components analysis
SQRT	Square-root
SWM	Spatial weights matrix
TC	Top coat
THg	Total mercury
QGIS	Quantum Geographic Information Systems
QSAR	Quantitative structure activity relationships
UC	Under coat
VIF	Variance inflation factor

Chapter 1

Introduction

1.1 General Introduction

Environmental exposure to potential contaminants is pervasive as a wide variety of compounds can be detected in even the most remote locations on earth [1]. One class of these detectable chemicals are metals. While metals are naturally occurring in the earth's crust, anthropogenic activities such as metallurgy, industrial activities, and fossil fuel burning, are anthropogenically increasing their circulation in both local environments and globally via wind and ocean currents [2]. Elevated exposure to certain metals can cause adverse health effects in humans and wildlife [3].

Mercury (Hg) is a metal with well-established negative impacts on immune responses, neural function, fertility, and fetal development in humans and wildlife [4–6]. Hg is released into the environment primarily through anthropogenic sources to the air, water, and terrestrial environments and to a lesser extent natural sources such as volcanoes. In ecosystems, the inorganic forms of Hg ($Hg^0$and Hg^{2+}) can be transformed into the more

toxic organic counterpart methylmercury (MeHg) by microbes. MeHg then bioaccumulates in organisms and biomagnifies in the food web, meaning that organisms of higher trophic position have higher MeHg body burdens [7]. Similarly, for humans, the primary route of MeHg exposure is through the diet. As a result, MeHg exposure is particularly of concern for individuals who consume diets high in freshwater and marine fish, and mammals [8,9].

Understanding spatial patterns of environmental Hg concentrations, exposures, and effects are essential to understanding the risk Hg poses on the health of humans and wildlife. This forms the basis of the relatively new discipline of landscape ecotoxicology. This interdisciplinary thesis integrates concepts and methods broadly from biology and geography to further develop this new field of landscape ecotoxicology, in order to spatially assess the relationship between Hg exposures and responses at the landscape level. This general introduction is meant to orient the reader and provides background on the main concepts used throughout this thesis.

1.1.1 Ecotoxicology

Toxicology is a science that studies the fate and transport of contaminants in the environment and the resulting relationship between chemical dose and biological response. As a subfield, ecotoxicology is the study of how chemicals can affect individuals in the ecosystem and the structure and function of an ecosystem as a whole [10]. In contrast to classic toxicology experiments that dose one organism with one chemical, typically in a laboratory setting, in ecotoxicology it is more difficult to measure the effects of chemicals on the physical and biological components due to the complexity of an ecosystem.

The IISD Experimental Lakes Area (IISD-ELA) in Canada is a rare example of how large ecosystem-level experiments can be performed. More commonly, "cosm" experiments are conducted where selected species of an ecosystem are added to a controlled environment as a surrogate of a corresponding ecosystem. However, the results of such experiments are limited in their usefulness to extrapolate to the population level [11–13].

Within the traditional risk assessment framework, assessing the risk that chemicals pose to human and ecological health is typically conducted using a chemical-by-chemical approach. The current framework of risk assessment involves identifying the hazard, evaluating dose-responses, quantifying exposure, and characterizing risk [14]. The potential risk is first identified through assessing chemical properties such as quantitative structure-activity relationships (QSAR) and related toxicokinetics, toxicodynamics typically based on *in vivo* and *in vitro* methods using human and animal cell lines and animal models [15]. These models establish dose-response relationships between chemical doses and effects. Recently, there has been a shift away from resource-intensive animal studies that typically use high dose and apical health endpoints which leave significant gaps in the understanding of the chemical mode of action and low dose extrapolation [16]. New high throughput assays that can screen many chemicals at a variety of doses within a short time period have improved the molecular methods used for toxicity testing. This methodological advancement in regulatory toxicology provides a better mechanistic understanding and predictive abilities, however modelling real-world exposures are still challenging [16–18].

Assessing the risk of exposures provide a link between laboratory toxicity tests and effects at the individual and population effects. In this process, the chemical exposure is

either estimated or measured to determine the frequency, concentration, and duration of exposure [14]. The routes of exposure (inhalation, ingestion, and dermal) and individual characteristics (including weight/size, sensitivity, and age) are important factors to consider in exposure assessment, as the chemical bioavailability and toxicity may vary with these factors. Exposure to a chemical can be measured both directly on or within the individual, or indirectly where the exposure is estimated using mathematical models [14]. Accurate exposure assessments are important as not all populations have the same chemical exposure and this spatial gradient of exposures needs to be accurately reflected in the exposure assessment. Results from the hazard identification, dose-response assessment, and exposure assessment are used to formulate the risk characterization. Primarily, the risk is based on the nature of the exposure; if there is no exposure, then there is no risk [14].

While high throughput methods have advanced traditional toxicology, there have been fewer methodological advances in exposure assessment and hazard characterization. Particularly, one aspect that has remained relatively unchanged is the non-spatial nature of human and ecological health risk assessments [19,20]. Inherently, everything in a non-controlled setting is subject to spatial variation, and therefore spatial considerations should be integral in ecotoxicology. Typically, these spatial variations have a quantifiable structure that can be summarized by Tobler's first law of geography that states, "everything is related to everything else, but near things are more related than distant things" [21]. This concept is highly relevant in ecotoxicology due to the diffusive nature of contaminant dispersion in the environment. As a result, there is an acknowledged need among ecotoxicologists to assess both the spatial distribution of chemicals across a landscape as

parameters that define the doses [22–24]. Further, the use of spatial methods has great potential to help improve risk assessment through more precise characterizations of exposure doses and resulting effects [25].

1.1.2 Ecological Health Indicators

Ecological risk assessments are conducted to quantify ecological effects caused by stressors and the effect of those stressors on individuals, populations, communities, and ecosystems [26]. However, complex systems, such as ecosystems, are difficult to understand and characterize due to the interdependencies and relationships between the components of the system [19]. The health and functioning of an ecosystem are reliant on these complex interactions which, can be evaluated in terms of the system's organization, function, productivity, resilience, and biodiversity. However, these emergent properties can be hard to measure [28], and as a result, it is difficult to quantify the health of an ecosystem and how it has deviated from baseline due to the impacts of stressors on the ecosystem, so relying on modeling exercises is often necessary [29]. Since the true complexity of ecological systems are beyond our ability to encode, model, and comprehend, developed models must strike a balance between including enough information that they are useful but not too much information rendering them uninterpretable [12].

Humans are an important part of an ecosystem as they both affect the ecosystem and are affected by the ecosystem in a reciprocal relationship. However, the traditional definition of ecosystem health lacks the integration and consideration of human health, even though the ecosystem and human health are intrinsically linked. As a result, a more

holistic framework of ecological health was developed to incorporate the health of humans, wildlife, and the environment [30,31]. This is the framework that underlays this thesis. Having a framework that incorporates the human aspect is important as the concept of health is value-laden. It is through the human lens that we can define what is a healthy ecosystem and what is an unhealthy ecosystem, a definition that will change person to person.

Sentinel Species

In contrast, humans and wildlife health can be easily measured through indicators such as blood pressure or body condition. Further, contaminant exposure can be measured by constructing dose-response relationships between internal doses of a chemical and a measured endpoint such as cardiovascular disease, neural impartment, or cancer [15]. These relationships are typically better established in humans than animals [32]. However, assessing the dose-response relationship of an ecosystem is not as simple. Ecosystem health cannot be measured or directly observed as health is the result of many complex interactions between parts of the ecosystem. Ecological indicators (i.e. air quality, water quality, contaminant burdens) are typically used as a way to summarize information about the health status of the ecosystem as well as make inferences about other unmeasured components [33]. Further, ecological indicators also serve an important purpose in a regulatory setting as predetermined values are typically used as the thresholds for action [33].

Due to the complexity of ecosystems, one indicator cannot be representative of overall ecosystem health, and thus multiple indicators must be chosen [34]. There are important

factors to consider when selecting an indicator. Jørgensen et al. (2011) outlines that indicators should be easy to collect, easily understood by laymen, relevant to the context, have scientific merit, and be cost effective. Ultimately, selection should take a pragmatic approach to balance the information that is desired, with the cost and time required for data collection [34,35]. Biological indicators (bioindicators) are the favoured method of assessing the response of a system to chemical exposure as they are time efficient and cost-effective and are typically easy to work with, sensitive to environmental changes, have a large geographic distribution, and are easy to quantify [33-34]. It is suggested that changes seen in key bioindicator species are the result of cumulative changes in the environment [35,36].

Wildlife bioindicators have been used to assess the effects of exposure to chemicals. Biomarkers of exposure and effect measured in tissue, fur, nail, whiskers, eggshells, and feathers are commonly used in biomonitoring [37,38]. Systems are complicated and individual or groups of bioindicators have been criticized as being too simple to properly represent the complexities of an entire ecological system. In addition to this, it can be hard to discern natural variability and natural phenomena from anthropogenic-related effects. Bioindicators are also criticized for being species and scale dependent. It is difficult to generalize to different species and can be difficult to extrapolate from one trophic level to another, especially if the species are not directly related [33]. By combining measured exposure data with measured effect data and other observed data including population information, behaviour, and diet, it is possible to determine how chemical exposures are affecting a population [39]. More recently, there has been an interest in collecting non-

invasive measurements using barbed wire snags to gather hair samples, collecting fecal matter, and bird feathers and eggshells [37,38,40]. This provides a method to monitor chemical exposure without interfering with wildlife. While bioindicators are superior from an economic standpoint and are the favoured method in regulatory decision making, there are still limitations to using indicators to assess ecological health.

Wildlife biomonitoring data can also be used as a sentential for human health [41,42]. Piscivorous (fish-eating) wildlife including mink and river otter, have been used as sentinel species providing integrated information about contaminants and their effects in an ecosystem. With high year-round fish consumptions, parallels can be drawn between mink, river otter, and humans as diet is the main pathway of exposure of MeHg for both humans and wildlife [43].

Western science bioindicators can also be integrated with social-ecological indicators which are typically guided by stakeholders and can be informed by traditional knowledge. This can be obtained through knowledge passed from previous generations, observations, and knowledge shared from other community members [44,45]. Such knowledge includes harvester and hunter's observations, consumption data, and Elder's knowledge [46]. Additionally, digital cartography provides a way of recording traditional knowledge as a method of preservation and a way to intuitively communicate traditional knowledge through the use of mapping to future generations and the public. It also provides a platform to disseminate and incorporate this knowledge of physical resources and traditional knowledge into biomonitoring, and resource development [47].

1.2 Landscape Ecotoxicology

Modelling chemical pollution across a landscape and assessing risk is challenging due to the heterogeneity and complexity of ecological systems. While a theoretical framework for understanding ecological exposure-response relationships was first proposed by Cairns and Niederlehner (1996), it has failed to gain traction in ecotoxicology as indicated by the small number of publications and a low number of citations of articles referencing landscape ecotoxicology [13]. Landscape ecotoxicology draws upon methods from ecology and toxicology and uses information from ecological function tests, toxicity tests, modelling approaches, and biomonitoring data to understand and predict dose-response relationships in spatially heterogeneous landscapes [29]. Geographic information systems (GIS) is increasing as a platform for landscape ecotoxicology.

GIS provides the platform to enhance ecological risk assessment and modelling by combining biomonitoring exposure and response data, environmental data, and social and cultural data with into one centralized location. Much of the work done in ecological risk assessments rely heavily on modelling to assess the relationships between different components of the ecosystem [48]. Once the mathematical relationships between the variables are developed and validated, it is then possible to understand the factors that drive relationships, and further assess how ecological health will be altered if ecosystem parameters change. Through established relationships, it is possible to guide ecological monitoring by identifying areas requiring further monitoring or remedial action [34].

Geographic Information Systems

A geographic information system is a digital platform that stores, organizes, analyzes, and visualizes multiple formats of both spatial and non-spatial (aspatial) data. Spatial data are also referred to as geospatial data when specifically relating to a numerical location on the surface of the earth. Typically, X, Y, Z (latitude-longitude-height) coordinates are used to represent where an item is located in geographic space. Also associated with these numeric coordinates are attributes that describe and characterize the item at that location [49]. As a platform, open source software such as Quantum GIS (QGIS) [50] is available at no cost to the user, as well as proprietary platforms such as ESRI's ArcGIS Desktop [51] that have licensing fees. Broadly, a GIS can store, organize, and maintain data quality as well as transform data into information through techniques such as geovisualizations (mapping), geospatial analyses, and geospatial statistics [49].

While these methods are commonplace within geographic information science and geography, they have yet to take hold in the other sciences, such as ecotoxicology, where they can provide many benefits. As a platform, the utility of a GIS within ecotoxicology research is the ability to identify population-level patterns and examine relationships between these patterns as they vary across geographic space [52]. Further, a GIS can support the incorporation of a spatial context into risk assessment analyses. Exposure assessments are necessary to quantify the risk associated with the exposure of contaminants for individuals in a community, both human and wildlife. Typically, exposure and the resulting risks associated with each exposure are distributed unevenly over space. Being able to accurately and cost effectively quantify those exposures is important [53].

In the ecotoxicology literature, there are many examples of using GIS to spatially map patterns of contaminants measured in abiotic (e.g. water, soil, air) media [54–57] and fewer examples assessing spatial patterns of contaminants in biological mediums [58–60]. Notably, there few examples in the literature using GIS for ecological risk assessment examining chemical stressor and response relationships [61–63]. This is an area that has been under-addressed in ecological risk assessment literature [61]. While not always explicitly stated, these examples use GIS to store and manage collected data from a variety of different data sources. All examples use GIS for some type geospatial analysis technique (e.g. kriging, interpolation, spatial regression, co-occurrence analysis) and some present geospatial visualizations. The reasons why GIS is an ideal platform for managing data, analyzing data, and producing geospatial visualizations are explored below.

GIS as a Platform for Data Management

Data management and integration is increasingly important as the need to address complex environmental health issues using a cross-discipline approach is required [64]. Differences in data semantics (terminology), structure, and organization produce barriers to such integration [65]. As the field of toxicology has grown to include many sub-disciplines, the type of data collected in these sub-disciplines varies and includes both quantitative data, such as water chemistry measurements, and qualitative data, such as perceptions of pollution. Thus, it is important to have a platform that allows for the seamless use and integration of all data. Interoperability, which is the ability of a system to allows for the seamless use of data within and between platforms, is a functional component of a GIS [66]. Having

interoperable data can help to facilitate collaborations between different projects, and between different disciplines [49]. While there are barriers to achieving a truly interoperable system, such as semantic and physical limitations, a GIS is an ideal platform to utilize and integrate data [66].

GIS is well suited to model both continuous and discrete phenomena. These are represented through two primary data models. Raster data consists of a matrix of square cells each containing one value. This model is best suited to represent continuous phenomena such as pollution gradients. The vector data consists of items represented as points, lines, and polygons. This model is best suited to represent discrete entities such as rivers, roads, or dwellings [49]. Through the file structure of a GIS, relationships are made between the spatial geographic coordinates and the aspatial attributes of that location. By making these relationships, a database of descriptive information at various locations in geographic space is created, and so through the use of location as the common link, both qualitative and quantitative data can be stored, overlaid, and utilized for analysis [67]. An integral part of ecotoxicological health risk assessments is the impact that a chemical exposure will have on different levels of organization in an ecosystem. GIS provides a way to organize data, and thereby allows us to assess the relationship between individuals

GIS as a Platform for Data Analysis

The strength of GIS comes from its analytical capabilities to assess patterns in data across space and time as well as between data sets. Methods range from simple overlays to advanced geospatial statistics. The objective of a risk assessment is to quantify the chemical

exposure and quantify the risk posed. Capitalizing on the unique properties of spatial data including spatial non-stationarity, anisotropy (directionality), and spatial autocorrelation can create more accurate estimations of exposure and, by extension, risk. Spatial non-stationarity is a property of spatial data whereby the relationships between variables will change unevenly across space as a result of anisotropy. In some cases, the spatial non-stationary can be further classified using the concept of anisotropy where this uneven change over space is directional [68]. The second property of spatial data are spatial autocorrelation where items that are located closer in space are likely to be more similar than items that are further apart [21]. Thus, attributes of the exposure including frequency, duration, and magnitude are subject to significant geospatial variability, as exposure and susceptibility are heterogeneous over a geographic region [64]. Special care needs to be given to all stages of the exposure assessment from designing the monitoring campaign to determining exposure and analyzing the data.

During study design, GIS can be used to plan optimal locations for monitoring sites. As monitoring equipment can be one of the most costly components of exposure assessments, developing sampling strategies that maximize the coverage using the fewest number of monitors is advantageous [69]. Location-allocation algorithms (also known as site selection models) are a commonly used method to determine the optimal locations based on a set of input parameters [49]. Using information including the number of available monitors, a continuous surface of monitoring need, and constraining features (i.e. no private property) the algorithm selects for the optimal sample locations [69].

Spatial patterns in data can be quantitatively assessed using geospatial statistics.

Global spatial autocorrelation metrics, such as Moran's I, assess how similar the data are in a given area [49]. However, due to the spatial nature of data, these clusters may not be evenly distributed across a surface, so there may be local clusters. Local indicators of spatial association (LISA) such as Getis and Ord's Gi* or a local Moran's I can be used to identify "hot spots" within a study area [70]. Both global and local clustering can provide indications of processes driving the observed patterns. Global spatial autocorrelation is indicative that one factor is being applied across the entire study area and is influencing the observed pattern, whereas local spatial autocorrelation is indicative of localized influences [71].

Spatial autocorrelation can also be used to statically fill unknown measurements between measured locations, also known as interpolation. Interpolation methods develop a mathematical estimation of new data, from a range of known data points [49]. A popular interpolation method, inverse weighted distance (IDW), estimates unknown values based on a matrix of surrounding known values where more weight is placed on nearby measurements and less weight on measurements further away. Other methods include natural neighbour, spline, and trend surface analyses which use similar mathematical weighting functions [49]. Kriging is a more advanced geostatistical method for interpolation which uses a measure of spatial dependence (semi-variance) to estimate values at locations where the value is unknown. Unlike other interpolation methods, kriging can estimate the standard errors of the predicted values, as well as minimize surface anisotropy to reduce these standard errors. This method can produce more accurate estimates than other interpolation methods [49]. Both IDW and Kriging are currently used within ecotoxicology literature [72–74].

To assess relationships between patterns, specialized spatial regressions can be used. Spatial regressions such as geographically weighted regression (GWR) and spatial autoregression (SAR) are necessary to mitigate the effects that spatial data can have on aspatial regression modelling methods. Due to anisotropy and spatial non-stationarity, the relationships between variables can change unevenly across space [68]. Therefore, where traditional regression coefficients produce one relationship between the dependent and independent variables, this coefficient is an average of all relationships. In heterogeneous relationships, this causes an increased error. A GWR addresses this issue by developing many localized regressions, which allows the beta coefficients to vary across space, addressing the issue of non-stationarity. In contrast to the traditional global regression, in the GWR method, the localized regressions are stationary which, induces stationarity, allowing the error to become identically distributed through the model. This decrease in the variance of the model increases the reliability of the beta estimates and therefore, creates more reliable predictions overall [68].

Spatial autocorrelation can also be problematic when conducting regression models. When the data are not independently distributed (spatially autocorrelated), the variance of the model estimates will be inflated and thereby less reliable. SAR considers the effect that neighbouring observations have on any given observation, by capturing any underlying spatial autocorrelation and including it as a parameter in the model (rho). By accounting for the spatial autocorrelation in the model, the error term can then become independently distributed and model estimates will be more reliable [75].

These methods have been used in exposure assessments to create predictive contaminant

distribution models for a variety of contaminants including oxides (NOx), sulphur oxides (SOx), particulate matter (PM), polycyclic aromatic hydrocarbon (PAHs), polychlorinated biphenyls (PCBs), persistent organic pollutants (POPs), and metals [76–78]. Generally, the R2 for these regressions are 0.70 or greater, yielding relatively high predictive power [76–78]. Land use regression models (LUR) have been validated for local, regional, and national air pollution modelling [79].

GIS as a Platform for Data Visualization

Traditional mapping that uses established cartographic conventions and representations is an intuitive way to communicate information. Visual representations of data can transcend barriers to traditional methods of information communication such as language and education [65]. This is particularly important when communicating complex scientific concepts to stakeholders who may lack an in-depth scientific background such as Indigenous communities, industry, the general public, and policy makers [80]. Typically, risk metrics are measured and estimated using advanced statistical models, which can be difficult to understand. However, illustrating this information using maps and other types of visualizations can help in communicating complex data to stakeholders by clearly highlighting areas of risk [80].

This information can be communicated through a variety of map types including contamination maps, exposure maps, hazard maps, and vulnerability maps. These maps can highlight spatial distributions of environmental contaminants, for instance, if there is any risk posed through exposure to individual chemicals or chemical mixtures [81]. This infor-

mation can then be used to inform stakeholders and policymakers to guide risk management. Further localized spatial analyses enable the identification of hot spots for targeted investigation and interventions, which is advantageous for industry and government bodies, as this enables the development of cost-effective targeted intervention strategies [60].

1.3 Thesis Rationale

While landscape ecotoxicology has a strong theoretical basis, drawing from fields such as ecotoxicology and ecology, a platform for practical implementation is lacking [13,23,24,29,82]. As a result, attempts to address spatially explicit dose-response effects at a landscape level are limited [82]. We need methods to integrate datasets, quantify dose-response patterns and pattern co-dispersion. Further, we are still limited in our methods to assess complex exposures. Since ecosystems undergo co-exposures of chemicals there is a need for analytical methods capable of assessing complex exposures in wildlife [63]. Without such methods, it is not possible to develop ecological risk assessments that are realistic and accurate. Finally, without methods for practical implementation, it is not possible to effectively analyse and communicate information to academics, policymakers, and the general public. Drawing on principles from geography and methods from GIS provides the opportunity to develop a complimentary spatial framework that supports the development of landscape ecotoxicology. This will support the development of spatial analyses using ecotoxicological data and improve modelling relating exposures back to potential sources and dose-response relationships across a landscape.

1.4 Thesis Objectives

The overarching objective of this thesis is to provide a unified and spatially explicit framework that uses GIS as a platform for conducting landscape ecotoxicology research and demonstrate applications of this spatial framework through assessing spatial patterns of biomarkers. This is presented through three sections where I develop a spatial framework for ecotoxicology (**Chapter 2**), test fur for use as a non-invasive biomarker medium for total Hg exposure in river otter (*Lontra canadensis*) and mink (*Neovison vison*) (**Chapters 3 and 4**), and quantify spatial patterns of exposure and effect biomarkers (**Chapters 5, 6, and 7**). All the chapters in my thesis were written as standalone manuscripts that have already been published in peer-reviewed journals or will be submitted for publication. Supplemental Information from each publication can be found in the corresponding Appendix. Finally, I conclude my thesis by providing a synthesis of my research contributions, discussion of implications, and suggestions for future research (**Chapter 8**). The following is a description of the structure of the thesis.

Section 1: Development of a Spatial Framework

The goal of this section is to extend the framework proposed by Cairns and Niederlehner (1996) to provide a spatially explicit platform for landscape ecotoxicology. The objective of **Chapter 2** is to develop a GIS platform to support geospatial methods that integrate biomonitoring data, assess spatial patterns of complex exposures, and assessing exposure-effect relationships across a landscape.

Section 2: Development of Fur Hg Biomarker

The goal of this section is to test the use of fur from semi-aquatic sentinel species, river otter and mink, as a non-invasive biomarker medium for total Hg exposure. The objective of **Chapter 3** is to develop a model to predict internal total Hg concentrations from measured fur Hg and determine a threshold of concern based on the measured fur Hg concentrations. I tested the prediction that measured the concentration of fur total Hg is positively associated with the total Hg concentrations measured in the internal tissues (brain, kidney, liver, and muscle).

The objective of **Chapter 4** is to determine the extent to which total Hg varies across the fur of a pelt, identify the relationship between total Hg in fur and methylated mercury (MeHg) in fur, and to identify the optimal fur sampling location for the purpose of biomonitoring. I tested the prediction that measured concentrations of fur total Hg is heterogeneously distributed across a pelt and hot spots of mercury excretion are quantifiable. I also tested the prediction that there is a positive association between the measured concentration of fur total Hg and the measured concentration of fur MeHg to ensure that total Hg is a good indicator of risk.

Section 3: Application of Spatial Analysis of Biomarkers

The goal of this section is to demonstrate how the spatial framework can be used to assess spatial patterns of biomarkers of exposure and effect. The objective of **Chapter 5** is to determine the relationship between sources of Hg and environmental factors that enhance methylmercury (MeHg) production and exposure to Hg in river otter and mink. I tested

the prediction that there is a linear relationship between the measured total Hg in the stomach contents and measured total Hg in fur. I also tested the hypothesis that stomach content total Hg and fur total Hg are associated with sources of Hg in the environment and relevant physio-chemical factors, including pH and organic carbon.

The objective of **Chapter 6** is to determine the spatial relationship between fur total Hg, a biomarker of exposure, and fur cortisol, a biomarker of effect. I tested the prediction that the relationship between fur total Hg and fur cortisol would vary across space and this spatial could be quantified using a geographically weighted regression.

The objective of **Chapter 7** is to demonstrate the utility of spatial principal component analysis (sPCA) for assessing spatial patterns of complex metal exposures in multiple species and life stages. I tested the prediction that a combination of biomarkers of metal exposure, measured in different species and life stages, cluster across the landscape quantifying hotspots of complex metal exposure across the landscape.

1.5 References

1.Poland JS, Riddle MJ, Zeeb BA. 2003. Contaminants in the Arctic and the Antarctic: a comparison of sources, impacts, and remediation options. Polar Rec. (Gr. Brit). 39:S0032247403002985.

2. Nriagu JO, Pacyna JM. 1988. Quantitative assessment of worldwide contamination of air, water and soils by trace metals. Nature. 333:134–139.

3. Pacyna JM, Scholtz MT, Li Y-F. 1995. Global budget of trace metal sources. Environ. Rev. 3:145–159.

4. Wolfe MF, Schwarzbach S, Sulaiman RA. 1998. Effects of mercury on wildlife: A comprehensive review. Environ. Toxicol. Chem. 17:146–160.

5. Chan HM, Scheuhammer AM, Ferran A, Loupelle C, Holloway J, Weech S. 2003. Impacts of Mercury on Freshwater Fish-Eating Wildlife and Humans. Hum. Ecol. Risk Assess. An Int. J. 9:867–883.

6. Ha E, Basu N, Bose-O'Reilly S, Dórea JG, McSorley E, Sakamoto M, Chan HM. 2017. Current progress on understanding the impact of mercury on human health. Environ. Res. 152:419–433.

7. Driscoll CT, Mason RP, Chan HM, Jacob DJ, Pirrone N. 2013. Mercury as a global pollutant: Sources, pathways, and effects. Environ. Sci. Technol. 47:4967–4983.

8. Mergler D, Anderson H a, Chan LHM, Mahaffey KR, Murray M, Sakamoto M, Stern AH. 2007. Methylmercury exposure and health effects in humans: a worldwide concern. Ambio. 36:3–11.

9. Eagles-Smith CA, Silbergeld EK, Basu N, Bustamante P, Diaz-barriga F, Hopkins WA, Kidd KA, Nyland JF. 2018. Modulators of mercury risk to wildlife and humans in the context of rapid global change. Ambio. 47:170–197.

10. Truhaut R. 1977. Ecotoxicology: objectives, principles and perspectives. Ecotoxicol. Environ. Saf. 1:151–173.

11. Van Den Brink PJ. 2008. Ecological Risk Assessment: From Book-Keeping to Chemical Stress Ecology. Environ. Sci. Technol. 42:8999–9004.

12. Beketov MA, Liess M. 2012. Ecotoxicology and macroecology - Time for integration. Environ. Pollut. 162:247–254.

13. Schäfer RB. 2014. In response: why we need landscape ecotoxicology and how it could be advanced—an academic perspective. Environ. Toxicol. Chem. 33:1193–1194.

14. Environment Canada. 2007. Overview of the Ecological Assessment of Substances under the Canadian Environmental Protection Act , 1999. Assessment.

15. Dix DJ, Houck KA, Martin MT, Richard AM, Setzer RW, Kavlock RJ. 2006. The ToxCast Program for Prioritizing Toxicity Testing of Environmental Chemicals. Toxicol. Sci. 95:5–12.

16. National Research Council. 2007. Toxicity testing in the 21st century: A vision and a strategy. National Academies Press, Washington, DC.

17. Villeneuve DL, Crump D, Garcia-Reyero N, Hecker M, Hutchinson TH, LaLone CA, Landesmann B, Lettieri T, Munn S, Nepelska M, Ottinger MA, Vergauwen L, Whelan M. 2014. Adverse outcome pathway (AOP) development I: Strategies and principles. Toxicol. Sci. 142:312–320.

18. Villeneuve DL, Crump D, Garcia-Reyero N, Hecker M, Hutchinson TH, LaLone CA, Landesmann B, Lettieri T, Munn S, Nepelska M, Ottinger MA, Vergauwen L, Whelan M. 2014. Adverse outcome pathway development II: Best practices. Toxicol. Sci. 142:321–330.

19. Monn C. 2001. Exposure assessment of air pollutants: a review on spatial heterogeneity and indoor/outdoor/ personal exposure to suspended particulate matter, nitrogen dioxide and ozone. Atmos. Environ. 35.

20. Briggs D. 2005. The role of GIS: Coping with space (and time) in air pollution exposure assessment. J. Toxicol. Environ. Heal. - Part A. 68:1243–1261.

21. Tobler W. 1970. A computer movie simulating urban growth in the Detroit region. Econ. Geogr. 46:234–240. 22. Clements WH, Hickey CA, Kidd KW. 2012. How Do Aquatic Communities Respond to Contaminants? It Depends on the Ecological Context. Environ. Toxicol. Chem. 31:1932–1940.

23. Price OR, Thorbek P. 2014. In Response: Challenges and opportunities for landscape ecotoxicology and spatially explicit risk assessment—An industry perspective. Environ. Toxicol. Chem. 33:1194–1196.

24. Wendt-Rasch L, Poulsen V, Duquesne S. 2014. In Response: Regulatory risk assessment and landscape ecotoxicology—A governmental perspective. Environ. Toxicol. Chem. 33:1196–1197.

25. Barnthouse LW, Munns Jr WR, Sorensen MT. 2007. Population-level ecological risk assessment. CRC Press.

26. Norton SB, Rodier DJ, Schalie van der, H W, Wood WP, Slimak MW, Gentile JH. 1992. A framework for ecological risk assessment at the EPA. Environ. Toxicol. Chem. 11:1663–1672.

27. Van Straalen N. 2003. Peer reviewed: ecotoxicology becomes stress ecology. Environ. Sci. Technol.:324A–330A.

28. Costanza R. 2012. Ecosystem health and ecological engineering. Ecol. Eng. 45:24–29.

29. Cairns J, Niederlehner BR. 1996. Developing a Field of Landscape Ecotoxicology. Ecol. Appl. 6:790–796.

30. Aguirre AA, Ostfeld RS, Tabor GM, House C, Pearl MC. 2002. Conservation medicine: ecological health in practice. Oxford University Press.

31. McLaren L, Hawe P. 2005. Ecological perspectives in health research. J. Epidemiol. Community Health. 59:6–14.

32. Depledge MH, Galloway TS. 2005. Healthy animals, healthy ecosystems. Front. Ecol. Environ. 3:251–258.

33. Jørgensen SE, Xu L, Costanza R. 2010. Handbook of ecological indicators for assessment of ecosystem health. CRC press.

34. Lu Y, Wang R, Zhang Y, Su H, Wang P, Jenkins A, Ferrier RC, Bailey M, Squire G. 2015. Ecosystem health towards sustainability. Ecosyst. Heal. Sustain. 1:1–15.

35. Siddig AAH, Ellison AM, Ochs A, Villar-Leeman C, Lau MK. 2016. How do ecologists select and use indicator species to monitor ecological change? Insights from 14 years of publication in Ecological Indicators. Ecol. Indic. 60:223–230.

36. Urban NA, Swihart RK, Malloy MC, Dunning JB. 2012. Improving selection of indicator species when detection is imperfect. Ecol. Indic. 15:188–197.

37. Lodenius M, Solonen T. 2013. The use of feathers of birds of prey as indicators of metal pollution. Ecotoxicology. 22:1319–1334. 38. Bechshoft T, Derocher a. E, Richardson E, Mislan P, Lunn NJ, Sonne C, Dietz R, Janz DM, St. Louis VL. 2015. Mercury and cortisol in Western Hudson Bay polar bear hair. Ecotoxicology. 24:1315–1321.

39. Burger J. 2006. Bioindicators: Types, Development, and Use in Ecological Assessment and Research. Environ. Bioindic. 1:22–39. 40. Hebert CE, Campbell D, Kindopp R, Macmillan S, Martin P, Neugebauer E, Patterson L, Shatford J. 2013. Mercury trends in colonial waterbird eggs downstream of the oil sands region of Alberta, Canada. Environ. Sci. Technol. 47:11785–11792.

41. Basu N. 2012. Piscivorous mammalian wildlife as sentinels of methylmercury exposure and neurotoxicity in humans. Methylmercury Neurotox., pp 357–370. doi:10.1007/978-1-46142383-6.

42. Basu N, Scheuhammer AM, Bursian SJ, Elliott J, Rouvinen-Watt K, Chan HM. 2007. Mink as a sentinel species in environmental health. Environ. Res. 103:130–144.

43. Yates DE, Mayack DT, Munney K, Evers DC, Major A, Kaur T, Taylor RJ. 2005. Mercury levels in mink (*Mustela vison*) and river otter (*Lontra canadensis*) from northeastern North America. Ecotoxicology. 14:263–274.

44. Royer MJS, Herrmann TM. 2011. Socioenvironmental changes in two traditional food species of the Cree first nation of subarctic James Bay. Cah. Geogr. Que. 55:575–601.

45. Parlee BL, Geertsema K, Willier A. 2012. Social-ecological thresholds in a changing boreal landscape: Insights from cree knowledge of the Lesser Slave Lake region of Alberta, Canada. Ecol. Soc. 17.

46. Parlee BL, Goddard E, Dene First Nation É, Smith M. 2014. Tracking Change: Traditional Knowledge and Monitoring of Wildlife Health in Northern Canada. Hum. Dimens. Wildl. An Int. J. 19:47–61.

47. Engler NJ, Scassa T, Taylor DRF. 2013. Mapping Traditional Knowledge: Digital Cartography in the Canadian North. Cartographica. 48:189–199.

48. Costanza R, Mageau M. 1999. What is a healthy ecosystem? Aquat. Ecol. 33:105–115.

49. De Smith MJ, Goodchild MF, Longley P. 2007. Geospatial analysis: a comprehensive guide to principles, techniques and software tools. Troubador Publishing Ltd.

50. QGIS Development Team. 2018. QGIS geographic information system. Open Source Geospatial Found. Proj. `http//qgis.osgeo.org`.

51. ESRI ArcGIS Desktop. 2011. Release 10. Redlands, CA Environ. Syst. Res. Inst.

52. Richardson DB, Volkow ND, Kwan M-P, Kaplan RM, Goodchild MF, Croyle RT. 2013. Spatial turn in health research. Sci. (New York, NY). 339:1390.

53. Ott WR, Steinemann AC, Wallace LA. 2006. Exposure analysis. CRC Press.

54. Bozon N, Sinfort C, Mohammadi B. 2009. A GIS-based atmospheric dispersion model.

55. Bertazzon S, Johnson M, Eccles K, Kaplan GG. 2015. Accounting for spatial effects in land use regression for urban air pollution modeling. Spat. Spatiotemporal. Epidemiol. 14–15:9–21.

56. Kirk JL, Muir DCG, Gleason A, Wang X, Lawson G, Frank RA, Lehnherr I, Wrona F. 2014. Atmospheric Deposition of Mercury and Methylmercury to Landscapes and Waterbodies of the Athabasca Oil Sands Region. Environ. Sci. Technol. 48:7374−7383.

57. Wang XN, Gu YG, Wang ZH, Ke CL, Mo MS. 2018. Biological risk assessment of heavy metals in sediments and health risk assessment in bivalve mollusks from Kaozhouyang Bay, South China. Mar. Pollut. Bull. 133:312–319.

58. Jariyasopit N, Harner T, Wu D, Williams A, Halappanavar S, Su K. 2016. Mapping Indicators of Toxicity for Polycyclic Aromatic Compounds in the Atmosphere of the Athabasca Oil Sands Region. Environ. Sci. Technol. 50:11282–11291.

59. Clifford PA, Barchers DE, Ludwig DF, Sielken RL. 1995. An Apporach to Quantify Spatial Components of Exposure for Ecological Risk Assessment. Environ. Toxicol. Chem. 14:895–906.

60. Thomas PJ, Eccles KM, Mundy LJ. 2017. Spatial modelling of non-target exposure to anticoagulant rodenticides can inform mitigation options in two boreal predators inhabiting areas with intensive oil and gas development. Biol. Conserv. 212:111–119.

61. Dyer SD, Posthuma L, de Zwart D, Kapo KE, Holmes CM. 2014. Developing a foundation for eco-epidemiological assessment of aquatic ecological status over large geographic regions utilizing existing data resources and models. Environ. Toxicol. Chem. 33:1665–1677.

62. Feist BE, Buhle ER, Arnold P, Davis JW, Scholz NL. 2011. Landscape Ecotoxicology of Coho Salmon Spawner Mortality in Urban Streams. PLoS One. 6:e23424.

63. Martin RW, Waits ER, Nietch CT. 2018. Empirically-based modeling and mapping to consider the co-occurrence of ecological receptors and stressors. Sci. Total Environ. 613:1228–1239.

64. Sexton K, Linder SH. 2011. Cumulative risk assessment for combined health effects from chemical and nonchemical stressors. Am. J. Public Health. 101:S81–S88.

65. Goodchild M, Guo H, Annoni A, Bian L, Bie K De, Campbell F, Craglia M, Ehlers M, Genderen J Van, Jackson D, Lewis AJ, Pesaresi M, Simpson R, Skidmore A, Wang C, Woodgate P, States U. 2012. Next-generation Digital Earth. Proc. Natl. Acad. Sci. 109:11088–11094.

66. Goodchild M, Egenhofer MJ, Fegeas R, Kottman C. 2012. Interoperating geographic information systems. 495, Springer Science & Business Media.

67. Laniak GF, Olchin G, Goodall J, Voinov A, Hill M, Glynn P, Whelan G, Geller G, Quinn N, Blind M, Peckham S, Reaney S, Gaber N, Kennedy R, Hughes A. 2013. Environmental Modelling & Software Integrated environmental modeling: A vision and roadmap for the future. Environ. Model. Softw. 39:3–23.

68. Fotheringham AS, Brunsdon C, Charlton M. 2002. Geographically weighted regression. John Wiley & Sons, Limited.

69. Kanaroglou PS, Jerrett M, Morrison J, Beckerman B, Arain MA, Gilbert NL, Brook JR. 2005. Establishing an air pollution monitoring network for intra- urban population exposure assessment: A location-allocation approach. Atmos. Environ. 39:2399–2409.

70. Ord A, Getis JK. 1995. Local Spatial Autocorrelation Statistics: Distributional Issues and an Application. Geogr. Anal. 27:286–306.

71. Nelson T, Boots B. 2008. Detecting spatial hot spots in landscape ecology. Ecography (Cop.). 31:556–566.

72. Li BG, Cao J, Liu WX, Shen WR, Wang XJ, Tao S. 2006. Geostatistical analysis and kriging of Hexachlorocyclohexane residues in topsoil from Tianjin, China. Environ. Pollut. 142:567–575.

73. Kim S-Y, Yi S-J, Eum YS, Choi H-J, Shin H, Ryou HG, Kim H. 2014. Ordinary kriging approach to predicting long-term particulate matter concentrations in seven major Korean cities. Environ. Health Toxicol. 29:e2014012. 74. Wang K, Chen X, Yang F, Porter DW, Wu N. 2014. A New Stochastic Kriging Method for Modeling Multi-Source Exposure − Response Data in Toxicology Studies. Sustain. Chem. Eng. 2:1581–1591.

75. Kissling WD, Carl G. 2008. Spatial autocorrelation and the selection of simultaneous autoregressive models. Glob. Ecol. Biogeogr. 17:59–71.

76. Gulliver J, de Hoogh K, Fecht D, Vienneau D, Briggs D. 2011. Comparative assessment of GIS-based methods and metrics for estimating long-term exposures to air pollution. Atmos. Environ. 45:7072–7080.

77. de Hoogh K, Wang M, Adam M, Badaloni C, Beelen R, Birk M, Cesaroni G, Cirach M, Declercq C, Dėdelė A, Dons E, de Nazelle A, Eeftens M, Eriksen K, Eriksson C, Fischer P, Gražulevičienė R, Gryparis A, Hoffmann B, Jerrett M, Katsouyanni K, Iakovides M, Lanki T, Lindley S, Madsen C, Mölter A, Mosler G, Nádor G, Nieuwenhuijsen M, Pershagen G, Peters A, Phuleria H, Probst-Hensch N, Raaschou-Nielsen O, Quass U, Ranzi A, Stephanou E, Sugiri D, Schwarze P, Tsai M-Y, Yli-Tuomi T, Varró MJ, Vienneau D, Weinmayr G, Brunekreef B, Hoek G. 2013. Development of land use regression models for particle composition in twenty study areas in Europe. Environ. Sci. Technol. 47:5778–86.

78. Melymuk L, Robson M, Helm P a., Diamond ML. 2013. Application of land use regression to identify sources and assess spatial variation in urban SVOC concentrations. Environ. Sci. Technol. 47:1887–1895.

79. Hystad P, Setton E, Cervantes A, Poplawski K, Deschenes S, Brauer M, van Donkelaar A, Lamsa L, Martin R, Jerrett M, Demers P. 2011. Creating national air pollution models for population exposure assessment in Canada. Environ. Health Perspect. 119:1123–1129.

80. Lahr J, Kooistra L. 2010. Environmental risk mapping of pollutants: State of the art and communication aspects. Sci. Total Environ. 408:3899–3907.

81. Lahr J, Münier B, Lange HJ De, Faber JF, Borgen P. 2010. Environment Wildlife vulnerability and risk maps for combined pollutants. Sci. Total Environ. 408:3891–3898.

82. Focks A. 2014. The Challenge: Landscape ecotoxicology and spatially explicit risk assessment. Environ. Toxicol. Chem. 33:1193–1198.

PART I

Development of a Spatial Framework for Ecotoxicology

Preface: This section provides the developmental foundations for the use of a geographic information system (GIS), spatial methods, and geospatial analysis in landscape ecotoxicology.

Chapter 2

The Use of Geographic Information Systems (GIS) for Spatial Ecological Risk Assessments: an example from the Athabasca Oil Sands area in Canada

Kristin M. Eccles[1,2], Bruce D. Pauli[2], and Hing Man Chan[1]

[1] Department of Biology, University of Ottawa, 30 Marie Curie, Ottawa, ON, K1N 6N5, Canada
[2] Science and Technology Branch, Environment and Climate Change Canada, National Wildlife Research Center, 1125 Colonel By Drive, Raven Road, Ottawa, ON K1A 0H3, Canada

This chapter is under review at *Environmental Toxicology and Chemistry*. The version presented in this paper has incorporated the comments and suggestions from the reviewers.

Author Contributions: KE conceived the idea, compiled the datasets, completed the statistical analysis, and wrote the manuscript. BP and LC contributed to the conceptualization of the project and provided guidance on the implementation and editing of the manuscript.

Supplemental information for this chapter can be found in Appendix A.

2.1 Abstract

There is an acknowledged need in ecotoxicology for methods that integrate spatial analyses in risk assessment. This has resulted in the emergence of landscape ecotoxicology, a subdiscipline of ecotoxicology. However, landscape ecotoxicology has yet to become common practice in risk assessment due to the underdevelopment of techniques and a lack of standardized methods. Here, we propose and demonstrate how the use of a geographic information system (GIS) provides a standardized platform for landscape ecotoxicological risks assessment using data collected under the Joint Oil Sands Monitoring (JOSM) Program in the Athabasca Oil Sands Regions (AOSR), Alberta, Canada. This dataset is comprised of concentrations of contaminants including metals and polycyclic aromatic hydrocarbons (PAHs), and health endpoints. The 1100 biological samples are comprised of various samples from tree swallows, amphibians, gull and tern eggs, plants, and mammals. We present three examples using GIS as a platform to: 1) integrate data and assess spatial patterns of contaminant exposure in the region; 2) assess spatial patterns of exposures to complex mixtures; and 3) examine patterns of exposures and responses across the landscape. We summarize the methods used in this paper into a workflow for ease of implementation. Using this GIS platform allows the results and related spatial patterns to be intuitively visualized and communicated through maps. The GIS platform will help researchers to identify hot spots of contamination, design and refine biomonitoring programs, and develop more ecologically realist risk assessments that incorporate complex exposures.

2.2 Introduction

Ecological risk assessments are conducted to quantify potential adverse effects caused by stressors, including chemicals of concern, on individuals, populations, communities, and ecosystems [1]. However, assessing the exposure of ecosystem components and determining the relationships with environmental contaminants is challenging, as species within ecosystems are typically exposed to complex mixtures of chemicals distributed heterogeneously across the landscape. This heterogeneity of exposures can lead to a range of possible effects resulting from varied exposures, further complicated by environmental factors that alter the exposure pathways and change the exposure-response relationship (Figure 2.1). Properties of a landscape can also cause chemical transformations and change the bioavailability of contaminants [2]. Thus, there is a need for methods that will allow for a better understanding of the complex relationships between exposures and responses across large geographic landscapes and how this influences the ultimate structure and functioning of an ecological system.

To address this methodological need, Cairns and Niederlehner (1996) proposed the development of a new subdiscipline of toxicology called landscape ecotoxicology. This subdiscipline draws upon methods from ecology, geography, and toxicology and uses the information generated from tests of ecological function, toxicity tests, modelling approaches, and biomonitoring data to understand and predict exposure-response relationships in spatially heterogeneous landscapes [3]. Since its inception, landscape ecotoxicology has not gained much traction in ecotoxicology; there are few publications and low a number of

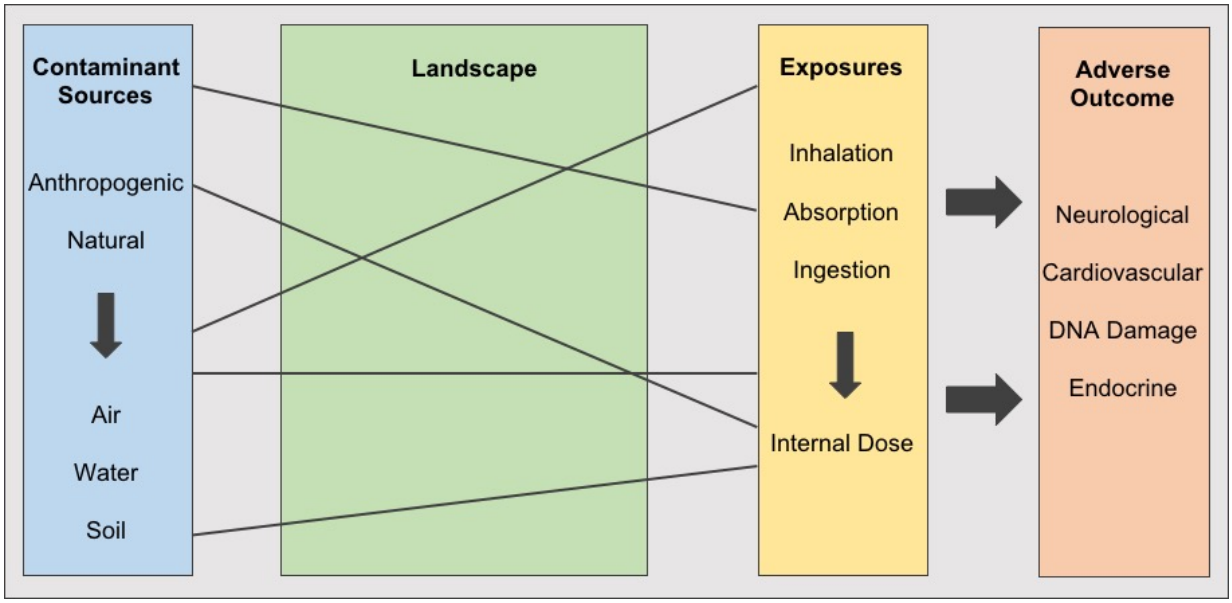

Figure 2.1: A conceptual representation of how contaminants released from both natural (e.g. volcanic eruptions, forest fires) and anthropogenic sources can be modified by the landscape. This can alter the exposure and the adverse outcomes that result from chemical exposure.

citations of articles referencing landscape ecotoxicology [4]. Nevertheless, the theoretical framework has been recently highlighted in the journal *Environmental Toxicology & Chemistry*, with perspectives from academia, government, and industry providing insight into the future development and utility of landscape ecotoxicology in spatially explicit risk assessments [5]. While there has been an increase in attention paid to spatial analyses in exposure assessments, spatial methods have not been fully applied to the assessment of exposures and biological responses across large landscapes, particularly through the lens of landscape ecotoxicology [6].

The theoretical basis of landscape ecotoxicology draws on concepts from a variety of disciplines. However, a unified method or platform for practical implementation is lacking [3–5,7,8]. While landscape ecotoxicology draws on methods from landscape ecology, there are some differences in the data collected in these two subdisciplines that limit the trans-

ferability of methods. Response data in ecotoxicology are commonly continuous (chemical burden), whereas landscape ecology has more discrete response data (presence/absence). Continuous and discrete data types rely on different underlying statistical distributions and thus some methods that have been developed for landscape ecology need to be adapted for landscape ecotoxicology [9]. As a result, practical applications that address spatially explicit chemical exposures and responses at a landscape level are limited [5].

Without a standardized platform for implementation, it is difficult to determine how to best integrate datasets, quantify exposure-response patterns, and assess spatial relationships. Moreover, ecosystems are exposed to mixtures of chemicals. Therefore, spatial analytical methods capable of assessing complex exposures and quantifying how the complex exposures and responses change across a landscape are needed [6]. As a result, it is difficult to effectively analyse, interpret, and communicate the results to regulators, policymakers, and other stakeholders including the general public.

A GIS is a combination of hardware and software programs that are able to store, manage, manipulate, and visualize geographic data (Figure 2.2). Geographic data are encoded with latitude and longitude coordinates, and these coordinates have associated attributes that provide information about processes happening on the landscape. GIS is well suited for the storage of ecotoxicology and landscape data. While ecosystems are complex in nature, components are organized into a nested hierarchy [10]. This nested hierarchical organization is similar to the tabular database structure of a shapefile, a common vector data format used by GIS software. Additionally, GIS can store both data with and without spatial information. This is advantageous for data management and integration,

which is becoming increasingly important as the need to address complex environmental health issues using a multi-disciplinary approach is required [11]. Using geolocations as the common link, both qualitative and quantitative data can be stored, overlaid, and utilized for analysis.

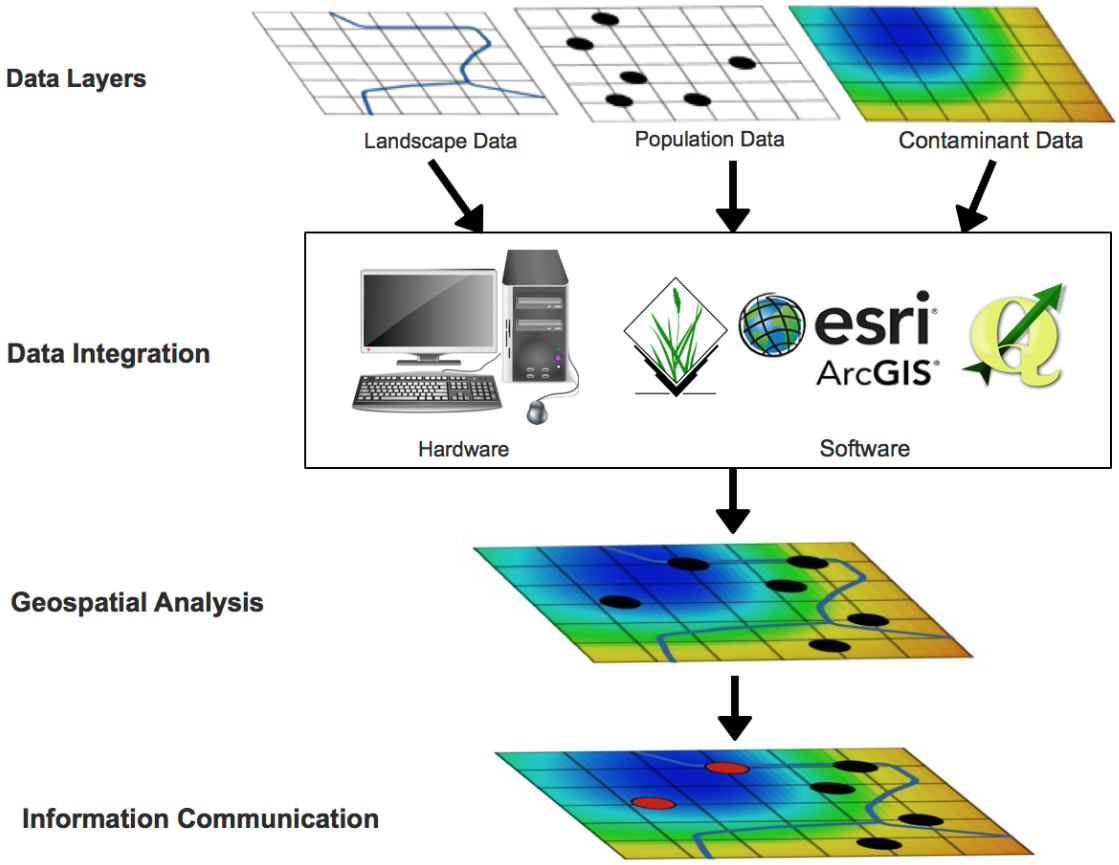

Figure 2.2: Schematic of how GIS can be used as a platform for landscape ecotoxicology.

A GIS is well suited for the storage of ecotoxicology and landscape data. While ecosystems are complex in nature, they can also be organized into a nested hierarchy [11]. This nested hierarchical organization is similar to the tabular database structure of a shapefile, a common vector data format used by GIS software. Additionally, GIS can store both data with and without spatial information. This is advantageous for data management

and integration, which is becoming increasingly important as the need to address complex ecological health issues using a multi-disciplinary approach is required [12]. Using geolocations as the common link, both qualitative and quantitative data can be stored, overlaid, and utilized for analysis.

GIS also provides a variety of spatial computational methods for the assessment of ecotoxicological data. This enables the identification of contaminant sources and factors modifying the exposures and responses of contaminants across a landscape. These methods range from simple overlays and mapping to high-level geospatial statistics [12]. Geospatial statistical methods can be used to assess patterns in data. For example, global metrics (i.e. Moran's I) can assess the similarity of different data over an entire region [12], while local indicators of spatial association (i.e. Getis and Ord's Gi*) can identify local clusters [13]. Investigating large scale (global) and small scale (local) influences on processes across a landscape, and the relationships between these patterns can provide information about what processes or factors are influencing the observed patterns of exposures and responses. Geospatial methods can also be used to assess relationships between patterns using specialized spatial regressions (i.e. geographically weighted regression and spatial autoregression). These methods address the often problematic properties of spatial data including spatial non-stationarity, anisotropy, and spatial autocorrelation [14], and help to reduce model variance (standard error) creating more reliable estimates [15]. A more detailed overview of computational tools available in GIS can be found in other review papers [16,17].

Mapping is an intuitive way to communicate information, which can transcend tradi-

tional barriers of information communication such as language and education [18]. This is particularly important when communicating complex scientific concepts to stakeholders who may lack an in-depth scientific background [19]. In addition, risk metrics are typically measured and estimated using advanced statistical models, which can be difficult to understand. However, illustrating this information using maps and other visualization aids can help in communicating complex data and relations to stakeholders by highlighting areas of risk [19]. Landscape-level ecotoxicological data can be communicated through a variety of map types including contamination maps, exposure maps, hazard maps, and vulnerability maps [20]. These maps can highlight spatial distributions of environmental contaminants, and potential risk resulting from exposure to individual chemicals or chemical mixtures [20]. This information can then be used to inform stakeholders and policymakers to guide risk management. Additionally, localized spatial analyses enable the identification of hot spots for targeted investigation and potential interventions. This is advantageous for industry and government regulators, as this enables the development of cost-effective, targeted intervention strategies [21].

There are a limited number of examples in the literature that use GIS to examine the spatial relationship between chemical exposure and responses across a landscape. Clifford et al. (1995) provided one of the first examples of how GIS and spatial data can be used for the purpose of ecological risk assessments. In this example, GIS was used to demonstrate and integrate measured dieldrin concentrations from the soil, the ratio of dieldrin concentrations in tissue to the soil concentrations in key species using bioaccumulation factors (BAF), and the home range of each species' prey. These three layers were intersected to

determine where the highest risk of exposures was in the food chain [22].

In a more recent example, Thomas et al. (2017) mapped and assessed the exposure of fisher (*Pekania pennanti*; formerly *Martes pennanti*) and American marten (*Martes americana*) in the Athabasca Oil Sands Region (AOSR) in Canada to second-generation anticoagulant rodenticides (SGARs). Using Getis and Ord's Gi* hotspot analysis and linear regression modelling, they demonstrated that the distribution of SGAR concentrations in these mammals was significantly associated with multiple factors on the landscape including total boreal disturbances, the number of oil sands mines, and broadleaf forest cover [21].

Feist et al. (2011) used GIS to make predictions about the mortality risk of adult coho salmon (*Oncorhynchus kisutch*) in unmonitored areas. In this example, they assess the spatial relationship between non-point source pollution produced in urban landscapes from run-off and rates of mortality in spawning adult coho salmon in Greater Puget Sound, Washington. Their results demonstrated a positive relationship between the proportion of local roads, impervious surfaces, commercial property within a basin, and salmon mortality [23].

Finally, Jariyasopit et al. (2016) provides an interesting example of how GIS and laboratory exposure-response data can be combined. In their study, polycyclic aromatic compounds (PACs) were extracted from passive air samplers at different locations in the AOSR and were used for the chemical exposures *in vitro* using salmonella mutagenicity and cytotoxicity bioassays. These toxicological assay results were spatially mapped. They found the highest measured levels of mutagenicity at sites located closer to mining activity,

which also had the highest PAC concentrations. Through the mapping of toxicity indicators, this study provides an example of how to assess the potential for chemically induced effects across a landscape [24].

While landscape ecotoxicology has a strong theoretical basis, the lack of a practical and standardized platform for data analysis has presented a barrier to implementation. In this paper, we use wildlife contaminant data from the Joint Oil Sands Monitoring (JOSM) program to demonstrate how a GIS platform using a variety of both proprietary and open source software can be used to: 1) integrate datasets collected under different biomonitoring programs from the AOSR, 2) assess spatial patterns of complex exposures using spatial principal components analysis; and 3) provide a proof-of-concept example of how to assess the spatial co-dispersion between exposures and responses. A workflow using GIS methods to address challenges at each step is proposed.

2.3 Methods

2.3.1 Data: The Joint Oil Sands Monitoring (JOSM) Program

The Canadian Alberta Joint Oil Sands Monitoring Program (JOSM) was a monitoring program developed in 2012 by Environment and Climate Change Canada and the Alberta Government. One component of the program aimed to systematically monitor exposures to contaminants of wildlife living in the Athabasca Oils Sands Region (AOSR). The wildlife contaminants monitoring program under JOSM was comprised of five individual projects assessing contaminant burdens in sentinel species. The species monitored include tree

swallows [25,26], wood frogs [27], gull and tern eggs [28,29], plants [30], and terrestrial and semi-aquatic mammals [21]. Biological samples from the monitoring activity were geolocated, and tissues were analysed for a variety of contaminants including metals and PAHs, and in some species, health indicators including thyroid hormones (triiodothyronine and thyroxine) and cortisol [31].

From these projects, the five datasets were compiled into one database which contains tissue concentrations for 31 metals, 93 alkyl and parent PAHs, and 28 health outcome endpoints measured in 1100 biological samples. The dataset matrix is not complete as there is missing data. For example, there are no metal data for tree swallows, but there is a high degree of spatial overlap in the metals in the other four data sets. Conversely, naphthenic acid concentrations were only measured in the wood frogs, and there is poor overlap between the PAHs measured in the five datasets. Additionally, health endpoint data are only available for tree swallows and wood frogs. Spatially the sampling efforts are focused north of Fort McMurray, Alberta around the tailings ponds, upgraders, and open pit mining area but also include samples from control areas away from the main oil sands development (Figure 2.3A). A summary map of all samples and the number of species in each hexagon tile after aggregation can be see in Appendix A Figure A.1 and Figure A.2 respectively.

In addition to wildlife contaminants data, abiotic data were also collected under JOSM including contaminants monitored in the air, water, and snow. Data can be accessed from the Canada-Alberta Joint Oil Sands Monitoring Portal (`https://www.canada.ca/en/environment-climate-change/services/oil-sands-monitoring.html`).

2.3.2 GIS Platform

GIS analyses can be executed through open source platforms available at no cost to the user (Quantum GIS (QGIS); QGIS Development Team 2018), proprietary software (ESRI's ArcGIS Desktop; ESRI ArcGIS Desktop 2011), and non-GIS specific software including R [34]. The methods in this paper are executed through a combination of software, which is noted in each section.

2.3.3 Data Integration

In this example, we integrate total Hg exposure data collected in wood frogs, gull eggs, plants, and terrestrial and semi-aquatic mammals. However, data for chemical exposure are often complex and multi-dimensional. Mercury analyses need to consider the biology of the receptor animals such as species and life stage prior to analysis [35]. Range standardizing (also termed ranging) is a common way to scale data to make datasets of different magnitudes comparable [9]. The end product is a value between 0 and 1 (Equation 2.1). In this example, we created subgroups for the species and life stage in all datasets before range standardization was conducted on these subgroups. Once all data were standardized, the tabular data were imported into ArcGIS 10.4 [33].

$$x_i = \frac{x - min(x)}{max(x) - min(x)} \tag{2.1}$$

Analysing biomonitoring data can pose some challenges, for example, when multiple samples are collected from the same location producing statistical pseudo-replication. This

issue occurred in both the gull eggs and mammals. To overcome this problem, the range standardized Hg values were aggregated to hexagon tiles with a 50 km diameter, chosen based on the calculated average nearest neighbour distance. This also helps to increase the spatial overlap of multiple species. Aggregating data to a coarser spatial resolution to increase spatial overlap is also a common practice in ecology [36]. The aggregate unit can be assessed for a variety of summary of statistics including mean, median, standard deviation, and variance.

Another challenge is the uneven sampling effort across the studied landscape. In our example, the highest density of samples are located in the area immediately surrounding Fort McMurray, Alberta and fewer samples are from areas remote from Fort McMurray. This uneven sampling regime in conjunction with the natural variation of chemical uptake in organisms creates bias when aggregated data are visualized. This issue has been thoroughly investigated in disease mapping [37–39]. Weighting methods are commonly used in statistical analyses to reduce biases in data resulting from uneven sample sizes or analytical errors as not all sample averages should be interpreted with the same confidence [39]. The second issue that arises here is that confidence intervals are not well suited to mapping and may even be non-existent if there is only one sample in the aggregate unit. To address this, we use an empirical Bayesian average which estimates a population mean using prior information. In this method, if the sample size in the sample unit is high, the mean calculated for the sample unit stays relatively the same as it is more likely to be a true average. However, if the sample size in the sample unit is low, the weighting method will pull the mean in the sample unit closer to the mean of the entire dataset, as a smaller

sample size be by affected by outliers. [39].

$$x_w = wR + (1 - w)c \tag{2.2}$$

where,

$$w = \frac{v}{v + m} \tag{2.3}$$

In this example, the Bayesian weighted average is (x_w) developed from a weight (w) which is a combination of the maximum number of samples in an individual hexagon (v) and the average number of samples in the hexagons (m) (Equation 2.3). This weight is applied to the average standardized Hg concentration in each hexagon (R) and the average standardized Hg concentration across all hexagons (c) (Equation 2.2). Using this method enables the comparison of standardized Hg concentrations independent of the sample size in each hexagon tile.

2.3.4 Spatial Assessment using Geospatial Cluster Analysis

Getis and Ord's Gi*

To identify clusters of high normalized Hg values (hot spots) and low normalized Hg values (cold spots), Getis and Ord's Gi* statistical method was used. This geostatistical method uses a spatial weights matrix to identify statistically significant local spatial autocorrelation based on a specified local neighbourhood [14].

Spatial Pincipal Components Analysis

In this example use the methods as described above to investigate the spatial pattern of 19 metal concentrations in 518 adult and recently metamorphosed wood frogs collected in 2012 and 2013 from 19 different sample locations (Table2.1). PCA, BCA, and MEM were performed using the ade4 package in R 3.43. [41]. We define the spatial connectivity through a spatial weights matrix (SWM) using a Gabriel graph, as this method is optimal for uneven sampling regimens [42]. A Monte-Carlo simulation is used to assess the ratio of the explained variance between the overall model (PCA) and different sites (BCA) to test the significance of collection location. To further investigate the spatial structure of the complex exposures, Moran's eigenvector maps (MEM) were used to account for the spatial autocorrelation of metal concentrations. Scores were generated by the combination of the eigenvector and eigenvalues from the BCA results and were mapped to assess the spatial patterns. The spatial analysis and mapping were completed in R 3.4.3 using the packages adespatial, spdep, and sp [43–45].

2.3.5 Quantifying Patterns of Co-dispersion for Exposure-Response Analysis

Models that assess the co-dispersion of species are commonly used in ecology [36]. However, these methods cannot be directly applied to ecotoxicology as the ecological methods are optimized for count data. Through modifications, integrating methods from ecology, ecotoxicology, and GIS, can also be applied to assess the co-occurrence between sources of

Table 2.1: Summary of tissue metal concentrations in adult and recently metamorphosed wood frogs collected in the AOSR measured in (μg/g) dry weight.

Metal	Min	Median	Mean	Max
Ag	0	0	0.02	0.63
As	0	0.11	0.22	2.2
Ba	4.3	20	24.85	108
Cd	0	0.15	0.21	1.3
Cu	1.3	8.15	8.75	20
Fe	167	390	529.2	1894
Ga	0.14	0.69	0.82	3.8
Hg	0.02	0.09	0.1	0.41
Li	0.03	0.14	0.17	0.82
Mn	4.4	50	77.33	639
Mo	0.16	0.36	0.73	21
Ni	0.9	2.5	2.69	5.3
Pb	0	0	0.1	1.2
Rb	1.2	10	11.69	36
Se	0.33	0.66	0.76	2.7
Sn	0	0	0.01	0.39
Sr	9.1	26.5	29.3	71
V	0	0.23	0.4	2.3
Zn	70	122	125.6	196

Min= variable minimum, Max= variable maximum

contaminants, exposures, and health outcomes in wildlife. This allows the evaluation of the assessment of exposure-response patterns across a landscape [46].

If samples are taken from the same location, then no data preprocessing is necessary. However, if data on exposure and response are not taken at the same location, then the data need to be spatially rescaled so that the spatial resolution will match. This involves aggregating, typically by averaging, to a coarser resolution [36]. Due to the mismatch in sampling locations in the dataset here, the data were first interpolated using inverse distance weighting (IDW) to create a regular grid for the exposure and response data.

For this example, we used the sum of the total parent PAH concentrations measured in the snow as the exposure data (n=118), and the total cortisol in adult amphibians (n=20)

averaged by site (n=4), as the response data. These two grids (rasters), were then range standardized (Equation 2.1) to generate two standardized grids. The raster calculator was then used to add these two grids together to provide a visual representation of how these two layers co-vary. All data manipulation, analysis, and mapping were completed in QGIS 2.18 [32]. The correlations between these two layers were further quantified using spatial statistics in R 3.4.3 using the package SpatialPack [47].

2.4 Results

2.4.1 Data Integration and Assessment of Spatial Patterns

Results of the total Hg aggregation can be seen in Figure 2.3B and results from the spatial analysis can be seen in Figure 2.4. Figure 2.4B shows that there is a hot spot of high standardized Hg values in the northeast corner of the ASOR and cold spots southwest of the ASOR. However, when compared with the weighted average, the cold spot disappears; this is due to the nature of the weighting metric, which selects for high standardized Hg values observed in many data points. This gives confidence that the high standardized values are true and that the corresponding hot spots are also true hot spots. The results of the analysis are supported in Figure 2.4. The hot spot in the northeastern corner of the ASOR is still present. This area corresponds to the area where open pit mining occurs, and the upgrader facilities are located.

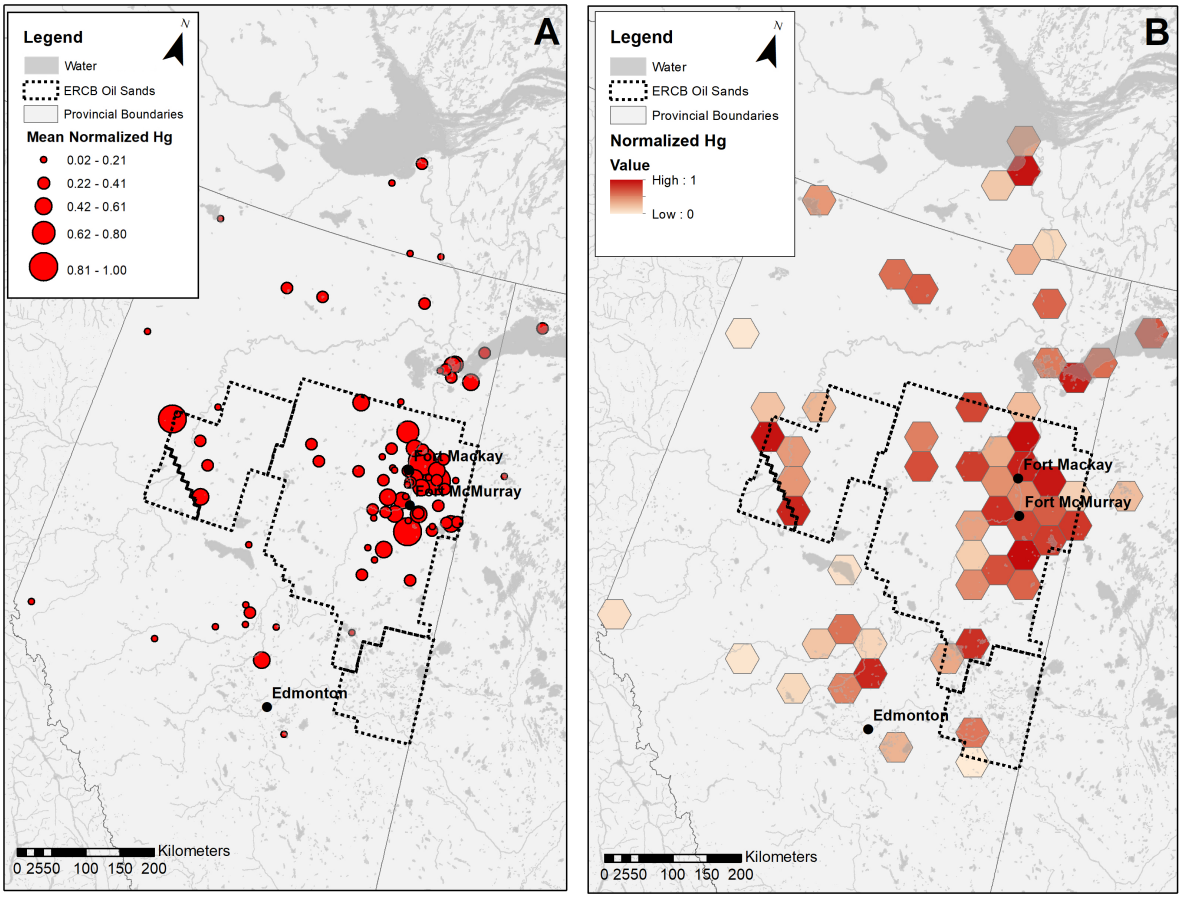

Figure 2.3: A. Individual range normalized mercury values of wildlife species (amphibians, gull eggs, plants, and terrestrial and semi-aquatic mammals) monitored in the oil sands and the surrounding region. The larger the red circle, the higher the range range-normalized mercury value. B. Averaged and weighted range normalized mercury values in 50 km diameter hexagon tiles. Light red tiles represent low average normalized mercury values and darker red tiles indicate higher average normalized mercury values.

2.4.2 Assessing Complex Exposures

The Monte-Carlo simulation result indicates that 46% (p=0.001) of the variance between the metal concentrations can be explained by the site and there is significant spatial structure in the exposure data. The MEM results of the assessment of complex metal exposures are summarized in Figure 2.5, where Figure 2.5A is a scree plot which represents the vari-

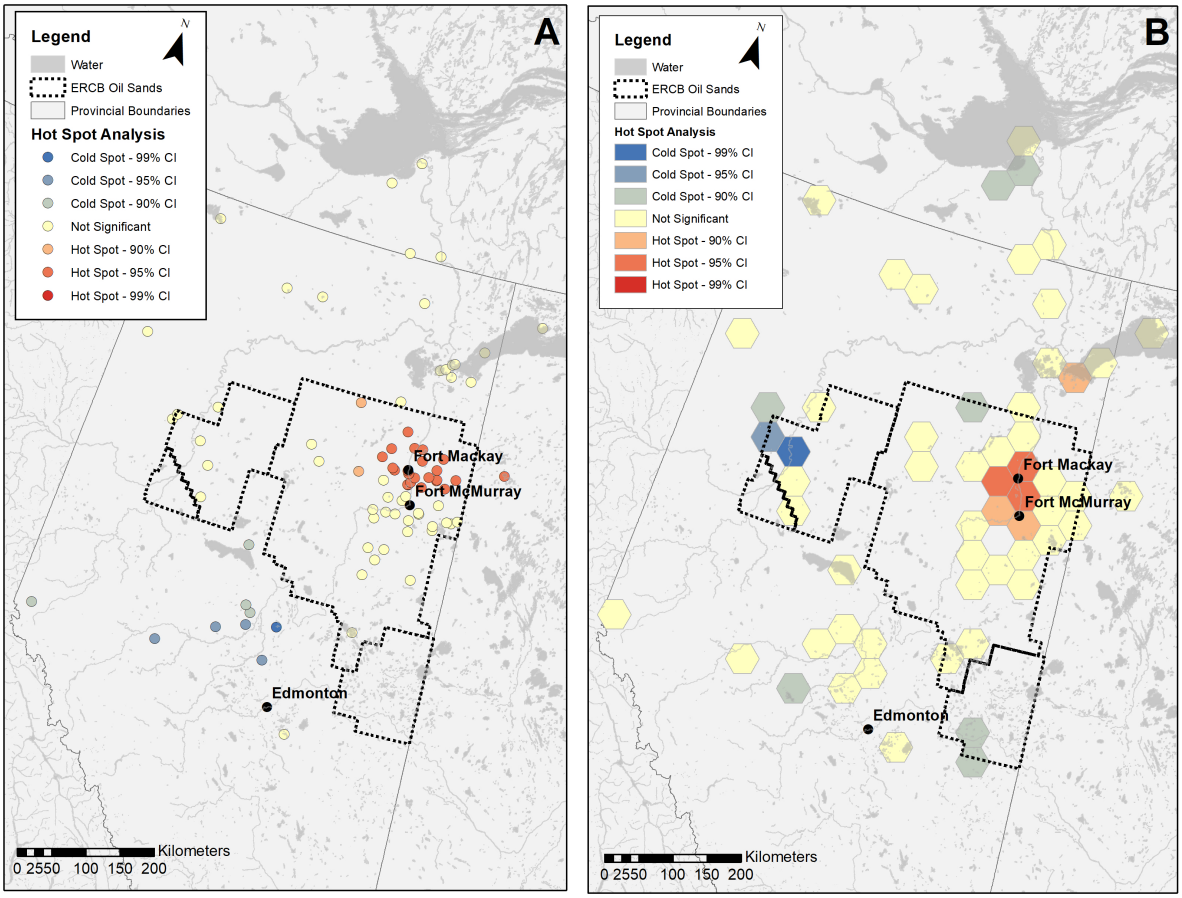

Figure 2.4: Getis and Ord's Gi* cluster maps for point data (A) and aggregated hexagon tiles (B). In both of these maps, red colouration represents differing levels of statistical confidence in the hot spot (cluster of high Hg normalized values in the integrated wildlife datasets) while the blue represents differing levels of statistical confidence in the cold spots (cluster of low normalized Hg values in the integrated wildlife datasets).

ance explained in each component of the PCA and Figure 2.5B is a biplot representing the correlation between metals in component 1 and component 2. The biplot in Figure 2.5B can be used to help interpret that spatial patterns of the complex metal mixture exposures of wood frogs are displayed in Figure 2.6. Component 1 (MEM1) is characterized by high levels Rb, Cu, Hg, Mn, and Ni in the north indicated by the black squares (positive loadings) and higher levels of Zn, cadmium, Se, As, and V in the south sample locations as indicated by the white squares (Cd loadings). Component 2 (MEM2, Figure 2.6B) is

characterized by three areas of metal combinations. In the north and the south, there are higher levels of Zn, Cd, Pb, Hg, and Rb in the wood frogs as indicated by the white squares (negative loadings). The band of black squares (positive loadings) in the middle of MEM2 is characterized by V and As. A table with the corresponding loadings can be seen in Appendix A Table A.1.

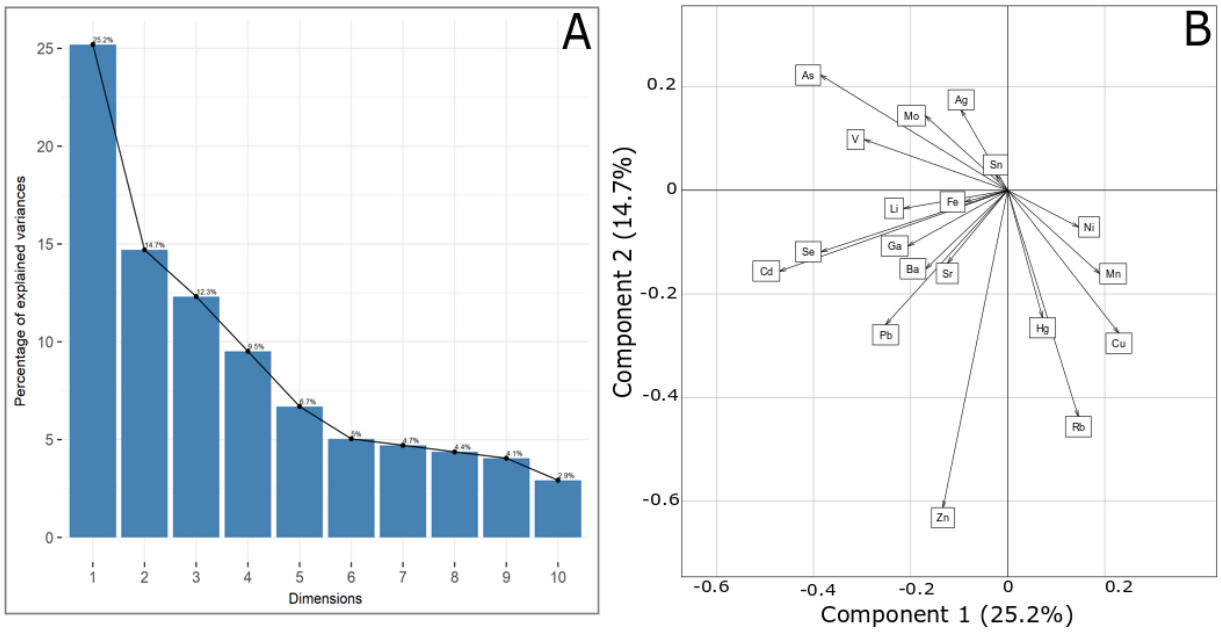

Figure 2.5: A. Results from the spatial principal components analysis (PCA) using recently metamorphosed and adult wood frogs (n=518) from 19 sample locations. Scree plot illustrating the amount of variance (y-axis) explained in the first 10 (of 24) components (x-axis). B. Biplot illustrating the correlation between factors metals loaded in component 1 (x-axis) and component 2 (y-axis).

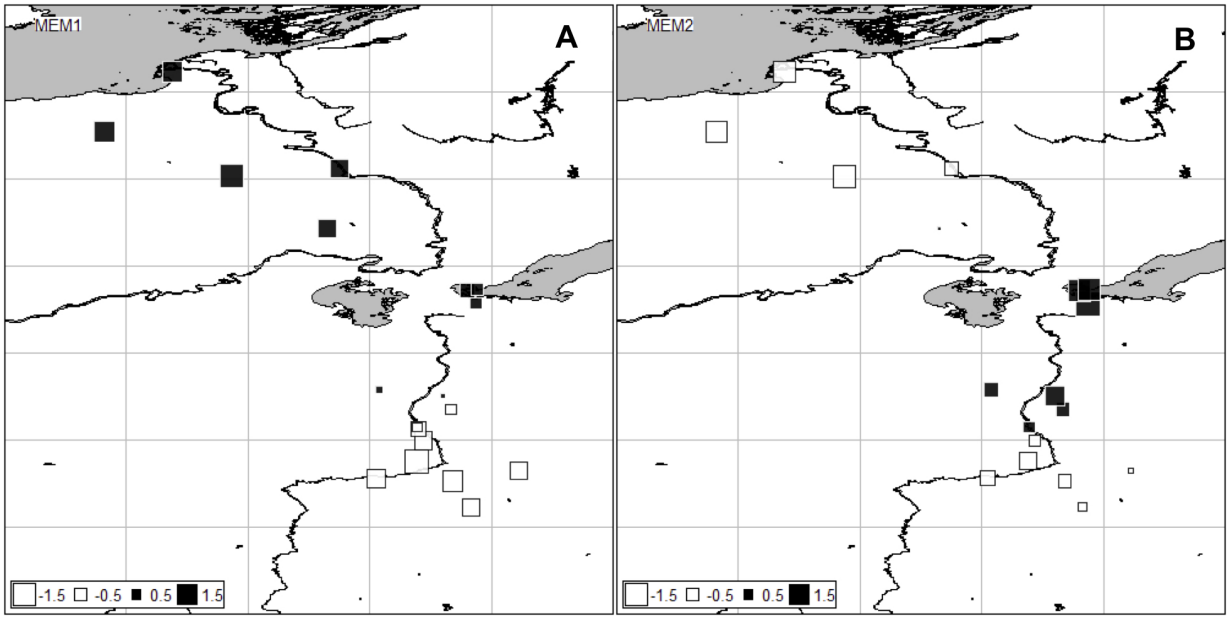

Figure 2.6: Moran's eigenvector maps highlighting the spatial distribution of between components analysis (BCA) scores in the first component (A) and the second component (B) for recently metamorphosed and adult wood frogs (n=518) from 19 sample locations. Figure 6A (MEM1) corresponds to component 1 (the x-axis of Figure 5B) and Figure 6B (MEM2) corresponds to component 2 (y-axis of Figure 5B).

2.4.3 Quantifying Patterns of Co-dispersion

The interpolation methods of the point data produced standardized grids demonstrating the spatially continuous patterns of PAH concentration in the snow (Figure 2.7C) and cortisol in the wood frogs (Figure 2.7D). By combining these layers (Figure 2.7E), the analysis demonstrates two hot spots (dark blue) where elevated cortisol co-occurred with higher total parent PAH deposition. This proof-of-concept statistical analysis shows how observed patterns in two datasets of exposure and response data can spatially correlated ($r = 0.28$).

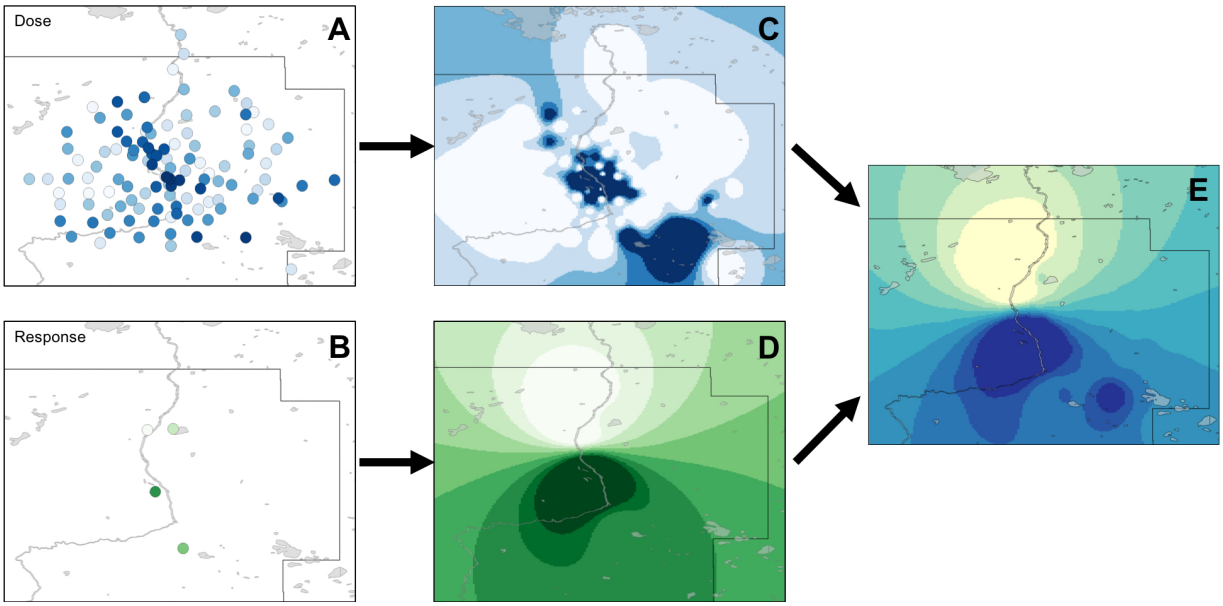

Figure 2.7: To assess co-dispersion, the point data (A, B) was interpolated using an inverse distance weighted (IDW) interpolation (C, D). The grids were normalized based on the data range and added together to illustrate the co-dispersion of the sum parent PAH and average amphibian cortisol concentration (E). In all of these images, lighter colours represent lower values (white and yellow) and darker colours (blue and green) represent higher values.

2.5 Discussion

The GIS platform and spatial methods presented in this paper are tools that can help fill the implementation gap of landscape ecotoxicology. We have created a generalized workflow to demonstrate steps of data preprocessing, geospatial analysis, and visualizations necessary to produce robust spatial analysis and communicate the information effectively (Figure 2.8). Also important to note is the selection of the correct datum and projection for the analysis (for more information see Iliffe (2000)), which a critical step for developing robust spatial analyses. The analyses presented in this paper used the North American Datum (NAD) 1983 with the Albers equal-area conic projection.

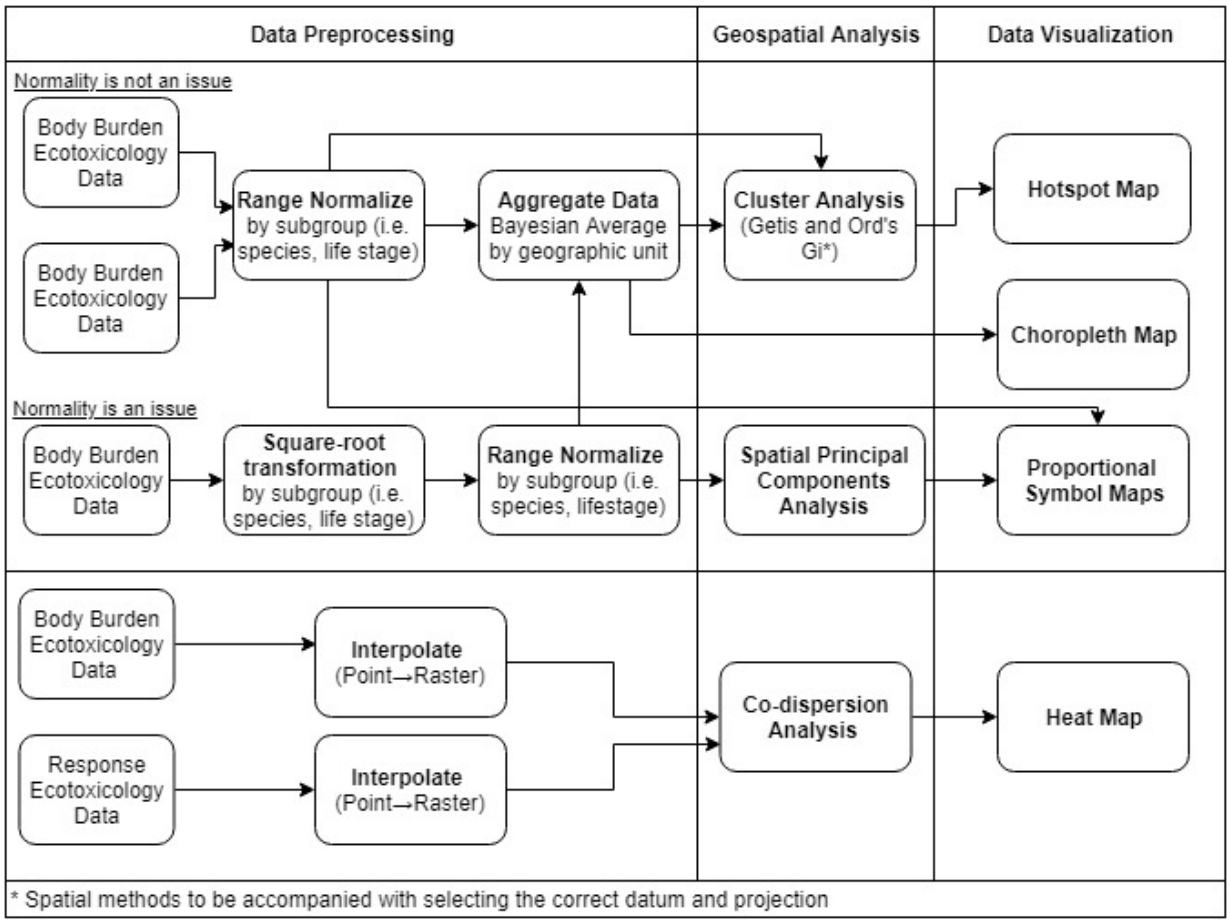

Figure 2.8: A workflow of methods that can be used to spatially assess ecotoxicological data using GIS as a platform for data pre-processing, geospatial analysis, and data visualization.

Spatial analyses provide opportunities to attribute patterns of body burdens seen in biota to potential sources. In the first example, integrating total Hg data from a number of monitoring projects conducted under JOSM, identified hot spots around the upgraders. This total Hg hot spots in wildlife tissue burdens of Hg also correspond with the highest intensity of areal deposition of total Hg in the AOSR [49]. Further, the clustering results from this example are similar to the mercury burdens observed in the eggs of California gull (*Larus californicus*), glaucous-winged gulls (*Larus glaucescens*), herring gulls (*Larus argentatus smithsonianus*), and ring-billed gull (*Larus delawarensis*) collected in the region [29]. Results from the second example, identifying spatial clusters of complex metal mea-

sured in wood frogs demonstrate there is a strong spatial component to the body burdens as the location explains almost half of the variance in the data. Scores around the Oil Sands in components 1 and 2 are highly loaded with As, V, Se, Cd, Zn, Pb, Cu, Hg, and Rb. Similarly, other research has shown that V and Zn are emitted in high quantities from the upgraders and metals including Hg exhibit strong distance decay from upgrader facilities [49]. Further, Cd, Cu, Pb, Hg, and Zn deposition into snowpack from the Oil Sands region exceed guidelines for the protection of aquatic life [50]. Overall, this approach enables us to move away from single chemical exposure assessments and provides a way to assess highly dimensional data by providing a multivariate summary of how exposures to complex mixtures vary spatially.

In the final example, while exploratory in nature, demonstrates methods that can be used to assess exposure-response relationships across landscapes. This geographical "dose-response" assessments and can help develop assessments that are more representative of realistic environmental exposures. Datasets with a with larger sample sizes could assess if exposure and response patterns change across a landscape and how landscape features modify these relationships. Finally, all of the examples above incorporate aspects of data visualization through mapping, which aids in the communication of results.

The application of GIS in ecotoxicology provides opportunities to improve risk assessments and can help develop and refine monitoring programs. Capitalizing on unique properties of spatial data and using them as a modelling advantage to assess spatial heterogeneity can help to develop more accurate estimations of exposure, effects, and risk [6].The lack of biomonitoring data is always a major challenge in ecotoxicology. If biomon-

itoring data exist, then the information gained from combining datasets and identifying spatial patterns can be used to inform future monitoring. Cluster analyses can identify regions that could be used as control/ reference areas and regions of exposure interest for continued monitoring. It is important that sampling efforts capture the full range of contaminant concentrations in order for hot or cold spots to be detected. Further, implementing a weight of evidence metric, such as a Bayesian weighted average, provides an evidence-based approach for identifying regions of highest risk, increasing the confidence that regions of high standardized exposures and corresponding clusters are true. Due to the range standardization, this method is not able to give any indication about the risk of exposure. However, this method can be extended to assess hotspots of not just exposure but also risk by using the same clustering methods on toxicological reference values (TRV) or benchmark doses.

GIS can be used to determine optimal sampling locations based on a set of input parameters, such as land cover types, desired sample size, landscape features, development, roads, landscape disturbances, and known contaminant emitters. These features can be used to plan optimal locations for monitoring sites and sample collection. Specifically, location-allocation (also known as site selection) algorithms are commonly used to mathematically determine the optimal locations based on the provided input parameters. This method maximizes spatial sampling coverage using the lowest possible sample size [51]. This method can be employed to design a monitoring campaign or can be integrated with existing samples and data analyses, such as the hot spot analysis conducted in this research, to refine future monitoring. The goal of a biomonitoring program is to determine

the state or condition of the environment and is typically related to anthropogenic impacts on the health of ecosystems and human health. Recent efforts have been made to provide a foundation for biomonitoring programs by grounding them in conceptual or theoretical frameworks [52]. A framework adopted for any biomonitoring program is guided by the research question and issues being addressed by the monitoring. For example, the Driving Forces-Pressures-State-Impacts-Response (DPSIR) framework has been recommended to standardize the examination of indicators of environmental quality [53]. For monitoring for the protection of human health, the Driving Force-Pressure-State-Exposure-Effect-Action (DPSEEA) framework has been recommended over the DPSIR framework as the most suitable framework for developing an integrated environmental health monitoring program [52]. The GIS and spatial analysis can support the practical implementation of the selected theoretical framework by quantifying patterns on the landscape and changes in the environment, which can arise from social, economic, and institutional systems [52]. Overall, the selection of the appropriate framework, which is supported by GIS, can lead to better design and evaluation of adaptive monitoring programs and more robust evidence-based decision making from the information produced.

Further, GIS may also be useful in supporting other methods of risk assessment including cumulative environmental effects monitoring (CEEM), adverse outcome pathway (AOP) development, cumulative risk assessments (CRA), and Aggregate Exposure Pathways (AEP) [54,55]. As field research cannot be as controlled as laboratory experiments, it is often difficult to draw causal inferences. Thus it can be challenging to extend some risk assessment methods including AOP and AEP to a population level as these models

rely on causal support for pathways [54]. GIS provides the methods to not only evaluate spatial patterns in datasets and the relationship between two variables across space, but it can also quantify patterns that occur in different locations and at different spatial scales [18]. The ability to quantify how patterns are repeated at different times, locations, and spatial scales, builds the weight of evidence necessary to give more power to correlational relationships typically seen in field studies. Other advantages of using a GIS to support population-level risk assessment development is the ability to store, organize, analyse, and display a variety of data types and sources, which helps synthesize the variety of data needed for risk assessments [54].

While GIS and spatial analyses provide methods for the practical implementation of landscape ecotoxicology, there are still limitations to the further development of this sub-discipline. First, it is both costly and time-consuming to collect samples that cover a landscape scale. As a result, most data are collected at the site level, which is insufficient for a landscape ecotoxicology analysis. As a result, Focks (2014) suggested stronger collaboration is needed between government and academia to capitalize on the large-scale biomonitoring programs conducted by the government. Biomonitoring projects such as JOSM provide an example of how government and academia can work together to use data collected at large spatial scales. However, without resources to collect data at a large spatial scale, this will still remain a challenge.

Other limitations to the implementation of landscape ecotoxicology are theoretical issues surrounding how we define and quantify aspects of ecosystem health. This issue is primarily due to the complexity of ecological systems. At the individual level, bioindicator

sentinel species are used to quantify an ecological response of an organism or population to changes in the environment [56]. Bioindicators are used to provide information not only about the health status of the individual but also regarding unmeasured parts of the system through inference related to the dose of exposures to a chemical, the susceptibility of the bioindicator species to dose-related effects, and the resulting adverse outcomes of exposure [57]. However, determining causal relationships between exposure and effect is difficult particularly in complex multi-stressor environments. As a result, it is commonly accepted that one indicator is not sufficient to properly describe a system, however, selecting what indicators to use can be challenging [56,58]. GIS provides a platform for integrating biomarkers from sentinel species as we showed in the first example, providing an opportunity to assess co-occurring patterns in biomarkers across species. This could be extended by adding co-variate to assess how exposures change across landscapes in a multi-stressor environment.

Further, evaluating health in a connected multi-level system at the individual, population, community, and ecosystem level poses additional challenges. To assess the health of an ecosystem, it is necessary to assess function, productivity, resilience, and biodiversity of the system. These emergent properties can only arise as a direct result of the interaction of many parts of the system and are hard to identify and measure [59]. Regardless of the indicator type, it is imperative that the indicators have biological, methodological, and societal relevance, which also includes cultural (traditional) importance and economic importance [60].

Computational barriers to implementation of landscape ecotoxicology include a lack of

awareness of the available tools, lack of knowledge on use or implementation of the tools, and large start-up costs related to software acquisition and training of personnel [61]. However, there have been recent developments in open source GIS applications, which can be acquired at no cost to the user and are also relatively user-friendly and intuitive. Examples of this are Google Maps, Google Earth, and QGIS. As a result, GIS is shifting from a primarily expert-controlled domain to having applications for novice users [18,61]. This shift presents opportunities for the applications of GIS within ecotoxicology and for use in community-based monitoring programs or citizen science initiatives [62].

While using GIS as a platform for landscape ecotoxicology provides tools to address some of the existing shortcomings, we also note some of the limitations of these tools. Notable are uncertainties related to scale dependence, spatial resolution, and zonation, also known as the modifiable areal unit problem (MAUP) [12]. MAUP is an issue where spatial analyses performed at different geographical aggregations or with different zonations may provide different results [63]. As a result, it is recommended to use natural units for analysis such as administrative boundaries or use the smallest level of aggregation available [64]. For this reason, when analyses are performed at an aggregate level, typically for confidentiality reasons, it is important to only make conclusions and recommendation at the level of aggregation at which the analysis was performed.

Finally, it is important to highlight that it is not possible to determine causality from correlational methods. However, the results presented in this paper can be used for making inferences about populations, guiding future hypothesis generation, designing and refining biomonitoring studies, and can help to develop a weight of evidence in support of causal

mechanisms. There are parallels between the results produced using the present methods and Hill's (1965) criteria for causation. While these criteria have been developed for environmental epidemiology, similarly they can support wildlife toxicology and support cause and effect relationships in ecotoxicology. Out of the nine criteria for determining causation most notably, the methods presented here and GIS can support the criteria of consistency, observing the same effect in different locations and populations, and biological gradient, where high exposure doses should elicit a response of greater magnitude. Further, the correlational results obtained can help guide related experiments, another Hill criterion, to assess biologic plausibility and mode of action to ultimately link molecular toxicology with ecotoxicology.

2.6 Data availability

Data are available from the Canada-Alberta Oil Sands environmental monitoring data portal: `https://www.canada.ca/en/environment-climate-change/services/oil-sands-monitoring.html`. R code used in these analyses can be found at: `https://github.com/kristineccles/landscape_ecotoxicology.git`

2.7 Acknowledgments

We would like to thank all the project leaders in the Wildlife Health component of the Canada- Alberta Joint Oil Sands Monitoring Programs (C. Boutin, K.J. Fernie, C. Hebert, L.J. Mundy, D. Schock, C. Soos, and P.J. Thomas). We thank S. Dray for support with

the spatial PCA analysis and A.R. Shifman for computational support. We acknowledge funding support from the Canada Research Chair Program and the National Sciences and Engineering Research Council Discovery Grant to H.M. Chan; the National Sciences and Engineering Research Council Collaborative Research and Training Experience Program, Research in Environmental and Analytical Chemistry and Toxicology to K.M. Eccles; and Environment and Climate Change Canada, Province of Alberta, Joint Oil Sands Monitoring program to B.D. Pauli.

2.8 References

1. Norton SB, Rodier DJ, Schalie van der, H W, Wood WP, Slimak MW, Gentile JH. 1992. A framework for ecological risk assessment at the EPA. Environ. Toxicol. Chem. 11:1663–1672.

2. Forbes VE, Palmqvist A, Bach L. 2006. The use and misuse of biomarkers in ecotoxicology. Environ. Toxicol. Chem. 25:272–280.

3. Cairns J, Niederlehner BR. 1996. Developing a Field of Landscape Ecotoxicology. Ecol. Appl. 6:790–796.

4. Schäfer RB. 2014. In response: why we need landscape ecotoxicology and how it could be advanced—an academic perspective. Environ. Toxicol. Chem. 33:1193–1194.

5. Focks A. 2014. The Challenge: Landscape ecotoxicology and spatially explicit risk assessment. Environ. Toxicol. Chem. 33:1193–1198.

6. Martin RW, Waits ER, Nietch CT. 2018. Empirically-based modeling and mapping to consider the co-occurrence of ecological receptors and stressors. Sci. Total Environ. 613:1228–1239.

7. Wendt-Rasch L, Poulsen V, Duquesne S. 2014. In Response: Regulatory risk assessment and landscape ecotoxicology—A governmental perspective. Environ. Toxicol. Chem. 33:1196–1197.

8. Price OR, Thorbek P. 2014. In Response: Challenges and opportunities for landscape ecotoxicology and spatially explicit risk assessment—An industry perspective. Environ. Toxicol. Chem. 33:1194–1196.

9. Legendre P, Legendre L. 2012. Numerical ecology: second English edition. In Elsevier, ed. Amsterdam;Boston.

10. Miller W. 2007. The Hierarchical Structure of Ecosystems: Connections to Evolution. Evol. Educ. Outreach. 1:16–24.

11. Sexton K, Linder SH. 2011. Cumulative risk assessment for combined health effects from chemical and nonchemical stressors. Am. J. Public Health. 101:S81–S88.

12. De Smith MJ, Goodchild MF, Longley P. 2007. Geospatial analysis: a comprehensive guide to principles, techniques and software tools. Troubador Publishing Ltd.

13. Ord A, Getis JK. 1995. Local Spatial Autocorrelation Statistics: Distributional Issues and an Application. Geogr. Anal. 27:286–306.

14. Fotheringham AS, Brunsdon C, Charlton M. 2002. Geographically weighted regression. John Wiley & Sons, Limited.

15. Kissling WD, Carl G. 2008. Spatial autocorrelation and the selection of simultaneous autoregressive models. Glob. Ecol. Biogeogr. 17:59–71.

16. Briggs D. 2005. The role of GIS: Coping with space (and time) in air pollution exposure assessment. J. Toxicol. Environ. Heal. - Part A. 68:1243–1261.

17. Jerrett M, Gale S, Kontgis C. 2010. Spatial Modeling in Environmental and Public Health Research. Int. J. Environ. Res. Public Health. 7:1302–1329.

18. Goodchild M, Guo H, Annoni A, Bian L, Bie K De, Campbell F, Craglia M, Ehlers M, Genderen J Van, Jackson D, Lewis AJ, Pesaresi M, Simpson R, Skidmore A, Wang C, Woodgate P, States U. 2012. Next-generation Digital Earth. Proc. Natl. Acad. Sci. 109:11088–11094.

19. Lahr J, Kooistra L. 2010. Environmental risk mapping of pollutants: State of the art and communication aspects. Sci. Total Environ. 408:3899–3907.

20. Lahr J, Münier B, Lange HJ De, Faber JF, Borgen P. 2010. Environment Wildlife vulnerability and risk maps for combined pollutants. Sci. Total Environ. 408:3891–3898.

21. Thomas PJ, Eccles KM, Mundy LJ. 2017. Spatial modelling of non-target exposure to anticoagulant rodenticides can inform mitigation options in two boreal predators inhabiting areas with intensive oil and gas development. Biol. Conserv. 212:111–119.

22. Clifford PA, Barchers DE, Ludwig DF, Sielken RL. 1995. An Apporach to Quantify Spatial Components of Exposure for Ecological Risk Assessment. Environ. Toxicol. Chem. 14:895–906.

23. Feist BE, Buhle ER, Arnold P, Davis JW, Scholz NL. 2011. Landscape Ecotoxicology of Coho Salmon Spawner Mortality in Urban Streams. PLoS One. 6:e23424.

24. Jariyasopit N, Harner T, Wu D, Williams A, Halappanavar S, Su K. 2016. Mapping Indicators of Toxicity for Polycyclic Aromatic Compounds in the Atmosphere of the Athabasca Oil Sands Region. Environ. Sci. Technol. 50:11282–11291.

25. Cruz-Martinez L, Fernie KJ, Soos C, Harner T, Getachew F, Smits JEG. 2015. Detoxification, endocrine, and immune responses of tree swallow nestlings naturally exposed to air contaminants from the Alberta oil sands. Sci. Total Environ. 502:8–15.

26. Fernie KJ, Marteinson SC, Chen D, Eng A, Harner T, Smits JEG, Soos C. 2018. Elevated exposure, uptake and accumulation of polycyclic aromatic hydrocarbons by nestling tree swallows (Tachycineta bicolor) through multiple exposure routes in active mining-related areas of the Athabasca oil sands region. Sci. Total Environ. 624:250–261.

27. Mundy LJ, Bilodeau JC, Schock DM, Thomas PJ, Blais JM, Pauli BD. 2018. Using wood frog (Lithobates sylvaticus) tadpoles and semipermeable membrane devices to monitor polycyclic aromatic compounds in boreal wetlands in the oil sands region of northern Alberta, Canada. Chemosphere. 214:148–157.

28. Hebert CE, Campbell D, Kindopp R, Macmillan S, Martin P, Neugebauer E, Patterson L, Shatford J. 2013. Mercury trends in colonial waterbird eggs downstream of the oil sands region of Alberta, Canada. Environ. Sci. Technol. 47:11785–11792.

29. Dolgova S, Popp BN, Courtoreille K, Espie RHM, Maclean B, McMaster M, Straka JR, Tetreault GR, Wilkie S, Hebert CE. 2018. Spatial trends in a biomagnifying contaminant: Application of amino acid compound–specific stable nitrogen isotope analysis to the interpretation of bird mercury levels. Environ. Toxicol. Chem. 37:1466–1475.

30. Boutin C, Carpenter DJ. 2017. Assessment of wetland/upland vegetation communities and evaluation of soil-plant contamination by polycyclic aromatic hydrocarbons and trace metals in regions near oil sands mining in Alberta. Sci. Total Environ. 576:829–839.

31. Government of Canada. 2017. Monitoring wildlife contaminants in Alberta oil sands. [cited 18 July 2018]. Available from https://www.canada.ca/en/environment-climate-change/services/oil-sands-monitoring/monitoring-wildlife-contaminants-alberta-oil-sands.html.

32. QGIS Development Team. 2018. QGIS geographic information system. Open Source Geospatial Found. Proj. http//qgis. osgeo. org.

33. ESRI ArcGIS Desktop. 2011. Release 10. Redlands, CA Environ. Syst. Res. Inst.

34. R Core Development Team. 2017. R: A Language and Environment for Statistical Computing.

35. Driscoll CT, Mason RP, Chan HM, Jacob DJ, Pirrone N. 2013. Mercury as a global pollutant: Sources, pathways, and effects. Environ. Sci. Technol. 47:4967–4983.

36. Buckley H, Case B, Ellison A. 2016. Using codispersion analysis to characterize spatial patterns in species co- occurrences. Ecology. 97:32–39.

37. Bingenheimer JB, Raudenbush SW. 2004. Statistical and substantive inferences in public health: Issues in the Application of Multilevel Models. Annu. Rev. Public Health. 25:53–77.

38. Best N, Richardson S, Thomson A. 2005. A comparison of Bayesian spatial models for disease mapping. Stat. Methods Med. Res. 14:35–59.

39. Carlin BP, Louis TA. 2010. Bayes and empirical Bayes methods for data analysis. Chapman and Hall/CRC.

40. Thioulouse J, Dray S, Dufour A-B, Siberchicot A, Jombart T, Pavoine S. 2018. Multivariate Analysis of Ecological Data with ade4. Springer.

41. Dray S, Dufour A-B, others. 2007. The ade4 package: implementing the duality diagram for ecologists. J. Stat. Softw. 22:1–20.

42. Bauman D, Drouet T, Fortin MJ, Dray S. 2018. Optimizing the choice of a spatial weighting matrix in eigenvector-based methods. Ecology. 99:2159–2166.

43. Dray S, Blanchet G, Borcard D, Guenard G, Jombart T, Larocque G, Legendre P, Madi N, Wagner HH. 2016. adespatial: Multivariate multiscale spatial analysis. R Packag. version 0.0. 3.

44. Bivand R, Piras G. 2015. Comparing Implementations of Estimation Methods for Spatial Econometrics. J. Stat. Softw. 63:1–36.

45. Pebesma EJ, Bivand RS. 2005. Classes and methods for spatial data in R. R News. 5:9–13.

46. Beketov MA, Liess M. 2012. Ecotoxicology and macroecology - Time for integration. Environ. Pollut. 162:247–254.

47. Vallejos R, Osorio F, Bevilacqua M. 2018. Spatial Relationships Between Two Georeferenced Variables: with Applications in R. Springer, New York. Available from http://srb2gv.mat.utfsm.cl.

48. Iliffe J. 2000. Datums and map projections for remote sensing, GIS, and surveying. CRC Press.

49. Kirk JL, Muir DCG, Gleason A, Wang X, Lawson G, Frank RA, Lehnherr I, Wrona F. 2014. Atmospheric Deposition of Mercury and Methylmercury to Landscapes and Waterbodies of the Athabasca Oil Sands Region. Environ. Sci. Technol. 48:7374−7383.

50. Kelly EN, Schindler DW, Hodson P V, Short JW, Radmanovich R, Nielsen CC. 2010. Oil sands development contributes elements toxic at low concentrations to the Athabasca River and its tributaries. Proc. Natl. Acad. Sci. 107:16178–16183.

51. Kanaroglou PS, Jerrett M, Morrison J, Beckerman B, Arain MA, Gilbert NL, Brook JR. 2005. Establishing an air pollution monitoring network for intra- urban population exposure assessment: A location-allocation approach. Atmos. Environ. 39:2399–2409.

52. Liu H-Y, Bartonova A, Pascal M, Smolders R, Skjetne E, Dusinska M. 2012. Approaches to integrated monitoring for environmental health impact assessment. Environ. Heal. 11:88.

53. Smeets E, Weterings R. 1999. Environmental indicators: Typology and overview. European Environment Agency, Copenhagen. Available from http://www.eea.europa.eu/publications/TEC25.

54. Kramer VJ, Etterson MA, Hecker M. 2011. Adverse outcome pathways and ecological risk assessment: Bridging to population-level effects. Environ. Toxicol. Chem. 30:64–76.

55. Hines DE, Edwards SW, Conolly RB, Jarabek AM. 2018. A Case Study Application of the Aggregate Exposure Pathway (AEP) and Adverse Outcome Pathway (AOP) Frameworks to Facilitate the Integration of Human Health and Ecological End Points for Cumulative Risk Assessment (CRA). Environ. Sci. Technol. 52:839–849.

56. Lu Y, Wang R, Zhang Y, Su H, Wang P, Jenkins A, Ferrier RC, Bailey M, Squire G. 2015. Ecosystem health towards sustainability. Ecosyst. Heal. Sustain. 1:1–15.

57. Holt EA, Miller SW. 2010. Bioindicators: Using Organisms to Measure Environmental Impacts. Nat. Educ. Knowl. 3:8.

58. Jørgensen SE, Xu L, Costanza R. 2010. Handbook of ecological indicators for assessment of ecosystem health. CRC press.

59. Costanza R. 2012. Ecosystem health and ecological engineering. Ecol. Eng. 45:24–29.

60. Burger J. 2006. Bioindicators: Types, Development, and Use in Ecological Assessment and Research. Environ. Bioindic. 1:22–39.

61. Ye H, Brown M, Harding J. 2013. GIS for All: Exploring the Barriers and Opportunities for Underexploited GIS Applications. FOSGeo J. 13, pp 19–28.

62. Richardson DB, Volkow ND, Kwan M-P, Kaplan RM, Goodchild MF, Croyle RT. 2013. Spatial turn in health research. Sci. (New York, NY). 339:1390.

63. Openshaw S, Openshaw S. 1984. The modifiable areal unit problem.

64. Bailey TC, Gatrell AC. 1995. Interactive spatial data analysis. 413, Longman Scientific & Technical, Essex.

65. Hill AB. 1965. The Environment and Disease: Association or Causation? Proc. R. Soc. Med.:295–300.

PART II

Fur as a Biomarker of Mercury Exposure

Preface: This section provides the foundations for developing and understanding fur as a non-invasive biomarker of mercury exposure to be used in a spatial context.

Chapter 3

Predictive Meta-Regressions Relating Mercury Tissue Concentrations of Freshwater Piscivorous Mammals

Kristin M. Eccles[1], Philippe J. Thomas[2], and Hing Man Chan[1]

[1] Department of Biology, University of Ottawa, 30 Marie Curie, Ottawa, ON, K1N 6N5, Canada
[2] Science and Technology Branch, Environment and Climate Change Canada, National Wildlife Research Center, 1125 Colonel By Drive, Raven Road, Ottawa, ON K1A 0H3, Canada

This chapter was published: Eccles KM, Thomas PJ, Chan HM. 2017. Predictive meta-regressions relating mercury tissue concentrations of freshwater piscivorous mammals. *Environ. Toxicol. Chem.* 36:2377-2384.

Author Contributions: KE conceived the idea, completed the mercury analysis, completed the statistical analysis, and wrote the manuscript. PT collected and prepared the samples and contributed to editing the manuscript. LC contributed to the conceptualization of the project and provided guidance on the implementation and editing of the manuscript.

3.1 Abstract

Mercury (Hg) is a pollutant of global concern. Sentinel species such as river otter (*Lontra canadensis*) and mink (*Neovison vison*) are often used to monitor environmental concentrations in freshwater ecosystems. Tissue total Hg (THg) concentrations are frequently used as biomarkers of exposure. However, there is no comprehensive model relating Hg tissue concentrations in different tissues, making interstudy comparisons challenging. Our objective was to establish conversion factors relating fur, brain, liver, kidney, and muscle THg concentrations using mean concentrations and standard errors reported in the literature. We used data from more than 6000 samples, pooled across 16 studies and 96 sampling sites in North America and Europe. Sixteen regressions were derived for the river otter and mink models, which were statistically significant at a 95% confidence interval and yielded high explained variances. The models were validated using an external data set of individually measured THg tissue concentrations. The validated conversions were used to evaluate the current fur Hg screening guidelines of 20 μg/g and 30 μg/g. At both of these fur concentrations, brain concentrations are of concern for altering brain neurochemistry. We suggest a more conservative fur Hg screening guideline of 15 μg/g to protect sensitive furbearers. The conversion factors can be used to predict internal organ THg concentrations from fur measurements, eliminating the need for invasive tissue sampling.

3.2 Introduction

Exposure to environmental pollutants such as inorganic mercury (IHg) and organic methylmercury (MeHg) is of concern because of their effects on wildlife and human health [1-3]. Both Hg and MeHg are often measured together and expressed as the total Hg (THg) burden (IHg + MeHg = THg). In mammals, Hg is readily absorbed through the gastrointestinal tract and rapidly distributed throughout the body [2]. Methyl Hg can cross the placenta, and exposure to Hg during critical times in fetal development can cause long-term neurological effects [2]. Furthermore, because MeHg can cross the blood-brain barrier, subchronic and chronic exposure to MeHg at any age can lead to impairments to cognition, motor control, coordination, intellect, hearing, and vision [2,4].

Mercury is released into the environment by both natural and anthropogenic sources. Once in the environment, IHg can be methylated into MeHg, which bioaccumulates in organisms, including biota and fish, and biomagnifies up trophic levels [5]. Therefore, the highest MeHg concentrations are found in predatory fish and mammals [5]. This is of particular concern for piscivorous mammals because diet is the main route of MeHg exposure and their high position in the food web produces higher exposure [6]. Sentinel species have been used widely to monitor environmental pollutants, including Hg. Piscivorous top predators such as river otter and mink are commonly used as sentinel species for risk assessments of freshwater ecosystems [7,8]. Unlike birds, they have small home ranges and do not hibernate or migrate, meaning they are exposed to contaminants year-round. In addition, these species are distributed throughout North America, making them good

bioindicator candidates [5,9]. Through the use of biomarkers of exposure, such as tissue concentrations, sentinel species can be used to determine environmental concentrations and assess risks posed to wildlife consumers [10].

Human hair and toenails, animal fur, whiskers (vibrissae), eggshells, and feathers have been used for the biomonitoring of exposure to contaminants, including Hg [11-13]. Hair and fur are excellent biomarkers of exposure in humans and other mammals because contaminants within the bloodstream are sequestered in these tissues. Mercury is highly stable within these media, and collected samples do not require preservation or refrigeration before analysis [14,15]. Moreover, they provide noninvasive sources to monitor exposure to contaminants over a period of months compared with blood, urine, or feces, which only reflect recent exposure [15]. Therefore, they are less subject to variability in terms of seasonality, food availability, diet, age, sex, and habitat [14-16]. Chemical exposure can also be measured in tissues such as brain, liver, kidney, muscle, and fat, although these samples are highly invasive and typically require postmortem collection [17]. To improve the utility of fur as a biomarker of tissue Hg concentrations, it is necessary to gain a more complete understanding of the relationship between fur THg concentrations and the THg concentrations of internal organs, such as brain, liver, kidney, and muscle.

Most reviews on mammalian Hg concentrations have focused on polar bears and other top predators in the Arctic [3,12,18], and no such review for Hg concentrations in river otter or mink is available. Although both species are well studied, no comprehensive models relating all Hg tissue concentrations exist for either of these species. Such information is imperative for assessing spatial trends in a non-lethal way to informing environmental

management in the mid and southern latitudes of the Northern Hemisphere. Therefore, the objective of the present study was to develop a predictive meta-regression model relating the concentrations of Hg among individual tissues compartments using the mean Hg tissue concentrations reported in the literature for both river otter and mink. We hypothesized that there would be constant ratios between the THg concentrations in fur and those in the internal organs of river otter and mink, which would allow us to develop statistically significant conversion factors useful to future monitoring programs.

3.3 Methods

3.3.1 Data Collection

The literature search methods used for the present review are summarized in Figure 3.1 . The databases Web of Science and Scopus were systematically searched for studies on the relationship between Hg concentrations in the diet and various body compartments, such as fur, brain, liver, kidney, and muscle between 1980 and 2016. The search phrases used in these meta-analyses were "(mink OR *Neovison vison* OR *Mustela vison*) AND (mercury OR methylmercury)" and "(river otter OR *Lontra canadensis*) AND (mercury OR *methylmercury*)".

After initially gathering articles using the search expressions, we removed duplicates and then screened the articles for use based on 2 criteria. First, they had to report on the target genus and species of mink (*M. vison*, now known as *N. vison*) or river otter (*L. canadensis*). This excluded the European otter (*Lutra lutra*), sea otter (*Enhydra lutris*), and neotropical

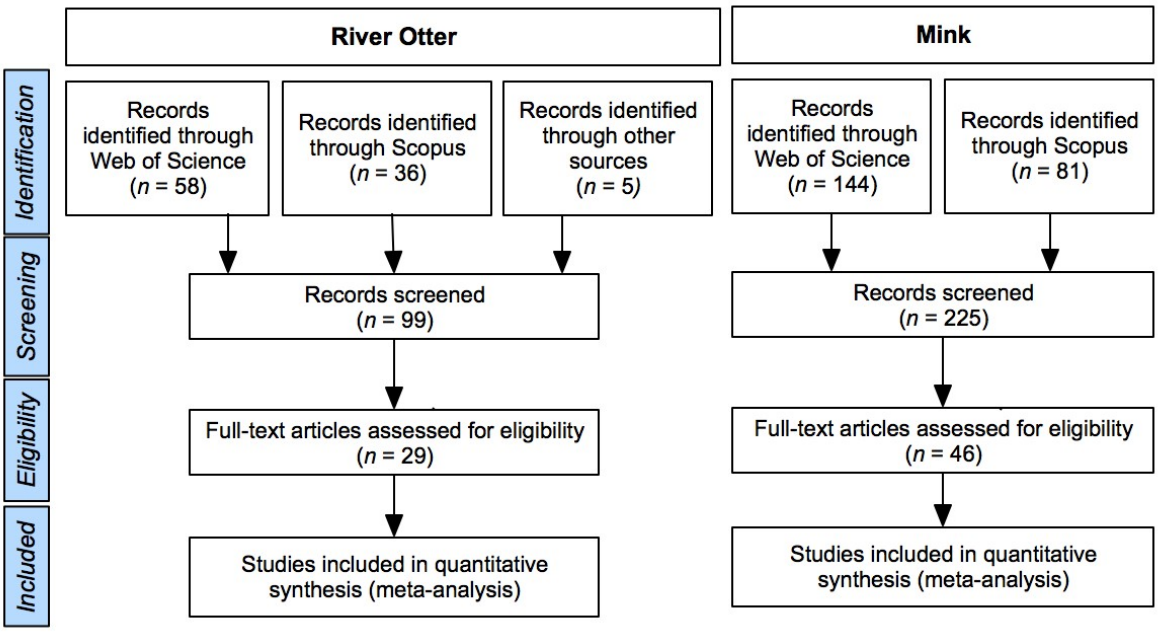

Figure 3.1: Summary of the screening process used for the meta-analysis.

otter (*Lontra longicaudis*). Second, the articles had to report concentrations for more than 1 tissue type. Eligible articles were used to compile mean tissue concentration, standard deviation (SD), standard error (SE), and number of samples at the locations surveyed. We did not account for the difference between different studies reported in the literature, such as the time of year that sampling was conducted or the performance of chemical measurement, because the present study focused only on the relationship between Hg concentrations in different tissues reported in each study.

When data were available, SD and SE were calculated. In addition, the corresponding antilog was taken for any studies that reported log-transformed values. Finally, all mean concentrations, SDs, and SEs were converted into micrograms per gram of dry weight for both the river otter and the mink analyses. If a conversion factor from wet weight to dry weight was provided in the study, this value was used. For example, in Kucera [19], the

conversion factor from dry weight to wet weight was provided for river otter, where liver values were divided by 0.41, kidney values were divided by 0.43, and brain concentrations were divided by 0.33. If no conversion was provided, values were converted from wet weight to dry weight assuming moisture contents of 80% for brain [20] and 75% for liver, kidney, and muscle [21,22]. For mink conversions from wet weight to dry weight, Kalisinska et al. [23] assumed a 71% moisture content when converting concentration values for kidney and liver. Basu et al. [8] assumed a brain moisture content of 74.6%. No conversion value specific to mink muscle concentrations could be found in the literature, so a moisture content of 75% was used based on the conversion value for river otters [22]. Using these moisture content values, the conversion formula in Equation 3.1 was used for the conversion from wet weight to dry weight concentrations. Only THg values were used in the analysis.

$$dry\,weight = \frac{wet\,weight}{1 - (\frac{percent\,moisture}{100})} \tag{3.1}$$

3.3.2 Analysis

For the analysis only total Hg values were used. Pearson's product-moment correlation coefficients were calculated to assess the linear correlations between the Hg tissue concentrations from the literature as all tissue combinations exhibited strong linearity. These mean Hg tissue concentrations were regressed against one another using either the ordinary least squares method or the subtype weighted least squares method. The weight was equal to $1/SE^2$ of the dependent variable. When the assumptions are met, these models produce the most robust estimates for predictive purposes [24].

The models were assessed for homoscedasticity of the residuals using a nonconstant variance test. When $p > 0.05$, the residuals were homoscedastic. If the residuals were heteroscedastic, both the dependent and independent variables were square root-transformed to meet this assumption. The intercept of each model was forced through 0 to produce a simple conversion factor. Optimal models were chosen based on a balance of meeting the assumptions, model fit assessed by the Akaike information criterion corrected for small sample size, and parsimony for ease of use and interpretation.

The river otter and mink models were validated using individual tissue concentrations measured from an independent collection. Carcases were sourced from a monitoring program for oil and gas resource development in Northern Alberta, Canada (Canada-Alberta Joint Oil Sands Monitoring Program) in 2015. The sampled animals inhabited both high Hg-impacted regions and low Hg-impacted regions around the Canadian Oil Sands, and samples were selected along a gradient of exposures. Once tissue samples were dissected, they were mechanically homogenized (Heidolph Silent Crusher homogenizer; Sigma-Aldrich) and then freeze-dried for 48 h to remove all water content (FreeZone Freeze Dry System; Labconco). Then, the samples were ground into powder in an acid-washed pestle and mortar, and 50 mg were subsampled for analysis. All THg measurements were based on dry weight. The samples were analysed using a direct thermal decomposition Hg analyser (Mercury Analyzer 3000; Nippon Instruments North America). Quality assurance/quality control measures, including blank samples, standard reference material (DORM-4 and DOLT-5), and 10% of both river otter and mink tissue samples, were run in duplicate. DORM-4 is a fish protein certified reference material for trace metals with a

known THg concentration of 0.44 ± 0.036 mg/kg (experiment mean=0.36 ± 0.002 mg/kg) and DOLT-5 is a dogfish liver certified reference material for trace metals with a known THg concentration of 0.44 ± 0.024 mg/kg (experiment mean = 0.34 ± 0.032 mg/kg). Duplicate coefficient of variation (CV) = 2.37%. The limit of detection, calculated as 3 times the standard deviation of the blank (boat blanks) was 0.36 ng.

For each model, the conversion factor (beta coefficient) was applied to predictor (independent) variables to estimate the response (dependent) variables. For each tissue relationship, the estimated response variables were compared with the measured concentration using the root mean square error (RMSE; Equation 3.2). In this equation, the using the squared sum of all estimates ($\hat{Y}$) measured value (Y). This value is divided by the number (n) of pairs summed and then square-rooted.

$$RMSE = \sqrt{\frac{\Sigma_{n}^{t=1}(\hat{Y}_t - Y_t)^2}{n}} \tag{3.2}$$

To enable comparisons, the RMSE was normalized (NRMSE) to the range of the data (Equation 3.3) to adjust for the large concentration range in the validation data set. The NRMSE is expressed as the percent of the error in relation to the range of data.

$$NRMSE = \frac{RMSE}{max(Y) - min(Y)} \tag{3.3}$$

Negative and positive residuals were summed to assess how conservative the conversion factors were. All statistical analyses were completed in the statistical program R, Ver 3.0.1.

3.4 Results

The river otter data were compiled from 13 studies; however, accounting for each sample site throughout North America within each study increased the number of river otter Hg tissue sample concentration groups to 39 (Table 3.1). Similarly, the mink data were compiled from 16 studies; however, accounting for each sample site throughout North America and Europe within each study increased the number of mink Hg tissue sample concentration groups to 57 (Table 3.2). Additional information on the studies, locations, and tissue concentrations used for these analyses can be found in the Supplemental Data, Tables S1 and S2.

Table 3.1: Summary of the number of samples and the number of sample groups for river otters with tissue total mercury tissue measurements.

Study	Year	Fur	Brain	Liver	Kidney	Muscle
Dornbos [20]	2013	65		96		
Klenavic [25]	2008	199	203	203		
Strom [26]	2008	82	104	105	105	105
Yates [27]	2005	80	89	206		
Fortin [28]	2001	12	11	10	10	11
Evans [29]	2000	40	40	40	40	
Evans [30]	1998	18		19		
Francis [31]	1994			11	11	
Halbrook [32]	1994	125		10		121
Ropek [33]	1993			43	30	
Wren [34]	1986		10	76	54	48
Kucera [19]	1983		38	38	38	
Total Number of Samples		621	495	857	223	285
Total Number of Sample Sites		23	29	39	22	11

Table 3.3 and Table 3.4 show the Pearson product-moment correlation coefficients calculated for river otters and mink. For river otter, the correlation coefficients ranged from 0.46 (brain and muscle) to 0.97 (fur and kidney). For mink, the correlation coefficients

Table 3.2: Summary of the number of samples and the number of sample groups for Mink with tissue total mercury tissue measurements.

Study	Year	Fur	Brain	Liver	Kidney	Muscle
Evans [35]	2016		59			
Brzezinski [36]	2014			133	133	
Kalisinska [23]	2012			13	15	
Klenavic [37]	2008	144	147	146		
Lake [38]	2007			210		208
Gamberg [39]	2005		30	98	98	
Yates [40]	2005	126	118	512		
Fortin [41]	2001	39	38	39	39	39
Evans [29]	2000	41	41	41	41	
Dansereau [42]	1998			20		
Harding [43]	1998			26	12	
Halbrook [44]	1997	40		40	40	
Halbrook [45]	1996			28	27	27
Wren [34]	1986		82	82	82	82
Kucera [19]	1982		172	172	172	
Total Number of Samples		390	687	1560	659	356
Total Number of Sample Sites		17	32	57	32	10

ranged from 0.62 (brain and muscle) to 0.87 (fur and liver).

Table 3.3: Pearson's product-moment correlation coefficients for river otter mean total mercury tissue concentrations.

	Mean Fur	Mean Brain	Mean Liver	Mean Kidney
Mean Fur	1			
Mean Brain	0.939	1		
Mean Liver	0.58	0.601	1	
Mean Kidney	0.973	0.693	0.809	1
Mean Muscle	0.887	0.461	0.92	0.917

Table 3.4: Pearson's product-moment correlation coefficients for river otter mean total mercury tissue concentrations.

	Mean Fur	Mean Brain	Mean Liver	Mean Kidney
Mean Fur	1			
Mean Brain	0.698	1		
Mean Liver	0.871	0.809	1	
Mean Kidney	0.618	0.732	0.863	1
Mean Muscle	NA	0.646	0.66	0.83

The predictive meta-regression modelling results for river otter and mink are sum-

marized in Table 3.5 and Table 3.6. All models represented were statistically significant (a=0.05, maximum p=0.02), and a high percentage of variance was explained for both river otter (range, 0.83-0.99) and mink (range, 0.65-0.99). All models met the regression assumptions, except for the model that used brain to predict muscle THg concentrations, where the model residuals exhibited heteroscedasticity (non-constant variance = 0.03).

Table 3.5: Summary of all predictive paths between total mercury tissue concentrations in river otter.

Path	Path (X → Y)	B1	SE	Adj R2	p	NCV	DF
A	Brain → Kidney	2.84	0.33	0.83	<0.001	0.1	2.84
B	Brain → Liver	2.04	0.07	0.97	<0.001	0.31	2.04
C	Brain → Muscle	1.59	0.06	0.99	<0.001	0.03	1.59
D	Fur → Brain	0.15	0.01	0.99	<0.001	0.75	0.15
E	Fur → Kidney	0.62	0.05	0.95	<0.001	0.77	0.62
F	Fur → Liver	0.7	0.03	0.97	<0.001	0.43	0.7
G	Fur → Muscle	0.46	0.06	0.9	<0.001	0.11	0.46
H	Kidney → Brain	0.22	0.01	0.95	<0.001	0.33	0.22
I	Kidney → Liver	1.12	0.05	0.97	<0.001	0.14	1.12
J	Kidney → Muscle	0.54	0.02	0.99	<0.001	0.51	0.54
K	Liver → Brain	0.45	0.01	0.99	<0.001	0.39	0.45
L	Liver → Kidney	0.58	0.06	0.84	<0.001	0.84	0.58
M	Liver → Muscle	0.53	0.04	0.94	<0.001	0.18	0.53
N	Muscle → Brain	0.39	0.03	0.96	<0.001	0.74	0.39
O	Muscle → Kidney	1.94	0.11	0.98	<0.001	0.18	1.94
P	Muscle → Liver	2.02	0.14	0.95	<0.001	0.62	2.02

B1=model beta coefficient, SE=standard error, Adj R^2=adjusted R^2, p=p-value, ncv=non-constant variance p-value, df=degrees of freedom

Table 3.7 shows the results of the model validation. For the river otter models, all NRMSEs were less than 31%, with the exception of the model that used liver to predict brain Hg concentrations (NRMSE=39.6%) and the model that used fur to predict muscle concentration (NRMSE=45.4%). Similarly, for the mink models, most NRMSEs were less than 30%, with the exception of the model that used fur to predict kidney Hg concentrations

Table 3.6: Summary of all predictive paths between total mercury tissue concentrations in mink.

Path	Path (X → Y)	B1	SE	Adj R^2	P	NCV	DF
A	Brain → Kidney	1.49	0.11	0.92	<0.001	0.9	15
B	Brain → Liver	2.02	0.12	0.91	<0.001	0.82	25
C	Brain → Muscle	1.21	0.06	0.99	<0.001	0.37	3
D	Fur → Brain	0.13	0.02	0.8	<0.001	0.32	11
E	Fur → Kidney	0.64	0.05	0.65	0.01	0.89	6
F	Fur → Liver	0.46	0.03	0.91	<0.001	0.75	16
G	Fur → Muscle[a]	0.301	0.043	0.797	<0.001	0.23	11
H	Kidney → Brain	0.6	0.03	0.96	<0.001	0.53	15
I	Kidney → Liver	0.6	0.03	0.96	<0.001	0.53	15
J	Kidney → Muscle	0.89	0.07	0.82	<0.001	0.53	31
K	Liver → Brain	0.99	0.06	0.98	<0.001	0.61	5
L	Liver → Kidney	0.3	0.02	0.9	<0.001	0.44	24
M	Liver → Muscle	0.77	0.03	0.94	<0.001	0.65	31
N	Muscle → Brain	0.78	0.05	0.95	<0.001	0.2	9
O	Muscle → Kidney	0.43	0.1	0.82	0.022	0.82	3
P	Muscle → Liver	0.77	0.05	0.98	<0.001	0.71	5

[a]Estimated based on generated data

B1=model beta coefficient, SE=standard error, Adj R^2=adjusted R^2, p=p-value, ncv=non-constant variance p-value, df=degrees of freedom

(NRMSE=82.7%). We determined the percentage of overprediction when comparing the predicted values to the measured values in the validation. Models that overpredict more often are more conservative, and thus more protective, than models that underpredict more often.

For the generated tissue values, the coefficient of variation (CV) of sample duplicates ranged from 0.36% (muscle) to 7.36% (fur) for river otter. In the mink sample duplicates, the CV ranged from 0.59% (liver) to 8.34% (brain). For both river otter and mink, the average CV was approximately 2% (Table 3.8).

The validated conversion factors produced based on the meta-regression models can be found in Table 3.9

Table 3.7: Results of the model validation for river otter and mink using Hg analysis of independent tissue samples. The normalized root mean square error (NRMSE) is expressed as a percentage.

		River Otter		Mink	
Path	Path (X → Y)	NRMSE %	% Over Predicted	NRMSE %	% Over Predicted
A	Brain → Kidney	14.8	72.2	18.4	0
B	Brain → Liver	22.1	0	11.1	16.7
C	Brain → Muscle	13.2	5.6	13.3	100
D	Fur → Brain	28.6	44.4	28.4	57.1
E	Fur → Kidney	30.1	77.8	82.7	80
F	Fur → Liver	30.4	70.6	32.4	0
G	Fur → Muscle	45.4	0	19.2**	85.7**
H	Kidney → Brain	22.7	0	16.1	92.9
I	Kidney → Liver	10	23.5	13.9	23.5
J	Kidney → Muscle	18.1	11.1	10.9	23.5
K	Liver → Brain	39.6	100	13.2	0
L	Liver → Kidney	16.8	11.8	17.6	23.5
M	Liver → Muscle	8.8	29.4	18.2	7.1
N	Muscle → Brain	14.5	0	9	71.4
O	Muscle → Kidney	15.6	88.9	13.8	0
P	Muscle → Liver	9.9	94.1	11.7	70.6

**Estimated based on generated data

Table 3.8: Summary of generated mercury (Hg) tissue concentrations for model validation.

	Muscle Hg (μg/g)	Fur Hg (μg/g)	Brain Hg (μg/g)	Liver Hg (μg/g)	Kidney Hg (μg/g)
River Otter					
Min	0.77	1.45	0.31	1.03	0.75
Max	3.85	15.41	1.82	7.71	7.76
Median	1.48	4.33	0.75	2.16	1.52
Mean	1.68	5.26	0.85	2.76	2.51
Mink					
Min	0.13	0.36	0.1	0.11	0.3
Max	2.73	7.65	1.4	4.14	2.73
Median	1.28	3.97	0.42	1.06	1.19
Mean	1.35	4.1	0.54	1.34	1.24

3.5 Discussion

The Pearson product-moment correlation coefficients that relate Hg levels among different tissues for river otter and mink were similar to those published in the literature. For river otter, studies have published correlation coefficients between fur THg and brain THg concentrations of 0.64, 0.80 [25], 0.64 [20], and 0.74 [26] and the correlation coefficient for

Table 3.9: Conversion Factors between mercury tissue concentrations for river otter and mink.

Path	Path (X → Y)	Conversion Factor River Otter	Conversion Factor Mink
A	Brain → Kidney	2.84	1.49
B	Brain → Liver	2.04	2.02
C	Brain → Muscle	1.59	1.21
D	Fur → Brain	0.15	0.13
E	Fur → Kidney	0.62	0.64
F	Fur → Liver	0.7	0.46
G	Fur → Muscle	0.46	0.3
H	Kidney → Brain	0.22	0.6
I	Kidney → Liver	1.12	0.89
J	Kidney → Muscle	0.54	0.99
K	Liver → Brain	0.45	0.3
L	Liver → Kidney	0.58	0.77
M	Liver → Muscle	0.53	0.78
N	Muscle → Brain	0.39	0.43
O	Muscle → Kidney	1.94	0.77
P	Muscle → Liver	2.02	1.1

the same relationship calculated in the present study was 0.94. Similarly, in mink, studies have published correlation coefficients between fur THg and liver THg concentrations of 0.56 [27], 0.708 [26], 0.73 [28], 0.50, and 0.60 [29] and the correlation coefficient for the same relationship in the present study was 0.87. This demonstrates that a higher correlation coefficients, representing the linear relationship between fur and brain in river otters and between fur and liver in mink, were developed from the mean tissue concentration meta-analysis.

Although the sensitivities of river otter and mink to Hg exposure differ [30] and should be modelled separately, there are commonalities between the models of these species for the same tissues. Many of the meta-regressions using the same dependent and independent variables had similar beta values. For example, predicting brain THg from fur THg concentrations yielded similar beta values (river otter, 0.15; mink, 0.13). In addition, in most

models, fur THg concentrations were good predictors of tissue concentrations as indicated by the results of the validation.

Although there was confidence in the relatively accurate predictive power of most models, some models offered better predictions than others. Most of the models predicted concentrations with accuracies of 30% or less of the actual concentrations. The majority of the river otter and mink conversions overpredicted some tissue concentrations (12/16 paths). These models were limited to the estimation of 1 unknown tissue concentration from 1 known tissue concentration. These relationships were not modeled or validated as paths, and using the estimated tissue concentrations to estimate additional tissue concentrations could result in grossly inaccurate predictions from inordinate compounding of error terms.

It should be noted that the conversion factors were generated based on mean tissue concentrations from many samples of various sexes and ages, over many sample sites, and across many years. The meta-analysis inclusion criteria were chosen specifically so that the produced conversion factors would be simple and universal. This reflects realistic conditions of a non-invasive biomonitoring program using hair snags where information on age or sex may be unavailable.

The high NRMSEs of some models could indicate that these models were not fit properly, possibly resulting from the low degrees of freedom. In addition, the THg tissue burdens of the river otters and mink samples used to validate these models may have been influenced by local confounding factors. For example, animals inhabiting areas that experience high persistent exposure to pollutants, such as those in northern Alberta near the

oil sands, may adapt to their environments, altering the way they metabolize and excrete toxicants. Moreover, studies have shown that animals inhabiting contaminated regions have upregulated cytochrome P450 genes that detoxify these compounds. Detoxification aids in the elimination of these compounds from the body, which could result in lower tissue burdens [31,32].

Although tissue residue levels can be good biomarkers of exposure, guidelines are necessary to aid in their interpretation. For humans, healthy ranges related to biochemical, physiological, and behavioral parameters are well established and widely available. However, such guidelines have not been developed to the same degree for wildlife [33]. The current screening lowest- observed adverse-effect level guideline for fur THg in furbearing mammals is conservatively 20 μg/g [34] and less conservatively 30 μg/g [8,35]. It should be noted that the water content of fur/hair is negligible; thus, these concentrations are considered dry weight. The no-observable-adverse-effect level in human hair, observed in the Faroese Island population, is 6.0 μg/g [36]. Comparing the sensitivity to the effects of Hg (irrespective of type) on brain among species, river otters are ranked as the least sensitive, followed by rats, mink, mice, and humans. This is reflected in hair/fur screening guidelines [30].

The relationships developed in the meta-model can be used to assess whether current screening guidelines are appropriate (Figure 3.2). Using the conservative screening fur guideline of 20 μg/g and the less conservative value of 30 μg/g in conjunction with the upper limit of the beta coefficient (beta plus SE) of model D (i.e., fur $\rightarrow$ brain) produced estimated brain THg concentrations. The estimates ranged from 3.10 μg/g dry weight

to 4.66 μg/g dry weight for river otter and from 2.97 μg/g dry weight to 4.46 μg/g dry weight for mink There is a negative relationship between brain THg concentration and cholinergic muscarinic acetylcholine receptor density and ligand affinity. This is a particularly important relationship because THg is a potent neurotoxicant [20,37,38] and elicits a dose-dependent response. A screening threshold of 3 μg/g dry weight to 5 μg/g dry weight has been proposed as the concentration required to observe THg-related changes to brain neurochemistry in mammalian wildlife [20]. This is currently the most sensitive endpoint for assessing the neurotoxicity of THg in mammals [3,20].

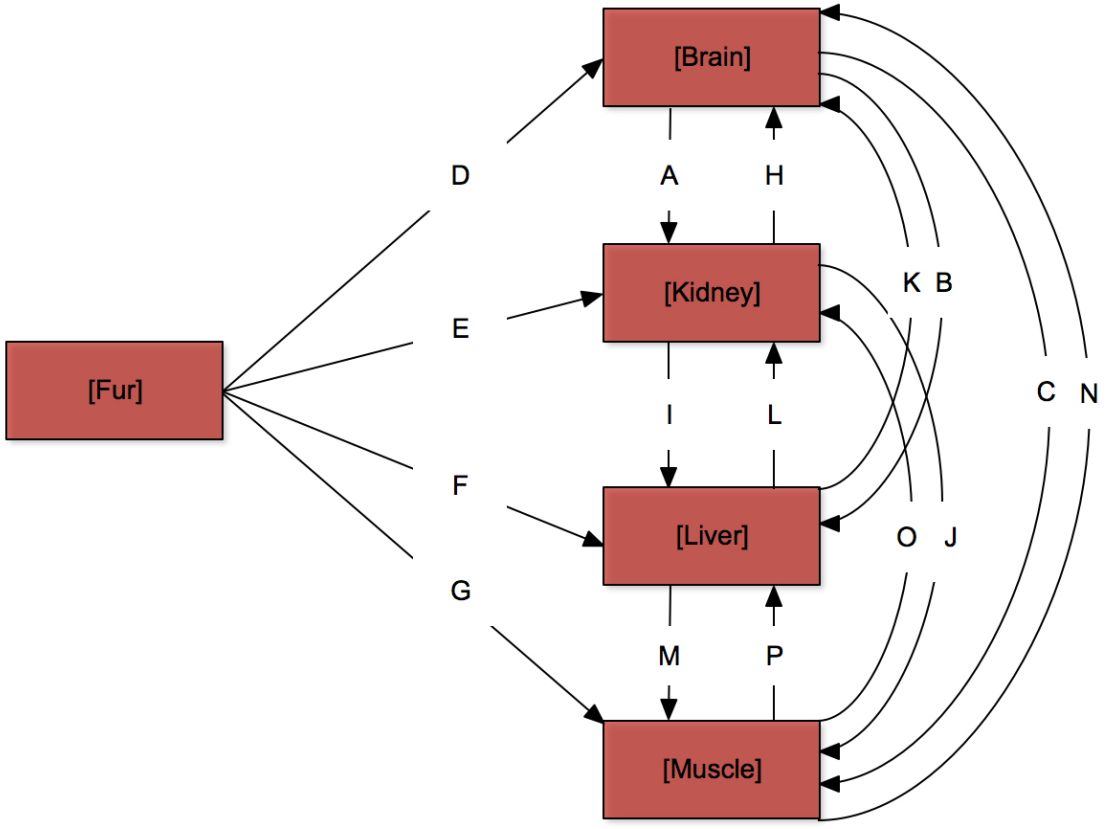

Figure 3.2: Conceptual model illustrating all calculated relational paths between different tissue compartments in river otter and mink.

Based on the brain concentration calculations from fur for river otters and mink, current fur screening guidelines may not be sufficiently conservative. At 30 μg/g, the predicted river otter and mink brain concentrations were above the upper limit of the threshold concentration of concern. At 20 μg/g, both species were at the threshold of concern. Furthermore, because river otters are reported to be the least sensitive species to the effects of brain THg, the current fur THg screening upper threshold guideline may not be appropriate for more sensitive species. A lower screening guideline or species-specific guidelines might be more appropriate to account for interspecies differences in sensitivity to THg in furbearing mammals. We suggest decreasing the fur THg screening guideline to 15 μg/g, which, based on the models, would be equivalent to brain THg concentrations of 2.33 μg/g dry weight in river otter and 2.23 μg/g dry weight in mink. This proposed guideline would keep more sensitive species near the lower limit of the threshold of concern. Of the samples measured for the validation, only 1 river otter had a fur THg concentration exceeding the proposed guideline of 15 μg/g.

Using the developed model, it is possible to estimate not only tissue concentrations in animals but also the concentrations required to produce the corresponding tissue concentrations. However, dietary information is available only for mink, as they are easier to raise in captivity [7]. Elucidating the relationship between tissue concentrations and dietary concentrations will provide useful information on environmental concentrations. Using the relationship between fur THg and dietary THg concentrations, the amount of THg in the diet can be estimated as an indirect measure of environmental THg concentrations. From this estimate, it may be possible to estimate the approximate THg concentration in fish

using food consumption information for mammals of concern. More work is needed to explore such applications of this model. In addition, more data are needed to determine the relationship between dietary intake in river otter and fur THg content.

Human, wildlife, and environmental health are intrinsically linked and improving our understanding of Hg exposure in mammals can provide insight into both environmental conditions and risk to humans. River otters and mink are considered to be good sentinel species for both environmental exposure and human health [7,8]. The meta-regressions developed in the present study can be used as a screening tool provides an indicator of ecosystem exposure to contaminants. These models can alleviate the need to measure concentrations in multiple tissues, saving both time and money. Moreover, they allow for the estimation of concentrations in more invasive tissues, such as brain, from less invasive samples, such as fur/ hair, which can be collected via fur/hair snags or from pelts from hunting and trapping. Similar meta-regression approaches can be applied to other species, such as polar bears, and to marine ecosystems. However, interspecies relationships must be investigated for each of the studied species.

3.6 Data availability

Data are available upon request from the authors.

3.7 Acknowledgments

We thank the Cree, Dene, and Métis communities who provided help and advice during the study and whose traditional lands contributed some of the wildlife collected for the present study (including Fort McMurray, Fort McKay, Mikisew Cree, and Athabasca Chipewyan First Nations and Métis); the Alberta Trappers Association and all registered trappers for their help and support during wildlife collection; B. Maile, M.Pybus, and the staff at Alberta Environment and Parks for their facilities and services rendered; and V. On Yee Yam and E. Littlewood for their help with sample preparation. We acknowledge funding support from the Canada Research Chair Program and the National Sciences and Engineering Research Council Discovery Grant to H.M. Chan; the National Sciences and Engineering Research Council Collaborative Research and Training Experience Program, Research in Environmental and Analytical Chemistry and Toxicology to K.M. Eccles; and Environment and Climate Change Canada, Province of Alberta, Joint Oil Sands Monitoring program to P.J.Thomas.

3.8 References

1. Chapman L, Chan HM. 2000. The influence of nutrition on methyl mercury intoxication. Environ Health Perspect 108(Suppl. 1):29-56.

2. Mergler D, Anderson HA, Chan LHM, Mahaffey KR, Murray M, Sakamoto M, Stern AH. 2007. Methylmercury exposure and health effects in humans: A worldwide concern. Ambio 36:3-11.

3. Dietz R, Sonne C, Basu N, Braune B, O-Hara T, Letcher RJ, Scheuhammer T, Andersen M, Andreasen C, Andriashek D, Asmund G, Aubail A, Baagøe H, Born EW, Chan HM, Derocher AE, Grandjean P, Knott K, Kirkegaard M, Krey A, Lunn N, Messier F, Obbard M, Olsen MT, Ostertag S, Peacock E, Renzoni A, Rig et FF, Skaare JU, Stern G, Stirling I, Taylor M, Wiig Ø, Wilson S, Aars J. 2013. What are the toxicological effects of mercury in Arctic biota- Sci Total Environ 443:775-790.

4. Basu N, Klenavic K, Gamberg M, O-Brien M, Evans D, Scheuhammer AM, Chan HM. 2005. Effects of mercury on neurochemical receptors in wild river otters (*Lontra canadensis*). Environ Sci Technol 39:3585-3591.

5. Lavoie RA, Jardine TD, Chumchal MM, Kidd KA, Campbell LM. 2013. Biomagnification of mercury in aquatic food webs: A worldwide meta-analysis. Environ Sci Technol 47:13385-13394.

6. Driscoll CT, Mason RP, Chan HM, Jacob DJ, Pirrone N. 2013. Mercury as a global pollutant: Sources, pathways, and effects. Environ Sci Technol 47:4967-4983.

7. Basu N, Scheuhammer AM, Bursian SJ, Elliott J, Rouvinen-Watt K, Chan HM. 2007. Mink as a sentinel species in environmental health. Environ Res 103:130-144.

8. Basu N, Klenavic K, Gamberg M, O-Brien M, Evans D, Scheuhammer AM, Chan HM. 2005. Effects of mercury on neurochemical receptor-binding characteristics in wild mink. Environ Toxicol Chem 24:1444.

9. Ben-David HN, Golden M. 2009. River otters (*Lontra canadensis*) in southcentral Alaska: Distribution, relative abundance, and minimum population size based on coastal latrine site surveys. SWAN I&M Progress Report. National Park Service, Anchorage, AK, USA.

10. Peterson EK, Schulte BA. 2016. Impacts of pollutants on beavers and otters with implications for ecosystem ramifications. J Contemp Water Res Educ 157:33-45.

11. Lodenius M, Solonen T. 2013. The use of feathers of birds of prey as indicators of metal pollution. Ecotoxicology 22:1319-1334.

12. Bechshoft T, Derocher AE, Richardson E, Mislan P, Lunn NJ, Sonne C, Dietz R, Janz DM, St Louis VL. 2015. Mercury and cortisol in western Hudson Bay polar bear hair. Ecotoxicology 24:1315-1321.

13. Pedro S, Xavier JC, Tavares S, Trathan PN, Ratcliffe N, Paiva H, Medeiros R, Pereira E, Pardal MA. 2015. Feathers as a tool to assess mercury contamination in gentoo penguins: Variations at the individual level. PLoS One 10:e0137622.

14. Pragst F, Balikova MA. 2006. State of the art in hair analysis for detection of drug and alcohol abuse. Clin Chim Acta 370:17-49.

15. Macbeth BJ, Cattet MRL, Stenhouse GB, Gibeau ML, Janz DM. 2010. Hair cortisol concentration as a noninvasive measure of long-term stress in free-ranging grizzly bears (*Ursus arctos*): Considerations with implications for other wildlife. Can J Zool 88:935-949.

16. Hernout V, McClean CJ, Arnold KE, Walls M, Baxter M, Boxall ABA. 2016. Fur: A non-invasive approach to monitor metal exposure in bats. Chemosphere 147:376-381.

17. Wolfe MF, Schwarzbach S, Sulaiman RA. 1998. Effects of mercury on wildlife: A comprehensive review. Environ Toxicol Chem 17:146-160.

18. Dietz R, Born EW, Riget F, Aubail A, Sonne C, Drimmie R, Basu N. 2011. Temporal trends and future predictions of mercury concentrations in northwest Greenland polar bear (*Ursus maritimus*) hair. Environ Sci Technol 45:1458-1465.

19. Kucera E. 1983. Mink and otter as indicators of mercury in Manitoba waters. Can J Zool Rev Can Zool 61:2250-2256.

20. Dornbos P, Strom S, Basu N. 2013. Mercury exposure and neurochemical biomarkers in multiple brain regions of Wisconsin River otters (*Lontra canadensis*). Ecotoxicology 22:469-475.

21. Kannan K, Newsted J, Halbrook RS, Giesy JP. 2002. Perfluoroocta- nesulfonate and related fluorinated hydrocarbons in mink and river otters from the United States. Environ Sci Technol 36:2566-2571.

22. Sleeman JM, Cristol DA, White AE, Evers DC, Gerhold RW, Keel MK. 2010. Mercury poisoning in a free-living northern river otter (*Lontra canadensis*). J Wildl Dis 46:1035-1039.

23. Kalisinska E, Budis H, Lanocha N, Podlasinska J, Jedrzejewska E, Kosik-Bogacka DI. 2012. Comparison of hepatic and nephric total mercury concentrations between feral and ranch American mink (*Neovison vison*) from northwestern Poland. Bull Environ Contam Toxicol 88:802-806.

24. Hsiao C. 2014. Analysis of Panel Data, 3rd ed. Cambridge University Press, New York, NY, USA.

25. Mierle G, Addison EM, MacDonald KS, Joachim DG. 2000. Mercury levels in tissues of otters from Ontario, Canada: Variation with age, sex, and location. Environ Toxicol Chem 19:3044-3051.

26. Klenavic K, Champoux L, Mike O, Daoust PY, Evans RD, Evans HE. 2008. Mercury concentrations in wild mink (*Mustela vison*) and river otters (*Lontra canadensis*) collected from eastern and Atlantic Canada: Relationship to age and parasitism. Environ Pollut 156:359-366.

27. Fortin C, Beauchamp G, Dansereau M, Larivi ere N, B elanger D. 2001. Spatial variation in mercury concentrations in wild mink and river otter carcasses from the James Bay territory, Qu ebec, Canada. Arch Environ Contam Toxicol 40:121-127.

28. Evans RD, Grochowina NM, Basu N, O-Connor EM, Hickie BE, Rouvinen-Watt K, Evans HE, Chan HM. 2016. Uptake of selenium and mercury by captive mink: Results of a controlled feeding experiment. Chemosphere 144:1582-1588.

29. Yates DE, Mayack DT, Munney K, Evers DC, Major A, Kaur T, Taylor RJ. 2005. Mercury levels in mink (*Mustela vison*) and river otter (*Lontra canadensis*) from northeastern North America. Ecotoxicology 14:263-274.

30. Basu N, Stamler CJ, Loua KM, Chan HM. 2005. An interspecies comparison of mercury inhibition on muscarinic acetylcholine receptor binding in the cerebral cortex and cerebellum. Toxicol Appl Pharmacol 205:71-76.

31. Brown AR, Hosken DJ, Bickley LK, Lepage G, Owen SF, Hetheridge MJ, Tyler CR. 2009. Genetic variation, inbreeding and chemical exposure-Combined effects in wildlife and critical considerations for ecotoxicology. Philos Trans R Soc Lond B Biol Sci 364:3377-3390.

32. Sonne C. 2010. Health effects from long-range transported contaminants in Arctic top predators: An integrated review based on studies of polar bears and relevant model species. Environ Int 36:461-491.

33. Depledge MH, Galloway TS. 2005. Healthy animals, healthy ecosystems. Front Ecol Environ 3:251-258.

34. Meador JP. 1996. Environmental Contaminants in Wildlife: Interpreting Tissue Concentrations. CRC, Boca Raton, FL, USA.

35. Evers DC, Han Y-J, Driscoll CT, Kamman NC, Goodale MW, Lambert KF, Holsen TM, Chen CY, Clair TA, Butler T. 2007. Biological mercury hotspots in the northeastern United States and southeastern Canada. Bioscience 57:29-43.

36. Grandjean P, Budtz-Jørgensen E. 2007. Total imprecision of exposure biomarkers: Implications for calculating exposure limits. Am J Ind Med 50:712-719.

37. Basu N, Scheuhammer AM, Rouvinen-Watt K, Grochowina N, Evans RD, O-Brien M, Chan HM. 2007. Decreased N-methyl-D-aspartic acid (NMDA) receptor levels are associated with mercury exposure in wild and captive mink. Neurotoxicology 28:587-593.

38. Basu N, Scheuhammer AM, Rouvinen-Watt K, Evans RD, Grochowina N, Chan LHM. 2008. The effects of mercury on muscarinic cholinergic receptor subtypes (M1 and M2) in captive mink. Neurotoxicology 29:328-334.

39. Strom SM. 2008. Total mercury and methylmercury residues in river otters (Lutra canadensis) from Wisconsin. Arch Environ Contam Toxicol 54:546-554.

40. Evans RD, Addison EM, Villeneuve JY, MacDonald KS, Joachim DG. 2000. Distribution of inorganic and methylmercury among tissues in mink (*Mustela vison*) and otter (*Lutra canadensis*). Environ Res 84:133-139.

41. Evans RD, Addison EM, Villeneuve JY, MacDonald KS, Joachim DG. 1998. An examination of spatial variation in mercury concentrations in otter (*Lutra canadensis*) in south-central Ontario. Sci Total Environ 213:239-245.

42. Francis DR, Bennett KA. 1994. Additional data on mercury accumulation in northern Michigan river otters. J Freshw Ecol 9:1-5.

43. Halbrook RS, Jenkins JH, Bush PB, Seabolt ND. 1994. Sublethal concentrations of mercury in river otters: Monitoring environmental contamination. Arch Environ Contam Toxicol 27:306-310.

44. Ropek RM, Neely RK. 1993. Mercury levels in Michigan river otters, Lutra canadensis. J Freshw Ecol 8:141-147.

45. Wren CD, Stokes PM, Fischer KL. 1986. Mercury levels in Ontario mink and otter relative to food levels and environmental acidification. Can J Zool Can Zool 64:2854-2859.

46. Brzezinski M, Zalewski A, Niemczynowicz A, Jarzyna I, Suska- Malawska M. 2014. The use of chemical markers for the identification of farm escapees in feral mink populations. Ecotoxicology 23:767-778.

47. Lake JL, Ryba SA, Serbst J, Brown CF, Gibson L. 2007. Mercury and stable isotopes of carbon and nitrogen in mink. Environ Toxicol Chem 26:2611-2619.

48. Gamberg M, Boila G, Stern G, Roach P. 2005. Cadmium, mercury and selenium concentrations in mink (*Mustela vison*) from Yukon, Canada. Sci Total Environ 351-352:523-529.

49. Fortin C, Beauchamp G, Dansereau M, Lariviere N, Belanger D. 2001. Spatial variation in mercury concentrations in wild mink and river otter carcasses from the James Bay territory, Quebec, Canada. Arch Environ Contam Toxicol 40:121-127.

50. Dansereau M, Lariviere N, Du Tremblay D, Belanger D. 1999. Reproductive performance of two generations of female semidomesticated mink fed diets containing organic mercury contaminated freshwater fish. Arch Environ Contam Toxicol 36:221-226.

51. Harding LE, Harris ML, Elliott JE. 1998. Heavy and trace metals in wild mink (*Mustela vison*) and river otter (*Lontra canadensis*) captured on rivers receiving metals discharges. Bull Environ Contam Toxicol 61:600-607.

52. Halbrook RS, Lewis LA, Aulerich RI, Bursian SJ. 1997. Mercury accumulation in mink fed fish collected from streams on the Oak Ridge Reservation. Arch Environ Contam Toxicol 33:312-316.

53. Halbrook RS, Woolf A, Hubert GF, Ross S, Braselton WE. 1996. Contaminant concentrations in Illinois mink and otter. Ecotoxicology 5:103-114.

Chapter 4

Distribution of organic and inorganic mercury across Canadian river otter (*Lontra canadensis*) pelts

Kristin M. Eccles[1], Eric S. Littlewood[1], Philippe J. Thomas[2], and Hing Man Chan[1]

[1] Department of Biology, University of Ottawa, 30 Marie Curie, Ottawa, ON, K1N 6N5, Canada
[2] Science and Technology Branch, Environment and Climate Change Canada, National Wildlife Research Center, 1125 Colonel By Drive, Raven Road, Ottawa, ON K1A 0H3, Canada

This chapter was published: Eccles KM, Littlewood ES, Thomas PJ, Chan HM. 2019. Distribution of organic and inorganic mercury across the pelts of Canadian river otter (*Lontra canadensis*). *Scientific Reports*. DOI:10.1038/s41598-019-39893-w.

Author Contributions: KE conceived the idea, completed the statistical analysis, prepared all figures, and contributed to the writing of the manuscript. EL processed the pelts and contributed to some of the manuscript preparation. PT collected the samples and contributed to editing the manuscript. LC contributed to the conceptualization of the project and provided guidance on the implementation and editing of the manuscript.

Supplemental information for this chapter can be found in Appendix B.

4.1 Abstract

Fur is a common biomarker of environmental mercury (Hg) exposure. Further, there are well-established relationships between total mercury (THg) in fur and organs. However, these models assumed that THg is uniformly distributed across the fur in a pelt. In this study, we assess the distribution of THg and methylmercury (MeHg) across the pelts of four river otters (*Lontra canadensis*). THg concentrations were measured in the topcoat ($n = 95$) and undercoat fur ($n = 95$). MeHg was measured in a subset of these samples ($n = 10$). Patterns of THg and MeHg were explored using cluster analyses and ANOVAs. Significant differences existed between THg in topcoat and undercoat and between anatomical region (head/body/tail/legs) and fur regions (dorsal/ventral/furline). The cluster analysis showed significant THg clusters in undercoat fur and to a lesser extent topcoat fur. Further, the error rate for predicting internal THg is lowest in the forebody region of the topcoat, thus, making this the optimal region to sample for biomonitoring. Fur samples taken outside of this region could result in prediction error as high as 140% when estimating internal organ THg. The ratio of MeHg in THg in topcoat fur was measured at $95.7 \pm 3.4\%$ indicating THg concentrations can be used to assess MeHg exposure.

4.2 Introduction

Mercury (Hg) is an environmental pollutant of global concern found in terrestrial and aquatic ecosystems. The methylated form of Hg (MeHg) is bioavailable and readily accumulates in the kidneys, liver, central nervous system and produces adverse effects on immune response, structure and function of nervous tissues, fertility, and fetal development in humans and wildlife [1]-[3]. In North American freshwater ecosystems, river otters (*Lontra canadensis*) are good sentinel species for MeHg exposure because of their non-migratory, non-hibernating behaviour, their small home range, as well as their high year-round fish consumption [4], [5]. These top predators are reliable indicators of environmental contamination as tissue Hg concentrations are correlated with Hg levels in fish prey species from the same watersheds [6].

Tissues examined in previous biomarker studies of Hg exposure in river otters include brain, liver, kidney, muscle and fur. Mercury concentrations in all organ tissues are directly related to the concentrations of mercury found in the blood and fur [7]-[9]. Hair is advantageous because it is a minimally-invasive matrix and an important excretory pathway which provides temporal trends in Hg exposure at concentrations that can be upwards of two orders of magnitude higher than those in blood [10]. Since both MeHg and Hg^{2+} ions have high affinities for thiol groups, the high sulphur content and slow growth rate of fur make this keratinous matrix ideal for assessing temporal trends of Hg exposure between seasonal moults of topcoat and undercoat fur [11]. Previous studies have also reported that total Hg (THg) concentrations in otter fur are strongly correlated with those concentrations found

in the brain [8], liver [8], [12], kidney [13], and muscle tissue [13].

Using fur to estimate THg exposure in river otters is similar to the well-established methods for using hair to estimate human THg exposure [4], [14]. Several studies have discussed the utility of fur THg concentrations to estimate the internal organ THg concentrations in these river otter and mink [15], [16], using predictive regression models [9] **(Chapter 3)**. The accuracy of estimates generated by this model vary between 28.6-45.4% based on a normalized root mean squared error (NRMSE) for river otter depending on the tissue [9]. While these relationships did not appear to be age or sex dependent, [8], [16] some of the unexplained variance could be attributed to differences in fur sample locations within each animal. A survey of the literature identified eight studies that reported fur THg sampled from a variety of locations (commonly on the limbs) (Table 4.1).

Table 4.1: Summary of fur sample locations in Hg biomonitoring studies in river otter.

Study	Sample Location
Halbrook et al. 1994	Unspecified Sample Location
Evans et al. 1998	Unspecified paw
Evans et al. 2000	Unspecified paw
Fortin et al. 2001	Forelimbs
Yates et al. 2005	Unspecified Sample Location
Strom 2008	Hind paw
Klenavic et al. 2008	Between the footpads
Dornbos et al. 2013	Unspecified paw

Few studies have assessed the potential difference in THg concentrations in different regions of the pelt. Klenavic et al. 2008 assessed the differences between the fur THg concentrations from all four footpads and concluded that no significant differences existed [8]. Wilkie et al. 2018 assessed fur THg concentrations on the dorsal surface of all paws, the dorsal base of the skull, the middle dorsal surface, the middle ventral surface, and the base

of the tail, in river otters from central Saskatchewan, Canada. This study concluded that there were significant differences between sampling locations but there was no difference in THg concentrations between the four paws. However, this study did not distinguish between topcoat or undercoat fur[17].

Biomonitoring programs using human hair have an established standard protocol of sampling from the occipital region [18]. In contrast, there is no standardized fur sampling location for biomonitoring in furbearing mammals [19]-[23]. Given the inconsistencies in sampling procedures for fur bearing mammals, and the potential for variation of THg concentrations across a pelt, we hypothesize that some of the unexplained variance in the regression models relating fur THg concentrations to the internal organ THg could be the result of a heterogeneous distribution of THg across the pelt. Further differences could exist between the concentrations of THg observed in the topcoat and undercoat layers in the analysed fur samples, thus if top coat and undercoat are analysed together it could produce more variability when trying to predict internal organ THg concentrations. If significant differences in accumulation patterns of THg exist across different regions or hair types of a pelt, then the generated predictive models for Hg concentrations could result in biased estimates if consistent locations and sample types are not used.

The objective of this research is to characterize the variability of excreted THg and MeHg compounds in otter pelts in order to identify the fur type (topcoat/undercoat) with the least variability and to determine if excretion of Hg compounds is dependent on anatomical region. Further, we will examine the relationship between the concentration of THg and internal organ THg to suggest an optimal sampling location as a standardized

sampling procedure for future biomonitoring programs.

4.3 Methods

4.3.1 Pelt Processing

Dried whole otter pelts and frozen carcasses were obtained from a trapline located in northern Alberta, Canada (n=4) in 2017. The pelts were flattened for sampling by cutting along the ventral sagittal axis (anus to middle of lower jaw). The dimensions of each pelt (median sagittal axis: length of nose to anus; transverse axis: midpoint between right fore/hind limb to midpoint between left fore/hind limb) were used to establish the proportions of the rectangular grid for each pelt, with the origin located at the intersection of the median sagittal and traverse axes. To account for the size difference between the pelts, the grid was scaled and then marked out using lab tape. Pictures of the gridded pelts can be seen in Appendix B Figures B.1-B.4. Topcoat and undercoat fur samples (50-150mg) were taken from the middle of each rectangle. Both topcoat (technically referred to as guard hair) have the same hair follicle composition, comprised of an outer cuticle, a cortex, and a medulla (central core). However, the topcoat hairs are longer and coarser than undercoat [31]. The pictures of the difference between these two hair types can be seen in Appendix B Figures B.5 and B.6.

4.3.2 Mercury Analysis

Approximately 10mg of topcoat and undercoat were subsampled and total mercury was measured using a direct thermal decomposition Hg analyser (Mercury Analyser 3000; Nippon Instruments North America, Texas, USA). Quality assurance/ quality control (QA/QC) methods included blank samples, standard reference material (DORM-4 and IAEA-085), and 10% of all samples were duplicated. A stratified random subset based on THg concentration tertiles and anatomical region was used to select samples for MeHg analysis. DORM-4 is a fish protein certified reference material for trace metals with a known THg concentration of 0.44 ± 0.036 mg/kg (experiment mean = 0.36 ± 0.017 mg/kg) and IAEA-085 is a human hair certified reference material for trace metals with a known THg concentration of 23.2 ± 0.8 mg/kg (experiment mean = 22.3 ± 0.61 mg/kg) and MeHg concentration of 22.9 ± 1.0 mg/kg (experiment mean = 19.17 ± 0.79 mg/kg). The limit of detection, calculated as 3 times the standard deviation of the blank (boat blanks) was 0.12 ng.

MeHg was measured using a method adapted from Cai (1997) and Laffont (2013) [32], [33]. Each topcoat fur sample was first digested in 7.0 mL of trace metal grade 3.0M HNO3 prepared with 18M deionized water (DIW) for 16 hours at 55°C in a clean glass vials with Teflon caps. Organic mercury species dissolved in the fur digestate solutions were extracted into 5mL Optima grade dichloromethane (DCM), shaken for 24 hours on an orbital shaker at 330 rpm, and centrifuged at 3000rpm for 10 mins. A known quantity of the DCM layer was transferred to a clean scintillation vial with 2.5 mL of 0.01M L-cysteine (Aldrich Chemical Company, Inc.) in DIW. This was shaken at 330 rpm for 45 mins, mixed for 20

s on a Fischer Scientific Vortex Mixer, and centrifuged at 3000rpm for 10mins. Finally, 100 uL of the aqueous layer was spread on a thin layer of Additive B (Nippon Instruments Corporation #282-62665) and analysed with the Mercury Analyser 3000.

Organ tissues were dissected, mechanically homogenized (Heidolph Silent Crusher homogenizer; Sigma-Aldrich), and then freeze-dried for 48 h (FreeZone Freeze Dry System; Labconco). Approximately 50 mg of ground tissue were subsampled and analysed using Mercury Analyser 3000. QA/QC methods included blanks samples, standard reference material (DOLT-5 and IAEA407), and 10% of all samples were duplicated. IAEA-407 is a fish homogenate certified reference material for trace metals with a known THg concentration of 0.222 ± 0.006 mg/kg (experiment mean=0.231 ± 0.002) and DOLT-5 is a dogfish liver certified reference material for trace metals with a known THg concentration of 0.44 ± 0.18 mg/kg (experiment mean=0.395 ± 0.009). The limit of detection, calculated as 3 times the standard deviation of the blank (boat blanks) was 0.03 ng.

4.3.3 Statistical analysis

All statistical analyses were performed in R 3.4.3 [34] using the packages car [35], gstat [36], lmtest [37], sp [38], and spdep [38]. A spatially, two- tailed paired Student's t-tests (equal variance) and Welch's t-test (unequal variance) were used to evaluate differences in THg in the topcoat and undercoat and to evaluate differences in the THg in the right and left hindlimbs. F-tests for equality of variances were used to quantify the relative variability of THg concentrations between topcoat and undercoat. A one-way Analysis of Variance (ANOVA) was used to determine if there are regional differences in THg between

anatomical region and fur region (front vs. back). The location of the anatomical region on each pelt can be seen in Appendix B Figure B.7 and the location of the fur regions on each pelt can be seen in Appendix B Figure B.8. A linear regression model was used to assess the relationship between the THg in the topcoat and undercoat across all pelts. Geospatial analyse include Getis and Ord's local Gi* cluster analysis to identify regions with statistically significant high or low fur THg concentration [39]. A semi-variogram was used to determine the range autocorrelation, as known as a neighbourhood. The range of spatial influence is quantified using the range of the semi-variogram. The calculated range distance was then used as the neighbourhood parameter in the Getis and Ord's Gi* analysis.

A linear regression was used to determine the relationship between MeHg and THg concentrations in topcoat fur in the subset sampled across all pelts. The model intercept was set to zero. Samples with MeHg to THg ratios greater than 110% were removed from the regression analysis to avoid bias due to analytical error [40]. Where necessary, models were tested for linearity (resettest: lmtest), homoscedasticity of residuals (ncvTest: car), residual normality (shapiro.wilks: lmtest) and no serial autocorrelation among residuals (dwtest: lmtest). All models presented met parametric test assumptions.

4.3.4 Pelt Average

The individual pelts' topcoat and undercoat were then normalized between zero and one (Equation 4.1). Points with the same coordinates were averaged to produce an average normalized THg value for both the topcoat and undercoat. Using the same methods

outlined in the statistical analysis, the composite was analysed for regional differences and hotspots.

$$c_{i\,normalized} = \frac{c_i - c_{min}}{c_{max} - c_{min}} \tag{4.1}$$

Optimal Sample Location. Using the conversion between fur THg and organ THg developed in Eccles et al. 2017, the brain, kidney, liver, and muscle concentrations were estimated based on the THg concentration at every sample point in the topcoat and undercoat. The percent error was calculated for each organ at each sample point for topcoat and undercoat (Equation 4.2).

$$Error_i = (abs(\frac{\hat{Y}_i - Y_i}{Y_i})) * 100 \tag{4.2}$$

Then a weighted average error for all organs in the topcoat and undercoat was calculated, where the brain had a weighting twice that of other organs due to its importance in mercury toxicity. Using the same methods outlined in the statistical analysis, the composite error rates was analysed for hotspots to identify the region of the pelt with the lowest error.

4.4 Results

4.4.1 THg in Individual Pelts

The measured THg and MeHg data for each pelt are summarized in Table 4.2 and a visual representation of the THg concentrations across the topcoat and the undercoat are summarized in Table 4.1. These plots illustrate the variability of THg in topcoat and undercoat fur. Quantitatively, a Welch's paired t-test showed that the concentrations of THg in topcoat fur were significantly lower than THg concentrations in undercoat fur sampled from the same location in all pelts ($p < 0.001$). Pearson product-moment correlation coefficients indicated that weak positive correlations ($r \leq 0.35$, $p<0.01$) existed between topcoat and undercoat fur THg concentrations in individual pelts and that these were statistically significant for pelt 2, pelt 3, and pelt 4.

Table 4.2: Summary of total mercury (THg) in the topcoat and undercoat, and methylmercury (MeHg) for each otter pelt, measured in μg/g.

Pelt	Mercury species	n	Mean	SD	Min	Max
Pelt 1	THg Topcoat	89	1.55	0.2	1.08	2.74
	THg Undercoat	89	2.19	0.62	0.61	4.37
	MeHg Topcoat	10	1.58	0.72	0.82	3.41
Pelt 2	THg Topcoat	98	4.6	0.2	4.23	5.3
	THg Undercoat	98	9.42	2.2	6.01	14.21
	MeHg Topcoat	10	4.54	0.59	4.08	6.11
Pelt 3	THg Topcoat	96	1.42	0.37	0.81	3.63
	THg Undercoat	96	2.86	1.51	0.62	7.84
	MeHg Topcoat	11	1.44	0.75	0.41	3.3
Pelt 4	THg Topcoat	95	4.44	0.16	4.04	4.81
	THg Undercoat	95	4.87	0.9	2.18	6.61
	MeHg Topcoat	9	4.44	0.16	4.12	4.59

Relative to the topcoat, the range of THg concentrations in the undercoat is 2.26, 7.66,

2.56, and 5.75 times higher in each of the pelts respectively (Figure 4.2 and Appendix B Table B.1). Further, the variance of undercoat fur THg concentrations were 10-118 times higher than the topcoat THg fur variances (Appendix B Table B.2).

There is a statistically significant difference in fur THg concentrations between the

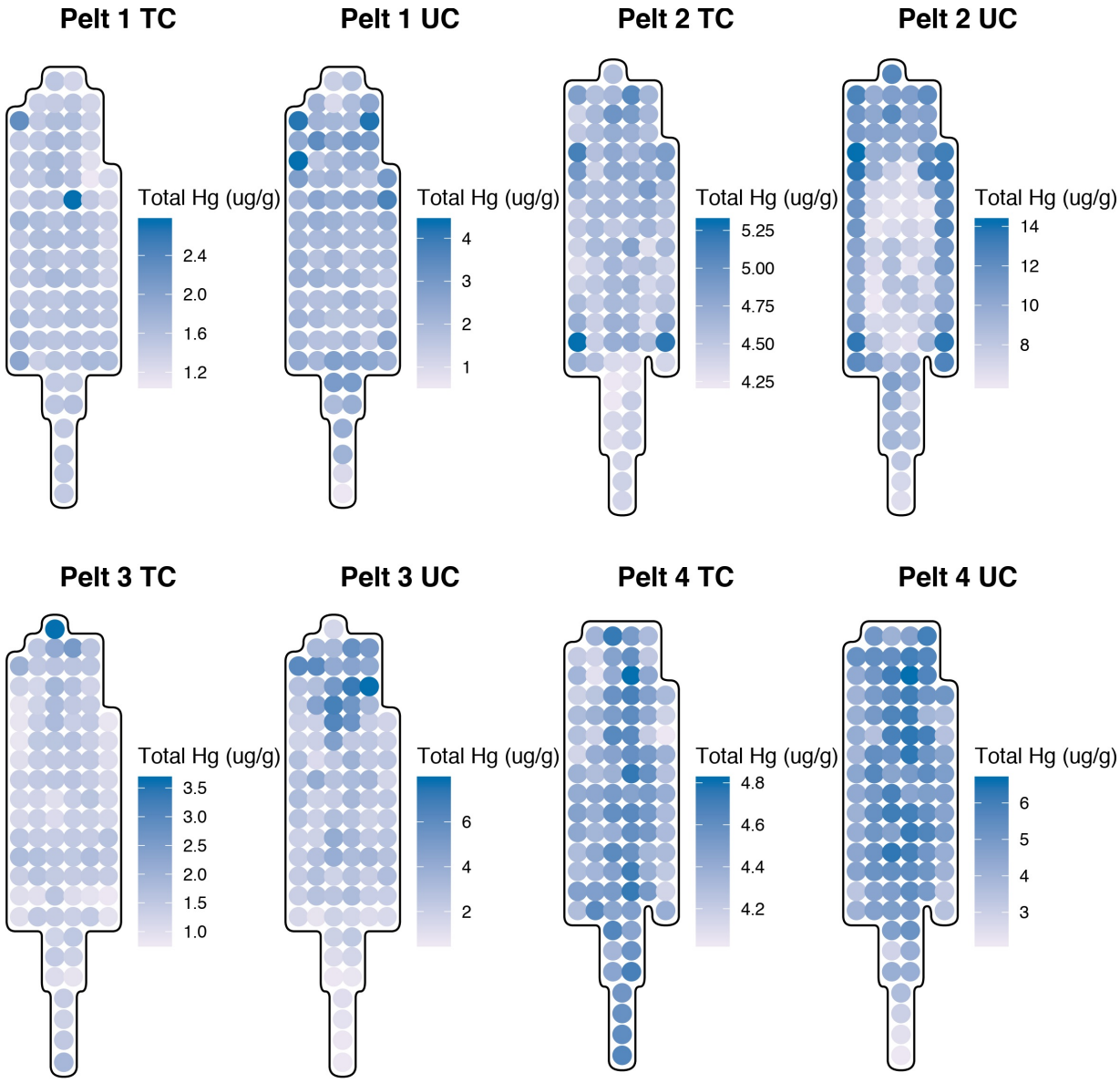

Figure 4.1: Distribution of THg concentrations in topcoat (TC) and undercoat (UC) fur in individual pelts.

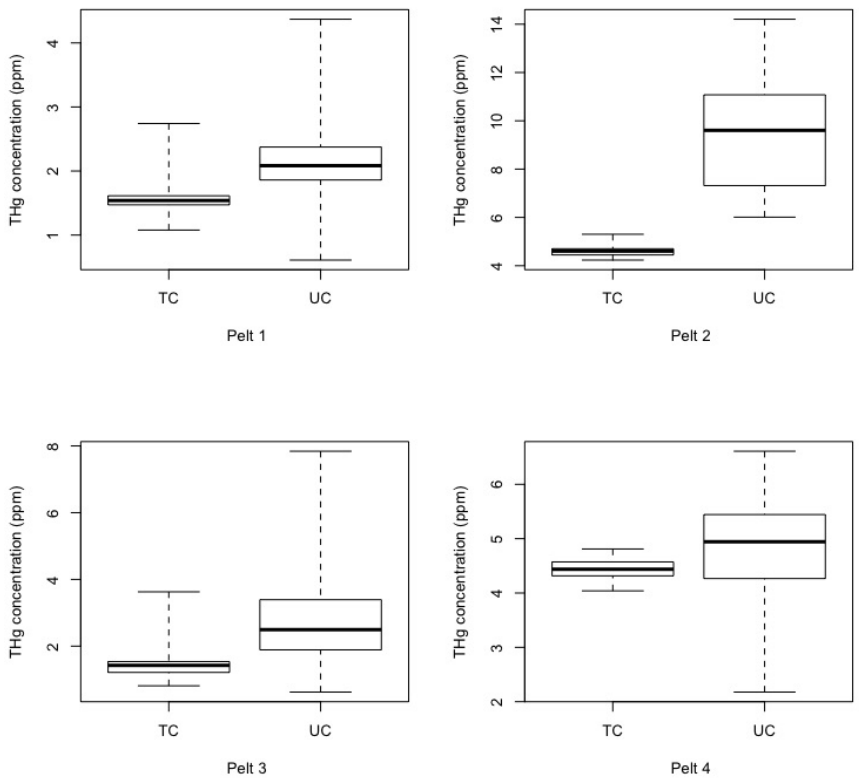

Figure 4.2: Boxplots of total mercury (THg) concentration ranges in topcoat (TC) and undercoat (UC) fur for individual pelts. In these boxplots, the line is the median, the boxes represent the interquartile range and the whiskers span the entire range of THg concentrations.

anatomical regions where fur is sampled (i.e. from the head, body, legs or tail) in some pelts. Significant effects of the anatomical region in topcoat fur THg concentrations existed in pelt 2 ($F_{3,94}$=9.831, p<0.001) and pelt 3 ($F_{3,92}$=14.31, p<0.001) and was significant in the undercoat of pelt 2 ($F_{3,94}$=3.088, p=0.031), pelt 3 ($F_{3,92}$=9.453, p<0.001) and pelt 4 ($F_{3,91}$=8.482, p<0.001). A post-hoc Tukey comparison of THg concentration between anatomical regions in the topcoat and undercoat fur is presented in Table 4.3. The magnitude of statistically significant differences ranged from 0.3-1.1 μg/g in topcoat fur and 1.2-2.6 μg/g in undercoat fur. The location of the anatomical regions on each pelt can be

found in Appendix B Figures B.7 and B.8.

Table 4.3: THg concentration differences between the levels of the anatomical region factor for topcoat and undercoat fur. Difference of the means is presented as the difference ± 95% confidence interval. P-values were adjusted for multiple comparison. Composite values have been normalized between zero and one.

Pelt	Region	Topcoat Difference (μg/g)	Adj. p-value	Undercoat Difference (μg/g)	Adj. p-value
Pelt 1	Head-Body	-0.1 ± 0.2	0.412	-0.5 ± 0.7	0.305
	Leg-Body	0.1 ± 0.3	0.724	0.1 ± 0.8	0.99
	Tail-Body	-0.1 ± 0.2	0.815	-0.1 ± 0.5	0.993
	Leg-Head	0.2 ± 0.3	0.248	0.6 ± 1.1	0.477
	Tail-Head	0.1 ± 0.3	0.869	0.4 ± 0.9	0.557
	Tail-Leg	-0.2 ± 0.3	0.496	-0.2 ± 1.0	0.975
Pelt 2	Head-Body	0.1 ± 0.2	0.873	1.9 ± 2.6	0.226
	Leg-Body	-0.1 ± 0.3	0.822	2.6 ± 3.3	0.177
	Tail-Body	-0.3 ± 0.1	< 0.001	-0.6 ± 1.7	0.758
	Leg-Head	-0.2 ± 0.3	0.642	0.7 ± 4.1	0.972
	Tail-Head	-0.3 ± 0.2	0.002	-2.5 ± 2.9	0.118
	Tail-Leg	-0.2 ± 0.3	0.348	-3.2 ± 3.6	0.095
Pelt 3	Head-Body	0.9 ± 0.4	< 0.001	0.7 ± 1.6	0.688
	Leg-Body	-0.2 ± 0.4	0.735	-1.9 ± 1.8	0.036
	Tail-Body	0.0 ± 0.3	0.996	-1.9 ± 1.1	< 0.001
	Leg-Head	-1.1 ± 0.6	< 0.001	-2.6 ± 2.4	0.026
	Tail-Head	-0.9 ± 0.4	< 0.001	-2.5 ± 1.9	0.003
	Tail-Leg	0.1 ± 0.5	0.86	0.0 ± 2.0	1
Pelt 4	Head-Body	0.1 ± 0.2	0.883	-0.1 ± 1.1	0.992
	Leg-Body	0.0 ± 0.2	0.997	-1.0 ± 1.2	0.176
	Tail-Body	0.1 ± 0.1	0.079	-1.2 ± 0.7	< 0.001
	Leg-Head	0.0 ± 0.3	0.986	-0.9 ± 1.6	0.507
	Tail-Head	0.1 ± 0.2	0.914	-1.1 ± 1.2	0.106
	Tail-Leg	0.1 ± 0.3	0.758	-0.2 ± 1.4	0.977
Composite (normalized THg)	Head-Body	0.001 ± 0.042	1	-0.015 ± 0.138	0.991
	Leg-Body	0.007 ± 0.037	0.953	-0.075 ± 0.121	0.370
	Tail-Body	-0.010 ± 0.029	0.801	-0.143 ± 0.094	< 0.001
	Leg-Head	0.006 ± 0.054	0.991	-0.060 ± 0.176	0.811
	Tail-Head	-0.011 ± 0.049	0.928	-0.127 ± 0.159	0.161
	Tail-Leg	NA	NA	-0.068 ± 0.144	0.612

Similarly, we detected a statistically significant difference in fur THg concentrations between fur regions (i.e. from the dorsal, fur line, or ventral regions) in some pelts. Significant effects of fur region on topcoat fur THg concentrations existed in pelt 3 ($F_{2,93}$=5.058, p=0.008) and pelt 4 ($F_{2,92}$=53.02, p<0.001) and significant differences in the undercoat were found in pelt 1 ($F_{2,86}$=9.294, p<0.001), pelt 2 ($F_{2,95}$=44.47, p<0.001) and pelt 4 ($F_{2,92}$=4.602, p=0.012). A post-hoc Tukey comparison of THg concentration differences between each fur region factor in topcoat and undercoat fur is presented in Table 4.4. The magnitude of statistically significant differences ranged from 0.1-0.3 μg/g in topcoat fur

and 0.4-3.3 μg/g in undercoat fur. The location of the fur regions on each pelt can be found in S1.

Table 4.4: THg concentration differences between the levels of the fur region factor for topcoat and undercoat fur. Difference of the means is presented as the difference ± 95% confidence interval. P-values were adjusted using the Tukey correction for multiple comparison.

Pelt	Comparison	Topcoat Difference (μg/g)	Adj. p-value	Undercoat Difference (μg/g)	Adj. p-value
Pelt 1	Fur Line-Dorsal	-0.1 ± 0.1	0.135	0.1 ± 0.4	0.624
	Ventral-Dorsal	-0.1 ± 0.1	0.110	0.6 ± 0.3	< 0.001
	Ventral-Fur Line	0.0 ± 0.1	0.989	0.4 ± 0.4	0.017
Pelt 2	Fur Line-Dorsal	0.0 ± 0.1	0.604	-0.1 ± 1.0	0.957
	Ventral-Dorsal	0.1 ± 0.1	0.12	3.2 ± 0.9	< 0.001
	Ventral-Fur Line	0.0 ± 0.1	0.722	3.3 ± 1.1	< 0.001
Pelt 3	Fur Line-Dorsal	-0.1 ± 0.2	0.854	0.1 ± 1.0	0.955
	Ventral-Dorsal	-0.3 ± 0.2	0.007	-0.1 ± 0.9	0.986
	Ventral-Fur Line	-0.2 ± 0.2	0.106	-0.2 ± 1.1	0.917
Pelt 4	Fur Line-Dorsal	-0.2 ± 0.1	< 0.001	0.1 ± 0.6	0.959
	Ventral-Dorsal	-0.3 ± 0.1	< 0.001	-0.5 ± 0.5	0.020
	Ventral-Fur Line	-0.1 ± 0.1	0.004	-0.6 ± 0.6	0.047
Composite (normalized THg)	Fur Line-Dorsal	-0.012 ± 0.024	0.428	-0.005 ± 0.079	0.989
	Ventral-Dorsal	-0.019 ± 0.020	0.057	0.103 ± 0.065	< 0.001
	Ventral-Fur Line	-0.007 ± 0.025	0.808	0.108 ± 0.085	0.009

Fur sampling points on individual pelts with statistically significant high or low THg concentrations were identified with Getis-Ord local Gi* analyses in Figure 4.3. All pelts showed some hotspots (i.e. regions where high values cluster together) and coldspots (i.e. regions of the pelt where low values cluster together). Typically, the undercoat has larger clusters than the topcoat, demonstrating greater heterogeneity of the undercoat in comparison with the topcoat. Most of the pelts demonstrate hotspots around the head region and coldspots around the tail region.

4.4.2 Methylmercury in Topcoat

The fraction of fur THg present as MeHg was determined by fitting a linear model with a zero intercept. Data where the MeHg in THg ratios exceeded 110% were removed, yielding a final sample size of n=34. The beta coefficient for this relationship was 0.957 ± 0.034

and relationship was highly significant (R^2=0.99, p-value < 0.001). This linear model met all regression assumptions of residual linearity, homoscedasticity, normality, and no autocorrelation.

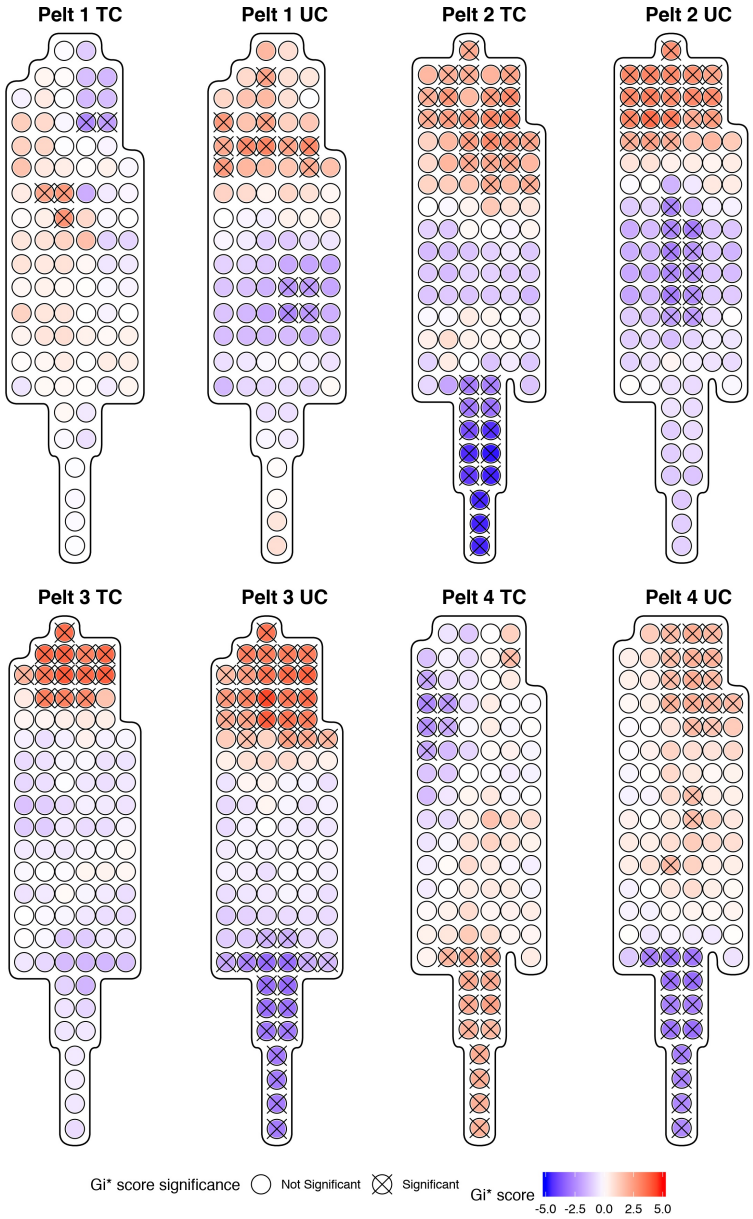

Figure 4.3: Getis-Ord local Gi* analyses for regions of statistically significant high and low THg concentrations in topcoat (TC) and undercoat (UC) fur of individual pelts. Statistically significant spots at the 95% CI (Gi*=+/- 1.96) are identified with an 'X'.

4.4.3 THg in Composite Pelts

As the topcoat and undercoat of pelts are going to have interindividual variation, a composite pelt of normalized THg concentrations averaged across the topcoat and undercoat was created. This composite pelt (normalized and averaged pelts) demonstrates average patterns of THg across the topcoat and undercoat (Figure 4A). Similar to the results of the individual pelts, the mean of the differences of the normalized THg concentrations in the topcoat and undercoat fur was highly significant. A Welch's paired t-test indicated that average normalized THg concentrations were 0.257 units lower (t_{104}= -19.06, p<0.001) in topcoat fur compared to undercoat fur. The ratio of the variances of the normalized topcoat and undercoat THg concentrations (ratio = 0.0817, $F_{104,104}$=0.0817, p<0.001) was also significant and indicates that the spread of THg concentrations is larger in the undercoat than in topcoat fur. The range of normalized THg concentrations in undercoat fur (0.061-0.860 units) was 2.88 times larger than the range of topcoat fur (0.063-0.341 units).

The composite pelt dataset showed no significant differences between anatomical regions ($F_{3,101}$=0.4167, p=0.7414) or fur regions ($F_{2,102}$=2.837, p=0.0632) in the normalized topcoat THg concentrations but there was a significant difference in anatomical regions ($F_{3,101}$= 5.648, p=0.001) and fur region ($F_{2,102}$= 8.146, p<0.001) in the undercoat fur. Tukey post-hoc comparisons of normalized THg concentration differences between anatomical regions and fur regions in the topcoat and undercoat can be found in Table 4.3 and Table 4.4 respectively.

The results of the Getis and Ord's Gi* cluster analysis (Figure 4.4B) indicate that in

the topcoat and bottom coat, there is a statically significant cluster of high values (hotspot) at the head and a statistically significant cluster of cold spots in the tail region (similar to results obtained in individual pelts). The clusters are smaller in the topcoat than in the undercoat demonstrating greater heterogeneity of the undercoat in comparison with the topcoat.

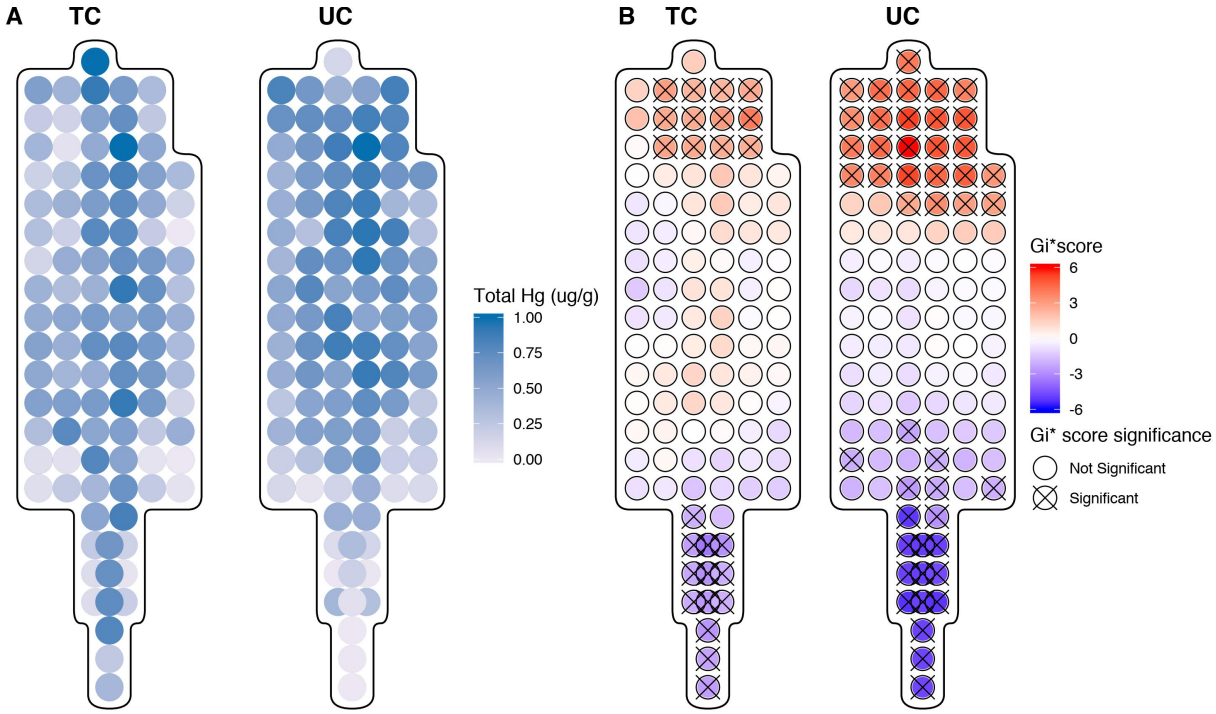

Figure 4.4: A. Distribution of normalized THg concentrations in topcoat (TC) and undercoat (UC) fur of the generated composite pelt. B. Getis-Ord local Gi* analyses for regions of statistically significant high and low THg concentrations the topcoat and undercoat of the composite pelt. Statistically significant spots at the 95% CI (Gi*=+/- 1.96) are identified with an 'X'.

4.4.4 Optimal Sampling Location

The percent residual from predicting internal organ THg concentrations from sampled fur THg at each sample point was used to demonstrate the accuracy of the predictor. The

distribution of average error across all organs, with brain having a heavier weighting, across all pelts can be seen in Figure 4.4A. The average topcoat error ranged from 30% to 89% error and in the undercoat the average percent error ranged from 26% to 143%. The results of the Getis and Ord's Gi* cluster analysis revealed a cluster of low error rates in the head region of the topcoat (Figure 4.5B). Conversely, in the undercoat at the head, there is a cluster of high error rates and a cluster of low error rates in the tail. This highlights the variability of error rates in the undercoat and differences between the topcoat and undercoat when using fur THg as a predictor of internal THg concentrations.

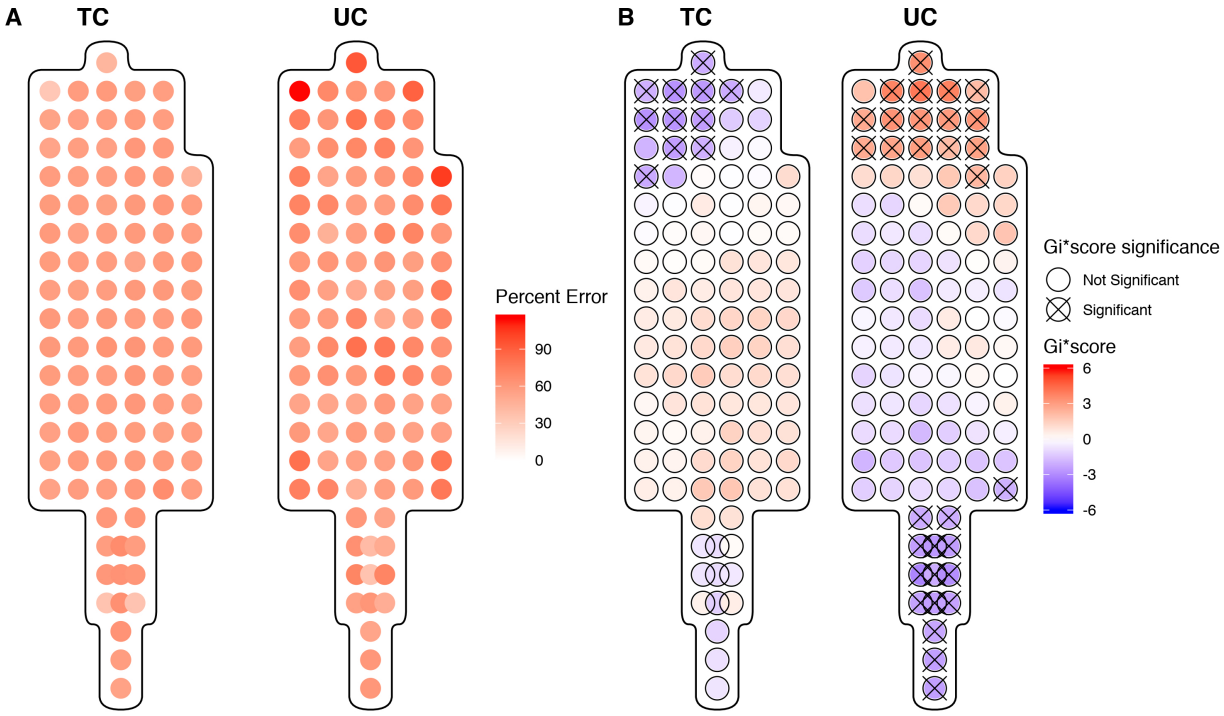

Figure 4.5: A. Average percent residual error for a weighted combination of residual error from brain, liver kidney, and muscle THg concentration based on fur THg in the top coat (TC) and undercoat (UC). B. Getis-Ord local Gi* analyses for regions of statistically significant high and low residual error in TC and UC. Statistically significant spots at the 95% CI (Gi*=+/- 1.96) are identified with an 'X'.

4.5 Discussion

Since there is no standardized sampling location for fur in wildlife biomonitoring studies, previous wildlife biomonitoring often collected hair randomly from different regions and assumed that THg is homogeneously distributed across the pelt. The results presented in this paper indicate that THg has a heterogeneous distribution across both the topcoat, and to a greater extent, the undercoat of a pelt in river otter. Further, this is the first study to quantify the difference in THg concentrations in both topcoat and undercoat. The differences between the THg concentrations in paired topcoat and undercoat fur samples were highly significant in all individuals; the concentration of THg in topcoat fur is significantly lower and less variable than the THg in undercoat. Fur sampled from the topcoat consistently had the smallest THg variances whereas undercoat variances were at least 10 times greater in individual pelts. This indicates that the excretion of Hg compounds into undercoat fur is more variable than the excretion into topcoat fur and also suggests that mean topcoat THg concentrations have a greater precision than mean undercoat THg concentrations. As a result, topcoat and undercoat fur should be analysed separately to avoid error introduced by changes in relative topcoat/undercoat abundance in samples.

Differences in anatomical and fur regions indicated that the variability of THg in topcoat and undercoat were statistically different, in some regions of the individual and composite pelts . Overall, in the composite pelt, there was no significant effect of anatomical and fur regions in topcoat fur while differences in THg concentration were detected in undercoat fur. These results suggest that for a pelt with an average THg distribution, the

differences in THg between topcoat fur THg concentrations in the head, body, legs or tail may be statistically significant but may not be biologically significant as the differences in THg are small. Individually, undercoat THg concentrations have greater variability than topcoat concentrations. The results from this study may explain the significant differences between THg in different anatomical regions in Wilkie et al. (2018) since the samples in that study consisted of both topcoat and undercoat fur [17]. However, it is important to note that paws were discarded during pelt process and therefore not analysed for THg concentrations in our study. Therefore, it was not possible to assess the THg in the fur in that region which presents itself as a limitation because we could not compare paw fur to other locations.

There were both interindividual and intraindividual variations of observed values in the distribution of THg across a pelt. A possible mechanism to explain the differences in THg concentrations observed in different anatomical and fur regions is varying levels of blood flow between these regions. Taylor & Minabe (1992) note that the structure of blood vessels in mammalian species is related to skin on parts of the animal that are more mobile[24]. In general, skin with higher mobility due to greater functional demands had larger and longer blood vessels [24]. Larger cutaneous blood vessels have the capacity to carry more blood and thus transport more Hg compounds at higher rates to the capillary beds that irrigate the hair follicles in these regions. As a result, skin regions with higher mobility may also excrete Hg compounds into fur from these regions at higher rates. Further, some of the interindividual variation could be explained by biological factors such as fur growth rate, fur growth period, seasonal moulting and seasonal diet changes, which may contribute to

the differences observed between the two fur types [25], [26]. Additional information on the age and sex of the river otters in this study may have also been useful. However, there is no consensus in the literature as to whether age or sex affects the fur THg concentrations in river otters [16], [27].

The fraction of MeHg in THg was 95.7±3.4% in topcoat fur. The ratio calculated in this study provided much higher precision than what has been reported MeHg in THg (78.6±25.9%) [28]. The greater variability could have resulted from a mixture of topcoat and undercoat fur as no distinction was made. The percentage of MeHg in otter fur is at the high end for the ratios found in humans (79-94%) [29]. This indicates that the majority of Hg compounds in fur consist of MeHg and supports previous research that fur is an important excretory pathway for MeHg [10]. Given that MeHg and THg concentrations are also correlated in the brain, kidney and liver, this suggests that fur THg measurements can be used to estimate organ MeHg concentrations [17], [28].

In all individual and composite pelts, topcoat fur contained fewer significant hotspots and coldspots than the undercoat fur. In general, the head region typically had higher THg concentrations than tail. The occurrence of significant THg hotspots in the head and upper body region is consistent with the high THg measurements in fur sampled from the base of the skull in Wilkie et al (2018) [17]. The existence of significant THg hotspots and coldspots in undercoat fur provides further evidence that undercoat fur concentrations are more variable than topcoat concentrations and suggests that heterogeneous regions may occur regularly in these locations on an average pelt. The average percent error for predicted organ THg was lower in the topcoat than the undercoat. Further, the cluster analysis of

the average percent error demonstrates that errors are lowest around the head region of the topcoat and the tail region of the undercoat. This indicates that concentrations found in the head of the topcoat and the tail of the undercoat are similar and result in similar predictive accuracy. Therefore, using fur THg to predict internal THg via the conversion factors, are most accurate when samples are taken from the forebody region. Previous samples taken from other regions may be subject to increased rates of error, especially samples taken from the undercoat of the forebody.

Based on our results, we suggest the development of a standardized fur sampling protocol for biomonitoring THg in river otter. It is important this protocol balances the need for accurate biomonitoring with the economic considerations for trappers. Thus, limbs are optimal locations for sampling. The composite pelt and cluster analyses help to identify the optimal biological sample region. Topcoat is better suited for sampling as the THg concentrations are less variable than the undercoat. Further, samples should be taken from the head/ forelimb region of the pelt to be most reflective of internal THg concentrations when using the conversion factor outlined in Eccles et al. 2017 [9]. Implications of estimating internal THg concentrations with fur sampled from other regions include the over or underestimation of the internal THg concentrations. These results also support the use of other non-invasive methods of fur sampling including the use of hair snares [30]. These samples are typically comprised of top coat from the head region. Thus, these samples would provide good estimates of internal THg concentrations and could be use in biomonitoring programs.

These results support the use of THg in the fur of river otters for biomonitoring pro-

grams to generate precise estimates of internal THg exposure based on fur THg concentrations when measured in topcoat fur in the fore body region. Simple sample collection protocols combined with the long-term stability of Hg in the fur matrix make this optimal for community-based monitoring programs to monitor Hg pollution in freshwater ecosystems. Future work includes assessing the distribution of THg of river otters with high mercury exposure to see if higher body burdens alter the distribution of THg across a pelt and assessing possible effects of age and sex on the distribution of THg across a pelt. Additionally, the characterization of THg distributions in other furbearing piscivorous mammals will be valuable for validating the use of fur biomonitoring programs in other sentinel species such as mink.

4.6 Data availability

Data are available upon request from the authors. R code used in these analyses can be found at: `https://github.com/kristineccles/pelt_hg.git`

4.7 Acknowledgments

The authors wish to acknowledge the Alberta Trappers' Association (Westlock, Alberta) and Mr. Reed Gauthier (Plamondon, Alberta) for all the help and support with sample collection, site access and local ecological knowledge that made this study possible. We also acknowledge E. Yumvihoze for laboratory support. We acknowledge funding support from the Canada Research Chair Program and the National Sciences and Engineering

Research Council Discovery Grant to H.M. Chan; the National Sciences and Engineering Research Council Collaborative Research and Training Experience Program, Research in Environmental and Analytical Chemistry and Toxicology to K.M. Eccles; and Environment and Climate Change Canada, the province of Alberta, and the Canada-Alberta Joint Oil Sands Monitoring Program to P. J. Thomas

4.8 References

1. Wolfe MF, Schwarzbach S, Sulaiman RA. 1998. Effects of mercury on wildlife: A comprehensive review. Environ. Toxicol. Chem. 17:146-160.

2. Chan HM, Scheuhammer AM, Ferran A, Loupelle C, Holloway J, Weech S. 2003. Impacts of Mercury on Freshwater Fish-Eating Wildlife and Humans. Hum. Ecol. Risk Assess. An Int. J. 9:867-883.

3. Ha E, Basu N, Bose-O'Reilly S, Dórea JG, McSorley E, Sakamoto M, Chan HM. 2017. Current progress on understanding the impact of mercury on human health. Environ. Res. 152:419-433.

4. Basu N. 2012. Piscivorous mammalian wildlife as sentinels of methylmercury exposure and neurotoxicity in humans. Methylmercury Neurotox., pp 357-370. doi:10.1007/978-1-46142383-6.

5. Evers DC, Mason RP, Kamman NC, Chen CY, Bogomolni AL, Taylor DL, Hammerschmidt CR, Jones SH, Burgess NM, Munney K, Parsons KC. 2008. Integrated mercury monitoring program for temperate estuarine and marine ecosystems on the North American Atlantic coast. Ecohealth. 5:426-441.

6. Foley RE, Jackling SJ, Sloan RJ, Brown MK. 1988. Organochlorine and mercury residues in wild mink and otter: Comparison with fish. Environ. Toxicol. Chem. 7:363-374.

7. Carrier G, Bouchard M, Brunet RC, Caza M. 2001. A Toxicokinetic Model for Predicting the Tissue Distribution and Elimination of Organic and Inorganic Mercury Following Exposure to Methyl Mercury in Animals and Humans. II. Application and Validation of the Model in Humans. Toxicol. Appl. Pharmacol. 171:50-60.

8. Klenavic K, Champoux L, Mike O, Daoust PY, Evans RD, Evans HE. 2008. Mercury concentrations in wild mink (*Mustela vison*) and river otters (*Lontra canadensis*) collected from eastern and Atlantic Canada: Relationship to age and parasitism. Environ. Pollut. 156:359-366.

9. Eccles KM, Thomas PJ, Chan HM. 2017. Predictive meta-regressions relating mercury tissue concentrations of freshwater piscivorous mammals. Environ. Toxicol. Chem. 36:2377-2384.

10. Wang W, Evans RD, Hickie BE, Rouvinen-Watt K, Evans HE. 2014. Methylmercury accumulation and elimination in mink (*Neovison vison*) hair and blood: results of a controlled feeding experiment using stable isotope tracers. Environ. Toxicol. Chem. 33:2873-2880.

11. Wang F, Lemes M, Khan MAK. 2012. Metallomics of mercury: role of thiol and selenol-containing biomolecules. In Liu, G, Cai, Y and O'Driscoll, N, eds, Environ. Chem. Toxicol. Mercur. John Wiley & Sons, Inc., Hoboken, NJ, pp 517-544.

12. Evans RD, Addison EM, Villeneuve JY, MacDonald KS, Joachim DG. 1998. An examination of spatial variation in mercury concentrations in otter (*Lutra canadensis*) in south-central Ontario. Sci. Total Environ. 213:239-245.

13. Strom SM. 2008. Total mercury and methylmercury residues in river otters (*Lutra canadensis*) from Wisconsin. Arch. Environ. Contam. Toxicol. 54:546-554.

14. Dietz R, Sonne C, Basu N, Braune B, O'Hara T, Letcher RJ, Scheuhammer T, Andersen M, Andreasen C, Andriashek D, Asmund G, Aubail A, Baagoe H, Born EW, Chan HM, Derocher AE, Grandjean P, Knott K, Kirkegaard M, Krey A, Lunn N, Messier F, Obbard M, Olsen MT, Ostertag S, Peacock E, Renzoni A, Rigèt FF, Skaare JU, Stern G, Stirling I, Taylor M, Wiig O, Wilson S, Aars J. 2013. What are the toxicological effects of mercury in Arctic biota? Sci. Total Environ. 443:775-790.

15. Fortin C, Beauchamp G, Dansereau M, Larivière N, Bèlanger D. 2001. Spatial variation in mercury concentrations in wild mink and river otter carcasses from the James Bay territory, Quèbec, Canada. Arch. Environ. Contam. Toxicol. 40:121-127.

16. Yates DE, Mayack DT, Munney K, Evers DC, Major A, Kaur T, Taylor RJ. 2005. Mercury levels in mink (*Mustela vison*) and river otter (*Lontra canadensis*) from northeastern North America. Ecotoxicology. 14:263-274.

17. Wilkie SC, Espie RHM, Basu N, Liber K, Hall BD. 2018. Trapped river otters (*Lontra canadensis*) from central Saskatchewan differ in total and organic mercury concentrations by sex and geographic location. Facets. 3:139-154.

18. McDowell MA, Dillon CF, Osterloh J, Bolger PM, Pellizzari E, Fernando R, Montes de Oca R, Schober SE, Sinks T, Jones RL, Mahaffey KR. 2004. Hair mercury levels in U.S. children and women of childbearing age: Reference range data from NHANES 1999-2000. Environ. Health Perspect. 112:1165-1171.

19. Dietz R, Riget F, Born EW, Sonne C, Grandjean P, Kirkegaard M, Olsen MT, Asmund G, Renzoni A, Baagoe H, Andreasen C. 2006. Trends in mercury in hair of greenlandic polar bears (*Ursus maritimus*) during 1892-2001. Environ. Sci. Technol. 40:1120-1125.

20. Cardona-Marek T, Knott KK, Meyer BE, O'Hara TM. 2009. Mercury concentrations in southern Beaufort sea polar bears: Variation based on stable isotopes of carbon and nitrogen. Environ. Toxicol. Chem. 28:1416-1424.

21. Dietz R, Born EW, Riget FF, Aubail A, Sonne C, Drimmie R, Basu N. 2011. Temporal Trends and Future Predictions of Mercury Concentrations in Northwest Greenland Polar Bear (*Ursus maritimus*) Hair. Environ. Sci. Technol. 45:1458-1465.

22. Dietz R, Riget F, Johansen P. 1996. Lead, cadmium, mercury and selenium in Greenland marine animals. Sci. Total Environ. 186:67-93.

23. Lieske CL, Moses SK, Castellini JM, Klejka J, Hueffer K, O'Hara TM. 2011. Toxicokinetics of mercury in blood compartments and hair of fish-fed sled dogs. Acta Vet. Scand. 53:66.

24. Taylor GI, Minabe T. 1992. The angiosomes of the mammals and other vertebrates. Plast. Reconstr. Surg. 89:181-215.

25. Bearhop S, Ruxton GD, Furness RW. 2000. Dynamics of mercury in blood and feathers of great skuas. Environ. Toxicol. Chem. 19:1638-1643.

26. Fraser E., Longstaffe FJ, Fenton MB. 2013. Moulting matters: the importance of understanding moulting cycles in bats when using fur for endogenous marker analysis. 91:533-544.

27. Mierle G, Addison EM, MacDonald KS, Joachim DG. 2000. Mercury levels in tissues of otters from Ontario, Canada: Variation with age, sex, and location. Environ. Toxicol. Chem. 19:3044-3051.

28. Evans RD, Addison EM, Villeneuve JY, MacDonald KS, Joachim DG. 2000. Distribution of inorganic and methylmercury among tissues in mink (*Mustela vison*) and otter (*Lutra canadensis*). Environ. Res. 84:133-9.

29. Harada M, Nakanishi J, Konuma S, Ohno K, Kimura T, Yamaguchi H, Tsuruta K, Kizaki T, Ookawara T, Ohno H. 1998. The present mercury contents of scalp hair and clinical symptoms in inhabitants of the Minamata area. Environ. Res. 77:160-164.

30. Depue JE, Ben-David M. 2007. Hair Sampling Techniques for River Otters. J. Wildl. Manage. 71:671-674.

31. Worthy GAJ, Rose J, Stormshak F. 1987. Anatomy and physiology of fur growth: The pelage priming process. Chapter. 54:827-841.

32. Cai Y, Tang G, Jaffe R, Jones R. 1997. Evaluation of some isolation methods for organomercury determination in soil and fish samples by capillary gas chromatography-atomic fluorescence spectrometry. Int. J. Environ. Anal. Chem. 68:331-345.

33. Laffont L, Maurice L, Amouroux D, Navarro P, Monperrus M, Sonke JE, Behra P. 2013. Mercury speciation analysis in human hair by species-specific isotope-dilution using GC-ICP-MS. Anal. Bioanal. Chem. 405:3001-3010.

34. Team RC. 2017. R: A Language and Environment for Statistical Computing.

35. Fox J, Weisberg S. 2011. An R Companion to Applied Regression.

36. Pebesma EJ. 2004. Multivariable geostatistics in S: the gstat package. Comput. Geosci. 30:683-691.

37. Zeileis A, Hothorn T. 2002. Diagnostic Checking in Regression Relationships. R News. 2:7-10.

38. Bivand RS, Pebesma E, Gomez-Rubio V. 2013. Applied spatial data analysis with R. Springer, NY.

39. Ord A, Getis JK. 1995. Local Spatial Autocorrelation Statistics: Distributional Issues and an Application. Geogr. Anal. 27:286-306.

40. Bloom NS. 1992. On the Chemical Form of Mercury in Edible Fish and Marine Invertebrate Tissue. Can. J. Fish. Aquat. Sci. 49:1010-1017.

PART III

Application of Spatial Analysis of Biomarkers

Preface: This section provides practical applications of using fur mercury as a biomaker of exposure, other biomarkers of metals exposures, and fur cortisol as a biomarker of biological response to assess spatial patterns of exposure, effect, and spatial dose-response relationships.

Chapter 5

Relationships between mercury concentrations in fur and stomach contents of river otter *(Lontra Canadensis)* and mink *(Neovison vison)* and their applications as proxys for environmental factors determining mercury bioavailability

Kristin M. Eccles[1], Philippe J. Thomas[2], and Hing Man Chan[1]

[1] Department of Biology, University of Ottawa, 30 Marie Curie, Ottawa, ON, K1N 6N5, Canada
[2] Science and Technology Branch, Environment and Climate Change Canada, National Wildlife Research Center, 1125 Colonel By Drive, Raven Road, Ottawa, ON K1A 0H3, Canada

This chapter is being prepared for submission in *Environmental Science and Technology.*

Author Contributions: KE conceived the idea, analysed the samples for mercury, completed the statistical analysis, and wrote the manuscript. PT collected and prepared the samples and contributed to editing the manuscript. LC contributed to the conceptualization of the project and provided guidance on the implementation and editing of the manuscript.

Supplemental information for this chapter can be found in Appendix C.

5.1 Abstract

The fur of piscivorous animals such as river otter (*Lontra canadensis*) and mink (*Neovison vison*) has been proposed to be used as a biomarker medium to assess mercury (Hg) exposure, but the relationship with dietary and environmental Hg exposure has not been fully characterized. The objective of this study is to investigate the relationship between fur total mercury (THg) and stomach content THg in river otter and mink, and their relationships with environmental factors. THg concentrations were measured in fur and stomach content of river otter (n=35) and mink (n=30) collected from Alberta, Canada between 2014-2017. The average fur THg concentration was 6.36 (SD=4.12) ppm and 5.25 (SD= 3.50) ppm and the average stomach content THg was 0.95 (SD=0.56) ppm and 0.71 (SD=0.54) in river otter and mink respectively. Regression analyses showed a significant positive relationship between the log fur THg and log stomach content THg for both species. Stomach content THg was significantly associated with soil pH (-) and % of deciduous forest (+). Fur THg was significantly associated with total fire burned (+) and % of wetlands (-). These results provide field evidence that fur can be used to reflect dietary Hg exposure and to identify sources and environmental factors that affect the bioavailable Hg in the habitats of these wildlife species.

5.2 Introduction

Mercury (Hg) is a global pollutant of ecological concern due to the established effects that methylated mercury (MeHg) has on the neurological health of multiple species of fish and mammals [1–4]. MeHg can bioaccumulate in organisms and biomagnify along the food chain in the aquatic environment [5]. Therefore, Hg pollution is particularly problematic for organisms at higher trophic levels including predatory fish, aquatic mammals, and humans. Water column properties such as dissolved organic carbon (DOC) concentration and water pH are important factors that control redox processes and methylation rates facilitated by bacteria. As a result, these factors regulate the bioaccumulation and biomagnification of MeHg in aquatic environments [6]. Anthropogenic impacts to the environment including climate change, land disturbance, overland flooding related to hydroelectric power generation, and industrial development and operations are projected to have both direct and indirect impacts on the transport, cycling, speciation, and bioavailability of Hg within ecosystems [7]. For example, the effects of climate change may alter the availability of prey and alter food web structure further increase the bioaccumulation and biomagnification of MeHg. As a result, this will alter the body burden of Hg in organisms at the top of the food chain [8].

River otter (*Lontra canadensis*) and mink (*Neovison vison*) have been used as sentinels for the health of freshwater ecosystems [9,10]. These two species are commonly used bioindicator species for Hg exposure due to their high fish consumption, and their non-migratory, non-hibernating natures [11]. Moreover, the relationships between total Hg

(THg) in fur and internal organ concentrations or internal doses in the target organs have been established [12–14]. Due to the overlap in diet items, particularly fish, between river otter, mink, and humans, these species have also been used as a sentinel for human health [10].

Fur is an ideal medium for biomonitoring as it can be collected non-invasively through hair snags or opportunistically through the fur trade [15,16]. The root of the hair follicle is supplied with arterial blood, so contaminants and circulating biomarkers get incorporated into new hair growth creating a chronological record of exposure within the stable keratin structure of the hair [17]. Due to seasonal moult, the exposures measured along the hair shaft are reflective of approximately one year of exposure [18]. Further, the majority of THg measured in fur is MeHg, which makes fur reflective of the MeHg body burden [19].

Since the diet is the main pathway of exposure to MeHg in aquatic mammals, understanding the environmental source and dietary exposures of Hg are important [20]. Due to the biomagnification potential of MeHg, the trophic position will affect the Hg body burden; organisms that feed at higher tropic positions tend to have higher MeHg body burdens [5,21]. Stable isotope analysis has been used to assess trophic position through δ^{15}N in organismal tissue and stomach contents [22,23]. In fish and mammals, higher δ^{15}N values indicate a higher trophic position and have been shown to be related to higher MeHg burden [24]. Similarly, δ^{13}C is used to determine dietary composition based on photosynthetic pathways of plants (e.g. C3 vs. C4). In freshwater ecosystems, this enrichment ratio has been used to distinguish between the consumption of littoral organisms such as algae and detritus and pelagic organisms such as phytoplankton in fish and mammals [25].

Hg biomonitoring has been conducted in many aquatic animals such as fish [3,27] birds including common loon [27,28], gull and tern [29], and a variety of mammals including river otter and mink [20,30], whales and polar bears [31]. However, few of these studies showed the direct relationship between Hg body burden, oral exposure, the external sources, and other environmental known factors for determining the bioavailability of MeHg such as pH and dissolved organic matters. Chen et al. (2005) evaluated lake attributes associated with increased Hg body burdens in a variety of fish species. They showed that chemical properties of the lakes including pH (-), SO_4(-), and alkalinity (-), and surrounding land use including % wetland (+), forest (+), and industrial land use (+) were important predictors for Hg contents in fish. Depew et al. (2013) assessed Hg burden in whole yellow perch and found similar significant predictors including pH, Hg deposition, and land cover variables including forest, urban, barren land, and agricultural land. No such studies have been conducted for aquatic mammals such as river otters and mink.

Our previously developed predictive models for the relationships between fur and organ THg concentrations in river otter and mink provide the basis to further develop these models to quantify the relationship between fur THg, dietary THg exposure, and environmental sources of Hg [13]. The relationships between fur Hg and dietary THg exposure and environmental sources of Hg have not been established and are necessary to understand the diet as a vector of mercury exposure[13]. The objective of this study is to assess the relationship between fur THg and dietary THg concentrations and their relationships with environmental factors that can affect Hg bioavailability. We predict that the concentration of THg in the stomach content will be positively correlated with THg concentration in the

fur. We also predict that sources of Hg in the environment and relevant physio-chemical factors, including soil pH and soil organic carbon, will be correlated to THg concentrations measured in the stomach content and the fur.

5.3 Methods

5.3.1 Sample collection

River otter (n=36) and mink (n=28) were obtained in collaboration with local trappers recruited through the Alberta Trappers Association (Westlock, AB) for a monitoring program for oil and gas resource development projects in Northern Alberta, Canada (Canada-Alberta Joint Oil Sands Monitoring Program) from 2014-2017. Since trapping occurred in the winter, carcasses were frozen upon capture and then were stored at -20°C until dissection.

5.3.2 Ethics

The carcasses used in this analysis were provided by Northern Alberta commercial trappers recruited through the Alberta Trappers Association. All animals were trapped under permit for the commercial fur trade following the Alberta Code for Responsible Trapping and the Agreement on International Humane Trapping Standards (AIHTS). Since the river otter and mink were collected for the commercial fur trade, they are not considered "experimental animals" and require no additional animal ethics or experimentation approvals as per Environment and Climate Change Canada's Animal Care Committee (ACC).

5.3.3 Mercury Measurement

The stomach contents were dissected and then mechanically homogenized (Heidolph Silent Crusher homogenizer; Sigma-Aldrich) under chemically-cleaned conditions. To remove all water content, the samples were freeze-dried for 48 hours (FreeZone Freeze Dry System; Labconco). Whole dried samples were ground, and 50 mg were subsampled for analysis. Stomach content THg measurements were expressed on a dry weight basis. Approximately 10mg of topcoat fur from the limb regions were subsampled for THg analysis. The fur samples were expressed as "fur weight". The samples were analysed using a direct thermal decomposition Hg analyser (Mercury Analyser 3000; Nippon Instruments North America). Quality assurance/quality control measures included blank samples, standard reference material (IAEA 085, DORM-4 and DOLT-5 from National Research Council of Canada), and 10% of tissue samples run in duplicate. IAEA-085 is a human hair certified reference material for trace metals with a known THg concentration of 23.2 $\pm$ 0.8 mg/kg (experiment mean = 22.5 $\pm$ 0.26 mg/kg). DORM-4 is a fish protein certified reference material for trace metals with a known THg concentration of 0.44 $\pm$ 0.036 mg/kg (experiment mean=0.37 $\pm$ 0.016 mg/kg) and DOLT-5 is a dogfish liver certified reference material for trace metals with a known THg concentration of 0.44 $\pm$ 0.024 mg/kg (experiment mean = 0.35 $\pm$ 0.018 mg/kg). Duplicate coefficient of variation (CV) = 4.1%. The limit of detection, calculated as 3 times the standard deviation of the blank (boat blanks) was 0.12 ng.

5.3.4 Fur Isotope Analysis

Fur samples were analysed for δ^{15}N (‰) and δ^{13}C (‰) in the Hatch Lab at the University of Ottawa using an elemental analyser (Vario EL Cube, Elementar, Germany) interfaced (Conflo III, Thermo, Germany) to an isotope ratio mass spectrometer (Delta Advantage,Thermo, Germany). The internal standards used included C-51 Nicotiamide (0.07, -22.95), C-52 mix of ammonium sulphate + sucrose (16.58, -11.94), C-54 caffeine (-16.61, -34.46), blind std C-55: glutamic acid (-3.98, -28.53). The δ^{15}N (‰) and δ^{13}C (‰) was calculated based on Eq (1). In this equation, R is the ratio of the abundance of the heavy to the light isotope, x denotes sample, and std is an abbreviation for the standard.

$$d = \frac{R_x - R_{std}}{R_{std}} * 1000 \tag{5.1}$$

5.3.5 Statistical Analysis

The statistical analysis was completed in R version 3.4.3. The concentration of THg in fur and stomach content between river otter and mink were compared using an unpaired Welch's (uneven variance) t-test. A Pearson product-moment correlation was also conducted to assess the association between fur THg and stomach content THg in river otter and mink. A weighted linear regression model was used to assess the relationships between fur and stomach content THg in river otter and mink. Weighing the regression models by a ratio between the total body weight of the animal and the amount of stomach content

recovered was important due to the wide range of stomach content recovered (1.91- 256.76 grams in river otter and 0.40-39.66 grams in mink). This is also important for the environmental modelling as it gives the appropriate amount of representation in the models, as higher stomach content to body weight ratios are likely to be more representative of feeding ecology, and thus, environmental conditions in their home range. Fur THg and stomach content THg were both base 10 log-transformed to meet model assumptions of residual normality, linearity, homoscedasticity, and independence were assessed using the appropriate tests.

Due to lack of sample, a subset analysed for stables isotopes δ^{13}C and δ^{15}N were used to individually assess the relationships between fur and stomach content THg with δ^{13}C and δ^{15}N signatures in the fur of the river otter (n=27) and mink (n=15) using a linear regression model.

A spatial analysis was used to assess the relationship between likely sources of THg with fur and dietary THg. Due to the similarity in diet composition (evaluated through isotopic signatures), the regression coefficients in the model assessing fur THg and stomach content THg, as well as the insignificant t-test results, river otter and mink were analysed together when assessing the relationship between fur and stomach content Hg and environmental variables (n=65). However, due to the difference in temporality between stomach content THg and fur THg, even though statistically related, these two dependent variables were modelled independently. The models between fur and stomach content THg and environmental factors were statistically adjusted for the trophic position using δ^{15}N , based on the assumption that the trophic position of primary producers is the similar across all regions

sampled.

River otter and mink with fur and stomach content THg were geolocated down to the trapline they were collected in. To account for animal movement, a buffer with a 9 km radius was created around the geolocation of each animal and all environmental variables were calculated based on this pseudo home range. This buffered distance was chosen based on reported radio collar home ranges [33,34]. Large buffers of 50 and 100 km were also used to obtain more encompassing environmental data. Environmental variables used include land cover, soil pH and organic carbon content, Hg deposition, forest fire burned area, and proximity to hydroelectric dams, oil and gas development, and contaminated sites. GIS was used to extract all data for the environmental variables. A table of the variables and how the variable was included in the model can be found in Table S1. However, since it is not feasible to obtain spatial data for the chemistry parameters associated with individual water bodies in the studied area. Therefore, we used soil pH as it has been significant in models assessing the Hg in yellow perch across Canada [35]. All spatial analysis was conducted in ArcGIS 10.5.

First, a Pearson Product Moment correlation was conducted with continuous environmental variables, and a Spearman Rank correlation was conducted with categorical variables to assess the correlation between log-transformed fur THg and stomach content THg. The results from the correlation analysis were used to guide a forwards-stepwise regression, using the Akaike Information Criterion corrected for small sample sizes (AICc) to assess model fit, independently fitting models for fur THg in the fur and stomach contents. Final models were assessed for the variance inflation factor (VIF) to ensure no multicollinearity

between independent variables. The regression models were further evaluated for adherence to model assumptions. A partial R^2 was computed to assess the contribution of each independent variable to the overall R^2.

5.4 Results

5.4.1 Diet and Hg

A summary of the THg concentrations for the total stomach content and fur can be found in Table 5.1. The t-test results demonstrate there was no statistical difference between mean THg in the fur (t=-1.13, p=0.20) or stomach content (t=-2.12 p=0.04) in river otter and mink.

Table 5.1: Summary of THg concentrations in fur and stomach content.

	River Otter		Mink	
	Fur THg (μg/g)	Stomach content THg (μg/g)	Fur THg (μg/g)	Stomach content THg (μg/g)
Min	1.21	0.11	0.36	0.04
Mean	6.36	0.95	5.25	0.71
SD	4.12	0.56	3.5	0.54
Max	19.72	2.5	17.78	1.81
n	36	36	28	28

Results from the Pearson product moment correlation indicate that there is a significant relationship between fur THg and stomach content THg in river otter (r=0.38, p=0.022) and mink (r=0.61, p= 0.0006). When these relationships are weighted by a ratio between the stomach contents recovered and total body weight, these relationships remain significant. The regression models assessing the relationship between fur log THg and stomach content log THg have similar beta coefficients (Table 5.3). While these models are both

statistically significant, the amount of variance the concentration of the stomach content THg can explain in the fur THg is lower in the river otter model (25%) than in the mink model (52%) (Figure 5.1 and Table 5.2).

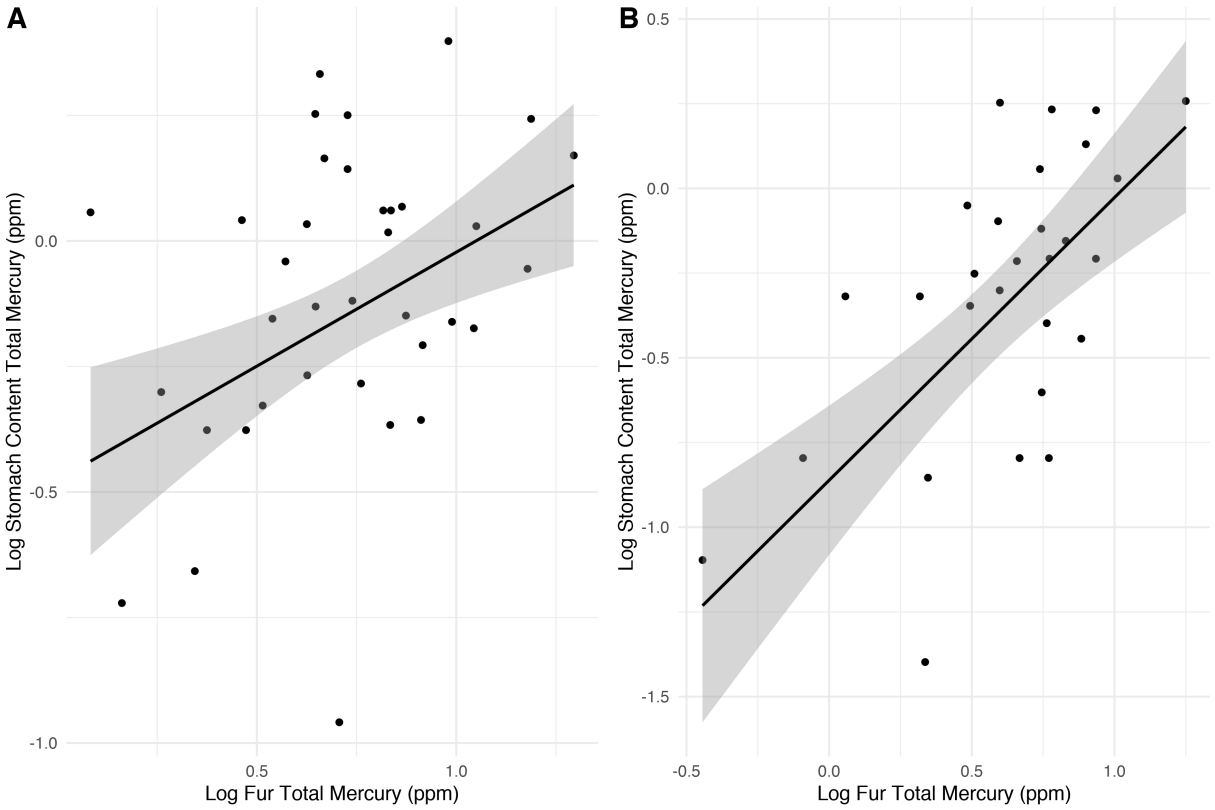

Figure 5.1: Line of best fit and standard error from the regression model between log total fur Hg and log total stomach content Hg in river otter (A) and mink (B)

Table 5.2: Summary of linear regression models between THg in the stomach content and fur of river otter and mink. Regressions were weighted by the weight of the stomach contents.

	River Otter			Mink		
	Estimate	Std. Error	P-value	Estimate	Std. Error	P-value
Intercept	0.83	0.05	< 2e-16	0.81	0.07	2.78E-11
Log stomach content THg	0.61	0.17	0.001	0.65	0.12	1.25e+00
P-value	0.001			1.25e-05		
DoF	33			25		
Adj. R2	0.25			0.52		

Mink (n=15) had an average δ^{13}C signature of -24.61 ±3.37(‰) and an average δ^{15}N

signature of 10.07 ±1.57 (‰). River otter (n=27) had an average δ^{13}C signature of -25.39 ±4.26 (‰) and an average δ^{15}N signature of 11.0 ±1.06 (‰). There was no difference between the isotopic signature for δ^{13}C (t=1.59, p=0.12) and δ^{15}N (t=-1.28, p=0.22) in river otter and mink.

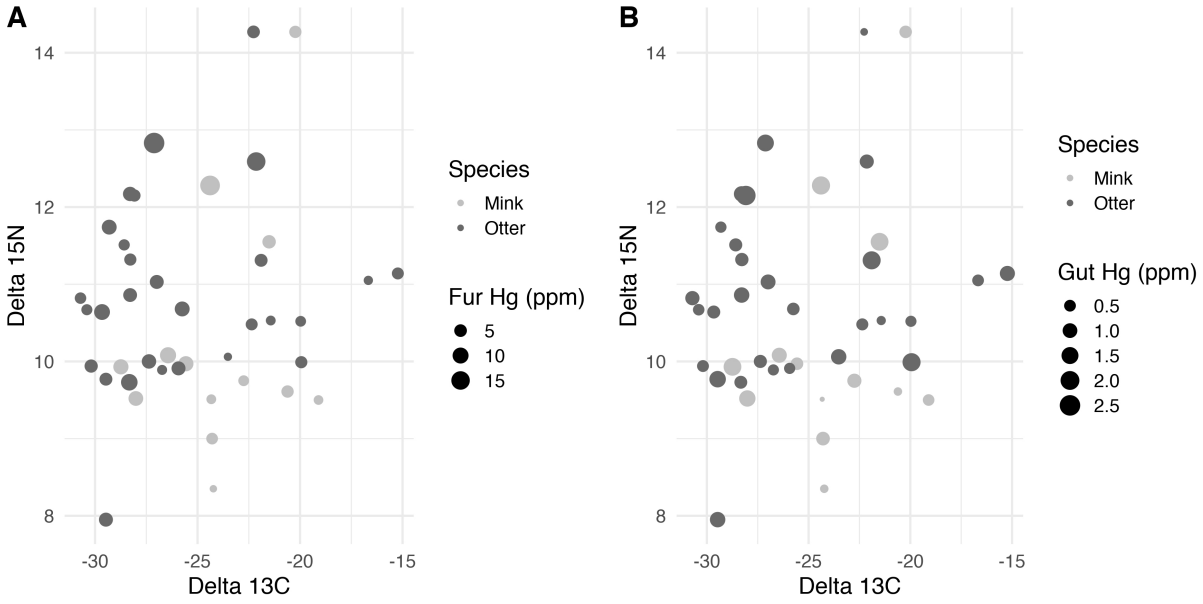

Figure 5.2: Stable isotope signature (δ^{13}C and δ^{15}N) of river otter and mink fur represented by position on the x and y-axes. The size the circle represents the fur THg (A) and the stomach content THg (B).

While river otter and mink have overlapping dietary patterns, river otter tends to eat at higher trophic positions than mink in the aquatic environment. Total mercury in fur and stomach content tends to increase with decreasing δ^{13}C and increasing δ^{15}N (Figure 5.2). These observations are confirmed in the results of the linear regression analysis. There is a significant positive relationship between fur THg and δ^{13}C and δ^{15}N values, and a significant positive relationship between stomach content THg and δ^{15}N (Table 5.3). Isotopic signature in hair can explain 20% of the variance of fur THg and 10% of the stomach content THg in both species. Thus, trophic position and composition of the diet

can explain 20% of the variance of THg observed in fur and 10% of the variance in stomach content THg.

Table 5.3: Summary of OLS regression model between log fur THg, log stomach content THg, and fur δ^{13}C and δ^{15}N isotopic signature.

	Fur THg (μg/g)			Stomach Content THg (μg/g)		
	Estimate	Std. Error	P-value	Estimate	Std. Error	P-value
Intercept	-0.96	0.44	0.03	-2.29	0.83	0.009
δ^{15}N	0.09	0.03	0.007	0.19	0.08	0.02461
δ^{13}C	-0.03	0.01	0.005			
P-value	0.002			0.025		
DoF	39			38		
Adj. R2	0.2			0.1		

5.4.2 Hg Sources

The best model for predicting stomach content THg (Table 5.4) included pH, and the area of deciduous forests in a pseudo-home range as significant predictors. While δ^{15}N was not significant, it was kept in the model to adjust for the trophic position. Also, important to note was the high multicollinearity between variables including soil OC and pH (r=-0.78, p=4.807e-14), and pH and proximity to the hydroelectric reservoir (r=-0.73, p=1.095e-11). The negative association of pH contributed the most to the overall variance explained as it has the highest partial R2. Overall, this model was statistically significant and explained 58% of the variance in stomach content THg. This model met all assumptions except residual heteroscedasticity (ncvTest p=0.0006), and independent variables were not correlated as indicated by VIF values <2.

The best model assessing the relationship between fur log THg and environmental variables (Table 5.5) showed that % Wetlands, Total Fire Area (sq. meters), and δ^{15}N were significant predictors. All these predictors contributed equally to the overall variance

Table 5.4: Relationships between log stomach content THg and environmental sources of Hg.

	Estimate	Std. Error	P-value	Partial R2
Intercept	3.38	1.126	0.005	-
pH	-0.85	0.134	2.50E-07	0.53
% Deciduous Tree	1.96	0.48	0.0003	0.31
δ^{15}N	0.055	0.062	0.38	0.02
P-value	1.16E-07	DoF	36	
R2	0.62	Adj. R2	0.58	

examples. The percent of wetlands found in the pseudo-home range had a negative impact on fur THg. There was also a significant relationship with the total area of forest fire, as the greater the forest fire burn area in the pseudo-home range is, the higher the log fur THg is. Overall this model was statistically significant and explained 25% of the variance in fur log THg. This model met all model assumptions and VIF <2.

Table 5.5: Relationship between log fur THg and environmental sources of Hg.

	Estimate	Std. Error	P-value	Partial R2
Intercept	0.045	0.33	0.89	-
% Wetlands	-5.52	2.56	0.039	0.11
Fire Burned Area (sq. meters)	0.004	0.002	0.039	0.11
δ^{15}N	0.063	0.03	0.03	0.12
P-value	0.003	DoF	38	
R2	0.3	Adj. R2	0.25	

5.5 Discussion

5.5.1 Relationship between stomach content and fur THg

While feeding studies have assessed the relationship between dietary THg concentrations in river otter [36] and mink [17,37], this is the first study to report this relationship in wild populations. In both river otter and mink, the relationship between fur THg and

stomach content THg were statistically significant, with the mink model accounting for more variance than the river otter model. In our regression models, 48% of the variance in mink stomach content THg and 75% of the variance in river otter stomach content THg was unexplained. The R-square of the relationships between fur THg and stomach content THg reported in this study are significantly lower than the relationship between diet Hg and fur THg reported in feeding studies which report R^2 values of >0.97 [36,37]. One likely reason for the large proportion of unexplained variance in our study could be due to the variability of Hg in the diet of wild animals when compared to a lab-controlled diet. Further, fur is reflective of the diet in approximately the past year, especially if the whole length fur sample is analysed, as fur bearers fully moult both their undercoat and topcoat once a year [38]. Conversely, stomach contents are reflective of the diet in approximately the last 24 hours and are subject to both daily and seasonal fluctuations [23,39]. Fur is a long term indicator of Hg exposure via diet and serves as an important excretion pathway of Hg [17]. In fur bearers, almost 90% of the Hg body burden is excreted into the fur [40]. The concentration of Hg exposure in a long-term diet may not be reflective of what was consumed prior to being trapped because, as Yaginuma-Sakurai et al. (2010) estimate, the time lag for THg to get incorporated into measurable hair growth is three weeks. Another possibility is the more varied diet in the wild

5.5.2 Relationship between THg and isotopic signatures

Stable isotopes provide valuable information on both diet trophic position through assessing δ^{15}N and locations of foraging through assessing δ^{13}C. Other studies have found that stable

isotopes in the fur were less variable than stable isotopes in the faeces as fur is not subject to daily dietary functions [42]. Thus, we analysed the stable isotopes in the fur, as opposed to the stomach contents, to better capture long term dietary patterns. Mink fur isotope results from our study (δ^{13}C:-24.61 and δ^{15}N: 10.07‰) are similar to the isotopic signature in muscle tissue reported for inland mink (δ^{13}C:-24.6‰- 26.4‰and δ^{15}N: 10.3-11.1‰) but had a different isotopic composition compared with coastal mink captured in Rhode Island, USA (δ^{13}C:-15.9‰and δ^{15}N: 13.9‰) [43] Similarly, the river otter fur isotope results from our study had a different composition (δ^{13}C: -25.39 and δ^{15}N: 11.03‰) from coastal river otter from Prince William Sound and Kachemak Bay, Alaska (δ^{13}C range: -18‰to -13‰and δ^{15}N: 14.9) [42,44]. This freshwater- marine δ^{13}C gradient has been observed in fish and the isotopic ratios similar to those reported in this study are observed in fish in Canadian freshwater ecosystems [45–47]. While we do not have sex information for the river otter or mink, which is a limitation of this study, other studies report no difference between stable isotopes in male and females [39,48].

River otters typically eat a diet comprised of more aquatic organisms (i.e. fish, clams) which are higher in Hg than diet items of mink which is typically comprised of more terrestrial organisms [33,49]. However, this research indicates that the average diet of mink and river otter captured in northern Alberta, Canada had similar Hg concentrations and similar δ^{13}C and δ^{15}N. This similarity in the diet of mink and river otter has been observed in other studies specific to the boreal region [33]. The positive relationship between THg and δ^{15}N in the pooled mink and river otter samples is supported by the large body of evidence between trophic position and THg due to the bioaccumulation and biomagnification of Hg

[24,47]. As a result, the trophic position of the diet is an important factor in predicting THg and thus will be included when assessing the relationship with environmental variable (section 4.3).

Ben-David et al. (2001) demonstrated that fur THg concentrations were positively associated with the δ^{13}C of fur for river otters in marine environments, whereas our results demonstrate a negative relationship between δ^{13}C and fur THg. This is likely due to the marine-freshwater δ^{13}C gradient highlighted above and the respective in nutrients available to the primary producer in that specific food chain. These results are similar to the relationship between δ^{13}C and THg and possibility indicates a higher reliance on pelagic prey items [50]. However, δ^{13}C does not necessarily add predictive power to models when assessing Hg concentrations in wildlife, as was the case with our models [51]

5.5.3 Relationship between THg exposure and environmental sources of THg

Soil pH explained a large proportion of the variation in the measured stomach content THg. Miskimmin et al. (1992) found that when the pH of boreal lake water was reduced from 7.0 to 5.0 there was a large increase in the net methylation rates regardless of the dissolved DOC concentration. The measured range of pH in lake water is similar to the range of soil pH values present in our study (4.6-6.4). Similar relationships have been found in common loons and their fish prey species where loons and prey from lakes with lower pH have higher mercury body burdens [53]. This evidence supports our findings that the soil pH in the locations where the animals were captured is an important driver for the Hg

stomach content or the dietary Hg exposure for these two species of mammals.

The percentage of the deciduous forest was also a significant positive predictor of stomach content THg in the pooled river otter and mink samples. The river otter and mink samples were collected in the boreal ecozone which, is characterized by a mixture of coniferous trees (mainly jack pine and balsam fir) and deciduous trees (mainly red maple, poplar, and paper birch) [54]. Productive forests are shown to have the highest amount of soil Hg when compared with other land cover classes [8,55,56]. Forests with canopy foliage, such as the boreal forest, are associated with increased levels of contaminants, including Hg, due to a larger surface area to collect atmospheric deposition [56–58]. Further, the litter-fall influences the distribution and magnitude of the available Hg to aquatic ecosystems and represents a pathway for the influx of mercury into the aquatic ecosystems [55,57].

Two discrete landscape-level features that were significant when assessing the relationship between fur THg and environmental sources were wetlands and total fire burned area. Wetlands are important features of the landscape that influence the supply and sequestration of Hg and MeHg in aquatic environments. While wetland Hg dynamics are complex, they can exhibit net Hg accumulation [59]. Wetlands are also a significant source of organic carbon and while there is a positive environmental relationship between DOC and Hg [60], DOC may exhibit a protective effect in the aquatic environment by inhibiting the uptake of MeHg, to some extent [61]. This is also supported by the significant positive relationship between fur THg and soil OC, which was not included as it was highly correlated with soil pH. These results are similar to those found by Chen et al. (2005), where an increasing percentage of wetland was associated with a decrease in fish Hg. It is important to note

other studies have found a positive relationship between wetlands and THg measured in fish, invertebrates, and zooplankton [62]. However, since the source of data used in this study was remotely sensed data, an important follow up would be to collect surface water samples in these regions to elucidate and validate the complex Hg dynamics in a northern boreal habitat and their relationship with bioavailability and exposure in food webs.

The amount of fire area burned within a 10 year period was also a significant positive predictor of fur THg. Similarly, research by Kelly et al. (2006) demonstrated that after forest fires there is enhanced bioaccumulation of Hg in fish by a factor of 5. This is attributed to the increase in nutrient inputs which promoting bacterial methylation of inorganic Hg to MeHg resulting in increased MeHg in the aquatic ecosystem and in the food chain. Further, the increased primary productivity from the input of nutrient can also influence food web structure and may stimulate restructuring of food webs through increased piscivory [63]. Forest fires also release particulate Hg and MeHg into the air which is deposited into the local environment providing an influx of Hg [64].

There was a difference in significant environmental predictors between the stomach content THg and the fur THg models (soil pH and deciduous trees for stomach content and wetland and forest fires for fur). This difference may be reflective of the temporality of the two biomarkers. Since stomach content THg is a short-term indicator of Hg exposure, the concentrations measured are more likely to be a localized indicator of environmental Hg sources. Further, since the regression model between stomach content THg was weighted by a ratio of stomach contents to body weight, organisms with large stomach contents had a larger influence in the model. River otter and mink with low stomach contents volume likely

had not eaten recently. Significant predictors in this model were spatially continuous (soil pH and % of the deciduous forest). These landscape-level features that are continuous over space tend to be spatially autocorrelated, where neighbouring land cover types or features are more likely to be similar [65]. Where the animal was trapped is likely reflective of their local environment. Conversely, in the model assessing the relationship between fur THg and environmental variables, significant predictors are discrete landscape-level features (% wetlands and total burned area). These predictors occur at discrete locations on the landscape which the animal may not have been near when they were trapped but are reflected in their Hg exposure that occurred prior to capture.

A relatively small spatial scale was used in this study; our samples come from an area approximately 250,000 square kilometres. This is possibly why variables such as air deposition of Hg was not found to be significant in this modelling but was significant in other national Hg biomonitoring programs [3,32,66]. This highlights the importance of using appropriate geographic methods such as a geographically weighted regression (GWR) when assessing the relationship between sources of mercury and exposures at large spatial scales. While global regression models, for example, ordinary least squares (OLS), fit one line-of-best-fit between dependent and independent variables, the geographically weighted regression fits many localized regressions [67]. This allows the beta coefficients of the models to vary geographically, which would enable the assessment of local factors of influence in Hg exposure. National Hg monitoring programs in Canada have yet to use this approach [3,66].

5.5.4 Applications

Developing fur, an easily accessible biomarker medium, as a proxy indicator for environmental Hg sources and bioavailability, helps to addresses Article 19 of the Minamata Convention, which is a legally binding international treaty developed to protect human and wildlife health by decreasing and monitoring Hg inputs into the environment. Article 19 addresses the development and improvement of current methods for monitoring Hg in wildlife and the environment in which they live. This research provides evidence that fur can be used as a proxy for environmental Hg bioavailability. Expanding the current dataset to a national scale will help further develop fur as a proxy of environmental bioavailability of Hg by assessing both global and local drivers of Hg exposure.

5.6 Data availability

Data is available upon request from the authors. R code used in these analyses can be found at: `https://github.com/kristineccles/fur_gut_hg.git`

5.7 Acknowledgments

The authors wish to acknowledge the Alberta Trappers' Association (Westlock, Alberta), Mr. Reed Gauthier (Plamondon, Alberta), and Treaty 8 First Nations including Mikisew Cree First Nation, Athabasca Chipewyan First Nation, and Fort Mackay First Nation, and the Metis nations for all the help and support with sample collection, site access and local

ecological knowledge. We also acknowledge E. Yumvihoze for laboratory support.

5.8 References

1. Basu N, Klenavic K, Gamberg M, O'Brien M, Evans D, Scheuhammer AM, Chan HM. 2005. Effects of Mercury on Neurochemical Receptor-Binding Characteristics in Wild Mink. Environ. Toxicol. Chem. 24:1444–1450.

2. Dornbos P, Strom S, Basu N. 2013. Mercury exposure and neurochemical biomarkers in multiple brain regions of Wisconsin River Otters (Lontra canadensis). Ecotoxicology. 22:469–475.

3. Depew DC, Burgess NM, Campbell LM. 2013. Spatial patterns of methylmercury risks to common loons and piscivorous fish in Canada. Environ. Sci. Technol. 47:13093–13103.

4. Chan HM, Scheuhammer AM, Ferran A, Loupelle C, Holloway J, Weech S. 2003. Impacts of Mercury on Freshwater Fish-Eating Wildlife and Humans. Hum. Ecol. Risk Assess. An Int. J. 9:867–883.

5. Driscoll CT, Mason RP, Chan HM, Jacob DJ, Pirrone N. 2013. Mercury as a global pollutant: Sources, pathways, and effects. Environ. Sci. Technol. 47:4967–4983.

6. Chiasson-Gould SA, Blais JM, Poulain AJ. 2014. Dissolved organic matter kinetically controls mercury bioavailability to bacteria. Environ. Sci. Technol. 48:3153–3161.

7. Selin H, Keane SE, Wang S, Selin NE, Davis K, Bally D. 2018. Linking science and policy to support the implementation of the Minamata Convention on Mercury. Ambio. 47:198–215.

8. Obrist D, Kirk JL, Zhang L, Sunderland EM, Jiskra M, Selin NE. 2018. A review of global environmental mercury processes in response to human and natural perturbations: Changes of emissions, climate, and land use. Ambio. 47:116–140.

9. Basu N, Scheuhammer AM, Bursian SJ, Elliott J, Rouvinen-Watt K, Chan HM. 2007. Mink as a sentinel species in environmental health. Environ. Res. 103:130–144.

10. Basu N. 2012. Piscivorous mammalian wildlife as sentinels of methylmercury exposure and neurotoxicity in humans. Methylmercury Neurotox., pp 357–370. doi:10.1007/978-1-46142383-6.

11. Ben-David, M., Golden HN. 2009. River Otters (Lontra canadensis) in Southcentral Alaska: Distribution, Relative Abundance, and Minimum Population Size Based on Coastal Latrine Site Surveys. SWAN I&M Progr. report, Natl. Park Serv. Anchorage, Alaska.

12. Strom SM. 2008. Total mercury and methylmercury residues in river otters (Lutra canadensis) from Wisconsin. Arch. Environ. Contam. Toxicol. 54:546–554.

13. Eccles KM, Thomas PJ, Chan HM. 2017. Predictive meta-regressions relating mercury tissue concentrations of freshwater piscivorous mammals. Environ. Toxicol. Chem. 36:2377–2384.

14. Wilkie SC, Espie RHM, Basu N, Liber K, Hall BD. 2018. Trapped river otters (Lontra canadensis) from central Saskatchewan differ in total and organic mercury concentrations by sex and geographic location. Facets. 3:139–154.

15. Vongraven D, Aars J, Amstrup S, Atkinson SN, Born EW, Debruyn TD, Derocher AE, Durner G, Gill M, Lunn N, Obbard ME, Omelak J, Ovsyanikov N, Peacock E, Vongraven D, Aars J, Amstrup S, Atkinson SN, Belikov S, Born EW, Debruyn TD, Derocher AE, Durner G, Gill M, Lunn N, Obbard ME, Omelak J, Ovsyanikov N, Peacock E, Richardson E, Sahanatien V, Stirling I. 2016. Monograph Series Number 5: A circumpolar monitoring framework for polar bears Richardson , Vicki Sahanatien , Ian Stirling and Øystein Wiig Source: Ursus , Vol . 23 , Special Issue: Monograph Series Number 5: A circumpolar monitoring framework for pol.

16. Macbeth BJ, Cattet MRL, Stenhouse GB, Gibeau ML, Janz DM. 2010. Hair cortisol concentration as a noninvasive measure of long-term stress in free-ranging grizzly bears (Ursus arctos): considerations with implications for other wildlife. Can. J. Zool. 88:935–949.

17. Wang W, Evans RD, Hickie BE, Rouvinen-Watt K, Evans HE. 2014. Methylmercury accumulation and elimination in mink (Neovison vison) hair and blood: results of a controlled feeding experiment using stable isotope tracers. Environ. Toxicol. Chem. 33:2873–2880.

18. Hyvärinen H, Tyni P, Nieminen P. 2003. Effects of moult, age, and sex on the accumulation of heavy metals in the otter (Lutra lutra) in Finland. Bull. Environ. Contam. Toxicol. 70:278–284.

19. Evans RD, Addison EM, Villeneuve JY, MacDonald KS, Joachim DG. 2000. Distribution of inorganic and methylmercury among tissues in mink (Mustela vison) and otter (Lutra canadensis). Environ. Res. 84:133–9.

20. Yates DE, Mayack DT, Munney K, Evers DC, Major A, Kaur T, Taylor RJ. 2005. Mercury levels in mink (Mustela vison) and river otter (Lontra canadensis) from northeastern North America. Ecotoxicology. 14:263–274.

21. Watras CJ, Back RC, Halvorsen S, Hudson RJM, Morrison KA, Wente SP. 1998. Bioaccumulation of Hg in Pelagic Freshwater foot Webs. Sci. Total Environ. 212:183–208.

22. Lake JL, McKinney RA, Osterman FA, Ryba SA, Cantwell MG, Tien RY, Brown C, Suprock L. 2002. Mercury and stable isotopes in mink. Abstr. Pap. Am. Chem. Soc. 223:U521.

23. Ben-David M, Flynn RW, Schell DM. 1997. Annual and seasonal changes in diets of martens: evidence from stable isotope analysis. Oecologia. 111:280–291.

24. Atwell L, Hobson KA, Welch HE. 1998. Biomagnification and bioaccumulation of mercury in an arctic marine food web: insights from stable nitrogen isotope analysis. Can. J. Fish. Aquat. Sci. 55:1114–1121.

25. Post D. 2002. Using stable isotopes to estimate trophic position: models , methods , and assumptions. Ecol. Soc. Am. 83:703–718.

26. Cardona-Marek T, Knott KK, Meyer BE, O'Hara TM. 2009. Mercury concentrations in southern Beaufort sea polar bears: Variation based on stable isotopes of carbon and nitrogen. Environ. Toxicol. Chem. 28:1416–1424.

27. Evers DC, Han Y-J, Driscoll CT, Kamman NC, Goodale MW, Lambert KF, Holsen TM, Chen CY, Clair T a., Butler T. 2007. Biological Mercury Hotspots in the Northeastern United States and Southeastern Canada. Bioscience. 57:29–43.

28. Scheuhammer AM, Lord SI, Wayland M, Burgess NM, Champoux L, Elliott JE. 2016. Major correlates of mercury in small fish and common loons (Gavia immer) across four large study areas in Canada. Environ. Pollut. 210:361–370.

29. Dolgova S, Popp BN, Courtoreille K, Espie RHM, Maclean B, McMaster M, Straka JR, Tetreault GR, Wilkie S, Hebert CE. 2018. Spatial trends in a biomagnifying contaminant: Application of amino acid compound–specific stable nitrogen isotope analysis to the interpretation of bird mercury levels. Environ. Toxicol. Chem. 37:1466–1475.

30. Klenavic K, Champoux L, Mike O, Daoust PY, Evans RD, Evans HE. 2008. Mercury concentrations in wild mink (Mustela vison) and river otters (Lontra canadensis) collected from eastern and Atlantic Canada: Relationship to age and parasitism. Environ. Pollut. 156:359–366.

31. Basu N, Scheuhammer AM, Sonne C, Letcher RJ, Born EW, Dietz R. 2009. Is dietary mercury of neurotoxicological concern to wild polar bears (Ursus maritimus)? Environ. Toxicol. Chem. 28:133–140.

32. Chen CY, Stemberger RS, Kamman NC, Mayes BM, Folt CL. 2005. Patterns of Hg bioaccumulation and transfer in aquatic food webs across multi-lake studies in the northeast US. Ecotoxicology. 14:135–147.

33. Reid DG, Code TE, Reid ACH, Herrero SM. 1994. Food habits of the river otter in a boreal ecosystem. Can. J. Zool. 72:1306–1313.

34. Haan DM, Halbrook RS. 2015. Home Ranges and Movement Characteristics of Minks in East-central New York. Am. Midl. Nat. 174:302–309.

35. Depew DC, Burgess NM, Campbell LM. 2013. Modelling mercury concentrations in prey fish: Derivation of a national-scale common indicator of dietary mercury exposure for piscivorous fish and wildlife. Environ. Pollut. 176:234–243.

36. Halbrook RS, Lewis LA, Aulerich RI, Bursian SJ. 1997. Mercury accumulation in mink fed fish collected from streams on the Oak Ridge Reservation. Arch. Environ. Contam. Toxicol. 33:312–316.

37. Evans RD, Grochowina NM, Basu N, O'Connor EM, Hickie BE, Rouvinen-Watt K, Evans HE, Chan HM. 2015. Uptake of selenium and mercury by captive mink: Results of a controlled feeding experiment. Chemosphere. 144:1582–1588.

38. Fraser E., Longstaffe FJ, Fenton MB. 2013. Moulting matters: the importance of understanding moulting cycles in bats when using fur for endogenous marker analysis. 91:533–544.

39. Gamberg M, Boila G, Stern G, Roach P. 2005. Cadmium mercury and selenium concentrations in mink (Mustela vison) from Yukon, Canada. Sci. Total Environ. 351:523–529.

40. Farris FF, Dedrick RL, Allen P V., Smith JC. 1993. Physiological model for the pharmacokinetics of methyl mercury in the growing rat. Toxicol. Appl. Pharmacol. 119:74–90.

41. Yaginuma-Sakurai K, Murata K, Shimada M, Nakai K, Kurokawa N, Kameo S, Satoh H. 2010. Intervention study on cardiac autonomic nervous effects of methylmercury from seafood. Neurotoxicol. Teratol. 32:240–245.

42. Ben-David M, Bowyer RT, Duffy L, Duffy LK, Roby DD, Schell DM. 1998. Social Behavior and Ecosystem Processes: River Otter Latrines and Nutrient Dynamics of Terrestrial. Ecology. 79:2567–2571.

43. Lake JL, Ryba SA, Serbst J, Brown CF, Gibson L. 2007. Mercury and Stable Isotopes of Carbon and Nitrogen in Mink. Environ. Toxicol. Chem. 26:2611.

44. Ben-David M, Duffy LK, Blundell GM, Bowyer RT. 2001. Natural exposure of coastal river otters to mercury: Relation to age, diet, and survival. Environ. Toxicol. Chem. 20:1986–1992.

45. Paszkowski, C. A., Hanisch JR, Tonn WM, Scrimgeour GJ. 2010. δ^{13}C and δ^{15}N Signatures in Muscle and Fin Tissues: Nonlethal Sampling Methods for Stable Isotope Analysis of Salmonid. North Am. J. Fish. Manag. 30:1–11.

46. Cunjak RA, Roussel J-M, Gray MA, Dietrich JP, Cartwright DF, Munkittrick KR, Jardine TD. 2005. Using stable isotope analysis with telemetry or mark-recapture data to identify fish movement and foraging. Oecologia. 144:636–646.

47. Burgess NM, Hobson KA. 2006. Bioaccumulation of mercury in yellow perch (Perca flavescens) and common loons (Gavia immer) in relation to lake chemistry in Atlantic Canada Bioaccumulation of mercury in yellow perch (Perca flavescens) and common loons (Gavia immer) in relation. Hydrobiologia. 567:275–282.

48. Hammershøj M, Pertoldi C, Asferg T, Møller TB, Kristensen NB. 2005. Danish free-ranging mink populations consist mainly of farm animals: Evidence from microsatellite and stable isotope analyses. J. Nat. Conserv. 13:267–274.

49. Gilbert FF, Nancekivell EG. 1982. Food habits of mink (Mustela vison) and otter (Lutra canadensis) in northeastern Alberta. Can. J. Zool. 60:1282–1288.

50. Power M, Klein GM, Guiguer KRRA, Kwan MKH. 2002. Mercury accumulation in the fish community of a sub-Arctic lake in relation to trophic position and carbon sources. J. Appl. Ecol. 39:819–830.

51. Chesney EJ, Blum JD, Shine JP. 2010. Stable Isotope (N , C , Hg) Study of Methylmercury Sources and Trophic Transfer in the Northern Gulf of Mexico. 44:1630–1637.

52. Miskimmin B, Rudd WM, Kelly CA. 1992. Influence of dissolved organic carbon, pH, and microbial respiration rates on mercury methylation and demethylation in lake water. Can. J. Fish. Aquat. Sci. 49:17–22.

53. Burgess NM, Meyer MW. 2008. Methylmercury exposure associated with reduced productivity in common loons. Ecotoxicology. 17:83–91.

54. Harris RC, Rudd JW, Amyot M, Babiarz CL, Beaty KG, Blanchfield PJ, Bodaly R, Branfireun BA, Gilmour CC, Graydon JA. 2007. Whole-ecosystem study shows rapid fish-mercury response to changes in mercury deposition. PNAS. 104:16586–16591.

55. Obrist D, Johnson D, Lindberg S, Luo Y, Hararuk O, Bracho R, Battles JJ, Dail D, Edmonds R, Monson R, Ollinger S, Pallardy S, Pregitzer K, Todd D. 2011. Mercury distribution across 14 U.S. Forests. Part I: Spatial patterns of concentrations in biomass, litter, and soils. Environ. Sci. Technol. 45:3974–3981.

56. Obrist D, Pearson C, Webster J, Kane T, Lin C, Aiken GR, Alpers CN. 2016. A synthesis of terrestrial mercury in the western United States: Spatial distribution de fined by land cover and plant productivity. Sci. Total Environ. 568:522–535.

57. Grigal DF. 2002. Inputs and outputs of mercury from terrestrial watersheds: a review. Environ. Rev. 10:1–39.

58. Driscoll CT, Han Y, Chen CY, Evers DC, Lambert KF, Holsen TM, Kamman NC, Munson RK. 2007. Mercury Contamination in Forest and Freshwater Ecosystems in the Northeastern United States. 57:17–28.

59. Grigal DF. 2003. Mercury Sequestration in Forests and Peatlands; A Review. 405:393–405.

60. Lavoie RA, Amyot M, Lapierre J. 2019. Global Meta-analysis on the Relationship between Mercury and Dissolved Organic Carbon in Freshwater Environments. J. Geophys. Res. Biogeosciences.124. https://doi.org/10.1029/2018JG004896

61. Lavoie RA, Jardine TD, Chumchal MM, Kidd KA, Campbell LM. 2013. Biomagnification of mercury in aquatic food webs: A worldwide meta-analysis. Environ. Sci. Technol. 47:13385–13394.

62. Chasar LC, Scudder BC, Stewart AR, Bell AH, Aiken GR. 2009. Mercury Cycling in Stream Ecosystems. 3. Trophic dynamics. Environ. Sci. Technol. 43:2733–2739.

63. Kelly EN, Schindler DW, Louis VLS, Donald DB, Vladicka KE. 2006. Forest fire increases mercury accumulation by fishes via food web restructuring and increased mercury inputs. PNAS. 103:19380–19385.

64. Witt EL, Kolka RK, Nater EA, Wickman TR. 2009. Forest fire effects on mercury deposition in the boreal forest. Environ. Sci. Technol. 43:1776–1782.

65. Bolliger J, Wagner HH, Turner MG. 2007. Identifying and quantifying landscape patterns in space and time. A Chang. World. Springer, pp 177–194.

66. Chételat J, Hickey MBC, Poulain AJ, Dastoor A, Ryjkov A, McAlpine D, Vanderwolf K, Jung TS, Hale L, Cooke ELL, Hobson D, Jonasson K, Kaupas L, McCarthy S, McClelland C, Morningstar D, Norquay KJO, Novy R, Player D, Redford T, Simard A, Stamler S, Webber QMR, Yumvihoze E, Zanuttig M. 2018. Spatial variation of mercury bioaccumulation in bats of Canada linked to atmospheric mercury deposition. Sci. Total Environ. 626:668–677.

67. Fotheringham AS, Charlton M, Brunsdon C. 1998. Geographically weighted regression: a natural evolution of the expansion method for spatial data analysis. Environ. Plan. A. 30:1905–1927.

Chapter 6

Spatial patterns of dose-response relationships between mercury and cortisol in the fur of river otter (*Lontra canadensis*)

Kristin M. Eccles[1], Philippe J. Thomas[2], and Hing Man Chan[1]

[1] Department of Biology, University of Ottawa, 30 Marie Curie, Ottawa, ON, K1N 6N5, Canada
[2] Science and Technology Branch, Environment and Climate Change Canada, National Wildlife Research Center, 1125 Colonel By Drive, Raven Road, Ottawa, ON K1A 0H3, Canada

This chapter is being prepared for submission to *Proceedings of the National Academy of Sciences of the United States of America*.

Author Contributions: KE conceived the idea, analysed the samples for mercury and cortisol, completed the statistical analysis, and wrote the manuscript. PT collected and prepared the samples and contributed to editing the manuscript. LC contributed to the conceptualization of the project and provided guidance on the implementation and editing of the manuscript.

Supplemental information for this chapter can be found in Appendix D

6.1 Abstract

Fur has been validated to non-invasively quantify exposures and biological responses in wildlife. Hg is known to act as an endocrine disruptor through altering brain neurochemistry, though the relationship between Hg and cortisol in wildlife is elusive. In this study, we use fur from river otter (*Lontra canadensis*) to quantify total Hg (THg) and cortisol and assess how this dose-response relationship changes over space. Geotagged fur samples were obtained from a wildlife biomonitoring program (n=72) and the North American Fur Auction (n=37) between 2014 and 2017. Fur THg was measured using a mercury analyser and fur cortisol was measured using an enzyme-linked immunosorbent assay (ELISA). The mean and standard deviation for fur THg was 11.50ug/g ± 12.40 ug/g and fur cortisol was 5.71pg/mg ± 8.24. Results from the ordinary least squares (OLS) regression show no relationship between fur cortisol and THg. However, both Hg and cortisol were heterogeneously distributed across the landscape. When a geographically weighted regression (GWR) was used to create localized regressions there was a positive relationship between fur THg and cortisol in Alberta and a negative relationship between fur THg and cortisol in Northern Ontario. We suggest this bidirectional relationship is associated with mercury exposure; in otters where fur THg exceed the fur screening guideline (15ug/g), the negative relationship is due to an inhibitory cortisol response. Conversely, in otters where fur THg is <15ug/g, the stress response functions normally. This highlights the need to consider spatial sampling locations when assessing dose-response relationships in wildlife across large geographical areas.

6.2 Introduction

Understanding the relationship exposure to contaminants and effects in free-ranging wildlife is a key part of understanding overall ecosystem health [1,2]. However, it is challenging to sample live animals to measure biomarkers of exposure and biological effects as accessing remote regions can be cost prohibitive. Live sampling can also be stressful for the animals leading to biases in results [3]. As a result, the use of non-invasive biomonitoring techniques including the analysis of fur, feathers, and eggs have become increasingly popular in wildlife ecotoxicology [4–6]. Specifically, fur samples can be collected non-invasively through barbed wire hair snags, opportunistically through monitoring and hunting activities, and historical samples can be obtained from archives, including private and public museum collections [3]. Non-invasive fur collections can provide a cost-effective and practical solution for assessing the impact of contaminant exposure in wildlife.

Fur serves as a detoxification pathway for contaminants and metabolites and can provide a long-term record of exposures and responses [3,7,8]. As contaminants are ingested, absorbed, and metabolized, the contaminants and biological responses produced through metabolism are incorporated into new hair growth via the root of the hair supplied with blood from the circulatory system [9]. As the hair grows, these biomarkers are bound into the keratin structure of hair producing a stable long-term record over a period of months in animals that moult [10]. Contaminant research shows that there is a strong correlation between the concentration of mercury (Hg) found in the fur and concentrations found in the blood and internal organs [11–13] (Chapter 3). This indicates that concentrations

measured in wildlife fur are reflective of the internal doses in different target organs.

Using fur from sentinel species can provide information on the health status of an individual and from this inferences can be made about the health of the ecosystem [14,15]. Using pelts with georeferenced harvest information provides researchers with the unique ability to spatially assess larger exposure datasets than were previously possible with more invasive methods. Further, spatial analyses supported by a geographic information system (GIS) provide the opportunity to assess patterns of exposures and biological responses in wildlife and quantity dose-response relationships across heterogeneous landscapes. Spatial assessments can also be used by policy makers and stakeholders to identify areas of potential concern when assessing the influence of a contaminant on an ecosystem. This can help to understand the spatial aspect of population health, and in the case of representative organisms, help to develop and implement regional regulations to protect human health.

River otters (*Lontra canadensis*) have been used as a sentinel species in freshwater ecosystems. Biomarkers measured in these species are reflective of the local environment due to their non-migratory and non-hibernating behaviour and small home range [14,16]. This species can also act as sentinels of human health since they are top predators with high year-round fish consumption [14,17]. Mercury (Hg) is a concern as it bioaccumulates in wildlife and biomagnifies up the food chain [18]. In its methylated form, Hg is a potent neurotoxin and is a contaminant of concern due to its impacts on the central nervous system, immune response, and endocrine system [4,19,20]. Using fur Hg as a biomarker of exposure is well established as the relationship with internal organs is well understood. A fur Hg screening of 15 ug/g was suggested as this is more protective against changes in

brain neurochemistry in river otter [13].

To date, there are few biomarkers of effect that can be measured non-invasively in fur. One established biomarker is hair cortisol, which assesses long-term (weeks/ months) stress in free-ranging wildlife [3,7]. Cortisol production and the adrenocortical stress response are necessary for survival, initiating the "fight or flight" response. Under normal conditions, when a stressful stimulus is experienced the hypothalamic-pituitary-adrenal (HPA) axis is activated through the release of a series of hormones. This produces the glucocorticoid cortisol, which is released into the bloodstream [21,22] and is consequently incorporated into hair follicles. Measuring circulating cortisol using concentrations found in fur has some advantages over short term biomarkers, such as blood cortisol since it is not subject to influence from the stress of capture [22,23]. Cortisol has been analysed in the fur to assess stress of free-range wildlife including caribou, reindeer, polar bear, black bear, grizzly bear, lynx, gray wolf, and primates [24]. A recent review by Koren et al. (2018) showed that there is good concordance between circulating serum cortisol and cortisol in fur in mammals. Cortisol has not been assessed in the fur of a river otter. There is evidence to suggest that Hg is an endocrine disruptor and since cortisol production is an endocrine-mediated process it is hypothesized that Hg can interfere with cortisol production [25,26]. However, the mechanisms of action that leads to Hg-related endocrine disruption, especially with respect to cortisol, is largely unknown [8,25,26].

Laboratory studies show that mercury is deposited in the pituitary of laboratory animals after mercury exposure in a dose-dependent [27]. Cultured male Sprague-Dawley rat adrenal cortical cells exposed to Hg found that low dose (10 μM) mercury chloride exposure

was not affected but at high doses (100 μM) corticosteroid production was inhibited [28]. Similarly, a study dosing catfish with methylmercury chloride found that, when compared to the control group, plasma cortisol levels were significantly decreased after 90 and 180 days of Hg exposure [29].

However, discrepancies exist regarding the strength and directional of the relationship between Hg and cortisol in the wild. A recent review by Tan et al (2009) cites that while the majority of research reports a negative relationship between cortisol and Hg, some studies report a positive relationship or no relationship [8,26,30]. Bechshoft et al. (2015) found a marginal relationship between Hg and cortisol in the fur of polar bear from the western Hudson Bay. This relationship was not significant in females. Wada et al. (2010) found no correlation between fur Hg and plasma cortisol in big brown bats. It is important to note that most research on the relationship between research on Hg and cortisol has been conducted in fish species, using plasma Hg and cortisol. These studies are susceptible to capture bias and are not able to be extrapolated to mammalian systems with a high degree of confidence [26].

The objective of this study is to investigate the effectiveness of fur cortisol as a biomarker of effect in relations to mercury exposure in free-ranging river otter. Further, we use geographic information systems (GIS) and spatial methods to assess spatial patterns of this dose-response relationship. To investigate the spatial heterogeneity of the dose-response relationships we compare a traditional non-spatial ordinary least squares (OLS) regression with a spatial geographically weighted regression (GWR) model. We hypothesize that fur Hg and cortisol biomarkers will exhibit spatial heterogeneity and as a result, the

relationship between the two variables will also exhibit spatial heterogeneity. Therefore, the GWR will provide a more statistically rigorous method of assessing the dose-response relationship.

6.3 Methods

6.3.1 Sample Collection

Samples were obtained from two different programs. The first set of samples (n=73) were collected as part of a biomonitoring program and were collected in the Northwest Territories (Figure 6.1A) and the Athabasca Oil Sands Region in Northern Alberta (Figure 6.1B) between 2014 and 2017. These samples have more available information such as sex. The second set of samples (n=37) were obtained from the North American Fur Auction (NAFA) conducted in Toronto, Ontario between 2014 and 2017. Animals trapped for the commercial fur trade are trapped as adults between 2-4 years of age. Topcoat fur samples were collected from the fore or hind limb region and approximately 10 mg were subsampled for analysis. These fur samples are geolocated and were checked for validity using GoogleEarth. Samples that were geolocated in urban centers were removed (n=4). Fur auction samples originated from Ontario, Quebec (Figure 6.1C) and Nova Scotia (Figure 6.1D).

6.3.2 Cortisol Analysis

The top coat fur was analysed for cortisol using the procedure described in Davenport et al. (2006) [7] and Macbeth et al., (2010) [3]. To remove any surface contamination,

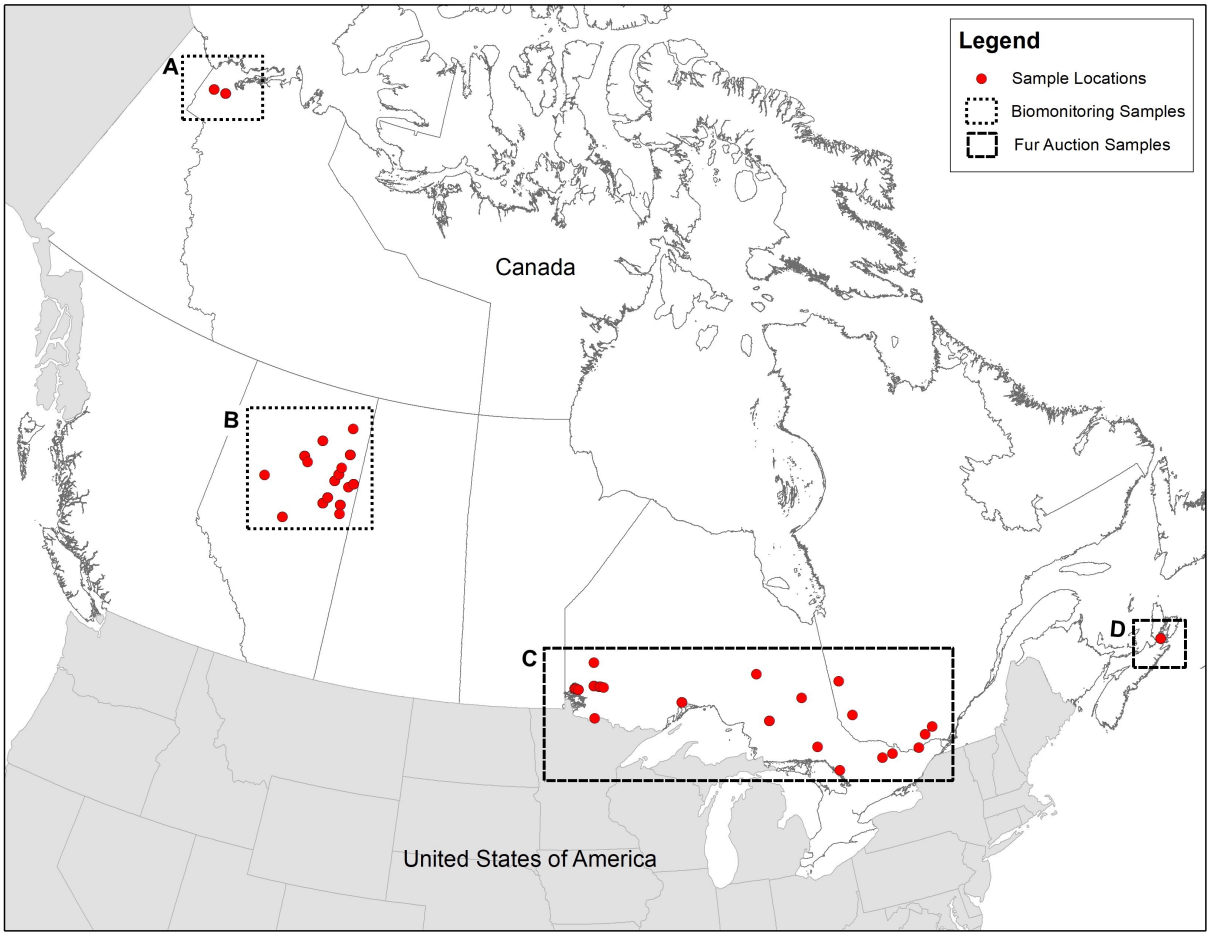

Figure 6.1: Overview of fur sample locations used in this analysis.

fur samples were washed three times in 2 mL of methanol for 3 min/wash using a slow rotator (Haematology and Chemistry Mixer 346; Fisher Scientific, Ottawa, ON, Canada). The solvent wash is an effective method of removing external cortisol without extracting cortisol from the internal hair shaft [32]. After the methanol wash, samples were dried for 24 hours at room temperature and then the decontaminated samples were ground to a powder using a Mixer Mill (Retsch, Inc., Newtown, PA; 30 Hz; 10-ml stainless-steel grinding jars; single 12-mm stainless-steel grinding ball). Between 5-25mg of ground fur was used to extract cortisol. Cortisol from the ground samples was extracted into 0.5 mL of methanol using a slow rotator (Haematology and Chemistry Mixer 346; Fisher Scientific,

Ottawa, ON, Canada) for a 24-hour period. The samples were vortexed and centrifuged to extract the supernatant which was then dried under nitrogen gas at 38°C. This procedure was completed two additional times using 0.5 ml of fresh methanol. The dried extract was reconstituted in 0.2 ml of phosphate buffer for 12 hours. Samples were run in duplicates of 50 ml aliquots using an enzyme-linked immunoassay kit (Oxford EA-65 Cortisol EIA kit; Oxford Biomedical, Lansing, MI). The cross-reactivity of the antibody used in the cortisol kit is as follows: cortisol (100%), prednisolone (66.9%), 11-deoxycortisol (58.1%), cortisone (15.9%), prednisone (13.7%), 17-hydroxyprogesterone (5.4%), and deoxycorticosterone (0.94%), as reported by the manufacturer. The intra-assay and inter-assay coefficients of variation (CV) were 4.8% and 26%, respectively. Samples that did not meet quality assurance-quality control (QA/QC) metrics were removed from the analysis. Cortisol concentrations are reported as pg of cortisol/mg of ground fur. The limit of detection of the EIA kit was 0.005 ng/ml which corresponds to approximately 0.04 pg cortisol/mg hair in a ground 25 mg hair sample.

6.3.3 Mercury Analysis

Approximately 10-25mg of top coat fur was subsampled for analysis. Samples were analysed using a direct thermal decomposition Hg analyser (Mercury Analyser 3000; Nippon Instruments North America). QA/QC measures included blank samples, standard reference material (IAEA 085, DORM-4, and DOLT-5 from National Research Council of Canada), and 10% of fur samples run in duplicate. The CV <5%. All Hg measurements are reported in μg/g fur weight total Hg (THg).

6.3.4 Statistical Analysis

The biomonitoring data were used to assess if sex differences exist between the total Hg (THg) and cortisol using a t-test. Due to the non-normal distribution of the data, measured cortisol and THg were log base10 transformed. However, since the assumption of equal variance between groups was violated, a Welch's two-sample t-test was used to assess if there was a difference in the median cortisol and THg concentrations between the two sexes. Then an analysis of variance (ANOVA) was conducted on the whole dataset to determine if there was a difference in measured cortisol and total Hg between locations. The data were grouped by provinces for ease and policy relevance. ANOVA assumptions were tested for residual normality and homogeneity.

First, an ordinary least squares (OLS) regression model was used to assess the non-spatial relationship between log fur THg and log fur cortisol. Human impact was also included as a predictor in the OLS regression model and was used as an underlay in mapping. This layer is a composite of all human disturbances to the land in Canada including settlements, roads, rail roads, industrial activities, and hydro corridors [33]. Since river otter fur THg data are geolocated to a trapline, a spatial averaging method was used to calculate an average human disturbance score using a 9km radius area around the trapline centroid. This 9km radius area was selected based on observed radio collar home ranges of wild river otter to account for animal movement [17,34]. In significant models, the model residuals were tested for residual normality, no serial autocorrelation, homogeneity, and linearity.

A geographically weighted regression (GWR) was used to assess the spatial relationship between fur log THg and fur log cortisol. This method classifies the study area into local neighbourhoods of influence through the development and use of a spatial weights matrix (SWM). In this analysis, the SWM was developed using a fixed Gaussian distance where the distance was selected using a data-led Akaike Information Criterion (AIC) optimization method. One localized regression is conducted per local neighbourhood, thus the number of samples in the global dataset is the same as the number of local regressions performed. Each local regression has its own model summary (e.g. beta coefficients, R2, etc.), thus the GWR model output is an averaged summary of all models. Since a GWR does not require the relationship (beta coefficient) to be stationary over the study area, it can produce more accurate regression coefficient estimates when compared to an OLS regression. This is demonstrated using an ANOVA comparing the residual sum of square errors between the global OLS regression and the GWR [35].

A second OLS regression model was developed based on GWR results and uses the screening guideline of 15 ug/g THg in fur that we proposed earlier. In this regression, we considered low Hg exposure as < 15ug/g and high Hg exposure as > 15ug/g. The low and high groups were run separately. In significant models, the model residuals were tested for residual normality, no serial autocorrelation, homogeneity, and linearity.

All aspatial statistical analyses were completed in R 3.5.2 [36] using the car [37], and lmtest [38] packages. The GWR was completed in GWR4.0 [39] and mapping was completed in ArcGIS 10.6.1 [40].

6.4 Results

A summary of the THg and cortisol data are shown by province in Table 6.1. Nova Scotia and the Northwest Territories had the highest median cortisol concentrations while Ontario had the lowest levels. Conversely, the highest median mercury concentrations were measured in Ontario, and the lowest was measured in Alberta and Nova Scotia. The measured fur THg concentrations are spatially mapped in three regions: (A) Oil Sands region, Alberta, (B) Inuvik, Northwest Territories, and (C) Ontario, Quebec, and Nova Scotia (Figure 6.2). Mapped results demonstrate a spatial heterogeneity, which means the concentrations of Hg and cortisol are unevenly distributed over space. Fur THg concentrations are below the 15 μg/g fur Hg screening guideline for fur-bearing mammals in most samples in Alberta, Quebec, and Nova Scotia. Conversely, in northern Ontario, most of the samples are above the 15 μg/g fur screening guideline as indicated by the yellow, orange, and red markers on the map (Figure 6.2). Fur cortisol concentrations are higher in Alberta, Quebec, and Nova Scotia with increasing cortisol concentrations closer to areas with higher human impact. Conversely, in Ontario, there are low concentrations of fur cortisol, as indicated by the light red circles (Figure 6.3).

The provincial differences were statistically assessed using an ANOVA. Results indicate the differences in the mean values of log THg ($F_{(4,109)}$= 23.08, p= 7.8e-14) and cortisol ($F_{(4,109)}$=4.92, p= 0.001) in each province is statistically different. The corresponding boxplot is shown in Figure 6.4 A and B respectively. The Tukey follow up test and corresponding plot can be seen in Appendix D Figure D.1 and Appendix D Table D.1 for THg

Table 6.1: Summary of total mercury (μg/g) and cortisol (pg/mg) in fur of river otters by province.

Province	Alberta	Nova Scotia	Northwest Territories	Ontario	Quebec	All
Cortisol (pg/mg)						
Mean	4.91	14.52	14.2	4.13	5.07	5.63
SD	8.7	13.11	5.98	4.97	0.79	8.24
Median	2.8	11.34	17.7	2.68	5.25	3.35
Min	0.03	3.84	6.07	0.14	3.96	0.03
Max	68.55	31.58	19.48	23.23	5.97	68.55
THg (μg/g)						
Mean	6.07	5.84	12.57	27.53	9.46	11.5
SD	3.49	2.9	7.7	16.32	6.3	12.4
Median	5.16	5.08	11.71	24.45	6.74	6.59
Min	1.13	3.43	3.53	3.09	3.35	1.13
Max	16.4	9.75	25.49	65.77	17.6	65.8
n	73	4	7	26	5	115

and Appendix D Figure D.2 and Appendix D Table D.2 for cortisol. This provides statistical evidence of spatial heterogeneity of measured fur THg and cortisol concentrations. A t-test on the subset of data with sex information demonstrates there was no differences in the mean fur log THg (t=-0.64, df=44, p=0.52) and was no differences in the mean fur log cortisol (t=-0.28, df=37, p=0.78) between males and females (Figure 6.5).

A t-test on the subset of data with sex information demonstrates there is no differences in the mean fur log THg (t=-0.64, df=44, p=0.52) and is no differences in the mean fur log cortisol (t=-0.28, df=37, p=0.77) between males and females (Figure 6.5).

Table 6.2: Summary of linear regression model between log THg and log cortisol in the fur of river otters.

	Estimate	Std. Error	P-value
Intercept	0.45	0.13	0.0009
Log fur THg	-0.0006	0.13	0.99
P-value	0.99		
DoF	113		
Adj. R^2	-0.009		

Using the whole dataset, the dose-response relationship between log THg and log cor-

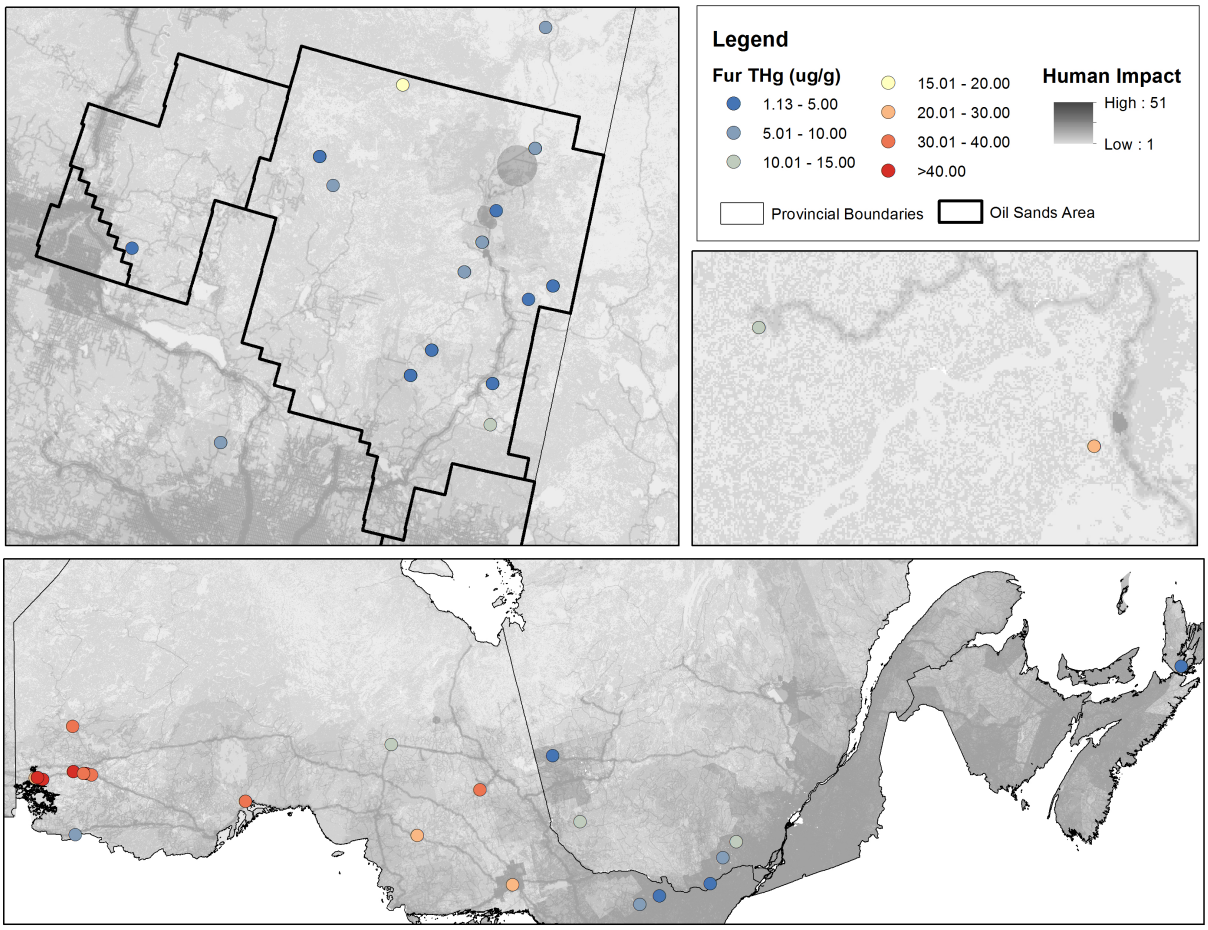

Figure 6.2: Measured fur THg (μg/g) concentrations in (A) Oil Sands region, Alberta, (B) Inuvik, Northwest Territories, and (C) Ontario, Quebec, and Nova Scotia. Concentrations below the fur mercury screening guidelines (<15 μg/g) are represented in cool colours (blue and green). Concentrations above the fur Hg screening guideline (>15 μg/g) are represented in warm colours (red and yellow). These data are overlaid on a human impact layer where darker grey indicate regions that have a higher human disturbance [28].

tisol was assessed using a global OLS regression. Regression results indicate there is no relationship between these two variables when analysed independently of spatial location (Table 2 and Figure 6A). Mapped results from the GWR use the t-value of the beta coefficient is used to summarize the significance and direction of the relationship (Figure 6.6). This highlights the dichotomy in the significance and direction of log THg as a predictor. In Alberta, log cortisol and log THg have a positive relationship, as indicated by the red

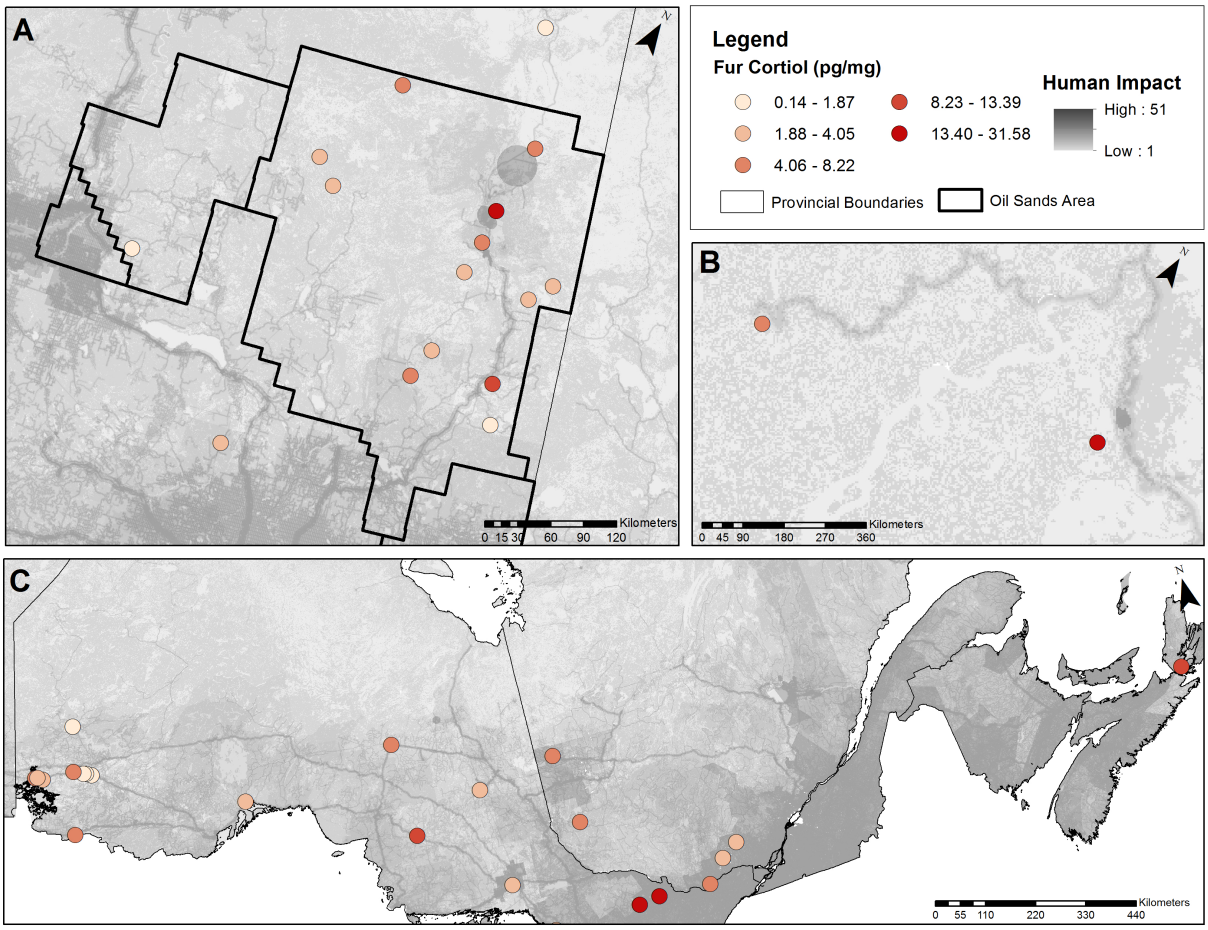

Figure 6.3: Measured fur cortisol (pg/mg) concentrations in (A) Oil Sands region, Alberta, (B) Inuvik, Northwest Territories, and (C) Ontario, Quebec, and Nova Scotia. Concentrations are represented in continuous scale where low fur cortisol concentrations are light red and high fur cortisol concentrations are dark red. These data are overlaid on a human impact layer where darker grey indicate regions that have a higher human disturbance [28].

circles (Figure 6.6A), but only a small portion of the variance (<10%) is explained by this relationship (Figure 6.6B). Conversely, in Ontario, the log cortisol and log THg have a negative relationship, as indicated by the blue circles (Figure 5A), and a higher amount of variance (>28%) is explained by this relationship than by OLS analysis alone (Figure 6.6B). This regression was not significant in other regions, such as the Northwest Territories and Nova Scotia. This is also evident in the GWR results, which summarizes all the regression models (Table 6.3), as the beta coefficient for log THg has a minimum of

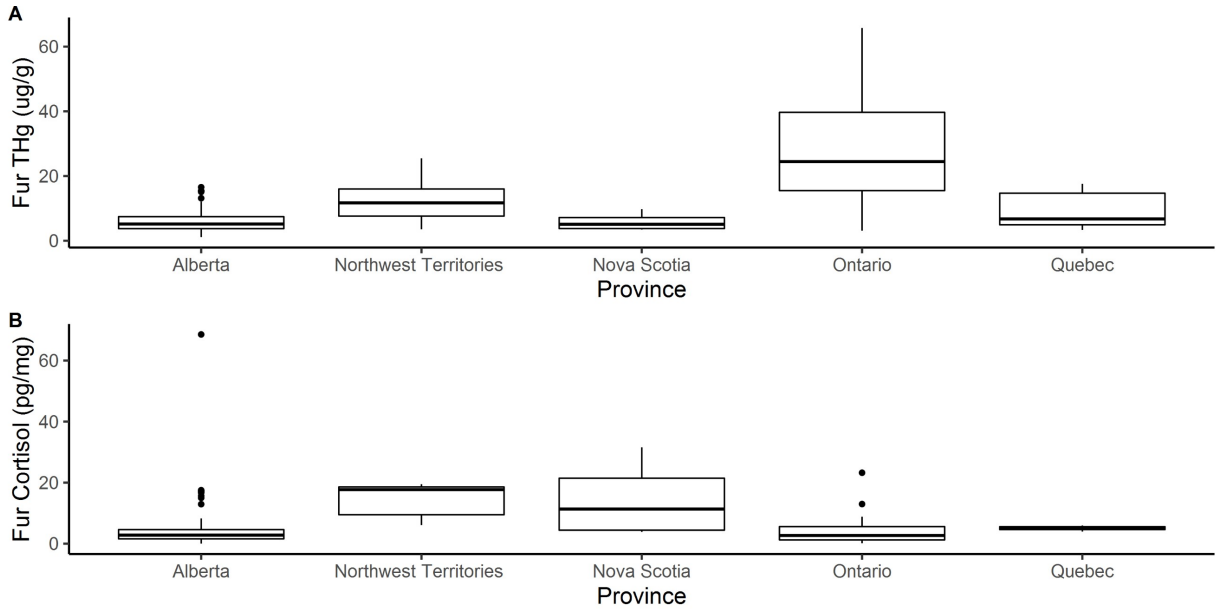

Figure 6.4: Boxplots showing (A) the difference in measured fur THg by province and (B) the difference in measured fur cortisol by province.

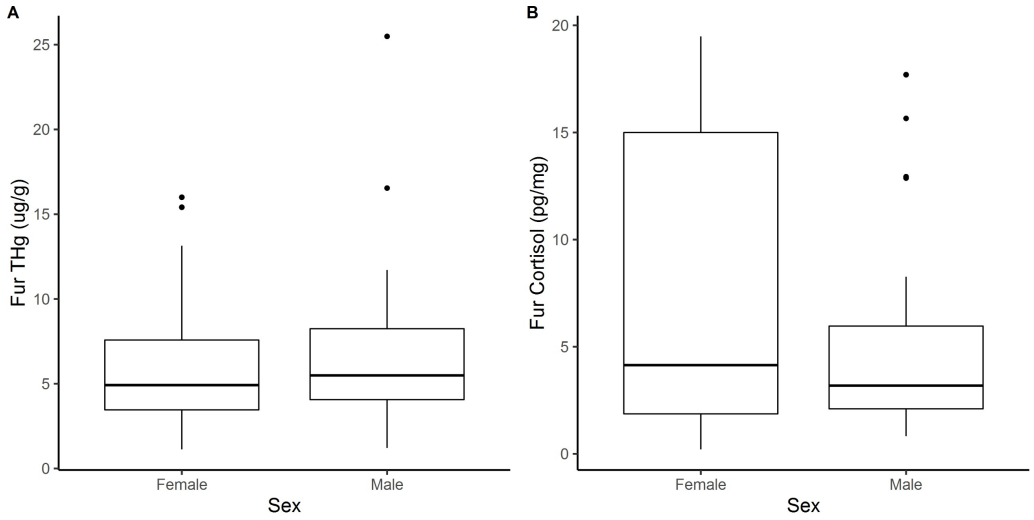

Figure 6.5: Boxplots showing (A) the difference in measured fur THg and (B) the difference in measured fur cortisol between sexes.

-0.82 and a maximum of 0.48. Further, results from the ANOVA show the GWR model significantly reduces the sum of the squares of errors which indicates the GWR model is a better fit than the global OLS model (F= 4.71, p=0.011). Over the study area, the R2 of each local regression in the GWR ranges from 0.008-37% variance explained, with an

average of 19% variance explained (Pseudo R^2) (Table 6.3).

Table 6.3: Summary of GWR results between measured log THg and measured log cortisol in the fur of river otter.

Variable	Mean	SD	Min	Max
Intercept	0.45	0.52	0.02	1.45
Log THg	0.11	0.46	-0.79	0.51
GWR ANOVA				
	Sum of Square	DoF	MS	F-value
Global Residuals	37.4	2		
GWR Improvement	9.28	7.52	1.24	
GWR Residuals	28.12	107.48	0.26	4.72
Global Adj R^2	-0.02			
GWR Pseudo R^2	0.18			

Based on the results from the GWR, the global OLS regression was rerun using 15ug/g as a cut off to designate a low and high THg exposure group (Figure 6.7B). In the low THg exposure group, there was a significant positive relationship with log cortisol which explained 5% of the variance. In the high THg exposure group, there was a significant negative relationship with log cortisol that explained 35% of the variance (Table 6.4). Further, the covariate human disturbance was added to the regression model. In the low exposure group, human disturbance was positively associated with log cortisol. Together these predictors explained 10% of the variance in log cortisol. Conversely, in the high exposure group, human influence did not have a significant relationship with log cortisol (Table 6.5).

6.5 Discussion

This is the first paper to report concentrations of fur cortisol in river otter and to use cortisol as a biomarker of effect in this sentinel species. The concentrations of cortisol we

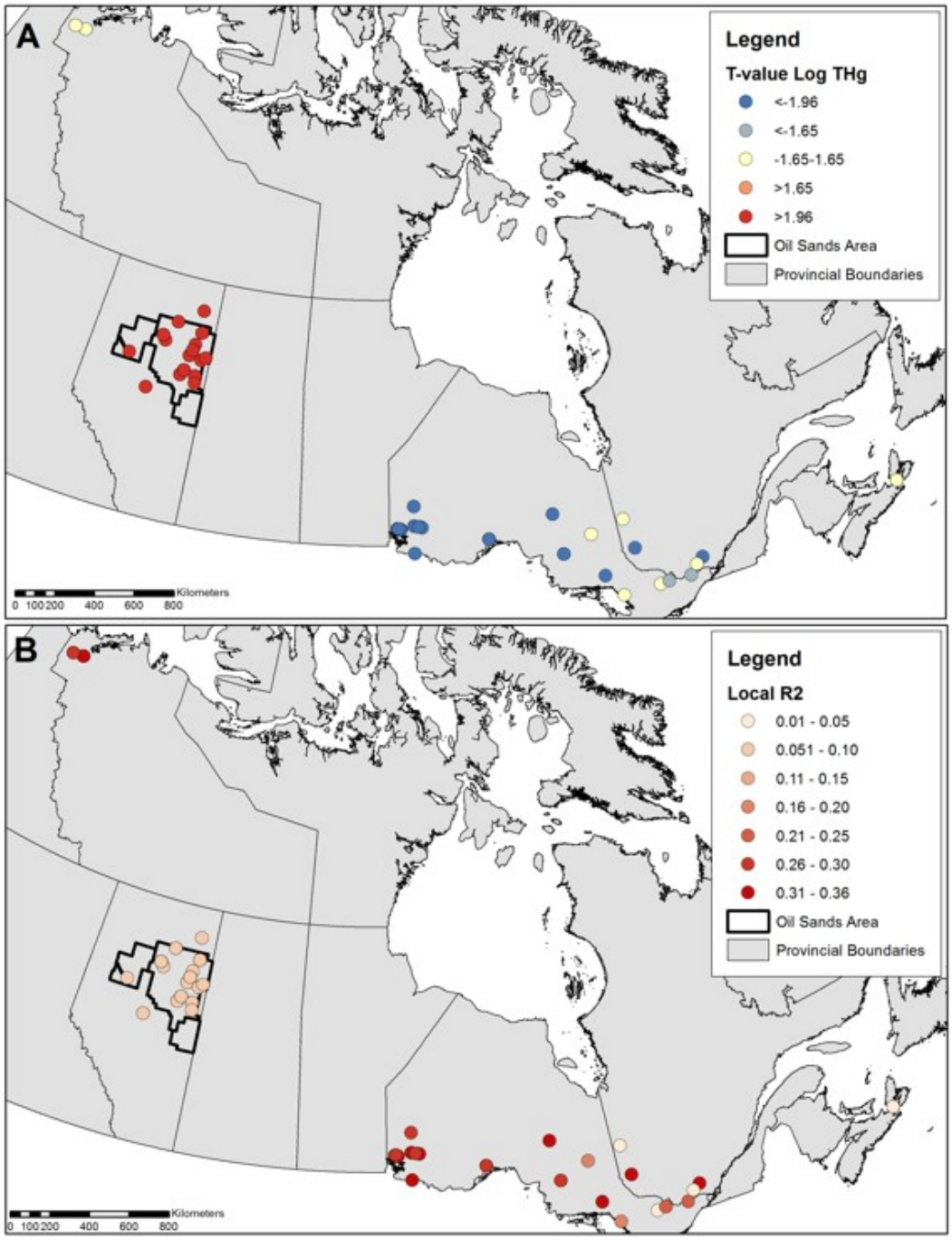

Figure 6.6: (A) T-value of the beta coefficient for log THg when regressed using log cortisol as the dependent variable. Blue circles represent a statistically significant (α=0.05) negative relationship. Red circles represent a statistically significant (α=0.05) positive relationship. Yellow circles are not statistically significant. (B) Circles represent the local R^2 value of each regression. Darker shades of red circles indicate a higher percentage of variance explained by log THg within the positive relationship.

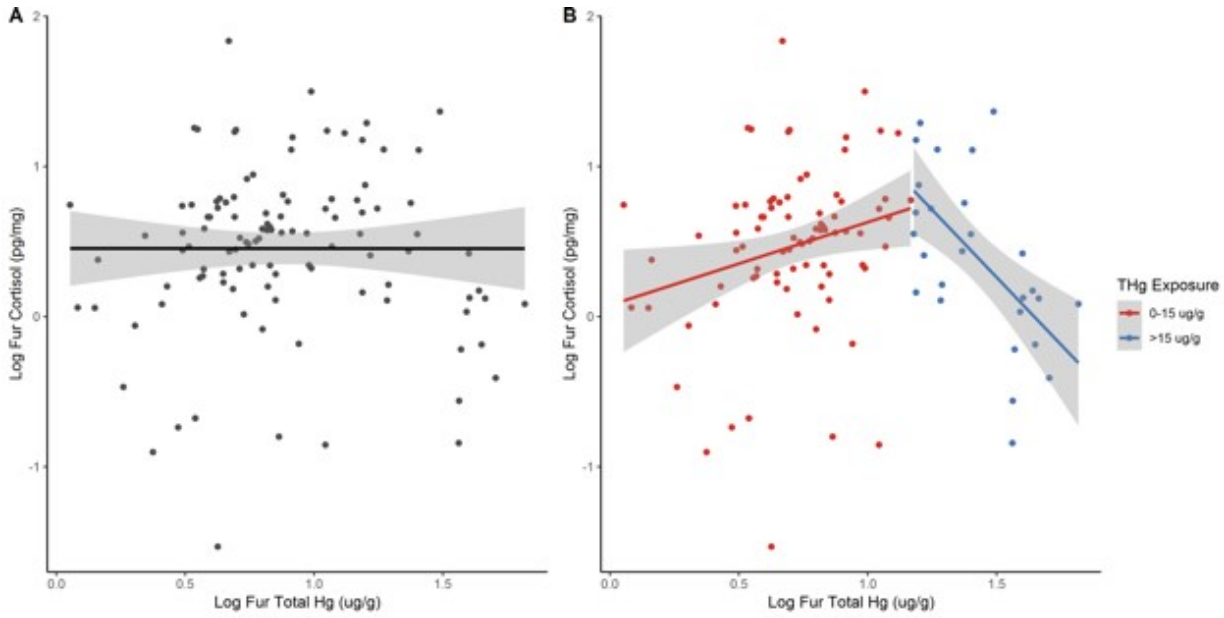

Figure 6.7: (A) Scatterplot showing the OLS regression relationship between log fur THg and log cortisol with a global regression line. (B) Scatterplot showing the amended OLS regression relationship between log fur THg and log cortisol with a regression splitting fur THg into two categories, 0-15μg/g (low exposure) and >15 μg/g (high exposure).

Table 6.4: OLS regression between log fur THg and log cortisol when fur THg is split into two categories, 0-15μg/g (low exposure) and >15 μg/g (high exposure).

	Low (0-15 μg/g)			High (>15μg/g)		
	Estimate	Std. Error	P-value	Estimate	Std. Error	P-value
Intercept	0.08	0.18	0.68	2.96	0.65	0.0001
Log fur THg	0.55	0.25	0.03	-1.8	0.46	0.000004
P-value	0.027			0.0005		
DoF	85			26		
Adj. R^2	0.045			0.35		

report in this study 5.63 pg/mg (range 0.03-68.55 pg/mg) are similar in comparison with ranges reported in other carnivores, such as grizzly bear (0.62–43.33 pg/mg) [3] and gray wolf (4.8–40.4 pg/mg) [41], but were higher than polar bears (males: 0.2-5.8 and females: 0.2-5.1) [8]. We found no sex differences in fur Hg and cortisol concentrations in river otters. Similarly, other studies reported no sex difference in contaminant burdens in river otter [12,42] and in cortisol concentrations in other mammal species [8,43]. This may be

Table 6.5: OLS regression between log fur THg and log cortisol with human influence as a covariate, when fur THg is split into two categories, 0-15μg/g (low exposure) and >15 μg/g (high exposure).

	Low (0-15 μg/g)			High (>15μg/g)		
	Estimate	Std. Error	P-value	Estimate	Std. Error	P-value
Intercept	-0.11	0.19	0.57	2.97	0.66	0.0001
Log fur THg	0.54	0.24	0.03	-1.72	0.48	0.001
Human Influence	0.032	0.013	0.02	-0.014	0.024	0.56
P-value	0.005			0.002		
DoF	84			25		
Adj. R^2	0.1			0.33		

due to the non-territorial and social nature of river otters [44]. The lack of sex differences in these biomarkers in the fur river otter supports the use of fur as a non-invasive biomarker, even when the information on the sex of the animal is not available.

This was also the first study to use a GWR to assess the heterogeneous relationship between dose-responses in free-ranging wildlife. Results from the global OLS regression model presented in this paper indicated there is no dose-response relationship between log THg and log cortisol measured in the fur of river otters. In contrast, the GWR results showed there was a statistically significant dose-response relationship that varies spatially. These results showed the importance of modelling geographically diverse data using appropriate methods that take spatial properties of data into consideration. When spatial properties of data, such as spatial heterogeneity, are not considered the coefficient estimate may be biased due to the heterogeneous error distribution of the model [45]. A more serious consequence of not accounting for the spatial properties of data is the failure to detect a significant relationship, which happened in the OLS regression in this research [35]. This highlights the need to consider spatial sampling location in studies assessing the influence of contaminant exposure on wildlife health in large geographical sampling areas.

The mapped results of biomarker concentrations in conjunction with the GWR results support the development of a hypothesis the relationship between Hg exposure and inhibition of cortisol production is dose dependent; at low fur THg concentrations have a positive relationship with cortisol and high fur THg concentrations have a negative relationship cortisol. In this study, we tested this hypothesis by classifying samples THg into low fur THg (<15ug/g) or high fur THg (>15ug/g) based on the results of our previous fur screening study [13]. This screening guideline was set based on the lowest observable effects in the change of brain neurochemistry in mink and river otter [13,46].

Considerably more research has been conducted in fish and bird on the relationship between Hg and cortisol than has been conducted in mammals [8,26,47]. However, the HPA axis is conserved across vertebrate species [48] and the main glucocorticoid stress hormone produced in birds is corticosterone. In avian research, Hg has been shown to both promote and inhibit the stress response [30,47,49]. Franceschini et al., (2009) found a negative relationship between corticosterone and blood Hg and egg Hg in tree swallows but a positive relationship between feather Hg and feather corticosterone. This may be due to the long temporal scale and integrated nature of exogenous biomarkers [30]. Further, the bidirectional relationship between Hg and cortisol observed in this study suggests that this relationship is complex and may be mediated by environmentally specific conditions including co-exposure to other contaminants [47]. Our research provides field evidence of a complex bidirectional relationship between Hg and cortisol in a mammalian species.

The negative relationship observed between THg and log cortisol measured in Ontario may be due to Hg-induced changes in brain neurochemistry affecting the HPA axis and

stress response. Hg is a potent neurotoxin that easily crosses the blood-brain barrier. In the brain, mercury has a high affinity for sulfur-rich thiol groups and can interfere with neurochemical signalling pathways [50]. Hg related changes in the brain neurochemistry have been reported in river otter and mink [51,52]. In those studies, the authors found negative correlations between Hg and cholinergic muscarinic acetylcholine (mACh) receptor level and dopamine-2 (D2) levels in the cerebral cortex [51,52]. Similarly, a negative relationship between NMDA receptor levels and Hg has been observed in mink and polar bears [53,54]. Accumulation rates in specific regions of the brain have not been quantified for river otter. However, other mammals report the highest concentrations of mercury in the pituitary gland, which is the site of ATCH secretion [8,55,56]. This could explain the negative relationship observed in this study in only high mercury exposure. More research is needed to better understand the phenotypic consequence of impairing cortisol synthesis and secretion through the KEGG pathway and its relationship with Hg.

The positive relationship observed between log THg and log cortisol measured in Alberta may be the result of mercury acting as a stressor. However, many chemicals can have an effect on the endocrine system including polycyclic aromatic hydrocarbons (PAH) [25]. Our results suggest that Hg may be acting as a proxy for the exposure to a suite of other factors that can induce a stress response, including anthropogenic activity or chemical co-exposure [26]. This positive relationship was observed in the Alberta Oil Sands. This region has the third largest reserve of crude oil in the world and rates of production are approximately 1.3 million barrels of crude oil per day [57]. The area is well documented to be elevated in trace elements, heavy metals and other persistent organic pollutants (POPs

such as PAHs) [58]. Additionally, there are a variety of land disturbances in the area, including industrial facilities, roads, and seismic lines, which has shown to have an impact on wolf and caribou in the region [59]. Wasser et al., (2011) found a change in glucocorticoids in the scat of wolf and caribou in response to human disturbance. Similarly, in our regression model, human influence was also a significant predictor explaining 10% of the variance in cortisol together with Hg.

Our results showing the inhibition of cortisol at high concentrations of Hg exposure using a non-invasive biomarker medium is the beginning of a promising new area for research in environmental assessments on the effects of chemicals on free-ranging wildlife. Future work can incorporate advanced quantitative techniques, such as metabolomics, to produce more robust response data to develop quick, accurate, and cost-effective methods for assessing complex responses. Metabolomics has been successfully completed in human hair [60–62] and in mice fur [63]. This response data can also with exposure data measured in hair using a non-targeted approach [64]. A developed ecotoxicological dataset comprised of multiple exposures and responses will enable the assessment of geospatial patterns of exposure and response data to identify patterns and environmental variables associated with the observed dose-response relationships.

6.6 Data availability

Data is available upon request from the authors. R code used in these analyses can be found at: `https://github.com/kristineccles/dose_reponse.git`

6.7 Acknowledgments

The authors wish to acknowledge the Alberta Trappers' Association (Westlock, Alberta), Mr. Reed Gauthier (Plamondon, Alberta), and Treaty 8 First Nations including Mikisew Cree First Nation, Athabasca Chipewyan First Nation, and Fort Mackay First Nation, and the Metis nations for all the help and support with sample collection, site access and local ecological knowledge that made this study possible. We also acknowledge Dr. David Janz and Luciene A Kapronczai for their support with the cortisol method and to E. Yumvihoze for laboratory support. We acknowledge funding support from the Canada Research Chair Program and the National Sciences and Engineering Research Council Discovery Grant to H.M. Chan; the National Sciences and Engineering Research Council Collaborative Research and Training Experience Program, Research in Environmental and Analytical Chemistry and Toxicology to K.M. Eccles; and Environment and Climate Change Canada, the province of Alberta, and the Canada-Alberta Joint Oil Sands Monitoring Program to P. J. Thomas.

6.8 References

1. J Kendall R. 2016. Wildlife Toxicology: Where We Have Been and Where We Are Going. J. Environ. Anal. Toxicol. 6:1–9.

2. Rattner BA. 2009. History of wildlife toxicology. Ecotoxicology. 18:773–783.

3. Macbeth BJ, Cattet MRL, Stenhouse GB, Gibeau ML, Janz DM. 2010. Hair cortisol concentration as a noninvasive measure of long-term stress in free-ranging grizzly bears (Ursus arctos): considerations with implications for other wildlife. Can. J. Zool. 88:935–949.

4. Wolfe MF, Schwarzbach S, Sulaiman RA. 1998. Effects of mercury on wildlife: A comprehensive review. Environ. Toxicol. Chem. 17:146–160.

5. Lodenius M, Solonen T. 2013. The use of feathers of birds of prey as indicators of metal pollution. Ecotoxicology. 22:1319–1334.

6. Evers DC, Han Y-J, Driscoll CT, Kamman NC, Goodale MW, Lambert KF, Holsen TM, Chen CY, Clair T a., Butler T. 2007. Biological Mercury Hotspots in the Northeastern United States and Southeastern Canada. Bioscience. 57:29–43.

7. Davenport MD, Tiefenbacher S, Lutz CK, Novak MA, Meyer JS. 2006. Analysis of endogenous cortisol concentrations in the hair of rhesus macaques. Gen. Comp. Endocrinol. 147:255–261.

8. Bechshoft T, Derocher a. E, Richardson E, Mislan P, Lunn NJ, Sonne C, Dietz R, Janz DM, St. Louis VL. 2015. Mercury and cortisol in Western Hudson Bay polar bear hair. Ecotoxicology. 24:1315–1321.

9. Wang F, Lemes M, Khan MAK. 2012. Metallomics of mercury: role of thiol and selenol-containing biomolecules. In Liu, G, Cai, Y and O'Driscoll, N, eds, Environ. Chem. Toxicol. Mercur. John Wiley & Sons, Inc., Hoboken, NJ, pp 517–544.

10. Kempson IM, Lombi E. 2011. Hair analysis as a biomonitor for toxicology, disease and health status. Chem. Soc. Rev. 40:3915–3940.

11. Carrier G, Bouchard M, Brunet RC, Caza M. 2001. A Toxicokinetic Model for Predicting the Tissue Distribution and Elimination of Organic and Inorganic Mercury Following Exposure to Methyl Mercury in Animals and Humans. II. Application and Validation of the Model in Humans. Toxicol. Appl. Pharmacol. 171:50–60.

12. Klenavic K, Champoux L, Mike O, Daoust PY, Evans RD, Evans HE. 2008. Mercury concentrations in wild mink (Mustela vison) and river otters (Lontra canadensis) collected from eastern and Atlantic Canada: Relationship to age and parasitism. Environ. Pollut. 156:359–366.

13. Eccles KM, Thomas PJ, Chan HM. 2017. Predictive meta-regressions relating mercury tissue concentrations of freshwater piscivorous mammals. Environ. Toxicol. Chem. 36:2377–2384.

14. Basu N. 2012. Piscivorous mammalian wildlife as sentinels of methylmercury exposure and neurotoxicity in humans. Methylmercury Neurotox., pp 357–370. doi:10.1007/978-1-46142383-6.

15. Basu N, Scheuhammer AM, Bursian SJ, Elliott J, Rouvinen-Watt K, Chan HM. 2007. Mink as a sentinel species in environmental health. Environ. Res. 103:130–144.

16. Evers DC, Mason RP, Kamman NC, Chen CY, Bogomolni AL, Taylor DL, Hammerschmidt CR, Jones SH, Burgess NM, Munney K, Parsons KC. 2008. Integrated mercury monitoring program for temperate estuarine and marine ecosystems on the North American Atlantic coast. Ecohealth. 5:426–441.

17. Reid DG, Code TE, Reid ACH, Herrero SM. 1994. Food habits of the river otter in a boreal ecosystem. Can. J. Zool. 72:1306–1313.

18. Driscoll CT, Mason RP, Chan HM, Jacob DJ, Pirrone N. 2013. Mercury as a global pollutant: Sources, pathways, and effects. Environ. Sci. Technol. 47:4967–4983.

19. Chan HM, Scheuhammer AM, Ferran A, Loupelle C, Holloway J, Weech S. 2003. Impacts of Mercury on Freshwater Fish-Eating Wildlife and Humans. Hum. Ecol. Risk Assess. An Int. J. 9:867–883.

20. Ha E, Basu N, Bose-O'Reilly S, Dórea JG, McSorley E, Sakamoto M, Chan HM. 2017. Current progress on understanding the impact of mercury on human health. Environ. Res. 152:419–433.

21. Sheriff MJ, Dantzer B, Delehanty B, Palme R, Boonstra R. 2011. Measuring stress in wildlife: Techniques for quantifying glucocorticoids. Oecologia. 166:869–887.

22. Russell E, Koren G, Rieder M, Van Uum S. 2012. Hair cortisol as a biological marker of chronic stress: Current status, future directions and unanswered questions. Psychoneuroendocrinology. 37:589–601.

23. Cattet M, Macbeth BJ, Janz DM, Zedrosser A, Swenson JE, Dumond M, Stenhouse GB. 2014. Quantifying long-term stress in brown bears with the hair cortisol concentration: A biomarker that may be confounded by rapid changes in response to capture and handling. Conserv. Physiol. 2:1–15.

24. Koren L, Bryan H, Matas D, Tinman S, Fahlman Å, Whiteside D, Smits J, Wynne-Edwards K. 2018. Towards the validation of endogenous steroid testing in wildlife hair. J. Appl. Ecol. 56:547–561.

25. Matthiessen P, Wheeler JR, Weltje L. 2018. A review of the evidence for endocrine disrupting effects of current-use chemicals on wildlife populations. Crit. Rev. Toxicol. 48:195–216.

26. Tan SW, Meiller JC, Mahaffey KR. 2009. The endocrine effects of mercury in humans and wildlife. Crit. Rev. Toxicol. 39:228–269.

27. Zhu X, Kusaka Y, Sato K, Zhang Q. 2000. The endocrine disruptive effects of mercury. Environ. Health Prev. Med. 4:174–183.

28. Ng TB, Liu WK. 1990. Toxic effect of heavy metals on cells isolated from the rat adrenal and testis. Vitr. Cell. Dev. Biol. 26:24–28.

29. Kirubagaran R, Joy KP. 1991. Changes in adrenocortical-pituitary activity in the catfish, Clarias batrachus (L.), after mercury treatment. Ecotoxicol. Environ. Saf. 22:36–44.

30. Franceschini MD, Lane OP, Evers DC, Reed JM, Hoskins B, Romero LM. 2009. The corticosterone stress response and mercury contamination in free-living tree swallows, Tachycineta bicolor. Ecotoxicology. 18:514–521.

31. Wada H, Yates DE, Evers DC, Taylor RJ, Hopkins WA. 2010. Tissue mercury concentrations and adrenocortical responses of female big brown bats (Eptesicus fuscus) near a contaminated river. Ecotoxicology. 19:1277–1284.

32. Kroshko T, Kapronczai L, Cattet MRL, Macbeth BJ, Stenhouse GB, Obbard ME, Janz DM. 2017. Comparison of methanol and isopropanol as wash solvents for determination of hair cortisol concentration in grizzly bears and polar bears. MethodsX. 4:68–75.

33. Canadian Wildlife Services. 2016. Anthropogenic Influence Layer Model 1.0.

34. Haan DM, Halbrook RS. 2015. Home Ranges and Movement Characteristics of Minks in East-central New York. Am. Midl. Nat. 174:302–309.

35. Fotheringham AS, Charlton M, Brunsdon C. 1998. Geographically weighted regression: a natural evolution of the expansion method for spatial data analysis. Environ. Plan. A. 30:1905–1927.

36. R Core Development Team. 2017. R: A Language and Environment for Statistical Computing.

37. Fox J, Weisberg S. 2011. An R Companion to Applied Regression.

38. Zeileis A, Hothorn T. 2002. Diagnostic Checking in Regression Relationships. R News. 2:7–10.

39. Nakaya T, Fotheringham AS, Brunsdon C, Charlton M. 2005. Geographically weighted Poisson regression for disease association mapping. Stat. Med. 24:2695–717.

40. ESRI ArcGIS Desktop. 2011. Release 10. Redlands, CA Environ. Syst. Res. Inst.

41. Bryan HM, Smits JEG, Koren L, Paquet PC, Wynne-Edwards KE, Musiani M. 2015. Heavily hunted wolves have higher stress and reproductive steroids than wolves with lower hunting pressure. Funct. Ecol. 29:347–356.

42. Yates DE, Mayack DT, Munney K, Evers DC, Major A, Kaur T, Taylor RJ. 2005. Mercury levels in mink (Mustela vison) and river otter (Lontra canadensis) from northeastern North America. Ecotoxicology. 14:263–274.

43. Bryan HM, Darimont CT, Paquet PC, Wynne-Edwards KE, Smits JEG. 2014. Stress and reproductive hormones reflect inter-specific social and nutritional conditions mediated by resource availability in a bear-salmon system. Conserv. Physiol. 2:1–18.

44. Gorman TA, Erb JD, McMillan BR, Martin DJ. 2006. Space and use of sociality of River Otters (Lontra canadensis) in Minnesota. J. Mammal. 87:740–747.

45. Stewart Fotheringham A, Charlton M, Brunsdon C. 1996. The geography of parameter space: an investigation of spatial non-stationarity. Int. J. Geogr. Inf. Syst. 10:605–627.

46. Dornbos P, Strom S, Basu N. 2013. Mercury exposure and neurochemical biomarkers in multiple brain regions of Wisconsin River Otters (Lontra canadensis). Ecotoxicology. 22:469–475.

47. Herring G, Eagles-Smith CA, Varland DE. 2018. Mercury and lead exposure in avian scavengers from the Pacific Northwest suggest risks to California condors: Implications for reintroduction and recovery. Environ. Pollut. 243:610–619.

48. Romero LM. 2004. Physiological stress in ecology: lessons from biomedical research. Trends Ecol. Evol. 19:249–255.

49. Provencher JF, Forbes MR, Hennin HL, Love OP, Braune BM, Mallory ML, Gilchrist HG. 2016. Implications of mercury and lead concentrations on breeding physiology and phenology in an Arctic bird. Environ. Pollut. 218:1014–1022.

50. Basu N. 2015. Applications and implications of neurochemical biomarkers in environmental toxicology. Environ. Toxicol. Chem. 34:22–29.

51. Basu N, Scheuhammer AM, Grochowina N, Klenavic K, Evans D, O'Brien M, Chan HM. 2005. Effects of Mercury on Neurochemical Receptors in Wild River Otters (Lontra canadensis). Environ. Sci. Technol. 39:3585–3591.

52. Basu N, Klenavic K, Gamberg M, O'Brien M, Evans D, Scheuhammer AM, Chan HM. 2005. Effects of Mercury on Neurochemical Receptor-Binding Characteristics in Wild Mink. Environ. Toxicol. Chem. 24:1444–1450.

53. Basu N, Scheuhammer AM, Sonne C, Letcher RJ, Born EW, Dietz R. 2009. Is dietary mercury of neurotoxicological concern to wild polar bears (Ursus maritimus)? Environ. Toxicol. Chem. 28:133–140.

54. Basu N, Scheuhammer AM, Rouvinen-Watt K, Grochowina N, Evans RD, O'Brien M, Chan HM. 2007. Decreased N-methyl-D-aspartic acid (NMDA) receptor levels are associated with mercury exposure in wild and captive mink. Neurotoxicology. 28:587–593.

55. Hahn LJ, Kloiber R, Leininger RW, Vimy MJ, Lorscheider FL. 1990. Whole-body imaging of the distribution of mercury released from dental fillings into monkey tissues. FASEB J. 4:3256–3260.

56. Friberg L, Mottet NK. 1989. Accumulation of methylmercury and inorganic mercury in the brain. Biol. Trace Elem. Res. 21:201–206.

57. Alberta Energy. 2018. Facts and Statistics. [cited 28 June 2018]. Available from https://www.energy.alberta.ca/OS/AO

58. Kelly EN, Schindler DW, Hodson P V, Short JW, Radmanovich R, Nielsen CC. 2010. Oil sands development contributes elements toxic at low concentrations to the Athabasca River and its tributaries. Proc. Natl. Acad. Sci. 107:16178–16183.

59. Wasser SK, Keim JL, Taper ML, Lele SR. 2011. The influences of wolf predation, habitat loss, and human activity on caribou and moose in the Alberta oil sands. Front. Ecol. Environ. 9:546–551.

60. Sulek K, Han T, Villas-boas SG, Wishart DS, Soh S, Gluckman PD, Chong Y, Kenny LC, Baker PN. 2014. Hair Metabolomics: Identification of Fetal Compromise Provides Proof of Concept for Biomarker Discovery. Theranostics. 4:253–259.

61. He X, de Seymour J V, Sulek K, Qi H, Zhang H, Han T-L, Villas-Bôas SG, Baker PN. 2016. Maternal hair metabolome analysis identifies a potential marker of lipid peroxidation in gestational diabetes mellitus. Acta Diabetol. 53:119–122.

62. Seymour JV De, Tu S, He X, Zhang H, Li T, Baker PN, Sulek K. 2018. Metabolomic profiling of maternal hair suggests rapid development of intrahepatic cholestasis of pregnancy. Metabolomics. 14:1–5.

63. Tsutsui H, Maeda T, Zhe J, Inagaki S, Higashi T, Kagawa Y, Toyo T. 2011. Clinica Chimica Acta Biomarker discovery in biological specimens (plasma, hair, liver, and kidney) of diabetic mice based upon metabolite profiling using ultra-performance liquid chromatography with electrospray ionization time-of- flight mass spect. Clin. Chim. Acta. 412:861–872.

64. Sela H, Karpas Z, Zoriy M, Pickhardt C, Becker JS. 2007. Biomonitoring of hair samples by laser ablation inductively coupled plasma mass spectrometry (LA-ICP-MS). Int. J. Mass Spectrom. 261:199–207.

Chapter 7

Geospatial Analysis of Complex Metal Exposures to Biota in the Athabasca Oil Sands

Kristin M. Eccles[1,2], Bruce D. Pauli[2], and Hing Man Chan[1]

[1] Department of Biology, University of Ottawa, 30 Marie Curie, Ottawa, ON, K1N 6N5, Canada
[2] Science and Technology Branch, Environment and Climate Change Canada, National Wildlife Research Center, 1125 Colonel By Drive, Raven Road, Ottawa, ON K1A 0H3, Canada

This chapter is being prepared for submission in *Science of the Total Environment*.

Author Contributions: KE conceived the idea, compiled the datasets, completed the spatial and statistical analyses, and wrote the manuscript. BP and LC contributed to the conceptualization of the project and provided guidance on the implementation and editing of the manuscript.

Supplemental information for this chapter can be found in Appendix E

7.1 Abstract

Understanding of patterns of chemical mixture exposure of the biota is challenging due to the spatial heterogeneity and complexity of the sources, pathways, and fate of the multiple chemicals. While spatially driven relationships between sources and body burden of a single chemical are commonly modelled, there is little effort on modelling chemical mixtures across multiple species in an impacted area. In this study, we use a spatial principal components analysis (sPCA) to assess spatial patterns of the body burden of 22 metals in 492 individual wildlife from a biomonitoring program including fur-bearing mammals, colonial waterbirds, and amphibians collected from Northern Alberta, Canada, an area impacted by the Athabasca Oil Sands. Our study demonstrates that range normalizing is an effective method for integrating metal body burden in different species and life stages. We found that spatial patterns of the body burden of 15 metals measured in the biomarkers demonstrated random spatial patterns which may indicate background/ non-point source exposures. There were seven metals including mercury, vanadium, lead, rubidium, lithium, strontium, and barium were clustered and were shown to be elevated in multiple species around the open pit mining area as well as regions downstream of a documented area of point source metal input. These methods provide tools for integrating biomonitoring datasets to get a more ecologically realistic representation of exposures of multiple species on a landscape. The results serve as a good case study of an integrative approach for identifying sources and drivers of exposure to a chemical mixture in biota across a landscape, and for developing more targeted monitoring efforts and intervention strategies.

7.2 Introduction

Traditional risk assessments in ecotoxicology have focused on a chemical by chemical exposure approach [1]. While these simple models are easy to develop and interpret, they are not representative of the true nature of environmental chemical exposure in the biota. As the biota in the ecosystem is often if not always, exposed to environmental mixtures, thus models on complex chemical mixture need to better reflect the ecological realism in risk assessments [2]. This is particularly true for biota living in regions of high anthropogenic disturbance such as the Alberta Oil Sands. The oil sands, located in the northeastern region of Alberta, covers approximately 142,200 km2. This region has the third largest reserve of crude oil in the world, after Venezuela and Saudi Arabia, and currently produces approximately 1.3 million barrels of crude oil per day [3]. Biota living in this region are exposed to a vast number of chemicals including metals primarily from the upgrading of bitumen and fugitive dust [4–6].

To monitor the potential impact of chemicals of concern associated with oil sands industrial operations on the environment and the health of wildlife in the Alberta Oil Sands, the Canadian federal government and the Provincial Alberta Government initiated the Canada-Alberta Joint Oil Sands Monitoring (JOSM) program in 2012. JOSM includes a total of 5 wildlife biomonitoring programs. Each of these monitoring programs included an annual sampling and measurement of chemical contaminants in wood frogs, fur-bearing mammals including river otter, mink, fisher, and marten, birds including the eggs of terns and gulls and, tree swallows, and plants. JOSM also included the monitoring of abiotic

matrices including air, water, aerial deposition of contaminants in the snow. In the wildlife biomonitoring projects, exposure to contaminants was measured tissues such as liver, as well as feathers and eggs as biomarkers of exposure. The goal of these contaminant monitoring projects under JOSM was to improve the understanding of the potential impacts of chemicals released on the health of the ecosystem in the Oil Sands Region [7].

In biomonitoring programs, bioindicator species and biomarkers are carefully chosen to be representative of not only the environmental conditions but also the inferences that can be made about ecosystem health, and by extension, human health [8,9]. However, it is well known that a single species or biomarker cannot be representative of the health of an ecosystem. Therefore, it is important to assess multiple bioindicator species and multiple biomarkers to gain a better understanding of the overall impacts of the environmental contaminants on ecosystem health [10,11]. Biomonitoring programs such as JOSM are designed to include multiple monitoring programs that monitor the burden of multiple chemicals in multiple species across a large landscape in the region. However, biomonitoring data collected from the oil sands monitoring programs under JOSM have yet to be integrated and analysed (9). This is due to the many challenges to spatially analysing large biomonitoring datasets with high dimensionality. For example, different species and life stages will accumulate and detoxify contaminants at different rates and use different mechanistic pathways [12]. Further, different matrices in the biomonitoring program may be measured using different units. As a result, many of the measurements are not comparable. Statistical methods such as normalizing the data using either a z-score or the range converts all measurements to a common scale can be used to integrate the datasets [13].

Also, when assessing data for spatial clusters during a spatial analysis, range normalization is superior as it retains more of the spatial structure in the data. The process of range normalizing uses the range of the dataset to standardize the individual values based on the data minimum and maximum. This process scales the values between zero and one [14].

Additionally, contaminant variables are often numerous and highly correlated. Correlated co-variates can prove problematic for some statistical methods such as regression. Therefore, multivariate analyses, such as principal components analysis (PCA) can be used to reduce the dimensionality of the data into uncorrelated orthogonal components that can explain the variance structure of the data [15]. While PCA is a commonly used method in ecotoxicology, the examination of the spatial aspect of principal components during this analysis has not yet been widely utilized [16].

A major aspect of ecotoxicology is to understand the distribution of contaminants in the environment and the relationships between contaminant exposure and effects in biota. As a result, the field is inherently spatial. Further, many ecotoxicological datasets are georeferenced, therefore enabling the investigation of spatial questions by using the common geospatial platform [17]. Moreover, it is important to include the spatial information in the PCA to control for any bias introduced by the sampling sites in the multivariate analyses. An ad hoc means to assess spatial patterns in a PCA is to map the scores produced from the multivariate analysis. However, this PCA is non-spatial and as a result, each location on the landscape is treated as independent when in the real world they are not [18].

A common way to integrate spatial information into a multivariate analysis is through a method called moran eigenvector maps (MEM). This method uses a spatial weights matrix

to define spatial connectivity and allow the quantification of spatial autocorrelation using Moran's I, which is a measure of self-similarity over space. This spatial information is then incorporated into the coefficients (scores) by quantifying the relationship between the data variables and their corresponding spatial lag using a co-inertia analysis [17]. This method has been used to assess spatial patterns in a variety of applications, some of which include genetic variability [19,20], metals in soil [21], and taxonomic and phylogenetic diversity of tadpoles [22].

In this study, we used a spatial analysis approach to integrate and analyse data from collected from three wildlife health biomonitoring programs that had complete metals data, under JOSM from 2012-2016. For more information about the individual monitoring projects and methods please see documents on the JOSM program [23]. These data sets are comprised of data on metal concentrations measured in the biomarkers collected from a variety of species and life stages. Our analysis addresses some of the challenges associated with integrating and analysing large datasets in ecotoxicology, including issues related to the data structure, and complexities associated with different species and life stages. Finally, we take a landscape ecotoxicology approach to analysing these biomonitoring datasets and assess overarching spatial patterns with respect to biomarkers of metal exposure and their relationships with the known sources and drivers of environmental availability using PCA and MEM analyses.

7.3 Methods

7.3.1 Chemical Analysis

Metal data was obtained from the three different wildlife monitoring programs (mammals, colonial waterbirds, and amphibians). The data was generated using inductively coupled plasma mass spectrometry (ICP-MS) with appropriate QA/QC methods in the liver of the mammals, eggs of the colonial waterbirds, and whole bodies of the amphibians . The samples used were collected between 2012 and 2016.

7.3.2 Data Preprocessing

Once compiled the dataset was first cleaned prior to analysis. Not all chemicals were analysed in all samples thus samples with missing data were removed. Then, to reduce the bias zero values impose on a PCA, all metals with greater than 50% non-detect in the dataset were removed; thus beryllium (Be), antimony (Sb), and uranium (U) were removed from the dataset. All measurements that were below the instrument detection limit were recoded to zero. In the cleaned dataset there were 22 metal co-variates and a sample size of 492. A summary of the species, life stages, and the number of samples from each monitoring project before data cleaning and after data cleaning can be seen in Table 7.1. An overview of the study area, the Athabasca oil sands in northern Alberta, Canada can be seen in Figure 7.1A and the location of each species collection location (from the cleaned data set) on the landscape can be seen in Figure 7.1B.

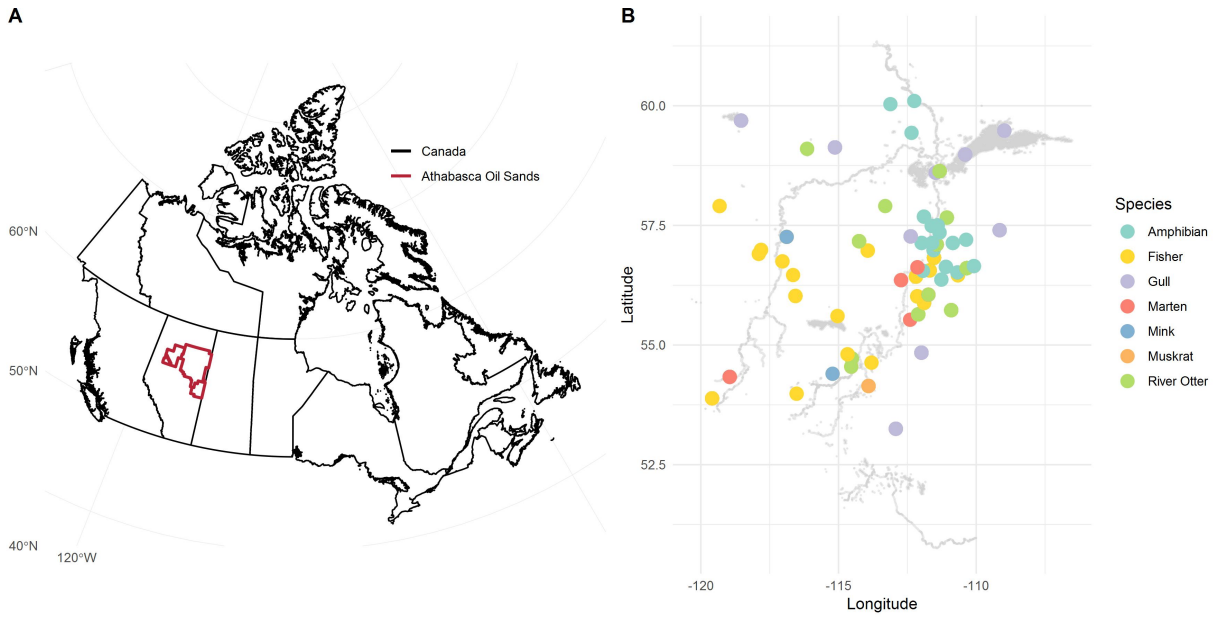

Figure 7.1: Overview of study location, the Athabasca Oil Sands in Canada. (B) Location of the difference species across the landscape (after data cleaning), n=492

Table 7.1: Summary of species and life stages samples used in this analysis pre and post data cleaning.

Species	Pre-cleaning n	Post-Cleaning n
Amphibian		
Adult	51	13
Recent Metamorph	32	8
Tadpole	44	21
Mammals		
River Otter	113	113
Marten	120	50
Mink	23	23
Muskrat	20	20
Fisher	63	63
Colonial Waterbirds		
Gull	255	181
Tern	24	0
Total	694	492

The dataset was assessed to ensure it met PCA assumptions, which includes assessment of sufficient sample size, the correlation between co-variates, linearity, and influence of outliers. In ecotoxicology data, measured exposures tend to be skewed left, where there

are many low exposures and few high exposures. Since PCA results can be highly influenced by outliers, this was addressed by performing both log10 and square-root transformation for comparison. The datasets were then normalized to zero and one using the range by species and life stage subgroups to make the datasets comparable. A workflow of the data preparation and analysis is summarized in Figure 7.2. All analyses were completed in R 3.4.3 using the packages ade4, adespatial, spdep, and sp [24–27].

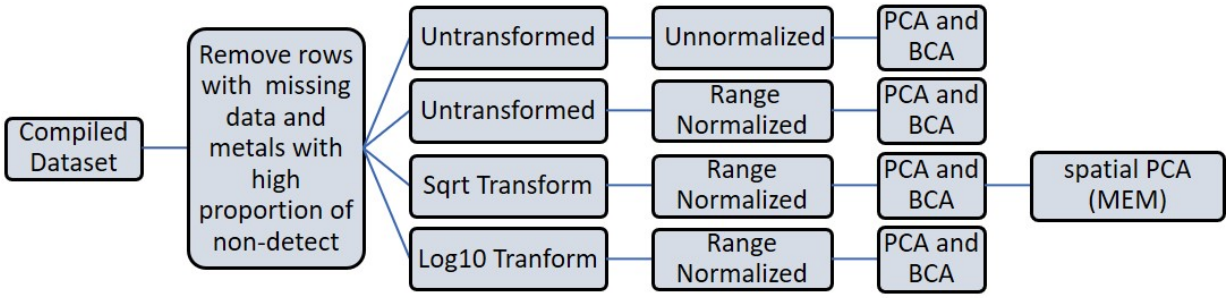

Figure 7.2: Overview of data processes and methods used in the integration and analysis wildlife contaminants of biomonitoring data from the Joint Oil Sands Monitoring (JOSM) program.

7.3.3 Data Analysis

For comparison, a PCA and a between-class analysis (BCA) were run on all transformed and range normalized data combinations (Figure 7.2). Range standardizing (also termed ranging) is a common way to scale data to make datasets of different magnitudes comparable [13]. The end product is a value between 0 and 1 (Equation 7.1).

$$x_i = \frac{x - min(x)}{max(x) - min(x)} \tag{7.1}$$

The BCA assess how much of the variance in the PCA can be attributed to dataset grouping. In this analysis, classes used in the BCA were sites, species. Species, life stage and site factors were compared pre and post-transformation and similarly for range normalization to assess the statistical significance of how much of the variance can be attributed to each factor using a Monte-Carlo permutation test. This test determines if the variance in the groups is statistically different and how much of the variance is attributed to the group classification [18]. This goal of this analysis was to minimize the amount of variance explained by species differences while mainlining the amount of variance explained by the sample site. Only the normalization method that retained the greatest amount of variance explained was spatially analysed using the MEM and interpreted.

To assess the multivariate spatial structure of the compiled dataset, a spatial weights matrix was created. This encodes the topological spatial relationships between samples and is used in the MEM to not only consider the variance of the variables but also the variance of spatially neighbouring points. Due to the irregular distribution of samples, a Gabriel graph with edges weighted by inverse distances was used to define the spatial connectedness [28]. The inverse distance weighting guarantees that samples closer together will have a greater influence than samples that are further apart. The spatial autocorrelation of the components was assessed using a Monte-Carlo based Moran's I and then mapped to assess the spatial patterns across the landscape. The mapped components are interpreted using biplots/loading values.

7.4 Results

BCA results comparing the two methods for data transformation (square-root and log base 10) to achieve more normal data and results from the range normalization methods can be seen in Figure 7.3. (A comparison of life stage difference can be found in Appendix E Figure E.1.) A lack of overlap between the amphibians and the other species in the unnormalized and untransformed data highlights the need to undertake normalization methods to make the datasets more comparable across species and possible to combine. This was achieved using the range normalization method when the datasets are range normalized, as seen by the overlap of all species (Figure 7.3). The goal of normalization is to minimize species differences so the variance captured in the PCA will instead be related to site differences. When the data is transformed and normalized, the "species effect" resulting from the lack of overlap of the amphibian data is reduced. While the effect that amphibians had on the explained variance was minimized, the normalization method increased the effect of gulls indicated by the slight separation of gulls from the rest of the species.

These visual patterns seen in Figure 3 can be statistically confirmed using the Monte-Carlo simulation to quantify the amount of variance that can be attributed to each factor (species, life stage, and site) in the compiled dataset under different transformation and normalization methods (Table 7.2). When comparing the transformation methods, the site explains the most variance, followed by species, and then the year the data were collected. When comparing the variance explained by each factor in the raw data versus the transformed and/or normalized data, transforming and normalizing the data reduces

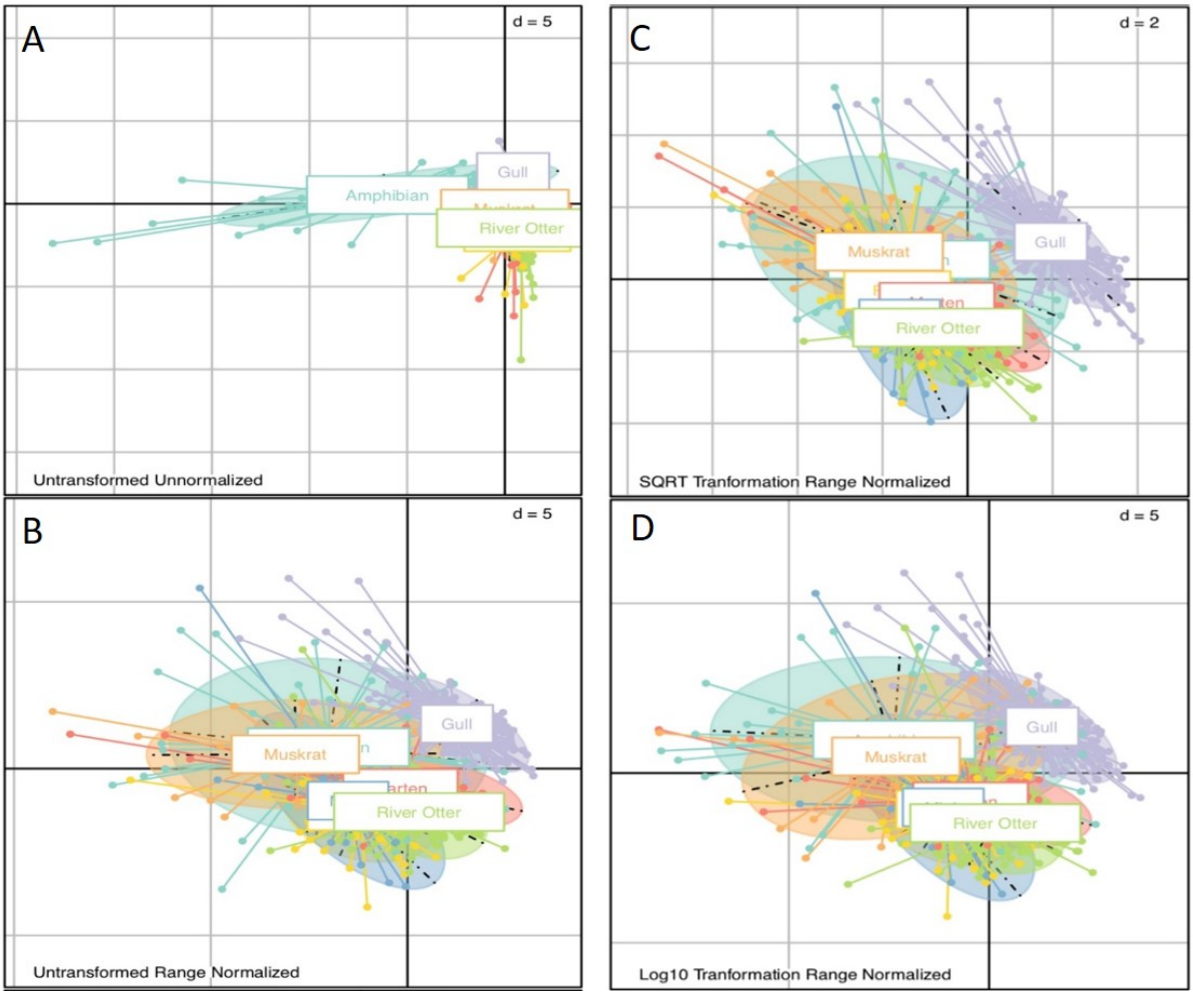

Figure 7.3: The variance attributed to each species groups comparing of transformations which include untransformed and unnormalized (A), untransformed and range normalized (B), square-root (SQRT) transformed and range normalized (C), and log10 transformed and range normalized (D). The transformation and normalization with the smallest species effect will have the most overlap between the species group.

the species and life stage effects. For comparison, after range normalization, 49% (p=0.02) of the variance was explained by the site in the amphibian dataset, 28% (p=0.001) of the variance was explained by the site in the gull dataset, and 25% (p=0.001) of the variance was explained by the site in the mammal dataset. As the largest amount of variance explained by the site is seen in the amphibian dataset, this might explain why this species appeared to be notably different in the untransformed and unnormalized dataset presented

in Figure 7.3. (PCA and BCA results from the individual datasets can be seen in Appendix E Figure E.2.)

Table 7.2: Summary from the Monte Carlo permutation test quantifying the amount of variance explained by each factor (species, life stage, and site).

	Untransformed Normalized (Raw)	Untransformed Normalized	SQRT Transformed Normalized	log base 10 Transformed Normalized
Variance Explained by Site	53.20%	39.70%	41.90%	41.30%
Variance Explained by Species	33.50%	18.70%	21.30%	20.00%
Variance Explained by Year	7.30%	7.30%	8.30%	7.50%
Total	94.00%	65.70%	71.20%	68.80%

*all tests were significant (p=<0.001)

The square-root normalization is the most optimal transformation method as it retains the largest amount of total variance explained while minimizing the variance explained by species differences and maximizing the amount of variance explained by the site. Due to this, only the square root transformed range normalized data were fully interpreted using a MEM to assess the spatial structure of metal exposure. (For comparison, the mapped BCA components, which do not take spatial relationships into consideration when orthogonally maximizing the variance, can be seen in Appendix E Figure E.2.) The MEM analysis has more distinct spatial patterns. The biplot from this analysis (Figure 7.4), and the loadings (Table 7.3) were used to interpret the mapped components (Figure 7.5).

In the first four components, 81% of the variance attributed to the positive spatial autocorrelation is explained. In component 1, the positively loaded metals are mercury, rubidium, and thallium. The pattern observed in these scores matches the location of gull egg samples (Appendix E Figure E.1. This variance is likely related to the species difference induced by the normalization. The negatively loaded metals are iron, arsenic, and cobalt. There is no apparent spatial pattern to these negatively loaded metals (Figure

Table 7.3: Table of loadings for moran's eigenvector maps (MEM) by site for square-rooted range normalized data. The metals with the highest positive and negative loading value have been bolded.

Metal	Component 1	Component 2	Component 3	Component 4
Silver (Ag)	-0.12	0.03	0.08	-0.2
Arsenic (As)	**-0.34**	**0.23**	-0.19	0.11
Barium (Ba)	0	**-0.39**	**-0.32**	-0.05
Bismuth (Bi)	-0.1	-0.07	0.15	0.11
Cadmium (Cd)	-0.15	0.15	0.18	0.25
Cobalt (Co)	**-0.33**	0.08	0.06	-0.22
Copper (Cu)	0.17	-0.03	-0.02	**0.39**
Iron (Fe)	**-0.39**	0.19	-0.09	-0.15
Gallium (Ga)	-0.01	-0.3	-0.11	-0.03
Mercury (Hg)	**0.3**	0.01	**0.54**	-0.02
Lithium (Li)	0.03	**-0.33**	**-0.24**	-0.3
Manganese (Mn)	-0.07	-0.11	0.13	-0.23
Molybdenum (Mo)	-0.22	-0.05	-0.16	0.15
Nickel (Ni)	-0.04	-0.23	0.19	0.19
Lead (Pb)	-0.13	-0.29	**0.33**	-0.14
Rubidium (Rb)	**0.28**	**0.34**	-0.16	**-0.41**
Selenium (Se)	-0.3	-0.04	0.03	**0.32**
Tin (Sn)	-0.27	-0.12	0.16	0.05
Strontium (Sr)	0.08	**-0.42**	-0.19	0.03
Thallium (Tl)	**0.28**	0.15	-0.01	0.14
Vanadium (V)	-0.15	-0.12	**0.37**	**-0.34**
Zinc (Zn)	0.16	-0.17	0.13	0.12

7.5A)

The positively loaded metals in component 2 are rubidium and arsenic and the negatively loaded metals are strontium, lithium, and barium. These positive scores are observed south of Fort McMurray and oil sands open pit mining and upgrading operations as well as south of this region (Figure 7.5B). The negatively loaded metals are strontium and barium. The most negative scores are located north and east of the open pit mining and upgrading operations as well as in sample locations further south.

Component 3 is positively loaded with mercury, vanadium, and lead. This pattern is observed to start around Fort McMurray, Alberta and continues northward. West of this area is negatively loaded with the metals barium and lithium (Figure 7.5C). Component

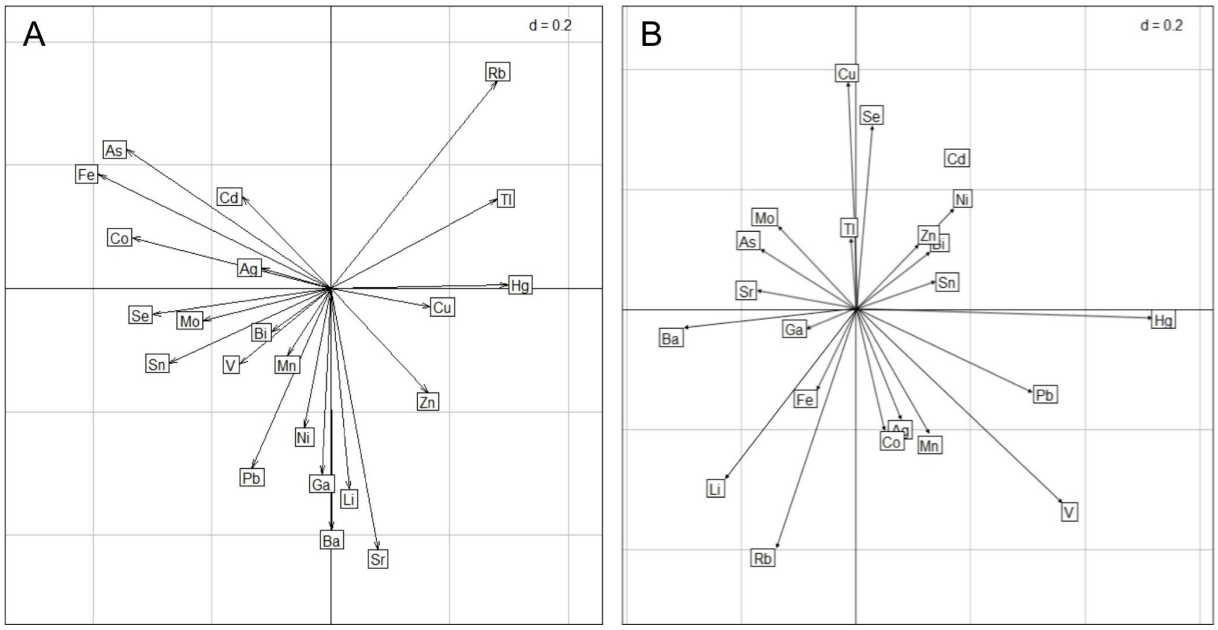

Figure 7.4: (A) Biplot between component 1 (x-axis) and 2 (y-axis) from the spatial PCA using Moran Eigenvector Maps (MEM). (B) Biplot between component 3 (x-axis) and 4 (y-axis) from the spatial PCA using MEM.

4 is positively loaded with the metals copper and selenium. These scores are highest in northwest Alberta as well as in the northernmost samples (Figure 7.5D). Negatively loaded metals include rubidium, vanadium, and lithium. The most negative scores are observed east of the oil sands area.

7.5 Discussion

This paper demonstrates a new application of methods for combining complex biomonitoring datasets comprised of multiple species and life stages; range normalizing data is an important step which allows datasets to be combined and assessed for overarching patterns of metal exposure. This methodology helps address one of the criticisms of biomonitoring programs: that assessing single sentinel species or single biomarkers may bias a true

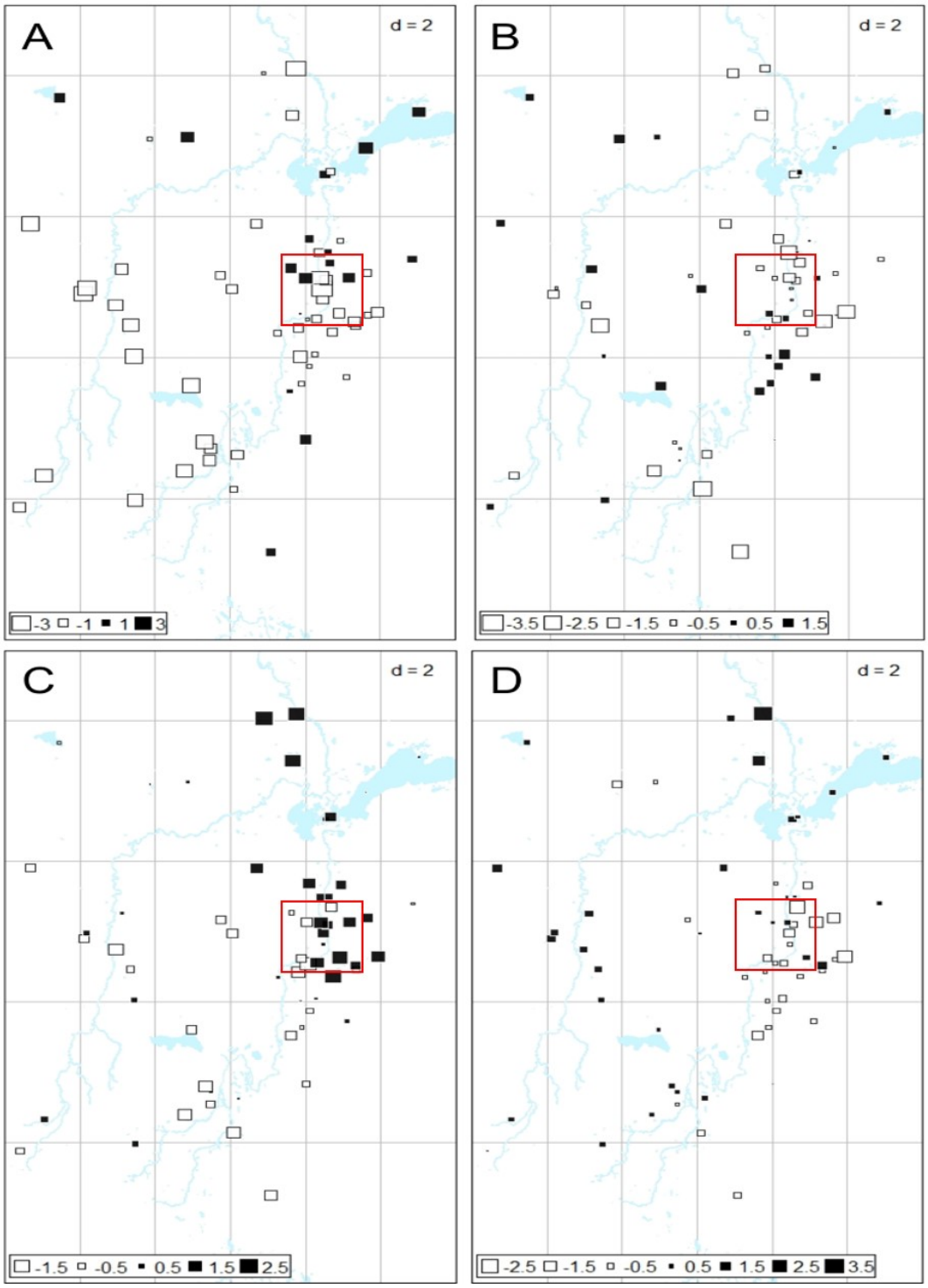

Figure 7.5: Mapped scores produced by the spatial Moran Eigenvector Maps (MEM) for component 1 (A), component 2 (B), component 3 (C) and component 4 (D). These scores are interpreted using the biplots from Figure 7.3 and Table 7.2. The red box highlights the Athabasca Oil Sands region.

evaluation of ecological health. At the same time, challenges to integrating and analysing biomonitoring data can arise from differences related to where the samples were collected and what chemicals were analysed. These differences can result in missing data and a lack of sample collection overlap, which is problematic for many statistical methods and can limit the types of analyses that can be done [29]. In this study, we attempted to address these issues.

The simplest way of handling missing data is to delete cases where there is missing information or to selectively remove co-variates with many missing values, which was how missing data was handled in this analysis. This resulted in a 29% reduction in sample size and losing all information on terns. While the simplest method, there is the risk of information loss which can lead to bias [30]. Other methods of dealing with missing data exist, such as imputation using maximum likelihood or multiple correspondence analysis (MCA). These methods rely on the patterns of missing data and the underlying mechanisms leading to the missing data. However, for these methods to be effective, there must be an understanding of the underlying structure of the data [30]. Due to the complexity of the dataset and the exploratory nature of the analysis, we opted for the simplest method. Other methods of imputation could be explored in the future.

This paper also presents the application of a new method for assessing the spatial structure of multidimensional datasets in ecotoxicology. To our knowledge, this is the first time that the MEM method has been applied to biomonitoring data. In the present study, the methods used to highlight the spatial distribution of metal exposures in different species across a landscape. Even though the positive loadings in the first component are primarily

related to the gull eggs and demonstrate a species difference, instead of a difference between metals, we argue that this is still an important pattern. In component 1, mercury is the metal with the highest loading value. The latitudinal gradient of the positive scores is similar to results from other studies assessing mercury in gull and tern eggs in northern Alberta [31,32].

In some of the components, there is no apparent clustering pattern (e.g. component 1-negative, component 2-positive). The most highly loaded metals in the components with no obvious clustering pattern have a similar metal composition (arsenic, iron, rubidium). Thus, this variance may be related to the geology of northern Alberta. For instance, in Northern Alberta arsenic levels are up to 10 times higher and iron level are up to 100 times higher than background concentrations in other regions of Alberta due to the naturally occurring shale deposits [33,34].

A variety of other metals including barium>strontium > rubidium> cobalt > lithium have a high natural abundance in the earth's crust, all of which are highly loaded in one or more of the components [35]. Rubidium is highly loaded across many components and generally shows no clustering pattern in any of the scores. This metal is discussed in Landis et al. (2017), they attribute sources of rubidium in the region to biomass burning and fugitive dust. Rubidium is highly reactive with oxygen and as a result, is typically found bound within caesium and lithium ores or minerals. It is possible that part of components 1 and 2 are highlighting variance related to naturally occurring metals.

Component 3 (positive loadings) and 4 (negative loadings) show a pattern of scores highly loaded with mercury, vanadium, lead, rubidium, lithium, strontium, and barium

around the open pit mining area as well as regions downstream of oil sands development. There are local inputs into the environment from oil sands operations that result in metal disposition from fugitive dust and upgrading processes such as metals being released in an aqueous solution from process water and tailings ponds [4]. Lynam et al. (2015) demonstrate that strontium is enriched in the oil sands region and is a tracer for deposition of crustal dust that results from mining and land clearing activities. In other research, local enrichment of mercury, vanadium, thallium, and lead from oil sands operations is documented [5,6,36]. The pattern observed with component 3 appears to separate anthropogenically- deposited metals from naturally occurring crustal elements.

Northern Alberta has very complex underlying natural geological and geochemical properties which are why natural resource extraction occurs in this region. The spatial analysis conducted in this study demonstrates that some while metals are naturally occurring in this region, it is apparent that other metals are being anthropogenically concentrated around the oil sands development. This is reflected in the patterns of metal exposures observed across multiple species and life stages. More specifically, mercury, vanadium, lead, rubidium, lithium, strontium, and barium were shown to be elevated in multiple species around the open pit mining area as well as regions downstream of oil sands development. This spatial analysis illustrates regions where metal exposures are elevated across samples in relation to other samples from other regions. Assessing patterns of exposure can help to identify priority metals, determine sources, identify priority areas for further study, and help develop targeted strategies for further monitoring or exposure reduction [37].

7.6 Data availability

Data is available upon request from the authors. R code used in these analyses can be found at: `https://github.com/kristineccles/complex_metal_exposures.git`

7.7 Acknowledgements

We would like to thank all the project leaders in the Wildlife Health component of the Canada- Alberta Joint Oil Sands Monitoring Programs (C. Boutin, K.J. Fernie, C. Hebert, L.J. Mundy, D. Schock, C. Soos, and P.J. Thomas). We thank S. Dray for support with the spatial PCA analysis and National Sciences and Engineering Research Council Collaborative Research and Training Experience Program, Research in Environmental and Analytical Chemistry and Toxicology to supporting a training opportunity in France and for funding support to K.M.Eccles. We acknowledge funding support from the Canada Research Chair Program and the National Sciences and Engineering Research Council Discovery Grant to H.M. Chan; and Environment and Climate Change Canada, Province of Alberta, Joint Oil Sands Monitoring program to B.D. Pauli.

7.8 References

1. Environment Canada. 2007. Overview of the Ecological Assessment of Substances under the Canadian Environmental Protection Act , 1999. Assessment. [cited 28 June 2018] Available from `https://www.canada.ca/content/dam/eccc/migration/main/lcpe-cepa/documents/substances/eas$_$overview-eng.pdf`

2. Vighi M, Villa S. 2013. Ecotoxicology: The Challenges for the 21st Century. Toxics. 1:18–35.

3. Alberta Energy. 2018. Facts and Statistics. [cited 28 June 2018]. Available from `https://www.energy.alberta.ca/OS/AOS/Pages/FAS.aspx`.

4. Landis MS, Patrick Pancras J, Graney JR, White EM, Edgerton ES, Legge A, Percy KE. 2017. Source apportionment of ambient fine and coarse particulate matter at the Fort McKay community site, in the Athabasca Oil Sands Region, Alberta, Canada. Sci. Total Environ. 584–585:105–117.

5. Kirk JL, Muir DCG, Gleason A, Wang X, Lawson G, Frank RA, Lehnherr I, Wrona F. 2014. Atmospheric Deposition of Mercury and Methylmercury to Landscapes and Waterbodies of the Athabasca Oil Sands Region. Environ. Sci. Technol. 48:7374−7383.

6. Lynam MM, Dvonch JT, Barres JA, Morishita M, Legge A, Percy K. 2015. Oil sands development and its impact on atmospheric wet deposition of air pollutants to the Athabasca Oil Sands Region , Alberta , Canada. Environ. Pollut. 206:469–478.

7. Hopke P, Jenkins A, Johnson D, Klanova J, Le C, Niemi G. 2016. Assessing the scientific integrity of the Canada–Alberta joint oil sands monitoring (2012–2015) expert panel review. Edmonton, Alberta.

8. Burger J. 2006. Bioindicators: Types, Development, and Use in Ecological Assessment and Research. Environ. Bioindic. 1:22–39.

9. Burger J, Gochfeld M, Niles L, Powers C, Brown K, Clarke J, Dey A, Kosson D. 2015. Complexity of bioindicator selection for ecological, human, and cultural health: Chinook salmon and red knot as case studies Joanna. 187:389–400.

10. Costanza R, Mageau M. 1999. What is a healthy ecosystem? Aquat. Ecol. 33:105–115.

11. Jørgensen SE, Xu L, Costanza R. 2010. Handbook of ecological indicators for assessment of ecosystem health. CRC press.

12. Luoma SN, Rainbow PS. 2005. Why is metal bioaccumulation so variable? Biodynamics as a unifying concept. Environ. Sci. Technol. 39:1921–1931.

13. Legendre P, Legendre L. 2012. Numerical ecology: second English edition. In Elsevier, ed. Amsterdam;Boston.

14. Milligan GW, Cooper MC. 1988. A Study of Standardization of Variables in Cluster Analysis. J. Classif. 5:181–204.

15. Berrendero JR, Justel A, Svarc M. 2011. Principal components for multivariate functional data. Comput. Stat. Data Anal. 55:2619–2634.

16. Van den Brink PJ, Van den Brink NW, Ter Braak CJF. 2003. Multivariate analysis of ecotoxicological data using ordination: Demonstrations of utility on the basis of various examples. Australas. J. Ecotoxicol. 9:141–156.

17. Dray S, Said S, Débias F. 2008. Spatial ordination of vegetation data using a generalization of Wartenberg's multivariate spatial correlation. J. Veg. Sci. 19:45–56.

18. Thioulouse J, Dray S, Dufour A-B, Siberchicot A, Jombart T, Pavoine S. 2018. Multivariate Analysis of Ecological Data with ade4. Springer.

19. Jombart T, Devillard S, Dufour A-B, Pontier D. 2008. Revealing cryptic spatial patterns in genetic variability by a new multivariate method. Heredity (Edinb). 101:92–103.

20. Frichot E, Schoville S, Bouchard G, François O. 2012. Correcting Principal Component Maps for Effects of Spatial Autocorrelation in Population Genetic Data. 3.

21. Saby NPA, Thioulouse J, Jolivet CC, Ratié C, Boulonne L, Bispo A, Arrouays D. 2009. Multivariate analysis of the spatial patterns of 8 trace elements using the French soil monitoring network data. Sci. Total Environ. 407:5644–5652.

22. Leão-Pires TA, Luiz AM, Sawaya RJ. 2018. The complex roles of space and environment in structuring functional, taxonomic and phylogenetic beta diversity of frogs in the Atlantic Forest. PLoS One. 13:e0196066.

23. Environment Canada. 2012. Joint Canada-Alberta implementation plan for oil sands monitoring. Available from http://www.publications.gc.ca/pub?id=9.697128&sl=0.

24. Dray S, Blanchet G, Borcard D, Guenard G, Jombart T, Larocque G, Legendre P, Madi N, Wagner HH. 2016. adespatial: Multivariate multiscale spatial analysis. R Packag. version 0.0. 3.

25. Bivand R, Piras G. 2015. Comparing Implementations of Estimation Methods for Spatial Econometrics. J. Stat. Softw. 63:1–36.

26. Pebesma EJ, Bivand RS. 2005. Classes and methods for spatial data in R. R News. 5:9–13.

27. Dray S, Dufour A-B, others. 2007. The ade4 package: implementing the duality diagram for ecologists. J. Stat. Softw. 22:1–20.

28. Bauman D, Drouet T, Fortin MJ, Dray S. 2018. Optimizing the choice of a spatial weighting matrix in eigenvector-based methods. Ecology. 99:2159–2166.

29. Gotway CA, Young LJ. 2002. Combining incompatible spatial data. J. Am. Stat. Assoication. 97:632–648.

30. Josse J, Pagès J, Husson F. 2011. Multiple imputation in principal component analysis. Adv. Data Anal. Classif. 5:231–246.

31. Hebert CE, Campbell D, Kindopp R, Macmillan S, Martin P, Neugebauer E, Patterson L, Shatford J. 2013. Mercury trends in colonial waterbird eggs downstream of the oil sands region of Alberta, Canada. Environ. Sci. Technol. 47:11785–11792.

32. Dolgova S, Popp BN, Courtoreille K, Espie RHM, Maclean B, McMaster M, Straka JR, Tetreault GR, Wilkie S, Hebert CE. 2018. Spatial trends in a biomagnifying contaminant: Application of amino acid compound–specific stable nitrogen isotope analysis to the interpretation of bird mercury levels. Environ. Toxicol. Chem. 37:1466–1475.

33. Dudas MJ. 1987. Accumulation of native arsenic in acid sulphate soils in Alberta. Can. J. Soil Sci. 67:317–331.

34. Bennett B, Dudas MJ. 2003. Release of arsenic and molybdenum by reductive dissolution of iron oxides in a soil with enriched levels of native arsenic. J. Environ. Eng. Sci. 2:265–272.

35. Steen B, Borg G. 2002. An estimation of the cost of sustainable production of metal concentrates from the earth's crust. Ecol. Econ. 42:401–413.

36. Kelly EN, Schindler DW, Hodson P V, Short JW, Radmanovich R, Nielsen CC. 2010. Oil sands development contributes elements toxic at low concentrations to the Athabasca River and its tributaries. Proc. Natl. Acad. Sci. 107:16178–16183.

37. Thomas PJ, Eccles KM, Mundy LJ. 2017. Spatial modelling of non-target exposure to anticoagulant rodenticides can inform mitigation options in two boreal predators inhabiting areas with intensive oil and gas development. Biol. Conserv. 212:111–119.

Chapter 8

Conclusion

8.1 Summary of Main Results

The overarching objective of my thesis research was to improve ecological risk assessment by using GIS as a platform for data management, integration, analysis, and visualizations. Through the three sections in my thesis, I have provided a spatial framework with practical examples of implementation. Specifically, I have developed fur as a non-invasive biomarker of mercury (Hg) exposure which is essential to understanding the spatial patterns of this biomarker, and I have provided examples of how biomarkers of exposure and effect can be used to assess spatial patterns and relationships at varying degrees of spatial scale. Overall, my thesis advances the field of landscape ecotoxicology and ecological risk assessment by providing tools to better understand biomonitoring data by capitalizing on data variance and spatial heterogeneity.

Chapters in the first two sections (**Chapter 2, 3 and 4**) were about developing GIS for the specific application of landscape ecotoxicology and developing biomarkers to be

used in a spatial context. Results from **Chapter 2** demonstrated that a spatial framework has many advantages over traditional non-spatial methods. First, it provided a way to integrate existing biomonitoring data to identify patterns of single chemical exposures across a landscape. This method can quantify exposure patterns across a landscape that can help to identify areas of higher risk that require further monitoring. This chapter also provided methods of assessing chemical exposures using a spatial principal component analysis (sPCA). This analysis identified hotspots of metal enrichment of mercury, zinc, lead, and vanadium around the upgraders in the Athabasca Oil Sands Regions. These patterns are observed across a variety of species and life stages. From this analysis, it is possible to identify spatial patterns of multiple exposures. The last methodological example in this chapter provides a proof of concept on how to characterize spatial exposure-response relationships across a landscape using co-dispersion analysis. This method can be used for hypothesis generation related factors that may influence exposures, responses, and the relationship between the two.

Chapter 3 and 4 provide a more complete understanding of fur as a non-invasive biomarker of Hg exposure in river otter and mink. Thus, when a fur sample is obtained, it is possible to use it for predicting the risk of Hg exposure. Specifically, **Chapter 3** provides a better understanding of Hg exposure in wildlife by quantifying the distribution of Hg within wildlife tissue and its relationship with fur Hg. The developed models between fur total Hg and the total Hg of internal organs developed in this chapter can be used to predict the kinetics of Hg in different tissues of piscivorous mammals and to establish fur concentrations as biomarkers for exposure or screening tools for freshwater ecosystem risk

assessments. These results suggest that furbearer guidelines [1–3] may be too high to be protective of fur-bearing mammals. As a result, I suggest a more conservative fur screening guideline of 15 μg/g of Hg in fur, which is based on brain neurochemical changes [4].

Chapter 4 further refines fur Hg as a non-invasive biomarker of Hg exposure by assessing the distribution of Hg across the pelt of river otters. This chapter shows an interesting use of spatial analyses, using spatial techniques for quantifying hot spots of Hg distribution that occurred primarily in the undercoat in the head region. Results from this research highlight the importance of sample location as Hg is heterogeneously distributed across the pelt and between fur types. Hg is higher and more variable spatially in the undercoat than the top coat. Further, when compared with internal Hg of organs fur from the forebody produces a more accurate prediction. As a result, I recommend fur is sampled for biomonitoring samples should be collected from the top coat of the forebody region. Fur samples taken outside of this region could result in prediction error as high as 140% when estimating internal organ THg. This chapter also assessed the ratio of methyl mercury (MeHg) in THg in topcoat fur. Results show that 95.7±3.4% of THg is MeHg indicating THg concentrations can be used to assess MeHg exposure in fur. This information is important for developing a biomonitoring program based on fur. Further, this work supports the use of hair fur snags for non-invasive biomonitoring as fur snags typically collect top coat fur from the forebody region.

Chapters in the third section (**Chapter 5,6, and 7**) demonstrate the application of GIS in landscape ecotoxicology using biomarkers of exposure and biomarkers of effect. **Chapter 5** examines the relationship between Hg and dietary exposures to THg by investigating the

relationship between fur and stomach content Hg and environmental sources of Hg, in order to examine the spatial relationship between physiochemical and environmental factors that contribute to MeHg production and environmental bioavailability. Results of regression models showed a significant positive relationship between the log fur THg and log stomach content THg for river otter and mink. There were also significant relationships between environmental sources and THg. Stomach content THg was significantly associated with soil pH (-) and % of deciduous forest (+). Fur THg was significantly associated with total fire burned (+) and % of wetlands (-) in a pseudo home range. These results provide field evidence that fur can be used as a proxy for environmental Hg concentrations and factors that affect Hg bioavailability.

Chapter 6 investigated the spatial dose-response relationships using fur THg as the exposure and fur cortisol as the response. Results from this chapter highlight how assessing spatial data using a non-spatial may make it appears there is no relationship between the two variables, as was the case in this chapter. Mapping the exposure data and response data gave evidence of a heterogeneous dose-response relationship which was confirmed statistically using a geographically weighted regression (GWR) as both positive dose-response relationships between THg and cortisol in fur and negative dose-response relationships were observed. These results were reconfirmed when reanalysed the global regression model using my previously suggested fur screening guideline of 15 μg/g to split the data into low ($<$15 μg/g) and high ($>$15 μg/g) Hg exposure groups. Results from this research highlight the importance of spatially assessing dose-response relationships, especially over large spatial areas. Results from this research also support the hypothesis that high Hg exposure

causes changes in brain neurochemistry that could lead to the impairment of the stress response [5].

Finally, in **Chapter 7** I examine spatial patterns of complex exposures using a spatial principal components analysis (sPCA). In this chapter, I use data normalization and transformation to combine datasets comprised of different species and life stages. Results from the research show that the normalization methods were able to remove the effect of species and life stages in the compiled dataset and were effective for combining data. This method can make exposure biomarkers comparable across species and life stages. As a result, the patterns observed in the sPCA were related to patterns of environmental exposures and not differences in species-specific accumulation rates. Other components in the sPCA were able to show patterns of complex exposures, with clustering around the Alberta Oil Sands, an area with concentrated deposition and exposure of metals. Methods and results in this chapter provide tools for integrating biomonitoring datasets to get a more ecologically realistic representation of exposures of multiple species on a landscape.

8.2 Research Contributions

8.2.1 Scientific Value

Complex problems that span multiple disciplines, such as environmental health issues and ecosystem health, need innovative interdisciplinary solutions for prevention, risk reduction, and mitigation. For this, the integration of knowledge across disciplinary boundaries is increasingly emphasized and required [6,7]. This interdisciplinary thesis integrates methods

from geography and biology and their respective subdisciplines to provide tools for assessing contaminant exposure and biological responses in wildlife. The methods demonstrated in my thesis provide the platform to advance the field of landscape ecotoxicology and improve spatial risk assessment.

Current methods of assessing ecological health typically use single chemical exposures in a single indicator. This is problematic as one indicator species may not be representative of the ecosystem also may not be applicable to other ecosystems [8]. Part of this thesis focused on the methods and implementation of integrating biomonitoring datasets with a variety of species and life stages and assessing patterns of exposure in these integrated datasets. Further, this thesis also demonstrated a method for analysing a complex biomonitoring dataset assessing complex exposures in multiple species using an sPCA. Approaches used in this research will make ecological risk assessments more realistic and informative.

My thesis also demonstrates methods and applications for assessing the heterogeneous distribution of dose-response relationships across a landscape. This is the first-time geospatial regression methods have been used to assess dose-response relationships in the ecotoxicology literature. Not considering a heterogeneous relationship between exposures and responses can lead to model misspecification, leading to the conclusions that there is no relationship. When the GWR is compared with the non-spatial model it indicates model misspecification. Using GWR methods in ecotoxicology will help to develop more statistically sound models and will be able to better capture dose-response relations across a landscape.

8.2.2 Social Value

Environmental health, wildlife health, and human health are highly interconnected within a complex system. While these three components are theoretically united under one framework – ecological health – until this point, these facets were not yet well- integrated methodologically. My thesis provides the platform to integrate social-ecological indicators and models and support community-based monitoring. While defining what is "healthy" was not the focus of this thesis, the indicators of health used were chosen to provide relevant information to those who rely on the land. First Nations in Canada are particularly vulnerable to the effect of environmental contaminants, as the health of the ecosystem in which they live is highly embedded in their spiritual, physical, mental, and cultural health through the provisions of traditional foods they hunt, gather, and fish. This interconnected concept of health is central to First Nation culture; health is much greater than the absence of disease [9]. Monitoring ecosystem health is important to First Nations, as one of the main concerns in many communities, is whether the water is safe to drink, and the food is safe to eat [10].

Further, mapping and visualization provide an intuitive way to communicate findings which will aid in knowledge translations to stakeholders, policymakers, and various interest groups. My thesis supports evidence-based decision making for interventions, programming, and policy decisions at the community, provincial, and national level by enabling the creation of localized interventions that target area of concern, to improve ecological health. The work presented in my thesis is already being used to identify regions of elevated Hg exposure (Figure 8.1) and guide community-based biomonitoring in the Alberta Oil Sands

and Northern Ontario through Environment and Climate Change Canada.

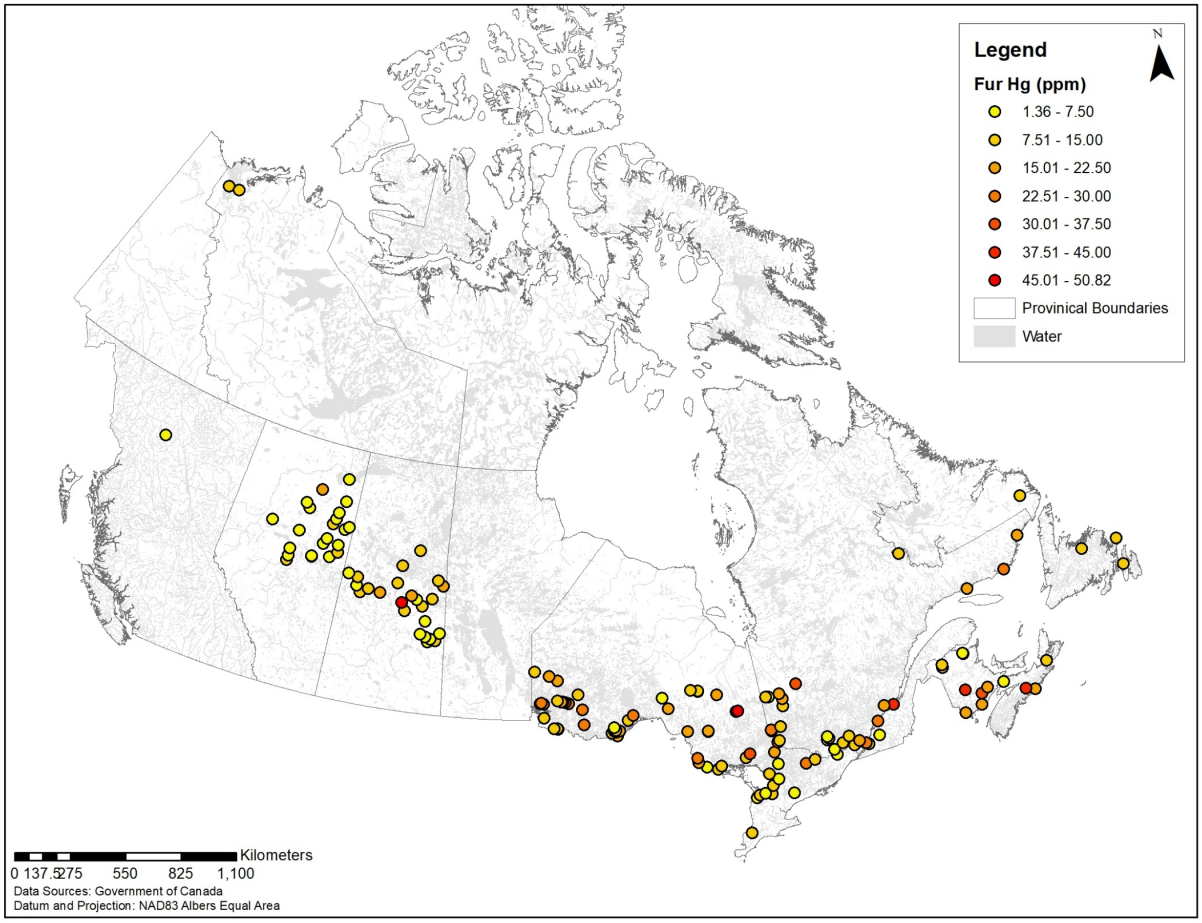

Figure 8.1: Mapped fur Hg concentrations (μg/g) in Canada. Samples from Saskatchewan were collected and measured by Wilkie et al. (2018) [11]. On this colour scale, yellow indicates low exposures and orange and red indicate high exposure as per the 15 μg/g fur mercury screening guideline [12].

8.3 Limitations and Future Work

While there is recognition that the inclusion of GIS would be beneficial to improve ecological risk assessments and develop the field of landscape ecotoxicology [13], there are technical barriers to implementation. GIS is a technical platform that has both organiza-

tional barriers and technical barriers to implementation including lack of awareness of the tool, lack of knowledge about how to use or implement the tool, and large startup costs for the software and trained personnel [14,15]. However, recent developments in open source GIS applications allow applications to be acquired at no cost to the user such as Google Maps, Google Earth, and QGIS. As a result, GIS is shifting from a primarily expert domain to having applications for novice users [14,15]. This shift presents opportunities for the applications of GIS within ecotoxicology, for example, use in community-based monitoring programs [16]. Throughout my thesis, I used a variety of different GIS software with the purpose of highlighting usability. To continue developing landscape applications of ecotoxicology, there needs to be more awareness around these methods, so spatial forethought can go into the design of biomonitoring studies. Geotagging all collected environmental data should be encouraged as a requirement for all biomonitoring programs as this will provide an opportunity for future spatial analyses to be performed. As demonstrated in my thesis, GIS analyses can quantify exposure-response relationships in biota that are inhabiting complex landscapes.

A theoretical limitation of this work and of spatial analyses as a whole is the fact that analyses are scale-dependent. This results in the modifiable areal unit problem (MAUP) where spatial analyses performed with different geographical aggregations or with different zonation may provide different results [17]. It is important that researchers are cognizant of this limitation and take measures to manage it. For example, when choosing a unit for analysis, it is best to choose natural units for analysis such as administrative boundaries or a unit relevant to planning and decision making. Another option is to use the smallest

level of aggregation available (the individual), which is the method used throughout this thesis. A related issue is an ecological fallacy whereby inferences about the individual (or a lower level of aggregation) cannot be deduced from the aggregate analyses [18]. For confidentiality reasons, often analyses are performed on aggregated data. However, this is more of an issue with humans than wildlife. Thus, it is important to only make conclusions about the aggregation in which the analysis was performed.

The field of landscape ecotoxicology also continues to be limited by available biomarker data. Our results showing the relationship between biomarkers of exposure and responses is the beginning of a promising new area for research in environmental assessments of the effects of chemicals on wildlife. Future work can incorporate advanced quantitative techniques, such as metabolomics, to produce more robust response data to allow for a more comprehensive assessment for complex responses. Metabolomics has been successfully completed in human hair [19–21] and in mice fur [22]. For example, metabolites associated with reactive oxygen metabolites including glutathione, 2-Oxobutyric acid, and 2-Hydroxybutyric acid have already been quantified in hair [19–22]. This response data can also be coupled with exposure data measured in hair using a non-targeted approach [23]. A developed ecotoxicological dataset collected using the "omics" approach that includes multiple exposures and response will enable a better assessment of the impacts of the industrial development on the ecosystem.

Special attention should be given to biomarker development that can assess ecological health and make inferences about human health [1]. The development of these biomarkers highlights the interconnected nature of health, especially for First Nations as an aspect of

cultural well-being, that is highly connected to the land and the state of the ecosystem. As such, social-ecological indicators should be developed in collaboration with stakeholders. This provides an opportunity to unite western science with traditional ecological knowledge [10,24]. Information related to harvester and hunter's observations, consumption data, and Elder's knowledge can help guide and inform the process of developing a socially and ecologically relevant biomarker [25]. Further, GIS can also be used as a platform to support this work. GIS is increasingly being used as a platform to map traditional knowledge and oral histories. Digital cartography provides a way of recording traditional knowledge as a method of preservation and a way to intuitively communicate traditional knowledge using maps and geovisualizations to future generations and the public. It also provides a platform to disseminate and incorporate this knowledge of physical resources and traditional knowledge into biomonitoring, and resource development [26].

8.4 References

1. Basu N, Scheuhammer AM, Bursian SJ, Elliott J, Rouvinen-Watt K, Chan HM. 2007. Mink as a sentinel species in environmental health. Environ. Res. 103:130–144.

2. Meador JP. 1996. Environmental contaminants in wildlife: interpreting tissue concentrations. CRC Press.

3. Evers DC, Han Y-J, Driscoll CT, Kamman NC, Goodale MW, Lambert KF, Holsen TM, Chen CY, Clair T, Butler T. 2007. Biological Mercury Hotspots in the Northeastern United States and Southeastern Canada. Bioscience. 57:29.

4. Dornbos P, Strom S, Basu N. 2013. Mercury exposure and neurochemical biomarkers in multiple brain regions of Wisconsin River Otters (*Lontra canadensis*). Ecotoxicology. 22:469–475.

5. Matthiessen P, Wheeler JR, Weltje L. 2018. A review of the evidence for endocrine disrupting effects of current-use chemicals on wildlife populations. Crit. Rev. Toxicol. 48:195–216.

6. Aguirre AA, Ostfeld RS, Tabor GM, House C, Pearl MC. 2002. Conservation medicine: ecological health in practice. Oxford University Press.

7. McLaren L, Hawe P. 2005. Ecological perspectives in health research. J. Epidemiol. Community Health. 59:6–14.

8. Burger J. 2006. Bioindicators: Types, Development, and Use in Ecological Assessment and Research. Environ. Bioindic. 1:22–39.

9. Reading J. 2009. The Crisis of Chronic Disease among Aboriginal Peoples: A Challenge for Public Health, Population Health and Social Policy.

10. Royer MJS, Herrmann TM. 2011. Socio Environmental changes in two traditional food species of the Cree first nation of subarctic James Bay. Cah. Geogr. Que. 55:575–601.

11. Wilkie SC, Espie RHM, Basu N, Liber K, Hall BD. 2018. Trapped river otters *(Lontra canadensis*) from central Saskatchewan differ in total and organic mercury concentrations by sex and geographic location. Facets. 3:139–154.

12. Eccles KM, Thomas PJ, Chan HM. 2017. Predictive meta-regressions relating mercury tissue concentrations of freshwater piscivorous mammals. Environ. Toxicol. Chem. 36:2377–2384.

13. Focks A. 2014. The Challenge: Landscape ecotoxicology and spatially explicit risk assessment. Environ. Toxicol. Chem. 33:1193–1198.

14. Goodchild M, Guo H, Annoni A, Bian L, Bie K De, Campbell F, Craglia M, Ehlers M, Genderen J Van, Jackson D, Lewis AJ, Pesaresi M, Simpson R, Skidmore A, Wang C, Woodgate P, States U. 2012. Next-generation Digital Earth. Proc. Natl. Acad. Sci. 109:11088–11094.

15. Ye H, Brown M, Harding J. 2013. GIS for All: Exploring the Barriers and Opportunities for Underexploited GIS Applications. Free Open Source Softw. Geospatial Conf. Proc.

16. Richardson DB, Volkow ND, Kwan M-P, Kaplan RM, Goodchild MF, Croyle RT. 2013. Spatial turn in health research. Sci. (New York, NY). 339:1390.

17. Openshaw S, Openshaw S. 1984. The modifiable areal unit problem.

18. Openshaw S. 1984. Ecological fallacies and the analysis of areal census data. Environ. Plan. A. 16:17–31.

19. Sulek K, Han T, Villas-boas SG, Wishart DS, Soh S, Gluckman PD, Chong Y, Kenny LC, Baker PN. 2014. Hair Metabolomics: Identification of Fetal Compromise Provides Proof of Concept for Biomarker Discovery. Theranostics. 4:253–259.

20. He X, de Seymour J V, Sulek K, Qi H, Zhang H, Han T-L, Villas-Bôas SG, Baker PN. 2016. Maternal hair metabolome analysis identifies a potential marker of lipid peroxidation in gestational diabetes mellitus. Acta Diabetol. 53:119–122.

21. Seymour JV De, Tu S, He X, Zhang H, Li T, Baker PN, Sulek K. 2018. Metabolomic profiling of maternal hair suggests rapid development of intrahepatic cholestasis of pregnancy. Metabolomics. 14:1–5.

22. Tsutsui H, Maeda T, Zhe J, Inagaki S, Higashi T, Kagawa Y, Toyo T. 2011. Clinica Chimica Acta Biomarker discovery in biological specimens (plasma , hair , liver and kidney) of diabetic mice based upon metabolite pro filing using ultra-performance liquid chromatography with electrospray ionization time-of-flight mass spectrometry. Clin. Chim. Acta. 412:861–872.

23. Sela H, Karpas Z, Zoriy M, Pickhardt C, Becker JS. 2007. Biomonitoring of hair samples by laser ablation inductively coupled plasma mass spectrometry (LA-ICP-MS). Int. J. Mass Spectrom. 261:199–207.

24. Parlee BL, Geertsema K, Willier A. 2012. Social-ecological thresholds in a changing boreal landscape: Insights from cree knowledge of the Lesser Slave Lake region of Alberta, Canada. Ecol. Soc. 17.

25. Parlee BL, Goddard E, Dene First Nation É, Smith M. 2014. Tracking Change: Traditional Knowledge and Monitoring of Wildlife Health in Northern Canada. Hum. Dimens. Wildl. An Int. J. 19:47–61.

26. Engler NJ, Scassa T, Taylor DRF. 2013. Mapping Traditional Knowledge: Digital Cartography in the Canadian North. Cartographica. 48:189–199.

Appendix

Appendix A

Supplement Information for Chapter 4: The Use of Geographic Information Systems (GIS) for Spatial Ecological Risk Assessments: an example from the Athabasca Oil Sands area in Canada

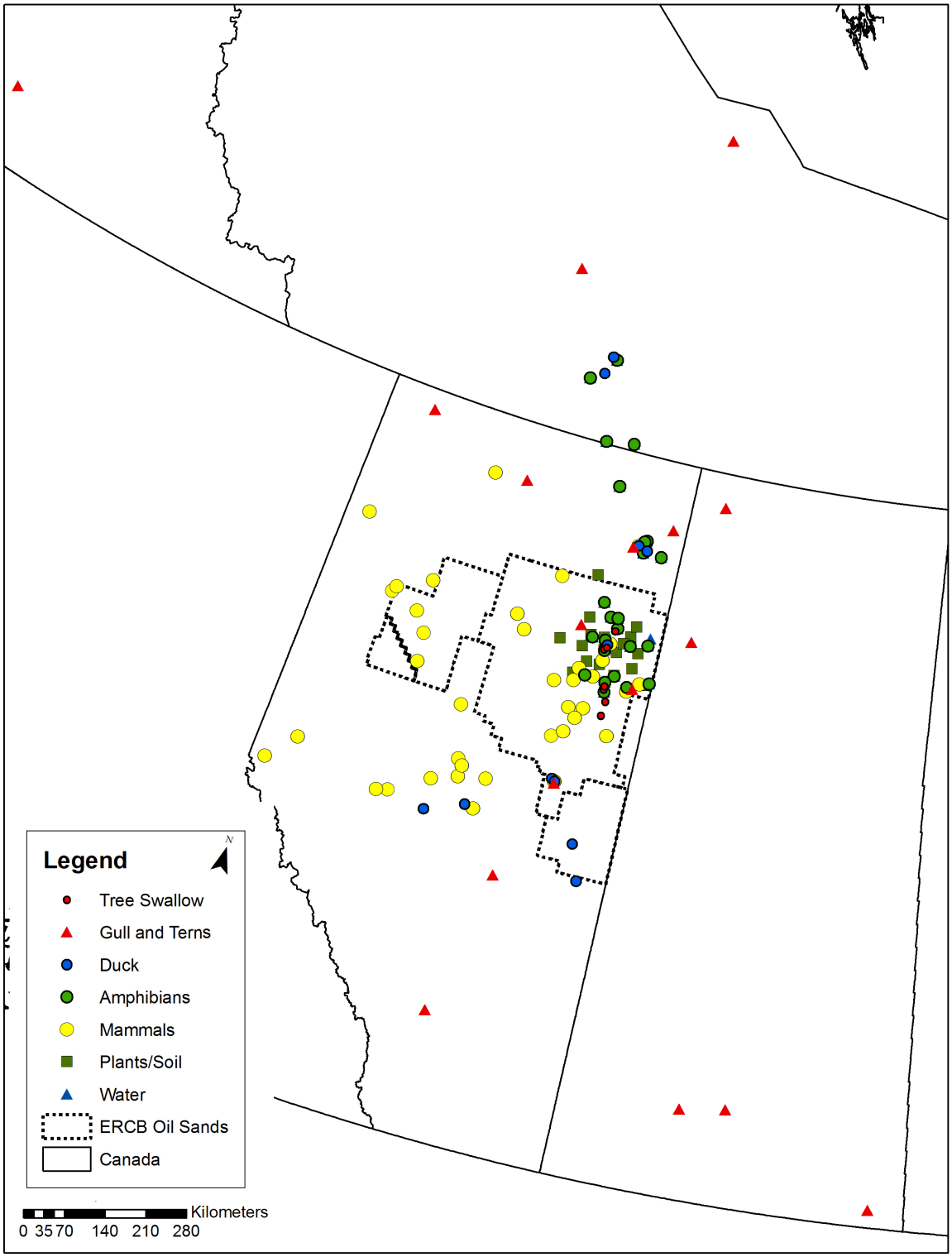

Figure A.1: A map showing the distribution of species sampled in the Joint Oil Sands Biomonitoring (JOSM) programs.

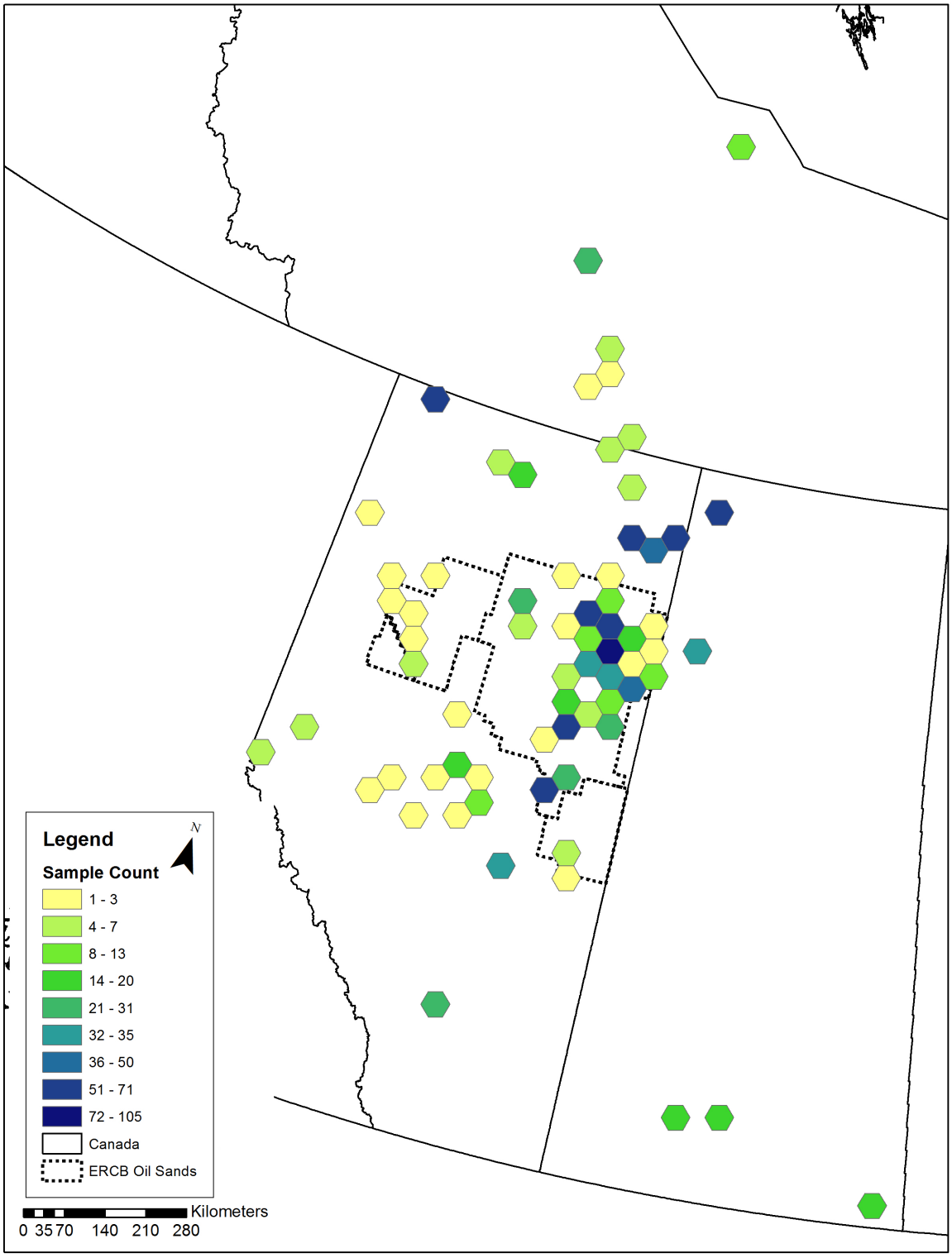

Figure A.2: The number of species from the Joint Oil Sands Biomonitoring (JOSM)programs within each cell after aggregation to a 25km hexagon grid.

Table A.1: Summary of the loadings for each metal in the multispati (MEM) analysis in components 1-4.

Metal	Component 1	Component 2	Component 3	Component 4
Ag	-0.10	0.16	-0.14	-0.16
As	-0.39	0.22	0.26	-0.68
Ba	-0.17	-0.15	0.19	0.01
Cd	-0.47	-0.16	0.20	0.53
Cu	0.23	-0.28	0.28	-0.05
Fe	-0.09	-0.02	-0.39	-0.08
Ga	-0.21	-0.11	0.23	0.05
Hg	0.07	-0.25	0.40	-0.11
Li	-0.21	-0.03	0.05	0.08
Mn	0.19	-0.16	-0.16	-0.17
Mo	-0.17	0.14	0.21	-0.18
Ni	0.15	-0.07	-0.07	-0.07
Pb	-0.25	-0.26	-0.16	0.09
Rb	0.15	-0.44	0.27	-0.09
Se	-0.38	-0.12	-0.06	-0.14
Sn	-0.02	0.03	-0.04	0.13
Sr	-0.12	-0.14	-0.31	-0.07
V	-0.30	0.10	-0.12	0.11
Zn	-0.13	-0.61	-0.32	-0.26

```
################################################################################
# PCA and BCA for complex exposures
# Written in R Version 3.5.2
################################################################################

# Load Libraries
library(factoextra)
library(ggplot2)
library(ade4)
library (adegraphics)
library(lattice)
library(sp)
library(adegenet)
library(spdep)
library(adespatial)
library(maptools)

# Combining plots for publication quality
library(ggpubr)
library(sjPlot)

################################################################################
# Read Data
data = read.csv("amphib_metals3.csv")

# Remove missing D\data
comp_data=na.omit(data)

################################################################################
### PCA ####
pca1= dudi.pca(df = comp_data[7:25], scannf = TRUE, nf = 5, center=TRUE)

#Plot PCA
g1=s.corcircle(pca1$co, plot=FALSE)
g2=s.label(pca1$li, plot=FALSE)
ADEgS(list(g1,g2))

#Scree Plot
scree=fviz_eig(pca1,
ncp=10,
ggtheme = theme_minimal(base_size = 18),
addlabels=TRUE,
```

```
main = NULL)

#### BCA ####
# Set up lat as a factor
lat=as.factor(comp_data$Lat)

#BCA by site
bca_site=bca(pca1,lat,scannf=TRUE)

# Plot BCA-Biplot
s.arrow(bca_site$co)

#Get loadings and write to csv
bca_loadings=bca_site$co
write.csv(bca_loadings, "bca_loadings.csv")

# Montecarlo to test between species differences
rt_between_site=randtest(bca_site)
rt_between_site
# 45% of the variance is explained by site differences (p=0.001)

############################################################
#### Spatial analysis ####
# Spatial Representation of BCA
# Create comp_dataset with bca scores and coordinates

# Aggregate the x y coordinates for site
xy=coordinates(comp_data[,3:4])
sitexy=aggregate(comp_data[,3:4], list(comp_data$Lat), mean)

# Extract information by site from BCA
dim(bca_site$tab)
scores_by_site=bca_site$li

# Attach Coordinates to sites
scores_xy=cbind(sitexy, scores_by_site)
write.csv(scores_xy, "site_scores_xy.csv")

# Prepare spatial data for mapping
colour=cbind(col="gray90", border="gray90")
rivers = readShapePoly("rivers_clip.shp", IDvar=NULL, proj4string=CRS(as.character(NA)),
verbose=FALSE, repair=FALSE, force_ring=FALSE)

# Map the scores of the BCA
g1.map.bca=s.value(scores_xy[,2:3],bca_site$li, symbol="circle",
pSp.col=as.factor(scores_xy$Group.1),
Sp=rivers, ppoints.cex=0.75,ylim=c(55,62), xlim=c(-115,-110))

#### Create BCA with spatial information integrated- Multispati ##### Defining spatial weights
# To explore other spatial weights matrices
# listw.explore()

# Gabriel Neighbourhood- best for uneven sampling schemes
nb <- chooseCN(scores_xy[,2:3], type = 2, plot.nb = FALSE)
lw <- nb2listw(nb, style = 'W', zero.policy = TRUE)

# Test spatial autcorrelation of BCA scores
# Moran's I
moran.randtest(scores_xy[,"Axis1"], listw=lw,nrepet=999)
moran.plot(scores_xy[,"Axis1"], listw=lw)
# Borderline positive spatial autocorrelation

moran.randtest(scores_xy[,"Axis2"], listw=lw,nrepet=999)
moran.plot(scores_xy[,"Axis2"], listw=lw)
#no spatial autocorrelation

# Write scores to csv
write.csv(cbind(xy,bca_site$li), "bca_scores.csv")

#Moran's eigenvector maps using gabriel neighbourhood
me=mem(lw)
map = s.value(scores_xy[,2:3], me[,c(1:2)], Sp=rivers, ppoints.cex=0.75,ylim=c(55,62), xlim=c(-115,-110))
scalo1=scalogram(scores_xy[,"Axis1"], me, nblocks=10)
plot(scalo1)
scalo2=scalogram(scores_xy[,"Axis2"], me, nblocks=10)
plot(scalo2)
s.arrow(me)

# Multispatial analysis
ms1=multispati(bca_site,lw,scannf=FALSE, nfposi=4,nfnega=0)
summary(ms1)
plot
s.arrow(ms1$c1)
# Output loadings
write.csv(ms1$c1, "multispati_loadings.csv")

#############################################################
# Publication Plots
# Figure 5
scree=fviz_eig(pca1,
ncp=10,
ggtheme = theme_minimal(base_size = 18),
```

```
addlabels=TRUE,
main = NULL)

save_plot("scree.tif", scree, width = 20, height = 20, dpi = 300,
legend.textsize = 20, legend.titlesize = 20,
legend.itemsize = 20)
```

```
#####################################################################
# Example 3: Codisperion Statistics
# Written in R Version 3.5.0
#####################################################################

#Load data
data = read.csv("data.csv")

#Load Libraries
library(SpatialPack)

summary(data)

x = data$amphib_cort
y = data$snow
coords = data [1:2]

data.test = modified.ttest(data$amphib_cort, data$snow, coords)
data.test

data.codisp = codisp(data$amphib_cort, data$snow, coords)
data.codisp
plot(data.codisp, xlab="distance (km)", title(main = NULL))

data.cor = cor.spatial(data$amphib_cort, data$snow, coords)
data.cor
```

Appendix B

Supplement Information for Chapter 4: Distribution of organic and inorganic mercury across Canadian river otter (*Lontra canadensis*) pelts

Table B.1: Equality of variances F-test results for topcoat (TC) and undercoat (UC) samples for individual pelts.

Pelt	Ratio of the variances (TC/UC)	F-value[1]	p-value
Pelt 1	0.1005	0.1005 (88,88)	< 0.001
Pelt 2	0.0084	0.0084 (97,97)	< 0.001
Pelt 3	0.0617	0.0617 (95,95)	< 0.001
Pelt 4	0.0331	0.0331 (94,94)	< 0.001

[1] Bracketed values are the degrees of freedom of the numerator and the denominator, respectively.

Table B.2: Student's t-test results for paired topcoat (TC) and undercoat (UC) samples with unequal variances for individual pelts.

Pelt	Mean of the differences (TC - UC) (μg/g)	t statistic[1]	p-value
Pelt 1	-0.6	-9.56 (88)	< 0.001
Pelt 2	-4.8	-22.3 (97)	< 0.001
Pelt 3	-1.4	-9.82 (95)	< 0.001
Pelt 4	-0.4	-4.83 (94)	< 0.001

[1] Bracketed values are degrees of freedom.

Figure B.1: Photo of gridding for pelt 1.

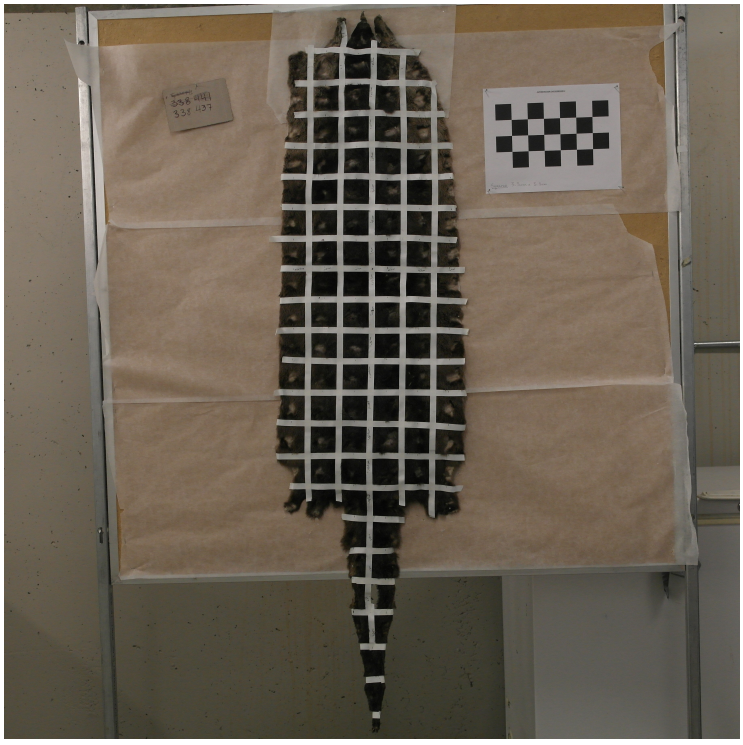

Figure B.2: Photo of gridding for pelt 2.

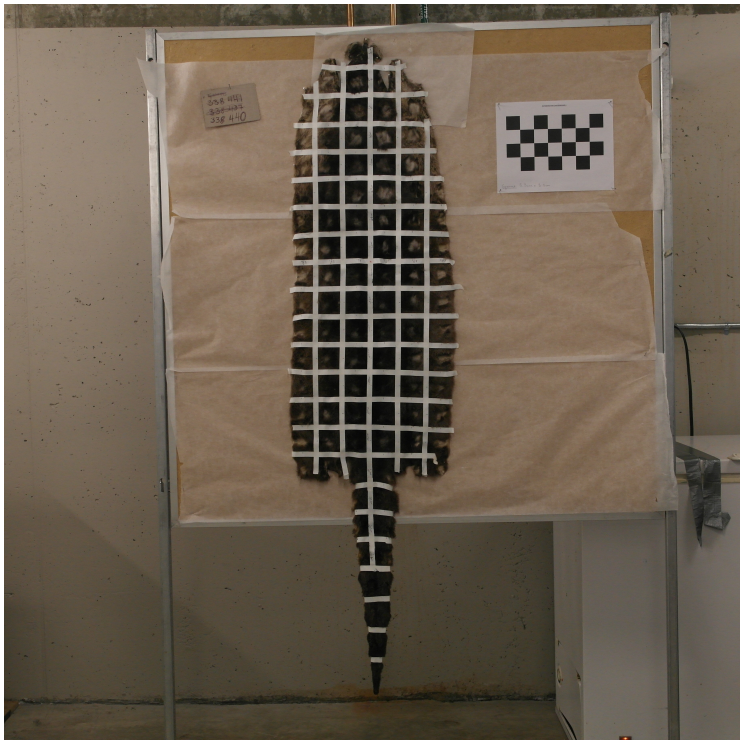

Figure B.3: Photo of gridding for pelt 3.

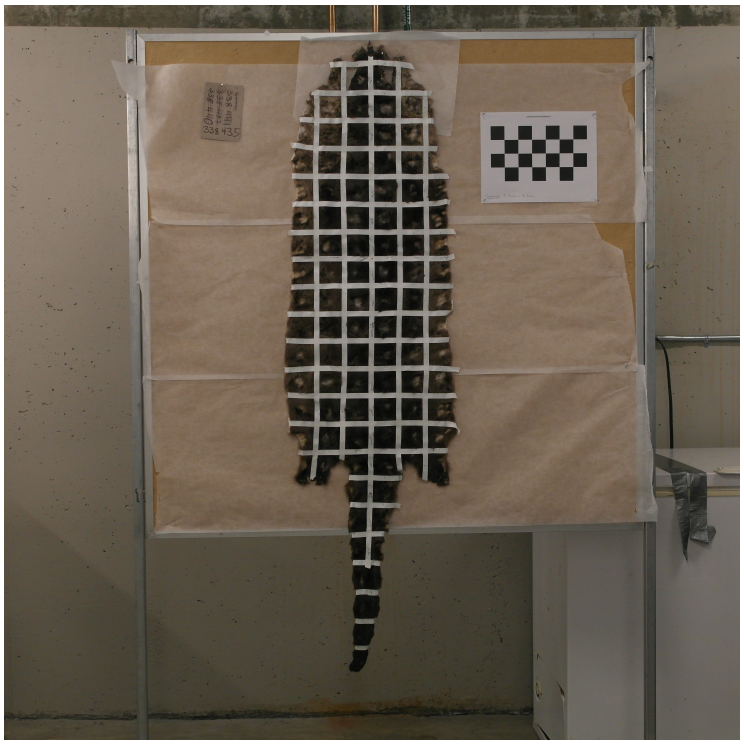

Figure B.4: Photo of gridding for pelt 4.

Figure B.5: Photo of fur sample after being removed from the pelt with topcoat (dark coarse hair) and undercoat (lighter thin hair).

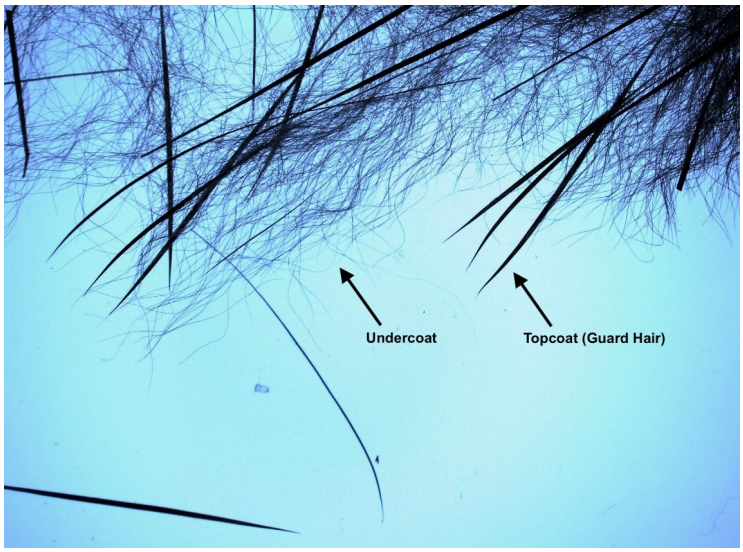

Figure B.6: Photo of fur sample under a dissecting microscope to show the difference between topcoat and undercoat fur; the topcoat is coarser and longer and undercoat is shorter and thinner.

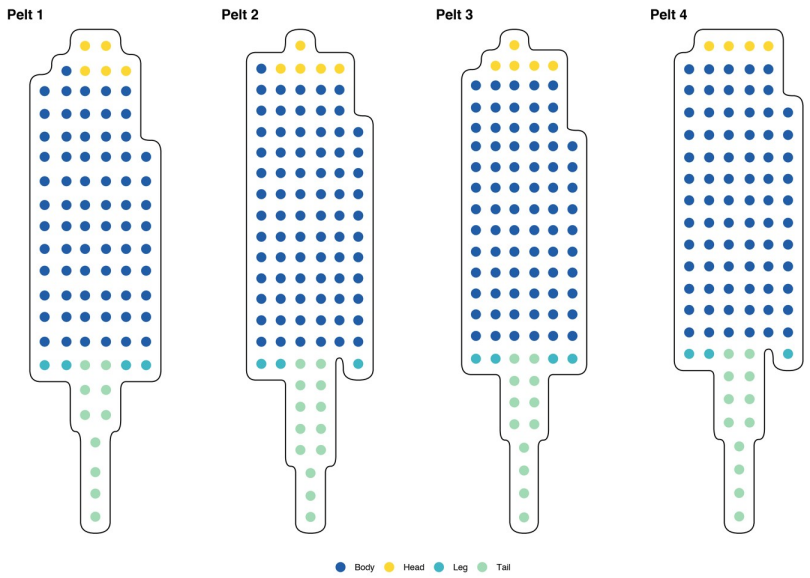

Figure B.7: A plot illustrating the different anatomical regions used for analysis on the pelt each.

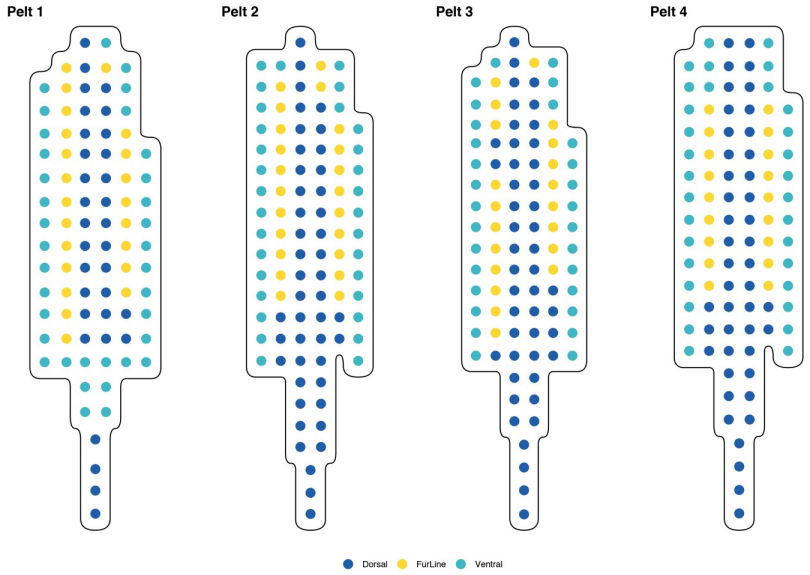

Figure B.8: A plot illustrating the different fur regions used for analysis on the pelt each.

```
##############################################################################
# Statistics for Pelt 1
# Written in R Version 3.5.0
##############################################################################
# Load data
pelt1 = read.csv("PELT1.csv")

# Load Libraries
library(ggplot2)
library(boot)
library(lmtest)
library(car)
library(multcomp)

#########################################################
#### Pelt 1 Statistical Analysis ####
#### T-test ####
# Check assumptions of raw variables
shapiro.test(pelt1$THg_TC) #Not normal
hist(pelt1$THg_TC, freq = FALSE, breaks = 30, xlab = "[THg] (ppm)") # Approximately normal

shapiro.test(pelt1$THg_UC) # Not normal
hist(pelt1$THg_UC, freq = FALSE, breaks = 30, xlab = "[THg] (ppm)") # Approximately normal

# Equal variances Levene's test
var.test(pelt1$THg_TC, pelt1$THg_UC) #variances are not equal

# Differene between TC and UC (paired)- Welch's paired t-test
t.test(pelt1$THg_TC, pelt1$THg_UC, paired = TRUE, var.equal = FALSE,
alternative = "two.sided")
shapiro.test((pelt1$THg_TC-pelt1$THg_UC)) # Differences Not normal
hist(pelt1$THg_TC-pelt1$THg_UC) # Differences Approximately normal

#### Variance between TC and UC ####
# Calculate absolute ranges
p1_TC_range = max(pelt1$THg_TC) - min(pelt1$THg_TC)
p1_UC_range = max(pelt1$THg_UC) - min(pelt1$THg_UC)

# Calculate ratio of ranges relative to TC THg range
UC_TC_ratio = (p1_UC_range)/(p1_TC_range)

# Calculate percent diff of ranges relative to TC THg range
percent_UC_TC_diff = (((p1_UC_range)/(p1_TC_range))-1)*100

# Calculate mean, SD and 95% CI (t(3, 0.05) = 3.1824) for percent diffs
paste(mean(percent_UC_TC_diff), "+/-",(3.1824*(260/sqrt(4))))

#### Anatomical Region Differences ####
# One-way ANOVA for Anatomical region
# TOP COAT
par(mfrow = c(2,2), mar = c(5,5,5,5))
p1_TC_anova1 = lm(pelt1$THg_TC ~ pelt1$Anatomical_region)
summary(p1_TC_anova1)
plot(p1_TC_anova1, main = "TC [THg] by anatomical region")

# Normality test of residuals
shapiro.test(residuals(p1_TC_anova1)) #not normal
hist(residuals(p1_TC_anova1), breaks = 30, freq = FALSE,
main = "Histogram of PELT 1 TC [THg] one-way ANOVA residuals by anatomical region")
curve(dnorm(x, mean(residuals(p1_TC_anova1)), sd(residuals(p1_TC_anova1))),
add=TRUE, col="darkblue", lwd=2)

# Homoscedasticity test of residuals
bptest(pelt1$THg_TC ~ pelt1$Anatomical_region) #homoscedastic

# Post-hoc Tukey's multiple comparison
# ANOVA
p1_TC_posthoc = aov(pelt1$THg_TC ~ pelt1$Anatomical_region)
p1_TC_tukey = TukeyHSD(p1_TC_posthoc)
plot(p1_TC_tukey)

# UNDERCOAT
par(mfrow = c(2,2), mar = c(5,5,5,5))
p1_UC_anova1 = lm(pelt1$THg_UC ~ pelt1$Anatomical_region)
summary(p1_UC_anova1)
plot(p1_UC_anova1, main = "UC [THg] by anatomical region")

# Normality test of residuals
shapiro.test(residuals(p1_UC_anova1)) #not normal
par(mfrow = c(1,1), las = 1, mar = c(5,5,5,5))
hist(residuals(p1_UC_anova1), breaks = 30, freq = FALSE)
curve(dnorm(x, mean(residuals(p1_UC_anova1)), sd(residuals(p1_UC_anova1))),
add=TRUE, col="darkblue", lwd=2) # Approximately normal

# Homoscedasticity test of residuals
leveneTest(pelt1$THg_UC ~ pelt1$Anatomical_region) # homoscedastic

#Tukey's multiple comparison
p1_UC_posthoc = aov(pelt1$THg_UC ~ pelt1$Anatomical_region)
p1_UC_tukey = TukeyHSD(p1_UC_posthoc)
plot(p1_UC_tukey)
```

```
#### Fur Region Differences ####
#TOP COAT
par(mfrow = c(2,2), mar = c(5,5,5,5))
p1_TC_anova2 = lm(pelt1$THg_TC ~ pelt1$Fur_region)
p1_TC_anova2
plot(p1_TC_anova2, main = "TC [THg] by fur region")

#normality test of residuals
shapiro.test(residuals(p1_TC_anova2)) # Not normal

par(mfrow = c(1,1), las = 1, mar = c(5,5,5,5))
hist(residuals(p1_TC_anova2), breaks = 30, freq = FALSE,
main = "Histogram of PELT 1 TC [THg] one-way ANOVA residuals by fur region")
curve(dnorm(x, mean(residuals(p1_TC_anova2)), sd(residuals(p1_TC_anova2))),
add=TRUE, col="darkblue", lwd=2) # Approx normal


# Homoscedasticity test of residuals
leveneTest(pelt1$THg_TC ~ pelt1$Fur_region) # Homoscedastic

#Tukey's multiple comparison
p1_TC_posthoc2 = aov(pelt1$THg_TC ~ pelt1$Fur_region)
p1_TC_tukey2 = TukeyHSD(p1_TC_posthoc2)
plot(p1_TC_tukey2)

# UNDERCOAT
par(mfrow = c(2,2), mar = c(5,5,5,5))
p1_UC_anova2 = lm(pelt1$THg_UC ~ pelt1$Fur_region)
p1_UC_anova2
plot(p1_UC_anova2, main = "UC [THg] by fur region")

#normality test of residuals
shapiro.test(residuals(p1_UC_anova2)) # Not normal

par(mfrow = c(1,1), las = 1, mar = c(5,5,5,5))
hist(residuals(p1_UC_anova2), breaks = 30, freq = FALSE,
main = "Histogram of PELT 1 UC [THg] one-way ANOVA residuals by fur region")
curve(dnorm(x, mean(residuals(p1_UC_anova2)), sd(residuals(p1_UC_anova2))),
add=TRUE, col="darkblue", lwd=2) # Approximately normal

# Homoscedasticity test of residuals
leveneTest(pelt1$THg_UC ~ pelt1$Fur_region) # Homoscedastic

#Tukey's multiple comparison
p1_UC_posthoc2 = aov(pelt1$THg_UC ~ pelt1$Fur_region)
p1_UC_tukey2 = TukeyHSD(p1_UC_posthoc2)
plot(p1_UC_tukey2)
```

```
##############################################################################
# Statistics for Pelt 2
# Written in R Version 3.5.0
##############################################################################
# Load data
pelt2 = read.csv("PELT2.csv")

# Load Libraries
library(ggplot2)
library(boot)
library(lmtest)
library(car)
library(multcomp)

#############################################################
#### Pelt 1 Statistical Analysis ####
#### T-test ####
# Check assumptions of raw variables
shapiro.test(pelt2$THg_TC) #Not normal
hist(pelt2$THg_TC, freq = FALSE, breaks = 30, xlab = "[THg] (ppm)") # Approximately normal

shapiro.test(pelt2$THg_UC) # Not normal
hist(pelt2$THg_UC, freq = FALSE, breaks = 30, xlab = "[THg] (ppm)") # Approximately normal

# Equal variances Levene's test
var.test(pelt2$THg_TC, pelt2$THg_UC) #variances are not equal

# Differene between TC and UC (paired)- Welch's paired t-test
t.test(pelt2$THg_TC, pelt2$THg_UC, paired = TRUE, var.equal = FALSE,
alternative = "two.sided")
shapiro.test((pelt2$THg_TC-pelt2$THg_UC)) # Differences Not normal
hist(pelt2$THg_TC-pelt2$THg_UC) # Differences Approximately normal

#### Variance between TC and UC ####
# Calculate absolute ranges
p2_TC_range = max(pelt2$THg_TC) - min(pelt2$THg_TC)
p2_UC_range = max(pelt2$THg_UC) - min(pelt2$THg_UC)

# Calculate ratio of ranges relative to TC THg range
UC_TC_ratio = (p2_UC_range)/(p2_TC_range)

# Calculate percent diff of ranges relative to TC THg range
percent_UC_TC_diff = (((p2_UC_range)/(p2_TC_range))-1)*100

# Calculate mean, SD and 95% CI (t(3, 0.05) = 3.1824) for percent diffs
paste(mean(percent_UC_TC_diff), "+/-",(3.1824*(260/sqrt(4))))

#### Anatomical Region Differences ####
# One-way ANOVA for Anatomical region
# TOP COAT
par(mfrow = c(2,2), mar = c(5,5,5,5))
p2_TC_anova1 = lm(pelt2$THg_TC ~ pelt2$Anatomical_region)
summary(p2_TC_anova1)
plot(p2_TC_anova1, main = "TC [THg] by anatomical region")

# Normality test of residuals
shapiro.test(residuals(p2_TC_anova1)) #not normal
hist(residuals(p2_TC_anova1), breaks = 30, freq = FALSE,
main = "Histogram of PELT 1 TC [THg] one-way ANOVA residuals by anatomical region")
curve(dnorm(x, mean(residuals(p2_TC_anova1)), sd(residuals(p2_TC_anova1))),
add=TRUE, col="darkblue", lwd=2)

# Homoscedasticity test of residuals
bptest(pelt2$THg_TC ~ pelt2$Anatomical_region) #homoscedastic

# Post-hoc Tukey's multiple comparison
# ANOVA
p2_TC_posthoc = aov(pelt2$THg_TC ~ pelt2$Anatomical_region)
p2_TC_tukey = TukeyHSD(p2_TC_posthoc)
plot(p2_TC_tukey)

# UNDERCOAT
par(mfrow = c(2,2), mar = c(5,5,5,5))
p2_UC_anova1 = lm(pelt2$THg_UC ~ pelt2$Anatomical_region)
summary(p2_UC_anova1)
plot(p2_UC_anova1, main = "UC [THg] by anatomical region")

# Normality test of residuals
shapiro.test(residuals(p2_UC_anova1)) #not normal
par(mfrow = c(1,1), las = 1, mar = c(5,5,5,5))
hist(residuals(p2_UC_anova1), breaks = 30, freq = FALSE)
curve(dnorm(x, mean(residuals(p2_UC_anova1)), sd(residuals(p2_UC_anova1))),
add=TRUE, col="darkblue", lwd=2) # Approximately normal

# Homoscedasticity test of residuals
leveneTest(pelt2$THg_UC ~ pelt2$Anatomical_region) # homoscedastic

#Tukey's multiple comparison
p2_UC_posthoc = aov(pelt2$THg_UC ~ pelt2$Anatomical_region)
p2_UC_tukey = TukeyHSD(p2_UC_posthoc)
plot(p2_UC_tukey)
```

```
#### Fur Region Differences ####
#TOP COAT
par(mfrow = c(2,2), mar = c(5,5,5,5))
p2_TC_anova2 = lm(pelt2$THg_TC ~ pelt2$Fur_region)
p2_TC_anova2
plot(p2_TC_anova2, main = "TC [THg] by fur region")

#normality test of residuals
shapiro.test(residuals(p2_TC_anova2)) # Not normal

par(mfrow = c(1,1), las = 1, mar = c(5,5,5,5))
hist(residuals(p2_TC_anova2), breaks = 30, freq = FALSE,
main = "Histogram of PELT 1 TC [THg] one-way ANOVA residuals by fur region")
curve(dnorm(x, mean(residuals(p2_TC_anova2)), sd(residuals(p2_TC_anova2))),
add=TRUE, col="darkblue", lwd=2) # Approx normal


# Homoscedasticity test of residuals
leveneTest(pelt2$THg_TC ~ pelt2$Fur_region) # Homoscedastic

#Tukey's multiple comparison
p2_TC_posthoc2 = aov(pelt2$THg_TC ~ pelt2$Fur_region)
p2_TC_tukey2 = TukeyHSD(p2_TC_posthoc2)
plot(p2_TC_tukey2)

# UNDERCOAT
par(mfrow = c(2,2), mar = c(5,5,5,5))
p2_UC_anova2 = lm(pelt2$THg_UC ~ pelt2$Fur_region)
p2_UC_anova2
plot(p2_UC_anova2, main = "UC [THg] by fur region")

#normality test of residuals
shapiro.test(residuals(p2_UC_anova2)) # Not normal

par(mfrow = c(1,1), las = 1, mar = c(5,5,5,5))
hist(residuals(p2_UC_anova2), breaks = 30, freq = FALSE,
main = "Histogram of PELT 1 UC [THg] one-way ANOVA residuals by fur region")
curve(dnorm(x, mean(residuals(p2_UC_anova2)), sd(residuals(p2_UC_anova2))),
add=TRUE, col="darkblue", lwd=2) # Approximately normal

# Homoscedasticity test of residuals
leveneTest(pelt2$THg_UC ~ pelt2$Fur_region) # Homoscedastic

#Tukey's multiple comparison
p2_UC_posthoc2 = aov(pelt2$THg_UC ~ pelt2$Fur_region)
p2_UC_tukey2 = TukeyHSD(p2_UC_posthoc2)
plot(p2_UC_tukey2)
```

```
##############################################################################
# Statistics for Pelt 1
# Written in R Version 3.5.0
##############################################################################
# Load data
pelt3 = read.csv("PELT3.csv")

# Load Libraries
library(ggplot2)
library(boot)
library(lmtest)
library(car)
library(multcomp)

#############################################################
#### Pelt 1 Statistical Analysis ####
#### T-test ####
# Check assumptions of raw variables
shapiro.test(pelt3$THg_TC) #Not normal
hist(pelt3$THg_TC, freq = FALSE, breaks = 30, xlab = "[THg] (ppm)") # Approximately normal

shapiro.test(pelt3$THg_UC) # Not normal
hist(pelt3$THg_UC, freq = FALSE, breaks = 30, xlab = "[THg] (ppm)") # Approximately normal

# Equal variances Levene's test
var.test(pelt3$THg_TC, pelt3$THg_UC) #variances are not equal

# Differene between TC and UC (paired)- Welch's paired t-test
t.test(pelt3$THg_TC, pelt3$THg_UC, paired = TRUE, var.equal = FALSE,
alternative = "two.sided")
shapiro.test((pelt3$THg_TC-pelt3$THg_UC)) # Differences Not normal
hist(pelt3$THg_TC-pelt3$THg_UC) # Differences Approximately normal

#### Variance between TC and UC ####
# Calculate absolute ranges
p3_TC_range = max(pelt3$THg_TC) - min(pelt3$THg_TC)
p3_UC_range = max(pelt3$THg_UC) - min(pelt3$THg_UC)

# Calculate ratio of ranges relative to TC THg range
UC_TC_ratio = (p3_UC_range)/(p3_TC_range)

# Calculate percent diff of ranges relative to TC THg range
percent_UC_TC_diff = (((p3_UC_range)/(p3_TC_range))-1)*100

# Calculate mean, SD and 95% CI (t(3, 0.05) = 3.1824) for percent diffs
paste(mean(percent_UC_TC_diff), "+/-",(3.1824*(260/sqrt(4))))

#### Anatomical Region Differences ####
# One-way ANOVA for Anatomical region
# TOP COAT
par(mfrow = c(2,2), mar = c(5,5,5,5))
p3_TC_anova1 = lm(pelt3$THg_TC ~ pelt3$Anatomical_region)
summary(p3_TC_anova1)
plot(p3_TC_anova1, main = "TC [THg] by anatomical region")

# Normality test of residuals
shapiro.test(residuals(p3_TC_anova1)) #not normal
hist(residuals(p3_TC_anova1), breaks = 30, freq = FALSE,
main = "Histogram of PELT 1 TC [THg] one-way ANOVA residuals by anatomical region")
curve(dnorm(x, mean(residuals(p3_TC_anova1)), sd(residuals(p3_TC_anova1))),
add=TRUE, col="darkblue", lwd=2)

# Homoscedasticity test of residuals
bptest(pelt3$THg_TC ~ pelt3$Anatomical_region) #homoscedastic

# Post-hoc Tukey's multiple comparison
# ANOVA
p3_TC_posthoc = aov(pelt3$THg_TC ~ pelt3$Anatomical_region)
p3_TC_tukey = TukeyHSD(p3_TC_posthoc)
plot(p3_TC_tukey)

# UNDERCOAT
par(mfrow = c(2,2), mar = c(5,5,5,5))
p3_UC_anova1 = lm(pelt3$THg_UC ~ pelt3$Anatomical_region)
summary(p3_UC_anova1)
plot(p3_UC_anova1, main = "UC [THg] by anatomical region")

# Normality test of residuals
shapiro.test(residuals(p3_UC_anova1)) #not normal
par(mfrow = c(1,1), las = 1, mar = c(5,5,5,5))
hist(residuals(p3_UC_anova1), breaks = 30, freq = FALSE)
curve(dnorm(x, mean(residuals(p3_UC_anova1)), sd(residuals(p3_UC_anova1))),
add=TRUE, col="darkblue", lwd=2) # Approximately normal

# Homoscedasticity test of residuals
leveneTest(pelt3$THg_UC ~ pelt3$Anatomical_region) # homoscedastic

#Tukey's multiple comparison
p3_UC_posthoc = aov(pelt3$THg_UC ~ pelt3$Anatomical_region)
p3_UC_tukey = TukeyHSD(p3_UC_posthoc)
plot(p3_UC_tukey)
```

```
#### Fur Region Differences ####
#TOP COAT
par(mfrow = c(2,2), mar = c(5,5,5,5))
p3_TC_anova2 = lm(pelt3$THg_TC ~ pelt3$Fur_region)
p3_TC_anova2
plot(p3_TC_anova2, main = "TC [THg] by fur region")

#normality test of residuals
shapiro.test(residuals(p3_TC_anova2)) # Not normal

par(mfrow = c(1,1), las = 1, mar = c(5,5,5,5))
hist(residuals(p3_TC_anova2), breaks = 30, freq = FALSE,
main = "Histogram of PELT 1 TC [THg] one-way ANOVA residuals by fur region")
curve(dnorm(x, mean(residuals(p3_TC_anova2)), sd(residuals(p3_TC_anova2))),
add=TRUE, col="darkblue", lwd=2) # Approx normal


# Homoscedasticity test of residuals
leveneTest(pelt3$THg_TC ~ pelt3$Fur_region) # Homoscedastic

#Tukey's multiple comparison
p3_TC_posthoc2 = aov(pelt3$THg_TC ~ pelt3$Fur_region)
p3_TC_tukey2 = TukeyHSD(p3_TC_posthoc2)
plot(p3_TC_tukey2)

# UNDERCOAT
par(mfrow = c(2,2), mar = c(5,5,5,5))
p3_UC_anova2 = lm(pelt3$THg_UC ~ pelt3$Fur_region)
p3_UC_anova2
plot(p3_UC_anova2, main = "UC [THg] by fur region")

#normality test of residuals
shapiro.test(residuals(p3_UC_anova2)) # Not normal

par(mfrow = c(1,1), las = 1, mar = c(5,5,5,5))
hist(residuals(p3_UC_anova2), breaks = 30, freq = FALSE,
main = "Histogram of PELT 1 UC [THg] one-way ANOVA residuals by fur region")
curve(dnorm(x, mean(residuals(p3_UC_anova2)), sd(residuals(p3_UC_anova2))),
add=TRUE, col="darkblue", lwd=2) # Approximately normal

# Homoscedasticity test of residuals
leveneTest(pelt3$THg_UC ~ pelt3$Fur_region) # Homoscedastic

#Tukey's multiple comparison
p3_UC_posthoc2 = aov(pelt3$THg_UC ~ pelt3$Fur_region)
p3_UC_tukey2 = TukeyHSD(p3_UC_posthoc2)
plot(p3_UC_tukey2)
```

```
##############################################################################
# Statistics for Pelt 4
# Written in R Version 3.5.0
##############################################################################
# Load data
pelt4 = read.csv("PELT4.csv")

# Load Libraries
library(ggplot2)
library(boot)
library(lmtest)
library(car)
library(multcomp)

#############################################################
#### Pelt 1 Statistical Analysis ####
#### T-test ####
# Check assumptions of raw variables
shapiro.test(pelt4$THg_TC) #Not normal
hist(pelt4$THg_TC, freq = FALSE, breaks = 30, xlab = "[THg] (ppm)") # Approximately normal

shapiro.test(pelt4$THg_UC) # Not normal
hist(pelt4$THg_UC, freq = FALSE, breaks = 30, xlab = "[THg] (ppm)") # Approximately normal

# Equal variances Levene's test
var.test(pelt4$THg_TC, pelt4$THg_UC) #variances are not equal

# Differene between TC and UC (paired)- Welch's paired t-test
t.test(pelt4$THg_TC, pelt4$THg_UC, paired = TRUE, var.equal = FALSE,
alternative = "two.sided")
shapiro.test((pelt4$THg_TC-pelt4$THg_UC)) # Differences Not normal
hist(pelt4$THg_TC-pelt4$THg_UC) # Differences Approximately normal

#### Variance between TC and UC ####
# Calculate absolute ranges
p4_TC_range = max(pelt4$THg_TC) - min(pelt4$THg_TC)
p4_UC_range = max(pelt4$THg_UC) - min(pelt4$THg_UC)

# Calculate ratio of ranges relative to TC THg range
UC_TC_ratio = (p4_UC_range)/(p4_TC_range)

# Calculate percent diff of ranges relative to TC THg range
percent_UC_TC_diff = (((p4_UC_range)/(p4_TC_range))-1)*100

# Calculate mean, SD and 95% CI (t(3, 0.05) = 3.1824) for percent diffs
paste(mean(percent_UC_TC_diff), "+/-",(3.1824*(260/sqrt(4))))

#### Anatomical Region Differences ####
# One-way ANOVA for Anatomical region
# TOP COAT
par(mfrow = c(2,2), mar = c(5,5,5,5))
p4_TC_anova1 = lm(pelt4$THg_TC ~ pelt4$Anatomical_region)
summary(p4_TC_anova1)
plot(p4_TC_anova1, main = "TC [THg] by anatomical region")

# Normality test of residuals
shapiro.test(residuals(p4_TC_anova1)) #not normal
hist(residuals(p4_TC_anova1), breaks = 30, freq = FALSE,
main = "Histogram of PELT 1 TC [THg] one-way ANOVA residuals by anatomical region")
curve(dnorm(x, mean(residuals(p4_TC_anova1)), sd(residuals(p4_TC_anova1))),
add=TRUE, col="darkblue", lwd=2)

# Homoscedasticity test of residuals
bptest(pelt4$THg_TC ~ pelt4$Anatomical_region) #homoscedastic

# Post-hoc Tukey's multiple comparison
# ANOVA
p4_TC_posthoc = aov(pelt4$THg_TC ~ pelt4$Anatomical_region)
p4_TC_tukey = TukeyHSD(p4_TC_posthoc)
plot(p4_TC_tukey)

# UNDERCOAT
par(mfrow = c(2,2), mar = c(5,5,5,5))
p4_UC_anova1 = lm(pelt4$THg_UC ~ pelt4$Anatomical_region)
summary(p4_UC_anova1)
plot(p4_UC_anova1, main = "UC [THg] by anatomical region")

# Normality test of residuals
shapiro.test(residuals(p4_UC_anova1)) #not normal
par(mfrow = c(1,1), las = 1, mar = c(5,5,5,5))
hist(residuals(p4_UC_anova1), breaks = 30, freq = FALSE)
curve(dnorm(x, mean(residuals(p4_UC_anova1)), sd(residuals(p4_UC_anova1))),
add=TRUE, col="darkblue", lwd=2) # Approximately normal

# Homoscedasticity test of residuals
leveneTest(pelt4$THg_UC ~ pelt4$Anatomical_region) # homoscedastic

#Tukey's multiple comparison
p4_UC_posthoc = aov(pelt4$THg_UC ~ pelt4$Anatomical_region)
p4_UC_tukey = TukeyHSD(p4_UC_posthoc)
plot(p4_UC_tukey)
```

```
#### Fur Region Differences ####
#TOP COAT
par(mfrow = c(2,2), mar = c(5,5,5,5))
p4_TC_anova2 = lm(pelt4$THg_TC ~ pelt4$Fur_region)
p4_TC_anova2
plot(p4_TC_anova2, main = "TC [THg] by fur region")

#normality test of residuals
shapiro.test(residuals(p4_TC_anova2)) # Not normal

par(mfrow = c(1,1), las = 1, mar = c(5,5,5,5))
hist(residuals(p4_TC_anova2), breaks = 30, freq = FALSE,
main = "Histogram of PELT 1 TC [THg] one-way ANOVA residuals by fur region")
curve(dnorm(x, mean(residuals(p4_TC_anova2)), sd(residuals(p4_TC_anova2))),
add=TRUE, col="darkblue", lwd=2) # Approx normal


# Homoscedasticity test of residuals
leveneTest(pelt4$THg_TC ~ pelt4$Fur_region) # Homoscedastic

#Tukey's multiple comparison
p4_TC_posthoc2 = aov(pelt4$THg_TC ~ pelt4$Fur_region)
p4_TC_tukey2 = TukeyHSD(p4_TC_posthoc2)
plot(p4_TC_tukey2)

# UNDERCOAT
par(mfrow = c(2,2), mar = c(5,5,5,5))
p4_UC_anova2 = lm(pelt4$THg_UC ~ pelt4$Fur_region)
p4_UC_anova2
plot(p4_UC_anova2, main = "UC [THg] by fur region")

#normality test of residuals
shapiro.test(residuals(p4_UC_anova2)) # Not normal

par(mfrow = c(1,1), las = 1, mar = c(5,5,5,5))
hist(residuals(p4_UC_anova2), breaks = 30, freq = FALSE,
main = "Histogram of PELT 1 UC [THg] one-way ANOVA residuals by fur region")
curve(dnorm(x, mean(residuals(p4_UC_anova2)), sd(residuals(p4_UC_anova2))),
add=TRUE, col="darkblue", lwd=2) # Approximately normal

# Homoscedasticity test of residuals
leveneTest(pelt4$THg_UC ~ pelt4$Fur_region) # Homoscedastic

#Tukey's multiple comparison
p4_UC_posthoc2 = aov(pelt4$THg_UC ~ pelt4$Fur_region)
p4_UC_tukey2 = TukeyHSD(p4_UC_posthoc2)
plot(p4_UC_tukey2)
```

```
#############################################################################
# Statistics for composite pelt and comparisons
# Written in R Version 3.5.0
#############################################################################
# Load data
pelt1 = read.csv("PELT1.csv")
pelt2 = read.csv("PELT2.csv")
pelt3 = read.csv("PELT3.csv")
pelt4 = read.csv("PELT4.csv")
compiled = read.csv("pelts_compiled.csv")

# Load Libraries
library(ggplot2)
library(boot)
library(lmtest)
library(car)
library(multcomp)

#############################################################
#### Pelt 1 Statistical Analysis ####
#### T-test ####
# Check assumptions of raw variables
shapiro.test(compiled$THg_TC) #Not normal
hist(compiled$THg_TC, freq = FALSE, breaks = 30, xlab = "[THg] (ppm)") # Approximately normal

shapiro.test(compiled$THg_UC) # Not normal
hist(compiled$THg_UC, freq = FALSE, breaks = 30, xlab = "[THg] (ppm)") # Approximately normal

# Equal variances Levene's test
var.test(compiled$THg_TC, compiled$THg_UC) #variances are not equal

# Differene between TC and UC (paired)- Welch's paired t-test
t.test(compiled$THg_TC, compiled$THg_UC, paired = TRUE, var.equal = FALSE,
alternative = "two.sided")
shapiro.test((compiled$THg_TC-compiled$THg_UC)) # Differences Not normal
hist(compiled$THg_TC-compiled$THg_UC) # Differences Approximately normal

#### Comparison of Ranges of TC and UC #####
par(mfrow=c(2,2))
# Create boxplots with whiskers as ranges
pelt1_stack=stack(pelt1[,7:8])
box_p1=boxplot(pelt1_stack$values ~ pelt1_stack$ind, range = 0,
names=c("TC", "UC"),
ylab = "THg concentration (ppm)",
xlab = " Pelt 1")

pelt2_stack=stack(pelt2[,7:8])
box_p2=boxplot(pelt2_stack$values ~ pelt2_stack$ind, range = 0,
names=c("TC", "UC"),
ylab = "THg concentration (ppm)",
xlab = " Pelt 2")

pelt3_stack=stack(pelt3[,7:8])
box_p3=boxplot(pelt3_stack$values ~ pelt3_stack$ind, range = 0,
names=c("TC", "UC"),
ylab = "THg concentration (ppm)",
xlab = " Pelt 3")

pelt4_stack=stack(pelt4[,7:8])
box_p4=boxplot(pelt4_stack$values ~ pelt4_stack$ind, range = 0,
names=c("TC", "UC"),
ylab = "THg concentration (ppm)",
xlab = " Pelt 4")

#### Variance between TC and UC ####
# Calculate absolute ranges
comp_TC_range = max(compiled$THg_TC) - min(compiled$THg_TC)
comp_UC_range = max(compiled$THg_UC) - min(compiled$THg_UC)

# Calculate ratio of ranges relative to TC THg range
UC_TC_ratio = (comp_UC_range)/(comp_TC_range)

# Calculate percent diff of ranges relative to TC THg range
percent_UC_TC_diff = (((comp_UC_range)/(comp_TC_range))-1)*100

# Calculate mean, SD and 95% CI (t(3, 0.05) = 3.1824) for percent diffs
paste(mean(percent_UC_TC_diff), "+/-",(3.1824*(260/sqrt(4))))

#### Anatomical Region Differences ####
# One-way ANOVA for Anatomical region
# TOP COAT
par(mfrow = c(2,2), mar = c(5,5,5,5))
comp_TC_anova1 = lm(compiled$THg_TC ~ compiled$Anatomical_region)
summary(comp_TC_anova1)
plot(comp_TC_anova1, main = "TC [THg] by anatomical region")

# Normality test of residuals
shapiro.test(residuals(comp_TC_anova1)) #not normal
hist(residuals(comp_TC_anova1), breaks = 30, freq = FALSE,
main = "Histogram of PELT 1 TC [THg] one-way ANOVA residuals by anatomical region")
curve(dnorm(x, mean(residuals(comp_TC_anova1)), sd(residuals(comp_TC_anova1))),
add=TRUE, col="darkblue", lwd=2)
```

```
# Homoscedasticity test of residuals
bptest(compiled$THg_TC ~ compiled$Anatomical_region) #homoscedastic

# Post-hoc Tukey's multiple comparison
# ANOVA
comp_TC_posthoc = aov(compiled$THg_TC ~ compiled$Anatomical_region)
comp_TC_tukey = TukeyHSD(comp_TC_posthoc)
plot(comp_TC_tukey)

# UNDERCOAT
par(mfrow = c(2,2), mar = c(5,5,5,5))
comp_UC_anova1 = lm(compiled$THg_UC ~ compiled$Anatomical_region)
summary(comp_UC_anova1)
plot(comp_UC_anova1, main = "UC [THg] by anatomical region")

# Normality test of residuals
shapiro.test(residuals(comp_UC_anova1)) #not normal
par(mfrow = c(1,1), las = 1, mar = c(5,5,5,5))
hist(residuals(comp_UC_anova1), breaks = 30, freq = FALSE)
curve(dnorm(x, mean(residuals(comp_UC_anova1)), sd(residuals(comp_UC_anova1))),
add=TRUE, col="darkblue", lwd=2) # Approximately normal

# Homoscedasticity test of residuals
leveneTest(compiled$THg_UC ~ compiled$Anatomical_region) # homoscedastic

#Tukey's multiple comparison
comp_UC_posthoc = aov(compiled$THg_UC ~ compiled$Anatomical_region)
comp_UC_tukey = TukeyHSD(comp_UC_posthoc)
plot(comp_UC_tukey)

#### Fur Region Differences ####
#TOP COAT
par(mfrow = c(2,2), mar = c(5,5,5,5))
comp_TC_anova2 = lm(compiled$THg_TC ~ compiled$Fur_region)
comp_TC_anova2
plot(comp_TC_anova2, main = "TC [THg] by fur region")

#normality test of residuals
shapiro.test(residuals(comp_TC_anova2)) # Not normal

par(mfrow = c(1,1), las = 1, mar = c(5,5,5,5))
hist(residuals(comp_TC_anova2), breaks = 30, freq = FALSE,
main = "Histogram of PELT 1 TC [THg] one-way ANOVA residuals by fur region")
curve(dnorm(x, mean(residuals(comp_TC_anova2)), sd(residuals(comp_TC_anova2))),
add=TRUE, col="darkblue", lwd=2) # Approx normal


# Homoscedasticity test of residuals
leveneTest(compiled$THg_TC ~ compiled$Fur_region) # Homoscedastic

#Tukey's multiple comparison
comp_TC_posthoc2 = aov(compiled$THg_TC ~ compiled$Fur_region)
comp_TC_tukey2 = TukeyHSD(comp_TC_posthoc2)
plot(comp_TC_tukey2)

# UNDERCOAT
par(mfrow = c(2,2), mar = c(5,5,5,5))
comp_UC_anova2 = lm(compiled$THg_UC ~ compiled$Fur_region)
comp_UC_anova2
plot(comp_UC_anova2, main = "UC [THg] by fur region")

#normality test of residuals
shapiro.test(residuals(comp_UC_anova2)) # Not normal

par(mfrow = c(1,1), las = 1, mar = c(5,5,5,5))
hist(residuals(comp_UC_anova2), breaks = 30, freq = FALSE,
main = "Histogram of PELT 1 UC [THg] one-way ANOVA residuals by fur region")
curve(dnorm(x, mean(residuals(comp_UC_anova2)), sd(residuals(comp_UC_anova2))),
add=TRUE, col="darkblue", lwd=2) # Approximately normal

# Homoscedasticity test of residuals
leveneTest(compiled$THg_UC ~ compiled$Fur_region) # Homoscedastic

#Tukey's multiple comparison
comp_UC_posthoc2 = aov(compiled$THg_UC ~ compiled$Fur_region)
comp_UC_tukey2 = TukeyHSD(comp_UC_posthoc2)
plot(comp_UC_tukey2)
```

```
##############################################################################
# Create pelt outlines
# Written in R Version 3.5.0
##############################################################################
# Load Libraries
pelt1 = read.csv("PELT1.csv")
pelt2 = read.csv("PELT2.csv")
pelt3 = read.csv("PELT3.csv")
pelt4 = read.csv("PELT4.csv")
compiled = read.csv("pelts_compiled.csv")

# Load libraries
library(smoothr)
library(rgeos)
##############################################################################
#### Pelt 1 Outline ####
# set up coordinates
coords = coordinates(cbind(pelt1$X_coord, pelt1$Y_coord))
p1 = SpatialPoints(coords)
plot(p1, axes = TRUE)

# Buffer
buf1 = gBuffer(p1, byid=FALSE, width=5, capStyle="SQUARE")
plot(buf1)

#Smooth edges
p1_smooth = smooth(buf1, method = "chaikin")
plot(p1_smooth)

#Plot final points and polygon
plot(p1_smooth)
points(coords)

#Write spatialpolygon to dataframe and then to shapefile
df = data.frame(id = getSpPPolygonsIDSlots(p1_smooth))
row.names(df) = getSpPPolygonsIDSlots(p1_smooth)
p1_spdf <- SpatialPolygonsDataFrame(p1_smooth, data =df)
writeOGR(p1_spdf, dsn = "C:/Users/keccl081/Dropbox/pelt", driver="ESRI Shapefile", layer = "p1_Outline")

##############################################################################
##### Pelt 2 Outline ####
# set up coordinates
coords = coordinates(cbind(pelt2$X_coord, pelt2$Y_coord))
p2 = SpatialPoints(coords)
plot(p2, axes = TRUE)

# Buffer
buf1 = gBuffer(p2, byid=FALSE, width=5, capStyle="SQUARE")
plot(buf1)

#Smooth edges
p2_outline = smooth(buf1, method = "chaikin")
plot(p2_outline)
#Plot final points and polygon
p2 = plot(p2_outline)
points(coords, col = pelt2$Anatomical_region, pch=16)

#Write spatialpolygon to dataframe and then to shapefile
df = data.frame(id = getSpPPolygonsIDSlots(p2_outline))
row.names(df) = getSpPPolygonsIDSlots(p2_outline)
p2_spdf = SpatialPolygonsDataFrame(p2_outline, data =df)
writeOGR(p2_spdf, dsn = "C:/Users/keccl081/Dropbox/pelt", driver="ESRI Shapefile", layer = "p2_Outline")

##############################################################################
##### Pelt 3 Outline ####
# set up coordinates
coords = coordinates(cbind(pelt3$X_coord, pelt3$Y_coord))
p3 = SpatialPoints(coords)
plot(p3, axes = TRUE)

# Buffer
buf1 = gBuffer(p3, byid=FALSE, width=5, capStyle="SQUARE")
plot(buf1)

#Smooth edges
p3_outline = smooth(buf1, method = "chaikin")
plot(p3_outline)
#Plot final points and polygon
p3 = plot(p3_outline)
points(coords, col = pelt3$Anatomical_region, pch=16)

#Write spatialpolygon to dataframe and then to shapefile
df = data.frame(id = getSpPPolygonsIDSlots(p3_outline))
row.names(df) = getSpPPolygonsIDSlots(p3_outline)
p3_spdf = SpatialPolygonsDataFrame(p3_outline, data =df)
writeOGR(p3_spdf, dsn = "C:/Users/keccl081/Dropbox/pelt", driver="ESRI Shapefile", layer = "p3_Outline")

##############################################################################
##### Pelt 4 Outline ####
# set up coordinates
coords = coordinates(cbind(pelt4$X_coord, pelt4$Y_coord))
p4 = SpatialPoints(coords)
```

```
plot(p4, axes = TRUE)

# Buffer
buf1 = gBuffer(p4, byid=FALSE, width=5, capStyle="SQUARE")
plot(buf1)

#Smooth edges
p4_outline = smooth(buf1, method = "chaikin")
plot(p4_outline)
#Plot final points and polygon
p4 = plot(p4_outline)
points(coords, col = pelt4$Anatomical_region, pch=16)

#Write spatialpolygon to dataframe and then to shapefile
df = data.frame(id = getSpPPolygonsIDSlots(p4_outline))
row.names(df) = getSpPPolygonsIDSlots(p4_outline)
p4_spdf = SpatialPolygonsDataFrame(p4_outline, data =df)
writeOGR(p4_spdf, dsn = "C:/Users/keccl081/Dropbox/pelt", driver="ESRI Shapefile", layer = "p4_Outline")

################################################################################
#### Pelt Compiled Outline ####
# set up coordinates
coords = coordinates(cbind(compiled$X_adj, compiled$Y_adj))
comp_p = SpatialPoints(coords)
plot(comp_p, axes = TRUE)

# Buffer
buf_comp = gBuffer(comp_p, byid=FALSE, width=.75, capStyle="SQUARE")
plot(buf_comp)

#Smooth edges
comp_smooth = smooth(buf_comp, method = "chaikin")
plot(comp_smooth)

#Plot final points and polygon
plot(comp_smooth)
points(coords)

#Write spatialpolygon to dataframe and then to shapefile
df = data.frame(id = getSpPPolygonsIDSlots(comp_smooth))
row.names(df) = getSpPPolygonsIDSlots(comp_smooth)
comp_spdf = SpatialPolygonsDataFrame(comp_smooth, data =df)
writeOGR(comp_spdf, dsn = "C:/Users/keccl081/Dropbox/pelt", driver="ESRI Shapefile", layer = "Comp_Outline_2")
```

```
################################################################################
# Figures illustrating different sample regions
# Written in R Version 3.5.0
################################################################################
# Load data
pelt1 = read.csv("PELT1.csv")
pelt2 = read.csv("PELT2.csv")
pelt3 = read.csv("PELT3.csv")
pelt4 = read.csv("PELT4.csv")

#Load Libraries
library(ggplot2)
library(ggspatial)
library(dplyr)
library(tidyr)
library(tidyverse)
library(rgeos)
library(smoothr)
################################################################################
##### Pelt 1 Outline ####
# Import shapefile created in "pelt_outlines_clean.R"
p1_shp = readOGR(dsn = ".", layer = "p1_Outline")

# Convert shapefile to a ggplot ready data frame
p1_shp_df <- fortify(p1_shp, region = "id")
p1_shp$id <- rownames(p1_shp@data)
p1_shp_df <- left_join(p1_shp_df, p1_shp@data,mby = "id")

# Plot outline and points
p1_fur = ggplot(p1_shp_df, aes(x = p1_shp_df$long, y = p1_shp_df$lat))+
geom_polygon(colour='black', fill='white')+
geom_point(data = pelt1, aes(x = X_coord, y = Y_coord, color = pelt1$Fur_region), size=4, shape=19)+
scale_colour_manual(values = c("#225ea8", "#FDD835", "#41b6c4", "#a1dab4"))+
labs(colour=" ")+
theme(legend.title = element_blank())+
coord_quickmap()+
theme_void()

################################################################################
##### Pelt 2 Outline ####
# Importshapefile
p2_shp = readOGR(dsn = ".", layer = "p2_Outline")

# Convert shapefile to a ggplot ready data frame
p2_shp_df <- fortify(p2_shp, region = "id")
p2_shp$id <- rownames(p2_shp@data)
p2_shp_df <- left_join(p2_shp_df, p2_shp@data,mby = "id")

# Plot outline and points
p2_fur = ggplot(p2_shp_df, aes(x = p2_shp_df$long, y = p2_shp_df$lat))+
geom_polygon(colour='black', fill='white')+
geom_point(data = pelt2, aes(x = X_coord, y = Y_coord, color = pelt2$Fur_region), size=4, shape=19)+
scale_colour_manual(values = c("#225ea8", "#FDD835", "#41b6c4", "#a1dab4"))+
labs(colour=" ")+
theme(legend.title = element_blank())+
coord_quickmap()+
theme_void()

################################################################################
##### Pelt 3 Outline ####
# Importshapefile
p3_shp = readOGR(dsn = ".", layer = "p3_Outline")

# Convert shapefile to a ggplot ready data frame
p3_shp_df <- fortify(p3_shp, region = "id")
p3_shp$id <- rownames(p3_shp@data)
p3_shp_df <- left_join(p3_shp_df, p3_shp@data,mby = "id")

# Plot outline and points
p3_fur = ggplot(p3_shp_df, aes(x = p3_shp_df$long, y = p3_shp_df$lat))+
geom_polygon(colour='black', fill='white')+
geom_point(data = pelt3, aes(x = X_coord, y = Y_coord, color = pelt3$Fur_region), size=4, shape=19)+
scale_colour_manual(values = c("#225ea8", "#FDD835", "#41b6c4", "#a1dab4"))+
labs(colour=" ")+
theme(legend.title = element_blank())+
coord_quickmap()+
theme_void()

################################################################################
##### Pelt 4 Outline ####
# Importshapefile
p4_shp = readOGR(dsn = ".", layer = "p4_Outline")

# Convert shapefile to a ggplot ready data frame
p4_shp_df <- fortify(p4_shp, region = "id")
p4_shp$id <- rownames(p4_shp@data)
p4_shp_df <- left_join(p4_shp_df, p4_shp@data,mby = "id")

# Plot outline and points
p4_fur = ggplot(p4_shp_df, aes(x = p4_shp_df$long, y = p4_shp_df$lat))+
geom_polygon(colour='black', fill='white')+
geom_point(data = pelt4, aes(x = X_coord, y = Y_coord, color = pelt4$Fur_region), size=4, shape=19)+
```

```
scale_colour_manual(values = c("#225ea8", "#FDD835", "#41b6c4", "#a1dab4"))+
labs(colour=" ")+
theme(legend.title = element_blank())+
coord_quickmap()+
theme_void()

################################################################################
#### Plot all fur region figures together ####
library(ggpubr)
library(sjPlot)

plot1=ggarrange(p1_fur, p2_fur, p3_fur, p4_fur,
labels = c("Pelt 1", "Pelt 2", "Pelt 3", "Pelt 4"),
ncol = 4, nrow = 1,
common.legend = TRUE,
legend = "bottom")

#Plot figures with dpi=300
save_plot("fur_region.tif", plot1, width = 30, height = 20, dpi = 300,
legend.textsize = 20, legend.titlesize = 20,
legend.itemsize = 20)

################################################################################
##### Anatomical Regions ####
p1_ana = ggplot(p1_shp_df, aes(x = p1_shp_df$long, y = p1_shp_df$lat))+
geom_polygon(colour='black', fill='white')+
geom_point(data = pelt1, aes(x = X_coord, y = Y_coord, color = pelt1$Anatomical_region), size=4, shape=19)+
scale_colour_manual(values = c("#225ea8", "#FDD835", "#41b6c4", "#a1dab4"))+
labs(colour=" ")+
theme(legend.title = element_blank())+
coord_quickmap()+
theme_void()

p2_ana = ggplot(p2_shp_df, aes(x = p2_shp_df$long, y = p2_shp_df$lat))+
geom_polygon(colour='black', fill='white')+
geom_point(data = pelt2, aes(x = X_coord, y = Y_coord, color = pelt2$Anatomical), size=4, shape=19)+
scale_colour_manual(values = c("#225ea8", "#FDD835", "#41b6c4", "#a1dab4"))+
labs(colour=" ")+
theme(legend.title = element_blank())+
coord_quickmap()+
theme_void()

p3_ana = ggplot(p3_shp_df, aes(x = p3_shp_df$long, y = p3_shp_df$lat))+
geom_polygon(colour='black', fill='white')+
geom_point(data = pelt3, aes(x = X_coord, y = Y_coord, color = pelt3$Anatomical), size=4, shape=19)+
scale_colour_manual(values = c("#225ea8", "#FDD835", "#41b6c4", "#a1dab4"))+
labs(colour=" ")+
theme(legend.title = element_blank())+
coord_quickmap()+
theme_void()

p4_ana = ggplot(p4_shp_df, aes(x = p4_shp_df$long, y = p4_shp_df$lat))+
geom_polygon(colour='black', fill='white')+
geom_point(data = pelt4, aes(x = X_coord, y = Y_coord, color = pelt4$Anatomical_region), size=4, shape=19)+
scale_colour_manual(values = c("#225ea8", "#FDD835", "#41b6c4", "#a1dab4"))+
labs(colour=" ")+
theme(legend.title = element_blank())+
coord_quickmap()+
theme_void()

################################################################################
#### Plot all figures together ####
plot2=ggarrange(p1_ana, p2_ana, p3_ana, p4_ana,
labels = c("Pelt 1", "Pelt 2", "Pelt 3", "Pelt 4"),
ncol = 4, nrow = 1,
common.legend = TRUE,
legend = "bottom")

#Plot figures with dpi=300
save_plot("anatomical_region.tif", plot2, width = 30, height = 20, dpi = 300)
```

```
#############################################################################
# Cluster analysis of pelt Hg using Getis and Ord's Gi*
# Written in R Version 3.5.0
#############################################################################
# Load data
pelt1 = read.csv("PELT1.csv")
pelt2 = read.csv("PELT2.csv")
pelt3 = read.csv("PELT3.csv")
pelt4 = read.csv("PELT4.csv")

# Load Libraries
library(spdep)
library(rgdal)
library(ggplot2)
library(gridExtra)
library(dplyr)
library(adespatial)

################################
### Pelt1 ###
#Set up spatial neighbourhood
p1_sppnt = SpatialPoints(cbind(pelt1$X_coord, pelt1$Y_coord))
p1_nb <- chooseCN(coordinates(p1_sppnt), type = 6, k = 12, plot.nb = FALSE)
p1_lw <- nb2listw(p1_nb, style = 'W', zero.policy = TRUE)

# Gi*
pelt1$Gi_TC = as.numeric(localG(pelt1$THg_TC, listw = p1_lw))
pelt1$Gi_UC = as.numeric(localG(pelt1$THg_UC, listw = p1_lw))

# Gi* p-value
#Z score values for levels of statistical significance:
# 90% significant: >= 1.645
# 95% significant: >= 1.960
# 99% significant: >= 2.576
# 99.9% significant: >= 3.291

# Bin gi* scores based on whether it is past the critical cut off
pelt1$Gi_pval_TC = as.factor(pelt1$Gi_TC >= 1.96 |  pelt1$Gi_TC <= -1.96)
pelt1$Gi_pval_UC <- as.factor(pelt1$Gi_UC >= 1.96 |  pelt1$Gi_UC <= -1.96)

# Plot 1
#TC THg Gi*
# Importshapefile
p1_shp = readOGR(dsn = ".", layer = "p1_Outline")
# Convert shapefile to a ggplot ready data frame
p1_shp_df <- fortify(p1_shp, region = "id")
p1_shp$id <- rownames(p1_shp@data)
p1_shp_df <- left_join(p1_shp_df, p1_shp@data,mby = "id")
pelt1 = as.data.frame(pelt1)

# Plot outline and points
p1_TC = ggplot(p1_shp_df, aes(x = p1_shp_df$long, y = p1_shp_df$lat)) +
geom_polygon(colour='black', fill='white') +
geom_point(data = pelt1, aes(x = X_coord, y = Y_coord, color = pelt1$Gi_TC), size=5, shape=19) +
geom_point(data = pelt1, aes(x = X_coord, y = Y_coord, shape = factor(pelt1$Gi_pval_TC)), size = 6) +
scale_shape_manual(values = c(1,13),
guide = guide_legend(title = "Gi* score significance"),
labels = c("Not Significant", "Significant")) +
scale_color_gradient2(high = "red", mid = "white", low = "blue", midpoint = 0, limits = c(-5, 5),
guide = guide_colourbar(title = "Gi* score")) +
coord_quickmap()+
theme_void()

p1_UC = ggplot(p1_shp_df, aes(x = p1_shp_df$long, y = p1_shp_df$lat)) +
geom_polygon(colour='black', fill='white') +
geom_point(data = pelt1, aes(x = X_coord, y = Y_coord, color = pelt1$Gi_UC), size=5, shape=19) +
geom_point(data = pelt1, aes(x = X_coord, y = Y_coord, shape = factor(pelt1$Gi_pval_UC)), size = 6) +
scale_shape_manual(values = c(1,13),
guide = guide_legend(title = "Gi* score significance")) +
scale_color_gradient2(high = "red", mid = "white", low = "blue", midpoint = 0, limits = c(-5, 5),
guide = guide_colourbar(title = "Gi* score")) +
coord_quickmap()+
theme_void()

################################################
### Pelt2 ###
#Set up spatial neighbourhood
p2_sppnt = SpatialPoints(cbind(pelt2$X_coord, pelt2$Y_coord))
p2_nb <- chooseCN(coordinates(p2_sppnt), type = 6, k = 12, plot.nb = FALSE)
p2_lw <- nb2listw(p2_nb, style = 'W', zero.policy = TRUE)

# Gi*
pelt2$Gi_TC = as.numeric(localG(pelt2$THg_TC, listw = p2_lw))
pelt2$Gi_UC = as.numeric(localG(pelt2$THg_UC, listw = p2_lw))

# Bin gi* scores based on whether it is past the critical cut off
pelt2$Gi_pval_TC = as.factor(pelt2$Gi_TC >= 1.96 |  pelt2$Gi_TC <= -1.96)
pelt2$Gi_pval_UC <- as.factor(pelt2$Gi_UC >= 1.96 |  pelt2$Gi_UC <= -1.96)

# Plot 2
#TC THg Gi*
# Importshapefile
```

```
p2_shp = readOGR(dsn = ".", layer = "p2_Outline")
# Convert shapefile to a ggplot ready data frame
p2_shp_df <- fortify(p2_shp, region = "id")
p2_shp$id <- rownames(p2_shp@data)
p2_shp_df <- left_join(p2_shp_df, p2_shp@data,mby = "id")
pelt2 = as.data.frame(pelt2)

p2_TC = ggplot(p2_shp_df, aes(x = p2_shp_df$long, y = p2_shp_df$lat)) +
geom_polygon(colour='black', fill='white') +
geom_point(data = pelt2, aes(x = X_coord, y = Y_coord, color = pelt2$Gi_TC), size=5, shape=19) +
geom_point(data = pelt2, aes(x = X_coord, y = Y_coord, shape = factor(pelt2$Gi_pval_TC)), size = 6) +
scale_shape_manual(values = c(1,13),
guide = guide_legend(title = "Gi* score significance"),
labels = c("Not Significant", "Significant")) +
scale_color_gradient2(high = "red", mid = "white", low = "blue", midpoint = 0, limits = c(-5, 5),
guide = guide_colourbar(title = "Gi* score")) +
coord_quickmap()+
theme_void()

#UC THg Gi*
p2_UC = ggplot(p2_shp_df, aes(x = p2_shp_df$long, y = p2_shp_df$lat)) +
geom_polygon(colour='black', fill='white') +
geom_point(data = pelt2, aes(x = X_coord, y = Y_coord, color = pelt2$Gi_UC), size=5, shape=19) +
geom_point(data = pelt2, aes(x = X_coord, y = Y_coord, shape = factor(pelt2$Gi_pval_UC)), size = 6) +
scale_shape_manual(values = c(1,13),
guide = guide_legend(title = "Gi* score significance"),
labels = c("Not Significant", "Significant")) +
scale_color_gradient2(high = "red", mid = "white", low = "blue", midpoint = 0, limits = c(-5, 5),
guide = guide_colourbar(title = "Gi* score")) +
coord_quickmap()+
theme_void()

#############################################################
### Pelt3 ###
#Set up spatial neighbourhood
p3_sppnt = SpatialPoints(cbind(pelt3$X_coord, pelt3$Y_coord))
p3_nb <- chooseCN(coordinates(p3_sppnt), type = 6, k = 12, plot.nb = FALSE)
p3_lw <- nb2listw(p3_nb, style = 'W', zero.policy = TRUE)

# Gi*
pelt3$Gi_TC = as.numeric(localG(pelt3$THg_TC, listw = p3_lw))
pelt3$Gi_UC = as.numeric(localG(pelt3$THg_UC, listw = p3_lw))

# Bin gi* scores based on whether it is past the critical cut off
pelt3$Gi_pval_TC = as.factor(pelt3$Gi_TC >= 1.96 |  pelt3$Gi_TC <= -1.96)
pelt3$Gi_pval_UC <- as.factor(pelt3$Gi_UC >= 1.96 |  pelt3$Gi_UC <= -1.96)

# Plot 3
# TC THg Gi*
# Importshapefile
p3_shp = readOGR(dsn = ".", layer = "p3_Outline")
# Convert shapefile to a ggplot ready data frame
p3_shp_df <- fortify(p3_shp, region = "id")
p3_shp$id <- rownames(p3_shp@data)
p3_shp_df <- left_join(p3_shp_df, p3_shp@data,mby = "id")
pelt3 = as.data.frame(pelt3)

p3_TC = ggplot(p3_shp_df, aes(x = p3_shp_df$long, y = p3_shp_df$lat)) +
geom_polygon(colour='black', fill='white') +
geom_point(data = pelt3, aes(x = X_coord, y = Y_coord, color = pelt3$Gi_TC), size=5, shape=19) +
geom_point(data = pelt3, aes(x = X_coord, y = Y_coord, shape = factor(pelt3$Gi_pval_TC)), size = 6) +
scale_shape_manual(values = c(1,13),
guide = guide_legend(title = "Gi* score significance"),
labels = c("Not Significant", "Significant")) +
scale_color_gradient2(high = "red", mid = "white", low = "blue", midpoint = 0, limits = c(-5, 6),
guide = guide_colourbar(title = "Gi* score")) +
coord_quickmap()+
theme_void()

#UC THg Gi*
p3_UC = ggplot(p3_shp_df, aes(x = p3_shp_df$long, y = p3_shp_df$lat)) +
geom_polygon(colour='black', fill='white') +
geom_point(data = pelt3, aes(x = X_coord, y = Y_coord, color = pelt3$Gi_UC), size=5, shape=19) +
geom_point(data = pelt3, aes(x = X_coord, y = Y_coord, shape = factor(pelt3$Gi_pval_UC)), size = 6) +
scale_shape_manual(values = c(1,13),
guide = guide_legend(title = "Gi* score significance"),
labels = c("Not Significant", "Significant"))+
scale_color_gradient2(high = "red", mid = "white", low = "blue", midpoint = 0, limits = c(-5, 7),
guide = guide_colourbar(title = "Gi* score")) +
coord_quickmap()+
theme_void()

#############################################################
### Pelt4 ###
#Set up spatial neighbourhood
p4_sppnt = SpatialPoints(cbind(pelt4$X_coord, pelt4$Y_coord))
p4_nb <- chooseCN(coordinates(p4_sppnt), type = 6, k = 12, plot.nb = FALSE)
p4_lw <- nb2listw(p4_nb, style = 'W', zero.policy = TRUE)

# Gi*
pelt4$Gi_TC = as.numeric(localG(pelt4$THg_TC, listw = p4_lw))
pelt4$Gi_UC = as.numeric(localG(pelt4$THg_UC, listw = p4_lw))
```

```
# Bin gi* scores based on whether it is past the critical cut off
pelt4$Gi_pval_TC = as.factor(pelt4$Gi_TC >= 1.96 |  pelt4$Gi_TC <= -1.96)
pelt4$Gi_pval_UC <- as.factor(pelt4$Gi_UC >= 1.96 |  pelt4$Gi_UC <= -1.96)

# Plot
#TC THg Gi*
# Importshapefile
p4_shp = readOGR(dsn = ".", layer = "p4_Outline")
# Convert shapefile to a ggplot ready data frame
p4_shp_df <- fortify(p4_shp, region = "id")
p4_shp$id <- rownames(p4_shp@data)
p4_shp_df <- left_join(p4_shp_df, p4_shp@data,mby = "id")

pelt4 = as.data.frame(pelt4)
# Plot outline and points
p4_TC = ggplot(p4_shp_df, aes(x = p4_shp_df$long, y = p4_shp_df$lat)) +
geom_polygon(colour='black', fill='white') +
geom_point(data = pelt4, aes(x = X_coord, y = Y_coord, color = pelt4$Gi_TC), size=5, shape=19) +
geom_point(data = pelt4, aes(x = X_coord, y = Y_coord, shape = factor(pelt4$Gi_pval_TC)), size = 6) +
scale_shape_manual(values = c(1,13),
guide = guide_legend(title = "Gi* score significance"),
labels = c("Not Significant", "Significant")) +
scale_color_gradient2(high = "red", mid = "white", low = "blue", midpoint = 0, limits = c(-5, 6),
guide = guide_colourbar(title = "Gi* score")) +
coord_quickmap()+
theme_void()

p4_UC = ggplot(p4_shp_df, aes(x = p4_shp_df$long, y = p4_shp_df$lat)) +
geom_polygon(colour='black', fill='white') +
geom_point(data = pelt4, aes(x = X_coord, y = Y_coord, color = pelt4$Gi_UC), size=5, shape=19) +
geom_point(data = pelt4, aes(x = X_coord, y = Y_coord, shape = factor(pelt4$Gi_pval_UC)), size = 6) +
scale_shape_manual(values = c(1,13),
guide = guide_legend(title = "Gi* score significance"),
labels = c("Not Significant", "Significant")) +
scale_color_gradient2(high = "red", mid = "white", low = "blue", midpoint = 0, limits = c(-5, 7),
guide = guide_colourbar(title = "Gi* score")) +
coord_quickmap()+
theme_void()

#####################################################
# Plot all figures together
library(ggpubr)
library(sjPlot)

p1=ggarrange(p1_TC, p1_UC, p2_TC, p2_UC,p3_TC, p3_UC,p4_TC, p4_UC,
labels = c("Pelt 1 TC", "Pelt 1 UC", "Pelt 2 TC", "Pelt 2 UC",
"Pelt 3 TC", "Pelt 3 UC","Pelt 4 TC", "Pelt 4 UC"),
vjust = 1,
hjust = -0.75,
ncol = 4, nrow = 2,
common.legend = TRUE,
legend = "bottom")

#Plot figures with dpi=300
save_plot("individual_getis.tif", p1, width = 20, height = 30, dpi = 300,
legend.textsize = 20, legend.titlesize = 20,
legend.itemsize = 20)
```

```
##############################################################################
# Cluster analysis for composite pelt
# Written in R Version 3.5.0
##############################################################################
# Load data
compiled = read.csv("pelts_compiled.csv")

# Load Libraries
library(ggplot2)
library(ggspatial)
library(dplyr)
library(tidyr)
library(rgeos)
library(smoothr)
library(sp)
library(rgdal)
library(ggpubr)
library(sjPlot)

#################################
# Importshapefile
comp_shp = readOGR(dsn = ".", layer = "Comp_Outline_2")
# Convert shapefile to a ggplot ready data frame
comp_shp_df <- fortify(comp_shp, region = "id")
comp_shp$id <- rownames(comp_shp@data)
comp_shp_df <- left_join(comp_shp_df, comp_shp@data,mby = "id")

#Layered lat long
ggplot(comp_shp_df, aes(x = comp_shp_df$long, y = comp_shp_df$lat))+
geom_polygon(colour='black', fill='white')+
geom_point(data = compiled, aes(x = X_adj, y = Y_adj, color = factor(compiled$Pelt)), size=4, shape=19)+
scale_colour_manual(values = c("#225ea8", "#FDD835", "#41b6c4", "#a1dab4"))+
labs(colour=" ")+
theme(legend.title = element_blank())+
coord_quickmap()+
theme_void()

# Plot Normalized Hg Values for TC and UC
comp_TC = ggplot(comp_shp_df, aes(x = comp_shp_df$long, y = comp_shp_df$lat)) +
geom_polygon(colour='black', fill='white') +
geom_point(data = compiled, aes(x = X_adj, y = Y_adj, color = compiled$TC_norm), size=7, shape=19) +
scale_color_gradient(low='#ece7f2', high='#0570b0',
guide = guide_colourbar(title = "Total Hg (ug/g)")) +
coord_quickmap()+
theme_void()

comp_UC = ggplot(comp_shp_df, aes(x = comp_shp_df$long, y = comp_shp_df$lat)) +
geom_polygon(colour='black', fill='white') +
geom_point(data = compiled, aes(x = X_adj, y = Y_adj, color = compiled$UC_norm), size=7, shape=19) +
scale_color_gradient(low='#ece7f2', high='#0570b0',
guide = guide_colourbar(title = "Total Hg (ug/g)")) +
coord_quickmap()+
theme_void()

#################################################################
#### Average Noralized values ####
adj_x_compiled = aggregate(compiled$X_adj, list(compiled$factor), mean)
adj_y_compiled = aggregate(compiled$Y_adj, list(compiled$factor), mean)
TC_compiled = aggregate(compiled$TC_norm, list(compiled$factor), mean)
UC_compiled = aggregate(compiled$UC_norm, list(compiled$factor), mean)
compiled_pelt = as.data.frame(cbind(adj_x_compiled[,2], adj_y_compiled[,2],TC_compiled[,2],UC_compiled[,2]))
colnames(compiled_pelt) <- c("x", "y", "TC", "UC")

# Plot
ggplot(comp_shp_df, aes(x = comp_shp_df$long, y = comp_shp_df$lat))+
geom_polygon(colour='black', fill='white')+
geom_point(data = compiled_pelt, aes(x = x, y = y, color = TC), size=4)+
labs(colour=" ")+
theme(legend.title = element_blank())+
coord_quickmap()+
theme_void()


################################################
### Compiled Pelt Hot Spot Analysis ####
#Set up spatial neighbourhood
comp_sppnt = SpatialPoints(cbind(compiled_pelt$x, compiled_pelt$y))
comp_nb <- chooseCN(coordinates(comp_sppnt), type = 6, k = 12, plot.nb = FALSE)
comp_lw <- nb2listw(comp_nb, style = 'W', zero.policy = TRUE)

# Gi*
compiled_pelt$Gi_TC = as.numeric(localG(compiled_pelt$TC, listw = comp_lw))
compiled_pelt$Gi_UC = as.numeric(localG(compiled_pelt$UC, listw = comp_lw))

# Gi* p-value
#Z score values for levels of statistical significance:
# 90% significant: >= 1.645
# 95% significant: >= 1.960
# 99% significant: >= 2.576
# 99.9% significant: >= 3.291

# Bin gi* scores based on whether it is past the critical cut off
```

```
compiled_pelt$Gi_pval_TC = as.factor(compiled_pelt$Gi_TC >= 1.96 |  compiled_pelt$Gi_TC <= -1.96)
compiled_pelt$Gi_pval_UC = as.factor(compiled_pelt$Gi_UC >= 1.96 |  compiled_pelt$Gi_UC <= -1.96)

# Plot 1
#TC THg Gi*
# Plot outline and points
hs_comp_TC = ggplot(comp_shp_df, aes(x = comp_shp_df$long, y = comp_shp_df$lat)) +
geom_polygon(colour='black', fill='white') +
geom_point(data = compiled_pelt, aes(x = x, y = y, color = compiled_pelt$Gi_TC), size=5, shape=19) +
geom_point(data = compiled_pelt, aes(x = x, y = y, shape = factor(compiled_pelt$Gi_pval_TC)), size = 6) +
scale_shape_manual(values = c(1,13),
guide = guide_legend(title = "Gi* score significance"),
labels = c("Not Significant", "Significant")) +
scale_color_gradient2(high = "red", mid = "white", low = "blue", midpoint = 0, limits = c(-6, 6),
guide = guide_colourbar(title = "Gi*score")) +
coord_quickmap()+
theme_void()

hs_comp_UC = ggplot(comp_shp_df, aes(x = comp_shp_df$long, y = comp_shp_df$lat)) +
geom_polygon(colour='black', fill='white') +
geom_point(data = compiled_pelt, aes(x = x, y = y, color = compiled_pelt$Gi_UC), size=5, shape=19) +
geom_point(data = compiled_pelt, aes(x = x, y = y, shape = factor(compiled_pelt$Gi_pval_UC)), size = 6) +
scale_shape_manual(values = c(1,13),
guide = guide_legend(title = "Gi*score significance")) +
scale_color_gradient2(high = "red", mid = "white", low = "blue", midpoint = 0, limits = c(-6, 6),
guide = guide_colourbar(title = "Gi* score")) +
coord_quickmap()+
theme_void()

#########################################################
# Plot composite figures together
plot1=ggarrange(comp_TC, comp_UC,
labels = c("Compiled TC", "Compiled UC"),
vjust = 1,
hjust = -0.5,
ncol = 2, nrow = 1,
common.legend = TRUE,
legend = "right")

#Plot figures with dpi=300
save_plot("compsite_pelt.tif", plot1, width = 15, height = 15, dpi = 300)

#Plot composite figure hotspots together
plot2=ggarrange(hs_comp_TC, hs_comp_UC,
labels = c("Hot Spot TC", "Hot Spot UC"),
vjust = 1,
hjust = -0.5,
ncol = 2, nrow = 1,
common.legend = TRUE,
legend = "right")

#Plot figures with dpi=300
save_plot("compsite_pelt_hs.tif", plot2, width = 15, height = 15, dpi = 300)
```

```
##############################################################################
# Plots of individual Hg concentrations
# Written in R Version 3.5.0
##############################################################################
# Load data
pelt1 = read.csv("PELT1.csv")
pelt2 = read.csv("PELT2.csv")
pelt3 = read.csv("PELT3.csv")
pelt4 = read.csv("PELT4.csv")

# Load Libraries
library(spdep)
library(rgdal)
library(dplyr)
library(ggplot2)
library(ggpubr)
library(sjPlot)

##############################################################################
# Plot 1
# Outline
# Importshapefile
p1_shp = readOGR(dsn = ".", layer = "p1_Outline")
# Convert shapefile to a ggplot ready data frame
p1_shp_df <- fortify(p1_shp, region = "id")
p1_shp$id <- rownames(p1_shp@data)
p1_shp_df <- left_join(p1_shp_df, p1_shp@data,mby = "id")

# Plot
p1_TC = ggplot(p1_shp_df, aes(x = p1_shp_df$long, y = p1_shp_df$lat)) +
geom_polygon(colour='black', fill='white') +
geom_point(data = pelt1, aes(x = X_coord, y = Y_coord, color = pelt1$THg_TC), size=4, shape=19) +
scale_color_gradient(low='#ece7f2', high='#0570b0',
guide = guide_colourbar(title = "Total Hg (ug/g)")) +
theme(legend.key.size=10)+
coord_quickmap()+
theme_void()

p1_UC = ggplot(p1_shp_df, aes(x = p1_shp_df$long, y = p1_shp_df$lat)) +
geom_polygon(colour='black', fill='white') +
geom_point(data = pelt1, aes(x = X_coord, y = Y_coord, color = pelt1$THg_UC), size=4, shape=19) +
scale_color_gradient(low='#ece7f2', high='#0570b0',
guide = guide_colourbar(title = "Total Hg (ug/g)")) +
coord_quickmap()+
theme_void()

##############################################################################
# Plot 2
# Outline
# Importshapefile
p2_shp = readOGR(dsn = ".", layer = "p2_Outline")
# Convert shapefile to a ggplot ready data frame
p2_shp_df <- fortify(p2_shp, region = "id")
p2_shp$id <- rownames(p2_shp@data)
p2_shp_df <- left_join(p2_shp_df, p2_shp@data,mby = "id")

# Plot
p2_TC = ggplot(p2_shp_df, aes(x = p2_shp_df$long, y = p2_shp_df$lat)) +
geom_polygon(colour='black', fill='white') +
geom_point(data = pelt2, aes(x = X_coord, y = Y_coord, color = pelt2$THg_TC), size=4, shape=19) +
scale_color_gradient(low='#ece7f2', high='#0570b0',
guide = guide_colourbar(title = "Total Hg (ug/g)")) +
coord_quickmap()+
theme_void()

p2_UC = ggplot(p2_shp_df, aes(x = p2_shp_df$long, y = p2_shp_df$lat)) +
geom_polygon(colour='black', fill='white') +
geom_point(data = pelt2, aes(x = X_coord, y = Y_coord, color = pelt2$THg_UC), size=4, shape=19) +
scale_color_gradient(low='#ece7f2', high='#0570b0',
guide = guide_colourbar(title = "Total Hg (ug/g)")) +
coord_quickmap()+
theme_void()

##############################################################################
# Plot 3
# Outline
# Importshapefile
p3_shp = readOGR(dsn = ".", layer = "p3_Outline")
# Convert shapefile to a ggplot ready data frame
p3_shp_df <- fortify(p3_shp, region = "id")
p3_shp$id <- rownames(p3_shp@data)
p3_shp_df <- left_join(p3_shp_df, p3_shp@data,mby = "id")

# Plot
p3_TC = ggplot(p3_shp_df, aes(x = p3_shp_df$long, y = p3_shp_df$lat)) +
geom_polygon(colour='black', fill='white') +
geom_point(data = pelt3, aes(x = X_coord, y = Y_coord, color = pelt3$THg_TC), size=4, shape=19) +
scale_color_gradient(low='#ece7f2', high='#0570b0',
guide = guide_colourbar(title = "Total Hg (ug/g)")) +
coord_quickmap()+
theme_void()
```

```
p3_UC = ggplot(p3_shp_df, aes(x = p3_shp_df$long, y = p3_shp_df$lat)) +
geom_polygon(colour='black', fill='white') +
geom_point(data = pelt3, aes(x = X_coord, y = Y_coord, color = pelt3$THg_UC), size=4, shape=19) +
scale_color_gradient(low='#ece7f2', high='#0570b0',
guide = guide_colourbar(title = "Total Hg (ug/g)")) +
coord_quickmap()+
theme_void()

################################################################################
# Plot 4
# Outline
# Importshapefile
p4_shp = readOGR(dsn = ".", layer = "p4_Outline")
# Convert shapefile to a ggplot ready data frame
p4_shp_df <- fortify(p4_shp, region = "id")
p4_shp$id <- rownames(p4_shp@data)
p4_shp_df <- left_join(p4_shp_df, p4_shp@data,mby = "id")

# Plot
p4_TC = ggplot(p4_shp_df, aes(x = p4_shp_df$long, y = p4_shp_df$lat)) +
geom_polygon(colour='black', fill='white') +
geom_point(data = pelt4, aes(x = X_coord, y = Y_coord, color = pelt4$THg_TC), size=4, shape=19) +
scale_color_gradient(low='#ece7f2', high='#0570b0',
guide = guide_colourbar(title = "Total Hg (ug/g)"))+
coord_quickmap()+
theme_void()

p4_UC = ggplot(p4_shp_df, aes(x = p4_shp_df$long, y = p4_shp_df$lat)) +
geom_polygon(colour='black', fill='white') +
geom_point(data = pelt4, aes(x = X_coord, y = Y_coord, color = pelt4$THg_UC), size=4, shape=19) +
scale_color_gradient(low='#ece7f2', high='#0570b0',
guide = guide_colourbar(title = "Total Hg (ug/g)")) +
coord_quickmap()+
theme_void()

################################################################################
# Plot all figures together
plot1=ggarrange(p1_TC, p1_UC, p2_TC, p2_UC,p3_TC, p3_UC,p4_TC, p4_UC,
labels = c("Pelt 1 TC", "Pelt 1 UC", "Pelt 2 TC", "Pelt 2 UC", "Pelt 3 TC", "Pelt 3 UC","Pelt 4 TC", "Pelt 4 UC"),
vjust = 1,
hjust = -0.5,
ncol = 4, nrow = 2,
common.legend = FALSE,
legend = "right")

#Plot figures with dpi=300
save_plot("individual_hg.tif", plot1, width = 20, height = 20, dpi = 300)
```

```
##############################################################################
# Otter fur THg to organ THg otter sampling spot optimization
# Written in R Version 3.5.0
##############################################################################
# Load data
compiled = read.csv("pelts_compiled.csv")

# Load Library
library(ggplot2)
library(Metrics)
library(rgdal)
library(ggpubr)
library(dplyr)
library(tidyr)
library(rgeos)
library(smoothr)
library(sp)
library(spdep)
library(gridExtra)
library(adespatial)
library(ggpubr)
library(sjPlot)

#Eccles et al. (2017) fur THg to organ THg predictive model eqns
#Fur to brain: y = 0.15x + 0
#Fur to kidney: y = 0.62x + 0
#Fur to liver: y = 0.70x + 0
#Fur to muscle: y = 0.46x + 0

########################################
# Import Shapefiles
# Composite Pelt
comp_shp = readOGR(dsn = ".", layer = "Comp_Outline_2")
# Convert shapefile to a ggplot ready data frame
comp_shp_df <- fortify(comp_shp, region = "id")
comp_shp$id <- rownames(comp_shp@data)
comp_shp_df <- left_join(comp_shp_df, comp_shp@data,mby = "id")

##############################################################################
#### Compiled TC ####
# Brain
compiled$TC_est_brain= 0.15*compiled$THg_TC
compiled$TC_resid_brain=compiled$TC_est_brain-compiled$Brain
compiled$TC_perc_brain= abs(((compiled$TC_est_brain-compiled$Brain)/(compiled$Brain))*100)

# Liver
compiled$TC_est_liver= 0.70*compiled$THg_TC
compiled$TC_resid_liver=compiled$TC_est_liver-compiled$Liver
compiled$TC_perc_liver= abs(((compiled$TC_est_liver-compiled$Liver)/(compiled$Liver))*100)

# Kidney
compiled$TC_est_kidney= 0.46*compiled$THg_TC
compiled$TC_resid_kidney=compiled$TC_est_kidney-compiled$Kidney
compiled$TC_perc_kidney= abs(((compiled$TC_est_kidney-compiled$Kidney)/(compiled$Kidney))*100)

# Muscle
compiled$TC_est_muscle = 0.62*compiled$THg_TC
compiled$TC_resid_muscle = compiled$TC_est_muscle-compiled$Muscle
compiled$TC_perc_muscle = abs(((compiled$TC_est_muscle-compiled$Muscle)/(compiled$Muscle))*100)
#####################################################################
# Average error TC
compiled$TC_comp_average_error = (compiled$TC_perc_brain/100*.4 + compiled$TC_perc_liver/100*.2 +
compiled$TC_perc_kidney/100*.2 + compiled$TC_perc_muscle/100*.2)*100

adj_x_compiled = aggregate(compiled$X_adj, list(compiled$factor), mean)
adj_y_compiled = aggregate(compiled$Y_adj, list(compiled$factor), mean)
TC_compiled = aggregate(compiled$TC_comp_average_error, list(compiled$factor), mean)
compiled_pelt_TC = as.data.frame(cbind(adj_x_compiled[,2], adj_y_compiled[,2],TC_compiled[,2]))
colnames(compiled_pelt_TC) <- c("x", "y", "TC")

#compiled_pelt_TC= subset(compiled_pelt_TC, TC < 40)

TC_error = ggplot(comp_shp_df, aes(x = comp_shp_df$long, y = comp_shp_df$lat))+
geom_polygon(colour='black', fill='white')+
geom_point(data = compiled_pelt_TC, aes(x = x, y = y, color = TC), size=5)+
scale_colour_gradient(low = "white", high = "red", limits =c(0,115))+
labs(colour="Percent Error")+
theme(legend.title = element_blank())+
coord_quickmap()+
theme_void()

#Set up spatial neighbourhood
comp_sppnt = SpatialPoints(cbind(compiled_pelt_TC$x, compiled_pelt_TC$y))
comp_nb <- chooseCN(coordinates(comp_sppnt), type = 6, k = 12, plot.nb = FALSE)
comp_lw <- nb2listw(comp_nb, style = 'W', zero.policy = TRUE)

# Gi*
compiled_pelt_TC$Gi_TC = as.numeric(localG(compiled_pelt_TC$TC, listw = comp_lw))

# Gi* p-value
#Z score values for levels of statistical significance:
# 90% significant: >= 1.645
```

```
# 95% significant: >= 1.960
# 99% significant: >= 2.576
# 99.9% significant: >= 3.291

# Bin gi* scores based on whether it is past the critical cut off
compiled_pelt_TC$Gi_pval_TC = as.factor(compiled_pelt_TC$Gi_TC >= 1.96 |  compiled_pelt_TC$Gi_TC <= -1.96)

#TC THg Gi*
# Plot outline and points
hs_comp_TC = ggplot(comp_shp_df, aes(x = comp_shp_df$long, y = comp_shp_df$lat)) +
geom_polygon(colour='black', fill='white') +
geom_point(data = compiled_pelt_TC, aes(x = x, y = y, color = compiled_pelt_TC$Gi_TC), size=5, shape=19) +
geom_point(data = compiled_pelt_TC, aes(x = x, y = y, shape = factor(compiled_pelt_TC$Gi_pval_TC)), size = 6) +
scale_shape_manual(values = c(1,13),
guide = guide_legend(title = "Gi*score significance"),
labels = c("Not Significant", "Significant")) +
scale_color_gradient2(high = "red", mid = "white", low = "blue", midpoint = 0, limits = c(-6, 6),
guide = guide_colourbar(title = "Gi*score")) +
coord_quickmap()+
theme_void()
################################################################################
#### Compiled UC ####
# Brain
compiled$UC_est_brain= 0.15*compiled$THg_UC
compiled$UC_resid_brain=compiled$UC_est_brain-compiled$Brain
compiled$UC_perc_brain= abs(((compiled$UC_est_brain-compiled$Brain)/(compiled$Brain))*100)

# Liver
compiled$UC_est_liver= 0.70*compiled$THg_UC
compiled$UC_resid_liver=compiled$UC_est_liver-compiled$Liver
compiled$UC_perc_liver= abs(((compiled$UC_est_liver-compiled$Liver)/(compiled$Liver))*100)

# Kidney
compiled$UC_est_kidney= 0.46*compiled$THg_UC
compiled$UC_resid_kidney=compiled$UC_est_kidney-compiled$Kidney
compiled$UC_perc_kidney= abs(((compiled$UC_est_kidney-compiled$Kidney)/(compiled$Kidney))*100)

# Muscle
compiled$UC_est_muscle = 0.62*compiled$THg_UC
compiled$UC_resid_muscle = compiled$UC_est_muscle-compiled$Muscle
compiled$UC_perc_muscle = abs(((compiled$UC_est_muscle-compiled$Muscle)/(compiled$Muscle))*100)

# Average error UC
compiled$UC_comp_average_error = (compiled$UC_perc_brain/100*.4 + compiled$UC_perc_liver/100*.2 +
compiled$UC_perc_kidney/100*.2 + compiled$UC_perc_muscle/100*.2)*100

adj_x_compiled = aggregate(compiled$X_adj, list(compiled$factor), mean)
adj_y_compiled = aggregate(compiled$Y_adj, list(compiled$factor), mean)
UC_compiled = aggregate(compiled$UC_comp_average_error, list(compiled$factor), mean)
compiled_pelt_UC = as.data.frame(cbind(adj_x_compiled[,2], adj_y_compiled[,2],UC_compiled[,2]))
colnames(compiled_pelt_UC) <- c("x", "y", "UC")

UC_error = ggplot(comp_shp_df, aes(x = comp_shp_df$long, y = comp_shp_df$lat))+
geom_polygon(colour='black', fill='white')+
geom_point(data = compiled_pelt_UC, aes(x = x, y = y, color = UC), size=5)+
scale_colour_gradient(low = "white", high = "red", limits =c(0,115))+
labs(colour="Percent Error")+
theme(legend.title = element_blank())+
coord_quickmap()+
theme_void()

#Set up spatial neighbourhood
comp_sppnt = SpatialPoints(cbind(compiled_pelt_UC$x, compiled_pelt_UC$y))
comp_nb <- chooseCN(coordinates(comp_sppnt), type = 6, k = 12, plot.nb = FALSE)
comp_lw <- nb2listw(comp_nb, style = 'W', zero.policy = TRUE)

# Gi*
compiled_pelt_UC$Gi_UC = as.numeric(localG(compiled_pelt_UC$UC, listw = comp_lw))

# Gi* p-value
#Z score values for levels of statistical significance:
# 90% significant: >= 1.645
# 95% significant: >= 1.960
# 99% significant: >= 2.576
# 99.9% significant: >= 3.291

# Bin gi* scores based on whether it is past the critical cut off
compiled_pelt_UC$Gi_pval_UC = as.factor(compiled_pelt_UC$Gi_UC >= 1.96 |  compiled_pelt_UC$Gi_UC <= -1.96)

#All THg Gi*
# Plot outline and points
hs_comp_UC = ggplot(comp_shp_df, aes(x = comp_shp_df$long, y = comp_shp_df$lat)) +
geom_polygon(colour='black', fill='white') +
geom_point(data = compiled_pelt_UC, aes(x = x, y = y, color = compiled_pelt_UC$Gi_UC), size=5, shape=19) +
geom_point(data = compiled_pelt_UC, aes(x = x, y = y, shape = factor(compiled_pelt_UC$Gi_pval_UC)), size = 6) +
scale_shape_manual(values = c(1,13),
guide = guide_legend(title = "Gi*score significance"),
labels = c("Not Significant", "Significant")) +
scale_color_gradient2(high = "red", mid = "white", low = "blue", midpoint = 0, limits = c(-6, 6),
guide = guide_colourbar(title = "Gi*score")) +
coord_quickmap()+
theme_void()
```

```
#####################################################################
p1 = ggarrange(hs_comp_TC, hs_comp_UC,
labels = c("TC Hotspot", "UC Hotspot"),
vjust = 1,
hjust = -.5,
ncol = 2, nrow = 1,
common.legend = TRUE,
legend = "right")

#Plot figures with dpi=300
save_plot("composite_error_hs.tif", p1, width = 15, height = 15, dpi = 300)

p2 = ggarrange(TC_error, UC_error,
labels = c("Average Error TC", "Average Error UC", "TC Hotspot", "UC Hotspot"),
vjust = 1,
hjust = -.5,
ncol = 2, nrow = 1,
common.legend = TRUE,
legend = "right")

#Plot figures with dpi=300
save_plot("composite_error.tif", p2, width = 15, height = 15, dpi = 300)

#####################################################################
#### Average TC and UC ####
compiled$all_comp_average_error = ((compiled$UC_perc_brain/100*.2 + compiled$UC_perc_liver/100*.1 +
compiled$UC_perc_kidney/100 *.1+ compiled$UC_perc_muscle/100*.1+
compiled$TC_perc_brain/100 *.2 + compiled$TC_perc_liver/100*.1 +
compiled$TC_perc_kidney/100*.1 + compiled$TC_perc_muscle/100*.1))*100

adj_x_compiled = aggregate(compiled$X_adj, list(compiled$factor), mean)
adj_y_compiled = aggregate(compiled$Y_adj, list(compiled$factor), mean)
all_compiled = aggregate(compiled$all_comp_average_error, list(compiled$factor), mean)
compiled_pelt_all = as.data.frame(cbind(adj_x_compiled[,2], adj_y_compiled[,2],all_compiled[,2]))
colnames(compiled_pelt_all) <- c("x", "y", "all")

all = ggplot(comp_shp_df, aes(x = comp_shp_df$long, y = comp_shp_df$lat))+
geom_polygon(colour='black', fill='white')+
geom_point(data = compiled_pelt_all, aes(x = x, y = y, color = all), size=4)+
scale_colour_gradient(low = "white", high = "red")+
labs(colour="Percent Error")+
theme(legend.title = element_blank())+
coord_quickmap()+
theme_void()

### Compiled Pelt Hot Spot Analysis ####
#Set up spatial neighbourhood
comp_sppnt = SpatialPoints(cbind(compiled_pelt_all$x, compiled_pelt_all$y))
comp_nb <- chooseCN(coordinates(comp_sppnt), type = 6, k = 12, plot.nb = FALSE)
comp_lw <- nb2listw(comp_nb, style = 'W', zero.policy = TRUE)

# Gi*
compiled_pelt_all$Gi_all = as.numeric(localG(compiled_pelt_all$all, listw = comp_lw))

# Gi* p-value
#Z score values for levels of statistical significance:
# 90% significant: >= 1.645
# 95% significant: >= 1.960
# 99% significant: >= 2.576
# 99.9% significant: >= 3.291

# Bin gi* scores based on whether it is past the critical cut off
compiled_pelt_all$Gi_pval_all = as.factor(compiled_pelt_all$Gi_all >= 1.96 |  compiled_pelt_all$Gi_all <= -1.96)

#All THg Gi*
# Plot outline and points
hs_comp_all = ggplot(comp_shp_df, aes(x = comp_shp_df$long, y = comp_shp_df$lat)) +
geom_polygon(colour='black', fill='white') +
geom_point(data = compiled_pelt, aes(x = x, y = y, color = compiled_pelt$Gi_TC), size=5, shape=19) +
geom_point(data = compiled_pelt, aes(x = x, y = y, shape = factor(compiled_pelt$Gi_pval_TC)), size = 6) +
scale_shape_manual(values = c(1,13),
guide = guide_legend(title = "Gi*score significance"),
labels = c("Not Significant", "Significant")) +
scale_color_gradient2(high = "red", mid = "white", low = "blue", midpoint = 0, limits = c(-6, 6),
guide = guide_colourbar(title = "Gi*score")) +
coord_quickmap()+
theme_void()
#####################################################################
plot1=ggarrange(all, hs_comp_all,
labels = c("          Average Error", "Average Error Hot Spots"),
vjust = 1,
hjust = -0.15,
ncol = 2, nrow = 1,
common.legend = FALSE,
legend = "right")

#Plot figures with dpi=300
save_plot("composite_error_hs.tif", plot1, width = 20, height = 15, dpi = 300)
```

Appendix C

Supplement Information for Chapter 5: Relationships between mercury concentrations in fur and stomach content of river otter *(Lontra Canadensis)* and mink *(Neovison vison)* and their applications as proxys for environmental factors determining mercury bioavailability

Table C.1: Summary of predictors used in the regression modelling.

Dataset Title	Author	Year	URL	Metric Calculated
Large Dams and Reservoirs of Canada	Global Forest Watch Canada	2010	https://databasin.org/datasets/b9b2e843d9b94b41abc8e76ebacfbe47	Distance to nearest reservoir Size of nearest reservoir
Soil pH	Atlas of the biosphere	1998	https://nelson.wisc.edu/sage/data-and-models/atlas/maps.php?catnum=2&type=Land%20Use	Average in home range (9 km) and 50km radius
Soil Organic Carbon	Atlas of the biosphere	1998	https://nelson.wisc.edu/sage/data-and-models/atlas/maps.php?catnum=2&type=Land%20Use)	Average in home range (9 km) and 50km radius
National Fire Database fire polygon data	Natural Resources Canada	2005-2015	http://cwfis.cfs.nrcan.gc.ca/datamart	Area sum in home range Number of fires in home range (9 km) and 50km radius
National Pollutant Release Inventory (NPRI)	Environment and Climate Change Canada	2014	https://open.canada.ca/data/en/dataset/40e01423-7728-429c-ac9d-2954385ccdfb	Distance to Hg emitter Hg emission volume from nearest emitter Count of mercury emitters in home range (9 km) and 50km radius
Modelled Hg Deposition	Environment and Climate Change Canada	2012-2015	Modeling and Integration Research Section Air Quality Research Division Science and Technology Branch	Average in home range (9 km)
Land Cover	Commission for Environmental Cooperation	2010	http://www.cec.org/tools-and-resources/map-files/land-cover-2010-landsat-30m	% of land cover in each polygon in home range (9 km)
Oil and Gas	Natural Resources Canada	2017	https://open.canada.ca/data/en/dataset/e46ede86-3bae-4479-8176-040cc5f2d9e6	Count of mines in home range (9 km) and 50km radius
Contaminated Sites	CAREX Emissions Mapping Project	2008	http://carexcanada.uvic.ca/emp/	Count of heavy metal contaminated sites in home range (9 km) and 50km radius buffer

```
##############################################################################
# Environmental Hg ~ Gut Hg ~ Fur Hg
# Written in R version 3.5.0
##############################################################################
# Load Data
data = read.csv("mink_ro_gut_bw.csv")

# Load Libraries
library(car)
library(corrplot)
library(AICcmodavg)
library(lmtest)
library(heplots) # partial r2
library(weights) # weighted correlation

# Plotting Libraries
library(ggplot2)
library(ggpubr)
library(sjPlot)

##############################################################################
#### Summarize Data ####
# Add logged variables to dataset
data$log_fur=log10(data$FurHg)
data$log_gut=log10(data$GutHg)

# Subset and summarize mink data
mink  = subset(data, data$Species == "Mink")
summary(mink)
sd(mink$FurHg)
sd(mink$GutHg)

#Subset and summarize river otter data
otter  = subset(data, data$Species == "Otter")
summary(otter)
sd(otter$FurHg)
sd(otter$GutHg)

##############################################################################
#### Relationship between Fur and Gut ####
# Test normality of variables
shapiro.test(otter$FurHg)
shapiro.test(otter$GutHg)
shapiro.test(mink$FurHg)
shapiro.test(mink$GutHg)
# Use logged variables due to the non-normal distrubtion
shapiro.test(otter$log_fur)
shapiro.test(otter$log_gut)
shapiro.test(mink$log_fur)
shapiro.test(mink$log_gut)

# Test Variance
leveneTest(data$log_fur~data$Species)
leveneTest(data$log_gut~data$Species)
# Equal variance among groups

##### T Test for difference in Hg between species ####
# Fur Hg
t.test(data$log_fur~data$Species)
wilcox.test(data$log_fur~data$Species)

# Gut Hg
t.test(data$log_gut~data$Species)
wilcox.test(data$log_gut~data$Species)

# Correlation Between Fur and Gut
# Pearson Poduct Moment Correlation
# River Otter
cor.test(otter$log_fur,otter$log_gut)
plot(otter$log_fur,otter$log_gut)

# Mink
cor.test(mink$log_fur,mink$log_gut)
plot(mink$log_fur,mink$log_gut)

##############################################################################
#### Regression Model: Gut ~ Fur ####
# Otter
# Null
lm1=lm(otter$log_fur~1)
AICc(lm1) # 13.72451

# Unweighted
lm1.1=lm(otter$log_fur~otter$log_gut)
summary(lm1.1)
AICc(lm1.1) # 10.50199

# Weighted
lm1.2=lm(otter$log_fur~otter$log_gut, weight=otter$bw_gut_ratio)
summary(lm1.2)
AICc(lm1.2) # 26.92151
```

```
# Mink
# Null
lm2=lm(mink$log_fur~1)
AICc(lm2) #24.31118

# Unweighted
lm2.1=lm(mink$log_fur~mink$log_gut)
summary(lm2.1)
AICc(lm2.1) # 13.83017

# Weighted
lm2.2=lm(mink$log_fur~mink$log_gut, weight=mink$bw_gut_ratio)
summary(lm2.2)
AICc(lm2.2) #37.1412

# Plot Models
plot_otter= ggplot(otter, aes(x = log_fur, y = log_gut)) +
geom_point(shape = 20, size=3) +
geom_smooth(method = "lm", mapping = aes(weight = bw_gut_ratio),
color = "black", show.legend = FALSE)+
theme_minimal(base_size=14)+
labs(x="Log Fur Total Mercury (ppm)", y="Log Stomach Content Total Mercury (ppm)")

plot_mink = ggplot(mink, aes(x = log_fur, y = log_gut)) +
geom_point(shape = 20, size=3) +
geom_smooth(method = "lm", mapping = aes(weight = bw_gut_ratio),
color = "black", show.legend = FALSE)+
theme_minimal(base_size = 14)+
labs(x="Log Fur Total Mercury (ppm)", y="Log Stomach Content Total Mercury (ppm)")

plot1=ggarrange(plot_otter, plot_mink,
labels = c("A", "B"),
ncol = 2, nrow = 1,
font.label = list(size = 20))
#Plot figures with dpi=300
save_plot("mink_otter_gut_hg.tif", plot1, width = 30, height = 20, dpi = 300)

#############################################################################
#### Test for interactions between site and species ####
# Boxplot All Species
ggplot(data, aes(x=as.factor(data$Lat), y=FurHg)) +
geom_boxplot(outlier.colour="red", outlier.shape=8,
outlier.size=4)+
theme_minimal()+
labs(x="Latitude", y="Fur Hg (ppm)")

#Box plot Mink and river otter seperated
ggplot(data, aes(x=as.factor(data$Lat), y=FurHg, fill=Species)) +
geom_boxplot(outlier.colour="red", outlier.shape=8,
outlier.size=4)+
theme_minimal()+
labs(x="Latitude", y="Fur Hg (ppm)")

# ANOVA All interactons
lm1=lm(data$FurHg~data$Species*as.factor(data$Lat))
anova(lm1) # No interaction
TukeyHSD(aov(data$FurHg~data$Species*as.factor(data$Lat)))

#Sites
lm1=lm(data$FurHg~as.factor(data$Lat))
anova(lm1) # No Interaction between site
t1 = TukeyHSD(aov(data$FurHg~as.factor(data$Lat)))
plot(t1)
```

```
##############################################################################
# Fur ~Gut: Isotopes
# Written in R version 3.5.0
##############################################################################
# Load Data
data = read.csv("mink_ro_gut_bw.csv")

# Load Libraries
library(car)
library(corrplot)
library(AICcmodavg)
library(lmtest)
library(heplots) # partial r2
library(weights) # weighted correlation

# Plotting Libraries
library(ggplot2)
library(ggpubr)
library(sjPlot)

##############################################################################
# Regression Gut and stable isotopes
lm3=lm(log_fur~Delta_13C+Delta_15N, data=data)
summary(lm3)
bptest(lm3)
dwtest(lm3)
resettest(lm3)
shapiro.test(resid(lm3))
# Meets all model assumptions

lm4=lm(log_gut~Delta_13C+Delta_15N, data=data, weight=bw_gut_ratio)
summary(lm4)

lm4.1=lm(log_gut~Delta_15N, data=data, weight=bw_gut_ratio)
summary(lm4.1)

bptest(lm4.1)
ncvTest(lm4.1) # Volated
resettest(lm4.1) # Violated
shapiro.test(resid(lm4.1)) # Violated

cor(data$Mass_Fraction_N,data$Delta_15N, use="complete.obs")

##############################################################################

# Plot
# delta 13C~ delta 15N
plot_fur=ggplot(data, aes(x=data$Delta_13C, y=data$Delta_15N)) +
geom_point(aes(colour = factor(Species), size = data$FurHg))+
labs(size = "Fur␣Hg␣(ppm)")+
scale_color_manual(name="Species", values=c("#C0C0C0","#696969"))+
labs(x = "Delta␣13C", y= "Delta␣15N")+
theme_minimal(base_size=16)

plot_gut=ggplot(data, aes(x=data$Delta_13C, y=data$Delta_15N)) +
geom_point(aes(colour = factor(Species), size = data$GutHg))+
labs(size = "Gut␣Hg␣(ppm)")+
scale_color_manual(name="Species", values=c("#C0C0C0","#696969"))+
labs(x = "Delta␣13C", y= "Delta␣15N")+
theme_minimal(base_size=16)

plot2=ggarrange(plot_fur, plot_gut,
labels = c("A", "B"),
ncol = 2, nrow = 1,
font.label = list(size = 20))

# Plot figures with dpi=300
save_plot("isotopes_gut_hg.tif", plot2, width = 30, height = 15, dpi = 300)

# Difference in Isotopes between groups
t.test(data$Delta_13C~data$Species)
t.test(data$Delta_15N~data$Species)
```

```
################################################################################
# Fur ~Gut: Gut~Environmental Sources
# Written in R version 3.5.0
################################################################################
#### Analysis Mink and River Otter Together ####

data = read.csv("mink_ro_gut_bw.csv")

# Load Libraries
library(car)
library(corrplot)
library(AICcmodavg)
library(lmtest)
library(heplots) # partial r2
library(weights) # weighted correlation

# Plotting Libraries
library(ggplot2)
library(ggpubr)
library(sjPlot)

################################################################################
# Correlation matrix between variables
cor=cor(data[,3:46], use="pairwise.complete.obs")
corrplot(cor,tl.col = "black")
#Significant of correlations
res1 <- cor.mtest(data[,3:46], use="pairwise.complete.obs",conf.level = .95)
corrplot(cor,p.mat = res1$p,tl.col = "black")
#Write to CSV
write.csv(cor, "cor_allspecies.csv")
#Write correlation matrix p-values to file
write.csv(res1$p, "pvalue_cor_allspecies.csv")

# Exploratory Data Analysis
cor=wtd.cor(data[,3:46], bootp=TRUE, weight=data$bw_gut_ratio)
# Write correlation matrix to file
write.csv(cor, "weighted_correlation_all.csv")

# River Otter EDA
#otter_cor = cor(otter[,3:46],use = "pairwise.complete.obs")
#corrplot(otter_cor)
#write.csv(otter_cor, "otter_cor.csv")
#hist(otter[,3:43],nclass = 10)

# Mink EDA
#mink_cor = cor(mink[,3:46], use = "pairwise.complete.obs")
#corrplot(mink_cor)
#write.csv(mink_cor, "mink_cor.csv")
#hist(mink[,3:43],nclass = 10)

#### Regression Model: Gut~Environmental Sources ####
### Unweighted ####
lm1=lm(log_gut~1, data=data_clean)
summary(lm1)
AICc(lm1) #56.74895

lm2=lm(log_gut~pH, data=data_clean)
summary(lm2)
AICc(lm2) #56.82

lm3=lm(log_gut~Grassland+Hg_dep, data=data_clean)
summary(lm3)
AICc(lm3) #54.98925
etasq(lm3)

bptest(lm3)
dwtest(lm3)
resettest(lm3)
shapiro.test(resid(lm3))# Violates

#### Weighted ####
lm4=lm(log_gut~1, weight=bw_gut_ratio, data=data_clean)
summary(lm4)
AICc(lm4) #119.3122

lm5=lm(log_gut~Delta_15N,weight=bw_gut_ratio, data=data_clean)
summary(lm5)
AICc(lm5) #82.66017

lm5=lm(log_gut~pH+Delta_15N,weight=bw_gut_ratio, data=data_clean)
summary(lm5)
AICc(lm5) #66.94067

lm3=lm(log_gut~near_resevoir_km+Delta_15N, weight=bw_gut_ratio, data=data_clean)
summary(lm3)
AICc(lm3) #70.18257

# pH and resevoir are correlated
cor.test(data_clean$near_resevoir_km, data_clean$pH)
ab=lm(data_clean$pH~data_clean$near_resevoir_km, weight=data_clean$bw_gut_ratio)
plot(data_clean$near_resevoir_km,data_clean$pH)
abline(ab)
```

```
# pH and OC are correlated
cor.test(data_clean$OC, data_clean$pH)

lm3=lm(log_gut~pH+deciduous.forest+Delta_15N, weight=bw_gut_ratio, data_clean=data_clean)
summary(lm3)
AICc(lm3) #54.57453
vif(lm3)
etasq(lm3)

bptest(lm3)
ncvTest(lm3)
resettest(lm3)
shapiro.test(resid(lm3))

cor(data_clean$OC,data_clean$near_resevoir_km)

#####################################################################

#### FUR Regression Model Environmental Sources ####
lm1=lm(log_fur~1, data=data)
summary(lm1)
AICc(lm1) #36.76426

lm1=lm(log_fur~Delta_15N, data=data)
summary(lm1)
AICc(lm1) #16.38723
vif(lm1)

lm1=lm(log_fur~Wetland+ Delta_15N, data=data)
summary(lm1)
AICc(lm1) #13.84876
vif(lm1)

lm1=lm(log_fur~Wetland+ Delta_15N+MinesCount, data=data)
summary(lm1)
AICc(lm1) #11.79771
vif(lm1)

lm1=lm(log_fur~Wetland+Delta_15N+MinesCount+sum_fire, data=data)
summary(lm1)
AICc(lm1) #13.4995
vif(lm1)

lm1=lm(log_fur~Wetland+Delta_15N+sum_fire+Hg_dep, data=data)
summary(lm1)
AICc(lm1) #13.01748
vif(lm1)

lm1=lm(log_fur~Wetland+Delta_15N+sum_fire+NPRI_Cnt, data=data)
summary(lm1)
AICc(lm1) #13.64913
vif(lm1)

lm1=lm(log_fur~Wetland+Delta_15N+sum_fire+pH, data=data)
summary(lm1)
AICc(lm1) #12.97571
vif(lm1)

lm1=lm(log_fur~Wetland+Delta_15N+sum_fire, data=data)
summary(lm1)
AICc(lm1) #11.18739
vif(lm1)
etasq(lm1)
# Test Assumptions
summary(lm1)
bptest(lm1)
dwtest(lm1)
resettest(lm1)
shapiro.test(resid(lm1))

#####################################################################

lm4=lm(log_gut~1, weight=bw_gut_ratio, data=data)
summary(lm4)
AICc(lm4) #119.3122

lm5=lm(log_gut~pH,weight=bw_gut_ratio, data=data)
summary(lm5)
AICc(lm5) #100.0504

lm3=lm(log_gut~near_mine_km, weight=bw_gut_ratio, data=data)
summary(lm3)
AICc(lm3) #84.53743
vif(lm3)
etasq(lm3)


cor(log10(data$near_resevoir_km),pH)
ggplot(data, aes(x = body_weight_kg, y = GutHg, color=as.factor(data$Species))) +
geom_point(shape = 20, size=3) +
geom_smooth(method = "lm", mapping = aes(weight = bw_gut_ratio),
```

```
color = "black", show.legend = FALSE)+
theme_minimal(base_size = 14)+
labs(x="pH", y="Log Stomach Content Total Mercury (ppm)")


ggplot(data, aes(x = bw_gut_ratio, y = log_gut, color=as.factor(data$Species))) +
geom_point(shape = 20, size=3) +
geom_smooth(method = "lm", mapping = aes(weight = Content_Weight_g),
color = "black", show.legend = FALSE)+
theme_minimal(base_size = 14)
# labs(x="pH", y="Log Stomach Content Total Mercury (ppm)")


plot(data$log_gut~log10(data$near_resevoir_km))

lm3=lm(log_gut~log10(near_oil_gas_km)+pH, data=data)
summary(lm3)
AICc(lm3) #81.7508
vif(lm3)etasq(lm3)

bptest(lm3)
dwtest(lm3)
resettest(lm3)
shapiro.test(resid(lm3))
```

Appendix D

Supplement Information for Chapter 6: Spatial patterns of dose-response relationships between mercury and cortisol in the fur of river otter (*Lontra canadensis*)

Table D.1: Comparison of fur log total mercury (μg/g) between provinces. P- value is adjusted for multiple comparison. Comparisons with a significant diffrence ($p<0.05$) are bolded.

Comparison	Difference	Lower CI	Upper CI	Adj. P
Northwest Territories -Alberta	0.29	-0.02	0.61	0.08
Nova Scotia-Alberta	0.02	-0.39	0.42	1
Ontario-Alberta	**0.62**	**0.44**	**0.8**	**0.0**
Quebec-Alberta	0.18	-0.19	0.55	0.66
Nova Scotia-Northwest Territories	-0.28	-0.78	0.22	0.53
Ontario-Northwest Territories	0.33	-0.01	0.67	0.06
Quebec-Northwest Territories	-0.12	-0.58	0.35	0.96
Ontario-Nova Scotia	**0.61**	**0.18**	**1.03**	**0.0**
Quebec-Nova Scotia	0.16	-0.37	0.7	0.91
Quebec-Ontario	**-0.44**	**-0.83**	**-0.06**	**0.02**

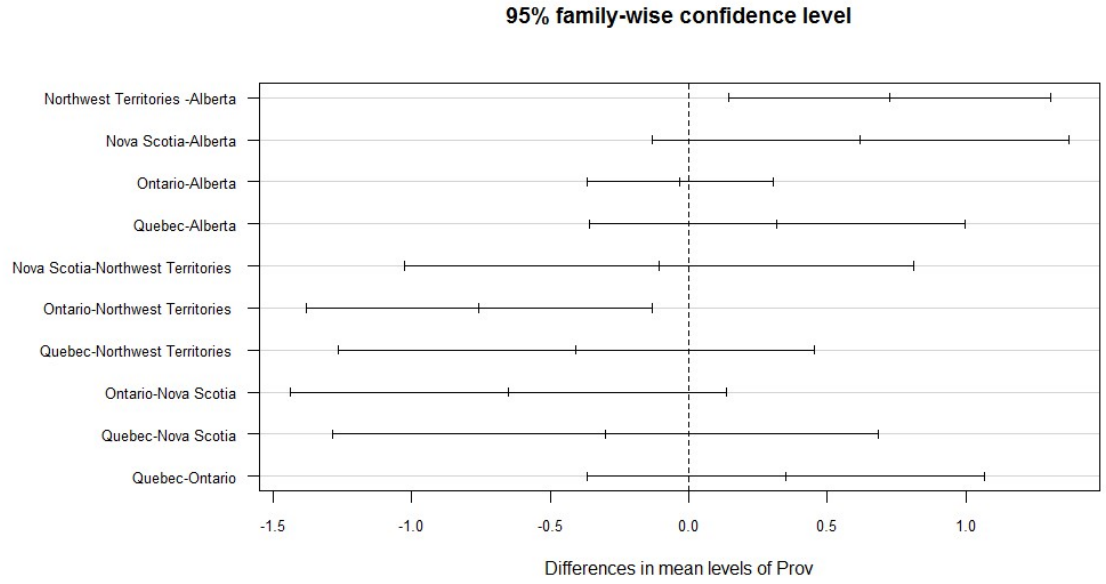

Figure D.1: Tukey plot comparison of fur log total mercury (μg/g) between provinces.

Table D.2: Comparison of fur log cortisol (pg/mg) between provinces. P- value is adjusted for multiple comparison. Comparisons with a significant difference ($p<0.05$) are bolded.

Comparison	Difference	Lower CI	Upper CI	Adj. P
Northwest Territories -Alberta	**0.73**	**0.15**	**1.31**	**0.01**
Nova Scotia-Alberta	0.62	-0.13	1.37	0.16
Ontario-Alberta	-0.03	-0.37	0.3	1
Quebec-Alberta	0.32	-0.36	1	0.69
Nova Scotia-Northwest Territories	-0.11	-1.03	0.81	1
Ontario-Northwest Territories	**-0.76**	**-1.38**	**-0.13**	**0.01**
Quebec-Northwest Territories	-0.41	-1.27	0.45	0.68
Ontario-Nova Scotia	-0.65	-1.44	0.14	0.16
Quebec-Nova Scotia	-0.3	-1.29	0.68	0.92
Quebec-Ontario	0.35	-0.37	1.07	0.66

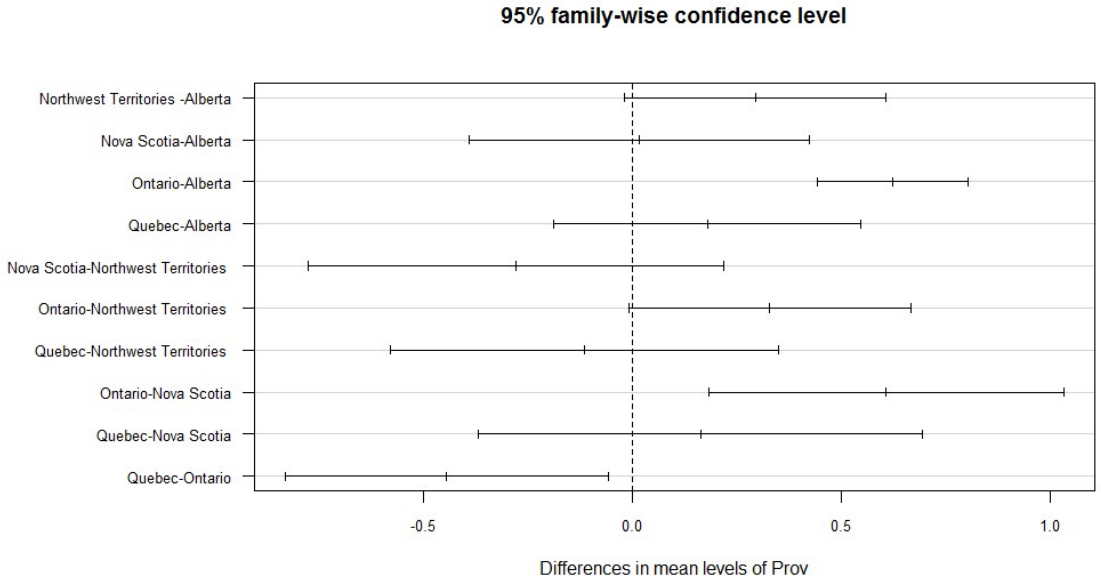

Figure D.2: Tukey plot comparison of fur log cortisol (pg/mg) between provinces.

```
#################################################################
# Dose Reponse ANOVAS Cortisol~Mercury
# Written in R Version 3.5.0
#################################################################
# Load Data
# All data
data=read.csv("compiled_cort_fur2.csv")
data$logcort=log10(data$fur_cort)
data$loghg=log10(data$fur_hg)

# Load Libraries
library(lmtest)
library(stats)
library(car)
library(psych)

# plots
library(ggpubr)
library(ggplot2)
library(sjPlot)
#################################################################
# EDA
# Summarize data
describeBy(data, data$Prov)

#Histograms
hist(data$fur_cort)
shapiro.test(data$fur_cort)
hist(data$logcort)
shapiro.test(data$logcort)

hist(data$fur_hg)
shapiro.test(data$fur_hg)
hist(data$loghg)
shapiro.test(data$loghg)

hist(data_site$hi)

#################################################################
#### Biomonitoring Data ####
#################################################################
# Sex Differences
# Subset Data
data_sex = subset(data, sex == "Female" | sex=="Male")

# Test for Variance for Hg
leveneTest(loghg ~ sex, data = data_sex) #homogenous
# Test for Variance for cortisol
leveneTest(logcort ~ sex, data = data_sex) #not homogenous

# T test and box plot for sex differences between Hg
t.test(data_sex$loghg~data_sex$sex)

p1 <- ggplot(data_sex, aes(x=sex, y=loghg)) +
geom_boxplot()+
theme_classic(base_size=16)+
xlab("Sex")+
ylab("Log Fur THg (ug/g)")
p1

# T test and box plot for sex differences between cortisol
t.test(data_sex$logcort~data_sex$sex)

p2 <- ggplot(data_sex, aes(x=sex, y=loghg)) +
geom_boxplot()+
theme_classic(base_size=16)+
xlab("Sex")+
ylab("Log Fur Cortisol (pg/mg)")
p2

# NO DIFFERENCE BETWEEN SEXES FOR CORT OR HG

# Make Plots Together
plot1=ggarrange(p1, p2,
labels = c("A", "B"),
vjust = 1,
hjust = -0.5,
ncol = 2, nrow = 1,
common.legend = TRUE,
legend = "right")

#Plot figures with dpi=300
save_plot("sex_boxplot.tif", plot1, width = 30, height = 15, dpi = 300)
```

```
#####################################################################
#### All data ####
#####################################################################
# Test for location differences
boxplot(data$loghg~data$Prov)
anova1=lm(data$loghg~data$Prov)
anova(anova1) # difference between provinces
summary(anova1)

bptest(anova1)# homoscedastic
shapiro.test(resid(anova1))
#not normal
hist(resid(anova1))
resettest(anova1)


#### Tukey Follow up Test ####
old.par <- par(mai=c(1.5,2,1,1))
tky1=TukeyHSD(aov(loghg~Prov, data=data))
tky1
plot(tky1, las=1,cex.axis=.7)


p1 <- ggplot(data, aes(x=Prov, y=loghg)) +
geom_boxplot()+
theme_classic(base_size=12)+
xlab("Province")+
ylab("Log Fur THg (ug/g)")
p1

# Difference by Province
boxplot(data$logcort~data$Prov)
anova2=lm(data$logcort~data$Prov)
anova(anova2) # difference between provinces
summary(anova2)

tky2=TukeyHSD(aov(logcort~Prov, data=data))
tky2
plot(tky2, las=1,cex.axis=.7)

p2 <- ggplot(data, aes(x=Prov, y=logcort)) +
geom_boxplot()+
theme_classic(base_size=12)+
xlab("Province")+
ylab("Log Fur Cortisol (pg/mg)")
p2

# Make Plots Together
plot1=ggarrange(p1, p2,
labels = c("A", "B"),
vjust = 1,
hjust = -0.5,
ncol = 1, nrow = 2,
common.legend = TRUE,
legend = "right")
plot1
#Plot figures with dpi=300
save_plot("prov_boxplot.tif", plot1, width = 30, height = 15, dpi = 300)
```

```
#################################################################
# Dose Reponse Relationship Cortisol~Mercury
# Written in R Version 3.5.0
#################################################################
# Load Data
# All data
data=read.csv("compiled_cort_fur2.csv")
data$logcort=log10(data$fur_cort)
data$loghg=log10(data$fur_hg)

# Load Libraries
library(lmtest)
library(stats)
library(car)
library(psych)

# plots
library(ggpubr)
library(ggplot2)
library(sjPlot)

#############################################################
# Test for Relationship between Hg and Cortisol
#############################################################
lm1=lm(data$logcort~data$loghg)
summary(lm1)

bptest(lm1) #homosedastic
shapiro.test(resid(lm1)) #not normal
dwtest(lm1) #autocorrelated
resettest(lm1) #not linear


# Plot
p3 = ggplot(data, aes(y=logcort, x=loghg)) +
geom_point(color="#4E4E4E") +
theme_classic()+
stat_smooth(method = "lm", color="black") +
xlab("Log Fur Total Hg (ug/g)")+
ylab("Log Fur Cortisol (pg/mg)")
p3

#Plot figures with dpi=300
save_plot("all_regression.tif", p3, width = 15, height = 15, dpi = 300)

p4=ggplot(data, aes(x=loghg, y=logcort, color=as.factor(hg_fac))) +
geom_point() +
geom_smooth(method=lm)+
theme_classic()+
xlab("Log Fur Total Hg (ug/g)")+
ylab("Log Fur Cortisol (pg/mg)")+
scale_colour_manual(values=c("#D62F27","#4575B5"),name ="THg Exposure", labels=c("0-15 ug/g", ">15 ug/g"))
p4
#Plot figures with dpi=300
save_plot("all_high_low.tif", p4, width = 15, height = 15, dpi = 300)

#############################################################
# Dichotomous high, low Hg
# subset Data
hg_high = subset(data, hg_fac == "1")
hg_low = subset(data, hg_fac == "0")

# High Hg
lm1=lm(hg_high$logcort~hg_high$loghg)
summary(lm1)

bptest(lm1)
shapiro.test(resid(lm1))
dwtest(lm1) #autocorrelation
resettest(lm1)
#Rest of assumptions are met

lm1.1=lm(hg_high$logcort~hg_high$loghg+hg_high$hi)
summary(lm1.1)
#HI is not signifcant

#Low Hg
lm2=lm(hg_low$logcort~hg_low$loghg)
summary(lm2)

bptest(lm2)
shapiro.test(resid(lm2)) #not normal
hist(resid(lm2)) #non-normality is not too bad
dwtest(lm2) #auotocorrelation
resettest(lm2)

lm2.2=lm(hg_low$logcort~hg_low$loghg+hg_low$hi)
summary(lm2.2)

bptest(lm2.2)
shapiro.test(resid(lm2.2)) #not normal
hist(resid(lm2.2)) #non-normality is not too bad
```

```
dwtest(lm2.2) #autocorrelation
resettest(lm2.2)

# Combine plots
# Make Plots Together
plot2=ggarrange(p3, p4,
labels = c("A", "B"),
vjust = 1,
hjust = -0.5,
ncol = 2, nrow = 1,
common.legend = TRUE,
legend = "right")
plot2

save_plot("combined_regression.tif", plot2, width = 30, height = 15, dpi = 300)
```

Appendix E

Supplement Information for Chapter 6: Spatial patterns of dose-response relationships between mercury and cortisol in the fur of river otter (*Lontra canadensis*)

```
##############################################################################
# Comparison of transformation and range normalization
# Written R version 3.4.3
##############################################################################
# Load Libraries
library(Hmisc)
library(ade4)
library (adegraphics)
library(lattice)
library(sp)
library(adegenet)
library(spdep)
library(adespatial)
library(rgdal)
library(factoextra)
library(ggplot2)

# Set up colour pallet
coul = c("#8dd3c7", "#ffd92f", "#bebada", "#fb8072", "#80b1d3", "#fdb462", "#b3de69")
##############################################################################
## RAW DATA ##
#Import Data
complete_data = read.csv("grid_complete_data.csv")
hist(complete_data[,10:31])

amphib = subset(complete_data, Species == "Amphibian")
gull =  subset(complete_data, Species == "Gull"| Species == "Tern")
mammal =  subset(complete_data, Species == "Fisher" | Species == "Marten"|
         Species == "Mink" | Species == "Muskrat"| Species == "River Otter")

# EDA of original data
hist(amphib[,10:31], nclass = 10)
hist(gull[,10:31], nclass = 10)
hist(mammal[,10:31], nclass = 10)

##############################################################################
#### Transform Data ####
#Sqrt Tranform
sqrt_df = sqrt(complete_data[,10:31])
summary(sqrt_df)
hist(sqrt_df)
sqrt_data = cbind(complete_data[,1:9], sqrt_df)

# Histogram by speices
amphib2 = subset(sqrt_data, Species == "Amphibian")
gull2 =  subset(sqrt_data, Species == "Gull"| Species == "Tern")
mammal2 =  subset(sqrt_data, Species == "Fisher" | Species == "Marten"|
         Species == "Mink" | Species == "Muskrat"| Species == "River Otter")

hist(amphib2[,10:31], nclass = 10)
hist(gull2[,10:31], nclass = 10)
hist(mammal2[,10:31], nclass = 10)

# Log10 Transform
log10_df = log10(complete_data[,10:31]+1)
summary(log10_df)
hist(log10_df)
log10_data = cbind(complete_data[,1:9], log10_df)

# Histogram by speices
amphib3 = subset(log10_data, Species == "Amphibian")
gull3 =  subset(log10_data, Species == "Gull"| Species == "Tern")
mammal3 =  subset(log10_data, Species == "Fisher" | Species == "Marten"|
         Species == "Mink" | Species == "Muskrat"| Species == "River Otter")

hist(amphib3[,10:31], nclass = 10)
hist(gull3[,10:31], nclass = 10)
hist(mammal3[,10:31], nclass = 10)

##############################################################################
#### Normalize between 0 and 1 data by speices and lifestage ####
# Untransformed
fac = interaction(factor(complete_data$Species),factor(complete_data$Lifestage), drop = T)
fnorm.var = function(y){ return((y - min(y)) / (max(y) - min(y)))}
fnorm.tab = function(tab) {apply(tab, 2, fnorm.var)}
range_norm_df=unsplit(lapply(split(as.data.frame(complete_data[,10:31]), fac),
FUN = function(x) as.data.frame(fnorm.tab(x))), fac)
summary(range_norm_df)
# Replace NA's with zeros
range_norm_df=rapply( range_norm_df, f=function(x) ifelse(is.nan(x),0,x), how="replace")
complete=as.data.frame(cbind(complete_data[,1:9],range_norm_df))

# Histogram by speices
amphib1 = subset(sqrt, Species == "Amphibian")
gull1 =  subset(sqrt, Species == "Gull"| Species == "Tern")
mammal1 =  subset(sqrt, Species == "Fisher" | Species == "Marten"|
         Species == "Mink" | Species == "Muskrat"| Species == "River Otter")

hist(amphib1[,10:31], nclass = 10)
hist(gull1[,10:31], nclass = 10)
hist(mammal1[,10:31], nclass = 10)
```

```
# SQRT
fac = interaction(factor(sqrt_data$Species),factor(sqrt_data$Lifestage), drop = T)
fnorm.var = function(y){ return((y - min(y)) / (max(y) - min(y)))}
fnorm.tab = function(tab) {apply(tab, 2, fnorm.var)}
range_norm_df=unsplit(lapply(split(as.data.frame(sqrt_data[,10:31]), fac),
FUN = function(x) as.data.frame(fnorm.tab(x))), fac)
summary(range_norm_df)
# Replace NA's with zeros
range_norm_df=rapply( range_norm_df, f=function(x) ifelse(is.nan(x),0,x), how="replace")
sqrt=as.data.frame(cbind(sqrt_data[,1:9],range_norm_df))

# Histogram by speices
amphib4 = subset(sqrt, Species == "Amphibian")
gull4 =  subset(sqrt, Species == "Gull"| Species == "Tern")
mammal4 =  subset(sqrt, Species == "Fisher" | Species == "Marten"|
        Species == "Mink" | Species == "Muskrat"| Species == "River Otter")

hist(amphib4[,10:31], nclass = 10)
hist(gull4[,10:31], nclass = 10)
hist(mammal4[,10:31], nclass = 10)

# LOG10
fac = interaction(factor(log10_data$Species),factor(log10_data$Lifestage), drop = T)
fnorm.var = function(y){ return((y - min(y)) / (max(y) - min(y)))}
fnorm.tab = function(tab) {apply(tab, 2, fnorm.var)}
range_norm_df=unsplit(lapply(split(as.data.frame(log10_data[,10:31]), fac),
FUN = function(x) as.data.frame(fnorm.tab(x))), fac)
summary(range_norm_df)
# Replace NA's with zeros
range_norm_df=rapply( range_norm_df, f=function(x) ifelse(is.nan(x),0,x), how="replace")
log10=as.data.frame(cbind(log10_data[,1:9],range_norm_df))

#Plot log10 Transformed data
amphib4 = subset(log10, Species == "Amphibian")
gull4 =  subset(log10, Species == "Gull"| Species == "Tern")
mammal4 =  subset(log10, Species == "Fisher" | Species == "Marten"|
        Species == "Mink" | Species == "Muskrat"| Species == "River Otter")

hist(amphib4[,10:31], nclass = 10)
hist(gull4[,10:31], nclass = 10)
hist(mammal4[,10:31], nclass = 10)

#####################################################################
#### PCA and BCA on Untransformed Unnormalized data ####
# Run the PCA
pca1 = dudi.pca(df = complete_data[,10:31], scannf = FALSE, nf = 2)
g1_1=s.arrow(pca1$co, plot=FALSE, plabels=list(cex=0.75,optim=TRUE),
        psub.text = "Untransformed Unnormalized")
g2_1=s.class(pca1$li,complete_data$Species, col=coul, plabels=list(optim=TRUE),
        psub.text = "Untransformed Unnormalized")
ADEgS(list(g1_1,g2_1))

# BCA: Site
bca_site = bca(x = pca1, fac = complete_data$Site, scannf = FALSE, nf = 4)
s.arrow(bca_site$co, plabels=list(cex=0.75,optim=TRUE))
rt_between_species=randtest(bca_site)
rt_between_species
# 53% of total inertia comes from the differences between sites

# BCA: Speices
bca_species = bca(x = pca1, fac = complete_data$Species, scannf = FALSE, nf = 2)
bca_species
s.arrow(bca_species$co)
rt_between_species=randtest(bca_species)
rt_between_species
# 34% of total inertia comes from the differences between species

# BCA: Year
bca_species = bca(x = pca1, fac = as.factor(complete_data$Year),
        scannf = FALSE, nf = 2)
bca_species
s.arrow(bca_species$co)
rt_between_species=randtest(bca_species)
rt_between_species
# 7.3% of total inertia comes from the differences between species

#####################################################################
#### PCA and BCA on Untransformed, range normalized data ####
# Run the PCA
pca2 = dudi.pca(df = complete[,10:31], scannf = FALSE, nf = 2)
g1_2=s.arrow(pca2$co, plot=FALSE, plabels=list(cex=0.75,optim=TRUE),
        psub.text = "Untransformed Range Normalized")
g2_2=s.class(pca2$li,complete$Species, col=coul, plabels=list(optim=TRUE),
        psub.text = "Untransformed Range Normalized")
ADEgS(list(g1_2,g2_2))

#BCA: Site
bca_site = bca(x = pca2, fac = complete$Site, scannf = FALSE, nf = 4)
#s.arrow(bca_site$co, plabels=list(cex=0.75,optim=TRUE))
rt_between_species=randtest(bca_site)
rt_between_species
# 39% of total inertia comes from the differences between sites
```

```
#BCA: Speices
bca_species = bca(x = pca2, fac = complete$Species, scannf = FALSE, nf = 2)
bca_species
s.arrow(bca_species$co)
rt_between_species=randtest(bca_species)
rt_between_species
# 18.7% of total inertia comes from the differences between species

#BCA: Year
bca_Year = bca(x = pca2, fac = as.factor(complete$Year), scannf = FALSE, nf = 2)
bca_Year
s.arrow(bca_Year$co)
rt_between_Year=randtest(bca_Year)
rt_between_Year
# 7.3% of total inertia comes from the differences between Year

#################################################################
#### PCA and BCA on sqrt Transform, range normalized data ####
pca3 = dudi.pca(df = sqrt[,10:31], scannf = FALSE, nf = 2)
g1_3=s.arrow(pca3$co, plot=FALSE, plabels=list(cex=0.75,optim=TRUE),
        psub.text = "SQRT Tranformation Range Normalized")
g2_3=s.class(pca3$li,sqrt$Species, col=coul, plabels=list(optim=TRUE),
        psub.text = "SQRT Tranformation Range Normalized")
ADEgS(list(g1_3,g2_3))

#BCA: Site
bca_site = bca(x = pca3, fac = sqrt$Site, scannf = FALSE, nf = 4)
#s.arrow(bca_site$co, plabels=list(cex=0.75,optim=TRUE))
rt_between_species=randtest(bca_site)
rt_between_species
# 41.6% of total inertia comes from the differences between sites

#BCA: Speices
bca_species = bca(x = pca3, fac = sqrt$Species, scannf = FALSE, nf = 2)
bca_species
s.arrow(bca_species$co)
rt_between_species=randtest(bca_species)
rt_between_species
# 21% of total inertia comes from the differences between species

#BCA: Year
bca_year = bca(x = pca3, fac = as.factor(sqrt$Year), scannf = FALSE, nf = 2)
bca_year
s.arrow(bca_year$co)
rt_bca_year=randtest(bca_year)
rt_bca_year
# 21% of total inertia comes from the differences between species

#################################################################
### PCA and BCA on log10 transformed range normalized data ###
pca4 = dudi.pca(df = log10[,10:31], scannf = FALSE, nf = 2)
g1_4=s.arrow(pca4$co, plot=FALSE, plabels=list(cex=0.75,optim=TRUE),
        psub.text = "Log10 Tranformation Range Normalized")
g2_4=s.class(pca4$li,log10$Species, col=coul, plabels=list(optim=TRUE),
        psub.text ="Log10 Tranformation Range Normalized")
ADEgS(list(g1_4,g2))

#BCA: Site
bca_site = bca(x = pca4, fac = log10$Site, scannf = FALSE, nf = 4)
#s.arrow(bca_site$co, plabels=list(cex=0.75,optim=TRUE))
rt_between_species=randtest(bca_site)
rt_between_species
# 41% of total inertia comes from the differences between sites

#BCA: Speices
bca_species = bca(x = pca4, fac = log10$Species, scannf = FALSE, nf = 2)
bca_species
s.arrow(bca_species$co)
rt_between_species=randtest(bca_species)
rt_between_species
# 20% of total inertia comes from the differences between species

#BCA: Year
bca_Year = bca(x = pca4, fac = as.factor(log10$Year), scannf = FALSE, nf = 2)
bca_Year
s.arrow(bca_Year$co)
rt_between_Year=randtest(bca_Year)
rt_between_Year
# 7.5% of total inertia comes from the differences between Year

#Combine Plots
ADEgS(list(g1_1,g2_1, g1_2,g2_2, g1_3,g2_3, g1_4,g2_4), layout=c(4, 2))

#################################################################
# Lifestage
#################################################################
# Set up colour pallet
coul = c("#8dd3c7", "#ffd92f", "#bebada", "#fb8072", "#80b1d3", "#fdb462", "#b3de69")

#### PCA and BCA on Untransformed Unnormalized data ####
# Run the PCA
```

```
pca1 = dudi.pca(df = complete_data[,10:31], scannf = FALSE, nf = 2)
g1_1=s.arrow(pca1$co, plot=FALSE, plabels=list(cex=0.75,optim=TRUE),
        psub.text = "Untransformed Unnormalized")
g2_1=s.class(pca1$li,complete_data$Lifestage, col=coul, plabels=list(optim=TRUE),
        psub.text = "Untransformed Unnormalized")
ADEgS(list(g1_1,g2_1))

# BCA: Site
bca_site = bca(x = pca1, fac = complete_data$Site, scannf = FALSE, nf = 4)
s.arrow(bca_site$co, plabels=list(cex=0.75,optim=TRUE))
rt_between_species=randtest(bca_site)
rt_between_species
# 53% of total inertia comes from the differences between sites

# BCA: Speices
bca_species = bca(x = pca1, fac = complete_data$Lifestage, scannf = FALSE, nf = 2)
bca_species
s.arrow(bca_species$co)
rt_between_species=randtest(bca_species)
rt_between_species
# 34% of total inertia comes from the differences between species

# BCA: Year
bca_species = bca(x = pca1, fac = as.factor(complete_data$Year), scannf = FALSE, nf = 2)
bca_species
s.arrow(bca_species$co)
rt_between_species=randtest(bca_species)
rt_between_species
# 7.3% of total inertia comes from the differences between species

#####################################################################
#### PCA and BCA on Untransformed, range normalized data ####
# Run the PCA
pca2 = dudi.pca(df = complete[,10:31], scannf = FALSE, nf = 2)
g1_2=s.arrow(pca2$co, plot=FALSE, plabels=list(cex=0.75,optim=TRUE),
        psub.text = "Untransformed Range Normalized")
g2_2=s.class(pca2$li,complete$Lifestage, col=coul, plabels=list(optim=TRUE),
        psub.text = "Untransformed Range Normalized")
ADEgS(list(g1_2,g2_2))

#BCA: Site
bca_site = bca(x = pca2, fac = complete$Site, scannf = FALSE, nf = 4)
#s.arrow(bca_site$co, plabels=list(cex=0.75,optim=TRUE))
rt_between_species=randtest(bca_site)
rt_between_species
# 39% of total inertia comes from the differences between sites

#BCA: Speices
bca_species = bca(x = pca2, fac = complete$Lifestage, scannf = FALSE, nf = 2)
bca_species
s.arrow(bca_species$co)
rt_between_species=randtest(bca_species)
rt_between_species
# 18.7% of total inertia comes from the differences between species

#BCA: Year
bca_Year = bca(x = pca2, fac = as.factor(complete$Year), scannf = FALSE, nf = 2)
bca_Year
s.arrow(bca_Year$co)
rt_between_Year=randtest(bca_Year)
rt_between_Year
# 7.3% of total inertia comes from the differences between Year

#####################################################################
#### PCA and BCA on sqrt Transform, range normalized data ####
pca3 = dudi.pca(df = sqrt[,10:31], scannf = FALSE, nf = 2)
g1_3=s.arrow(pca3$co, plot=FALSE, plabels=list(cex=0.75,optim=TRUE),
        psub.text = "SQRT Tranformation Range Normalized")
g2_3=s.class(pca3$li,sqrt$Lifestage, col=coul, plabels=list(optim=TRUE),
        psub.text = "SQRT Tranformation Range Normalized")
ADEgS(list(g1_3,g2_3))

#BCA: Site
bca_site = bca(x = pca3, fac = sqrt$Site, scannf = FALSE, nf = 4)
#s.arrow(bca_site$co, plabels=list(cex=0.75,optim=TRUE))
rt_between_species=randtest(bca_site)
rt_between_species
# 41.6% of total inertia comes from the differences between sites

#BCA: Speices
bca_species = bca(x = pca3, fac = sqrt$Lifestage, scannf = FALSE, nf = 2)
bca_species
s.arrow(bca_species$co)
rt_between_species=randtest(bca_species)
rt_between_species
# 21% of total inertia comes from the differences between species

#BCA: Year
bca_year = bca(x = pca3, fac = as.factor(sqrt$Year), scannf = FALSE, nf = 2)
bca_year
s.arrow(bca_year$co)
rt_bca_year=randtest(bca_year)
```

```
rt_bca_year
# 21% of total inertia comes from the differences between species

#################################################################
### PCA and BCA on log10 transformed range normalized data ###
pca4 = dudi.pca(df = log10[,10:31], scannf = FALSE, nf = 2)
g1_4=s.arrow(pca4$co, plot=FALSE, plabels=list(cex=0.75,optim=TRUE),
        psub.text = "Log10 Tranformation Range Normalized")
g2_4=s.class(pca4$li,log10$Lifestage, col=coul, plabels=list(optim=TRUE),
        psub.text ="Log10 Tranformation Range Normalized")
ADEgS(list(g1_4,g2))

#BCA: Site
bca_site = bca(x = pca4, fac = log10$Site, scannf = FALSE, nf = 4)
#s.arrow(bca_site$co, plabels=list(cex=0.75,optim=TRUE))
rt_between_species=randtest(bca_site)
rt_between_species
# 41% of total inertia comes from the differences between sites

#BCA: Speices
bca_species = bca(x = pca4, fac = log10$Lifestage, scannf = FALSE, nf = 2)
bca_species
s.arrow(bca_species$co)
rt_between_species=randtest(bca_species)
rt_between_species
# 20% of total inertia comes from the differences between species

#BCA: Year
bca_Year = bca(x = pca4, fac = as.factor(log10$Year), scannf = FALSE, nf = 2)
bca_Year
s.arrow(bca_Year$co)
rt_between_Year=randtest(bca_Year)
rt_between_Year
# 7.5% of total inertia comes from the differences between Year
#################################################################
#Combine Plots
ADEgS(list(g1_1,g2_1, g1_2,g2_2, g1_3,g2_3, g1_4,g2_4), layout=c(4, 2))
```

```
#################################################################
# Analysis By Species
# # Written R version 3.4.3
#################################################################
##### Import Data ####
#Take the aboslute values of the imputed data
data=read.csv("grid_complete_data.csv")

#### Load Libraries ####
library(ade4)
library(adespatial)
library(adegenet)
library(sp)
library(spdep)
library(maptools)
library(adegraphics)
library(RColorBrewer)
library(readOGR)
library(rgdal)

#################################################################
#### Set up data ####
#Normalize between 0 and 1 data by speices and lifestage
fac = interaction(factor(data$Species),factor(data$Lifestage), drop = T)
fnorm.var = function(y){ return((y - min(y)) / (max(y) - min(y)))}
fnorm.tab = function(tab) {apply(tab, 2, fnorm.var)}
range_norm_df=unsplit(lapply(split(as.data.frame(data[,9:31]), fac),
FUN = function(x) as.data.frame(fnorm.tab(x))), fac)
summary(range_norm_df)
# Replace NA's with zeros
range_norm_df=rapply( range_norm_df, f=function(x)
        ifelse(is.nan(x),0,x), how="replace")
norm_data=as.data.frame(cbind(data[,2:8],range_norm_df))

# Subets data
amphib = subset(norm_data, Species == "Amphibian")
gull =  subset(norm_data, Species == "Gull"| Species == "Tern")
mammal =  subset(norm_data, Species == "Fisher" | Species == "Marten"|
          Species == "Mink" | Species == "Muskrat"| Species == "River Otter")

#################################################################
#### Amphibians ####
# PCA
pca1= dudi.pca(df = amphib[,9:30], center = TRUE, scannf = FALSE, nf = 4)
g1=s.corcircle(pca1$co, plot=FALSE)
g2=s.label(pca1$li, plot=FALSE)
ADEgS(list(g1,g2))

# Between group analysis: SITE
amphib_site=bca(pca1,as.factor(amphib$Lat),scannf=FALSE)
#plot(amphib_site, row.pellipse.col=adegpar()$ppalette$quali(6))
rt_between_site=randtest(amphib_site)
rt_between_site

# Spatial Analysis
# Aggregate the x y coordinates for sites
xy=coordinates(amphib[,3:2])
sitexy=aggregate(amphib[, 3:2], list(amphib$Site), mean)

# Extract information by site from BCA
dim(amphib_site$tab)
scores_by_site=amphib_site$li

# Attach Coordinates to sites
scores_xy=cbind(sitexy, scores_by_site)
write.csv(scores_xy, "amphib_site_scores_xy.csv")

# Make the Maps
rivers = readOGR(dsn = "C:/Users/keccl081/Dropbox/
        Chapter4_PCA/All_Species/PCA_All","rivers_clip")
r2 = plot(rivers, col="#CBF6FF", border="#CBF6FF")

amphib_map_bca=s.value(scores_xy[,2:3],amphib_site$li,
         symbol="circle", pgrid.draw = FALSE,
         Sp=rivers, pSp.col="#CBF6FF", pSp.border="#CBF6FF",
         ylim = c(55, 62), xlim = c(-115, -109))
amphib_bi = s.arrow(amphib_site$co)

#################################################################
#### Gulls ####
# PCA
pca1= dudi.pca(df = gull[,8:30], center = TRUE, scannf = FALSE, nf = 4)
g1=s.corcircle(pca1$co, plot=FALSE)
g2=s.label(pca1$li, plot=FALSE)
ADEgS(list(g1,g2))

# Between group analysis: SITE
gull_site=bca(pca1,as.factor(gull$Lat),scannf=FALSE)
#plot(gull_site, row.pellipse.col=adegpar()$ppalette$quali(6))
rt_between_site=randtest(gull_site)
rt_between_site
```

```
# Spatial Analysis
# Aggregate the x y coordinates for sites
xy=coordinates(gull[,3:2])
sitexy=aggregate(gull[, 3:2], list(gull$Site), mean)

# Extract information by site from BCA
dim(gull_site$tab)
scores_by_site=gull_site$li

# Attach Coordinates to sites
scores_xy=cbind(sitexy, scores_by_site)
write.csv(scores_xy, "gull_site_scores_xy.csv")

# Make the Maps
rivers = readOGR(dsn = "C:/Users/keccl081/Dropbox/Chapter4_PCA/
        All_Species/PCA_All","rivers_clip")
#plot(rivers, col="#CBF6FF", border="#CBF6FF")

gull_map_bca=s.value(scores_xy[,2:3],gull_site$li,
         symbol="circle", pgrid.draw = FALSE,
         Sp=rivers, pSp.col="#CBF6FF", pSp.border="#CBF6FF",
         ylim = c(46, 62), xlim = c(-120, -101))
gulls_bi = s.arrow(gull_site$co)

#####################################################################
#### Mammals ####
# PCA
pca1= dudi.pca(df = mammal[,9:30], center = TRUE, scannf = FALSE, nf = 4)
g1=s.corcircle(pca1$co, plot=FALSE)
g2=s.label(pca1$li, plot=FALSE)
ADEgS(list(g1,g2))

# Between group analysis: SITE
mammal_site=bca(pca1,as.factor(mammal$Lat),scannf=FALSE)
#plot(mammal_site, row.pellipse.col=adegpar()$ppalette$quali(6))
rt_between_site=randtest(mammal_site)
rt_between_site

# Spatial Analysis
# Aggregate the x y coordinates for sites
xy=coordinates(mammal[,3:2])
sitexy=aggregate(mammal[, 3:2], list(mammal$Site), mean)

# Extract information by site from BCA
dim(mammal_site$tab)
scores_by_site=mammal_site$li

# Attach Coordinates to sites
scores_xy=cbind(sitexy, scores_by_site)
write.csv(scores_xy, "mammal_site_scores_xy.csv")

# Make the Maps
rivers = readOGR(dsn = "C:/Users/keccl081/Dropbox/Chapter4_PCA/
        All_Species/PCA_All","rivers_clip")
#plot(rivers, col="#CBF6FF", border="#CBF6FF")

mammal_map_bca=s.value(scores_xy[,2:3],mammal_site$li,
         symbol="circle", pgrid.draw = FALSE,
         Sp=rivers, pSp.col="#CBF6FF", pSp.border="#CBF6FF",
         ylim = c(53, 59), xlim = c(-120, -109))
mammals_bi = s.arrow(mammal_site$co)

#################################################
# Plot all figures together

ADEgS(list(amphib_map_bca, amphib_bi,
gull_map_bca, gulls_bi,
mammal_map_bca, mammals_bi), layout = c(3, 2))
```

```
#########################################################
# Spatial PCA
# written in R version 3.4.3
#########################################################
# Library
library(Hmisc)
library(ade4)
library (adegraphics)
library(lattice)
library(sp)
library(adegenet)
library(spdep)
library(adespatial)
library(rgdal)
library(factoextra)
library(ggplot2)

# Set up colour pallet
coul = c("#8dd3c7", "#ffd92f", "#bebada", "#fb8072", "#80b1d3", "#fdb461", "#b3de69")
#########################################################
## RAW DATA ##
#Import Data
complete_data = read.csv("grid_complete_data.csv")

#### Transform Data ####
#Sqrt Tranform
sqrt_df = sqrt(complete_data[,10:31])
sqrt_data = cbind(complete_data[,1:9], sqrt_df)

# SQRT
fac = interaction(factor(sqrt_data$Species),factor(sqrt_data$Lifestage), drop = T)
fnorm.var = function(y){ return((y - min(y)) / (max(y) - min(y)))}
fnorm.tab = function(tab) {apply(tab, 2, fnorm.var)}
range_norm_df=unsplit(lapply(split(as.data.frame(sqrt_data[,10:31]), fac),
FUN = function(x) as.data.frame(fnorm.tab(x))), fac)
summary(range_norm_df)
# Replace NA's with zeros
range_norm_df=rapply(range_norm_df, f=function(x) ifelse(is.nan(x),0,x), how="replace")
sqrt=as.data.frame(cbind(sqrt_data[,1:9],range_norm_df))

#### PCA and BCA on sqrt Transform, range normalized data ####
pca3 = dudi.pca(df = sqrt[,10:31], scannf = FALSE, nf = 4)
g1_3=s.arrow(pca3$co, plot=FALSE, plabels=list(cex=0.75,optim=TRUE),psub.text = "SQRT␣Tranformation␣Range␣Normalized")
g2_3=s.class(pca3$li,sqrt$Species, col=coul, plabels=list(optim=TRUE),psub.text = "SQRT␣Tranformation␣Range␣Normalized")
ADEgS(list(g1_3,g2_3))

#BCA: Site
bca_site = bca(x = pca3, fac = sqrt$Site, scannf = FALSE, nf = 4)
#s.arrow(bca_site$co, plabels=list(cex=0.75,optim=TRUE))
rt_between_species=randtest(bca_site)
rt_between_species
# 41.9% of total inertia comes from the differences between sites

s.arrow(bca_site$co)
write.csv(bca_site$C1, "sqrt_bca_loadings.csv")

#####################################################################
#### Map the BCA components ####
# Extract data for mapping
# Aggregate the x y coordinates for sites
sitexy=aggregate(sqrt[,3:4], list(sqrt$Site), mean)

# Extract information by site from BCA
dim(bca_site$tab)
scores_by_site=bca_site$li

# Attach Coordinates to sites
scores_xy=cbind(sitexy, scores_by_site)
write.csv(scores_xy, "site_scores_sqrt_norm.csv")

# Set up Spatial DataFrame
rivers = readOGR(dsn = "C:/Users/Kristin/Dropbox/chapter4_pca/
␣␣␣␣␣␣␣␣All_Species/PCA_All", layer = "rivers_clip")
rivers_convert <- fortify(rivers)
g1.map.bca=s.value(scores_xy[,3:2],bca_site$li, symbol="circle",
pgrid.draw = FALSE,ppoints.cex=0.75,
Sp=rivers, pSp.col="#CBF6FF", pSp.border="#CBF6FF", ylim = c(52, 61),
        xlim = c(-122, -106))

# Map Species Locations
ggplot(complete_data, aes(x=Long, y=Lat)) +
xlab("Longitude")+
ylab("Latitude")+
geom_polygon(data=rivers_convert, aes(long, lat, group = group, fill = hole),
        colour = alpha("lightgrey", 1/2), size = 0.7) +
scale_fill_manual(values = c("lightgrey", "white"), guide=FALSE)+
geom_point(aes(color = factor(complete_data$Species)),size=4)+
scale_color_manual(values=c("#8dd3c7", "#ffd92f", "#bebada", "#fb8072",
        "#80b1d3", "#fdb461", "#b3de69"), name="Species")+
theme_minimal()

#####################################################################
```

```
#### Spatia PCA ####
# Defining spatial weights
# Create spatial coordinates
xy=coordinates(scores_xy[,3:2])
# To explore other spatial weights matrices
#listw.explore()

#No weights on the edges
#nb <- chooseCN(coordinates(xy), type = 2, plot.nb = FALSE)
#lw <- nb2listw(nb, style = 'W', zero.policy = TRUE)

# Weighted edges
nb <- chooseCN(coordinates(xy), type = 2, plot.nb = FALSE)
distnb <- nbdists(nb, xy)
fdist <- lapply(distnb, function(x) 1 - x/max(dist(xy)))
lw <- nb2listw(nb, style = 'W', glist = fdist, zero.policy = TRUE)

# Plot neighbourhoods
g1=s.label(scores_xy[,3:2],nb=nb, pub.edge.col="red", ppoints.cex=0.25)

# Moran's I IDW
moran.randtest(scores_xy[,"Axis1"], listw=lw,nrepet=999)
moran.plot(scores_xy[,"Axis1"], listw=lw) # clustered

moran.randtest(scores_xy[,"Axis2"], listw=lw,nrepet=999)
moran.plot(scores_xy[,"Axis2"], listw=lw) #Clustered

moran.randtest(scores_xy[,"Axis3"], listw=lw,nrepet=999)
moran.plot(scores_xy[,"Axis3"], listw=lw) #clustered

moran.randtest(scores_xy[,"Axis4"], listw=lw,nrepet=999)
moran.plot(scores_xy[,"Axis4"], listw=lw) # Clustered

#Moran's eigenvector maps using gabriel neighbourhood
(me=mem(lw))
s.value(scores_xy[,3:2], me[,c(1:4)], ppoints.cex=0.75,
        ylim = c(52, 61), xlim = c(-120, -108))
scalo1=scalogram(scores_xy[,"Axis1"], me, nblocks=10)
plot(scalo1)
scalo2=scalogram(scores_xy[,"Axis2"], me, nblocks=10)
plot(scalo2)
scalo3=scalogram(scores_xy[,"Axis3"], me, nblocks=10)
plot(scalo3)
scalo4=scalogram(scores_xy[,"Axis4"], me, nblocks=10)
plot(scalo4)


### multispqti
ms1 = multispati(bca_site, lw)
ms1_weight_c1=as.data.frame(ms1$c1)
plot(ms1)
s.value(sitexy[,3:2], ms1$li, porigin.include = FALSE)
s.value(sitexy[,3:2], ms1$li[,1], porigin.include = FALSE, ppoints.cex=0.5, ylim = c(52, 61), xlim = c(-120, -108),
Sp=rivers, pSp.col="#CBF6FF", pSp.border="#CBF6FF")
s.value(sitexy[,3:2], ms1$li[,2], porigin.include = FALSE, ppoints.cex=0.5, ylim = c(52, 61), xlim = c(-120, -108),
Sp=rivers, pSp.col="#CBF6FF", pSp.border="#CBF6FF")
s.value(sitexy[,3:2], ms1$li[,3], porigin.include = FALSE, ppoints.cex=0.5, ylim = c(52, 61), xlim = c(-120, -108),
Sp=rivers, pSp.col="#CBF6FF", pSp.border="#CBF6FF")
s.value(sitexy[,3:2], ms1$li[,4], porigin.include = FALSE, ppoints.cex=0.5, ylim = c(52, 61), xlim = c(-120, -108),
Sp=rivers, pSp.col="#CBF6FF", pSp.border="#CBF6FF")
s.arrow(ms1$c1)

write.csv(ms1$c1, "multispati_loadings_site_all.csv")
```

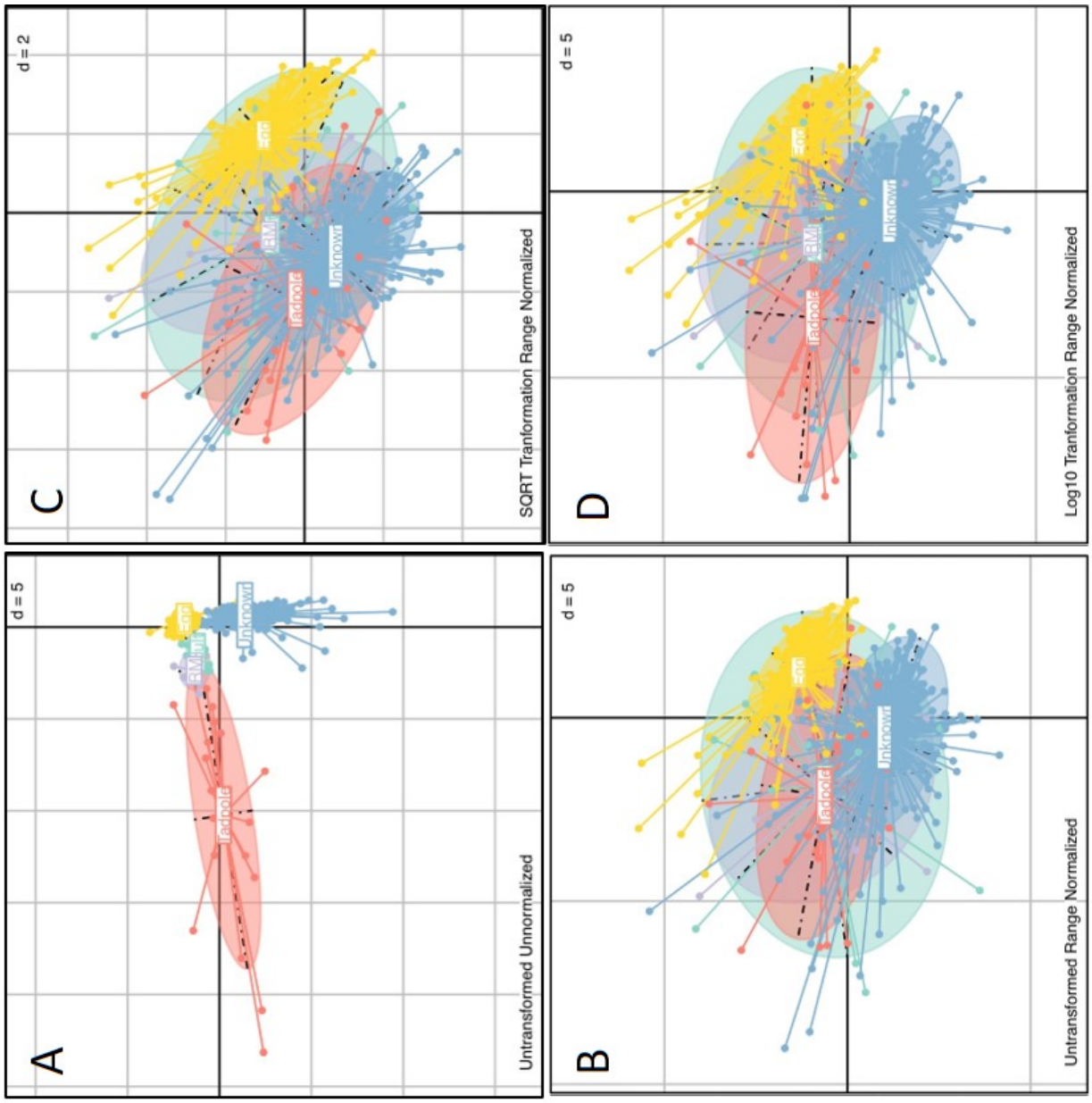

Figure E.1: Principal Components Analysis (PCA) and between components analysis (BCA) results for each combination of transformation and normalization method which controls for skewed data and the effects of life stage differences.

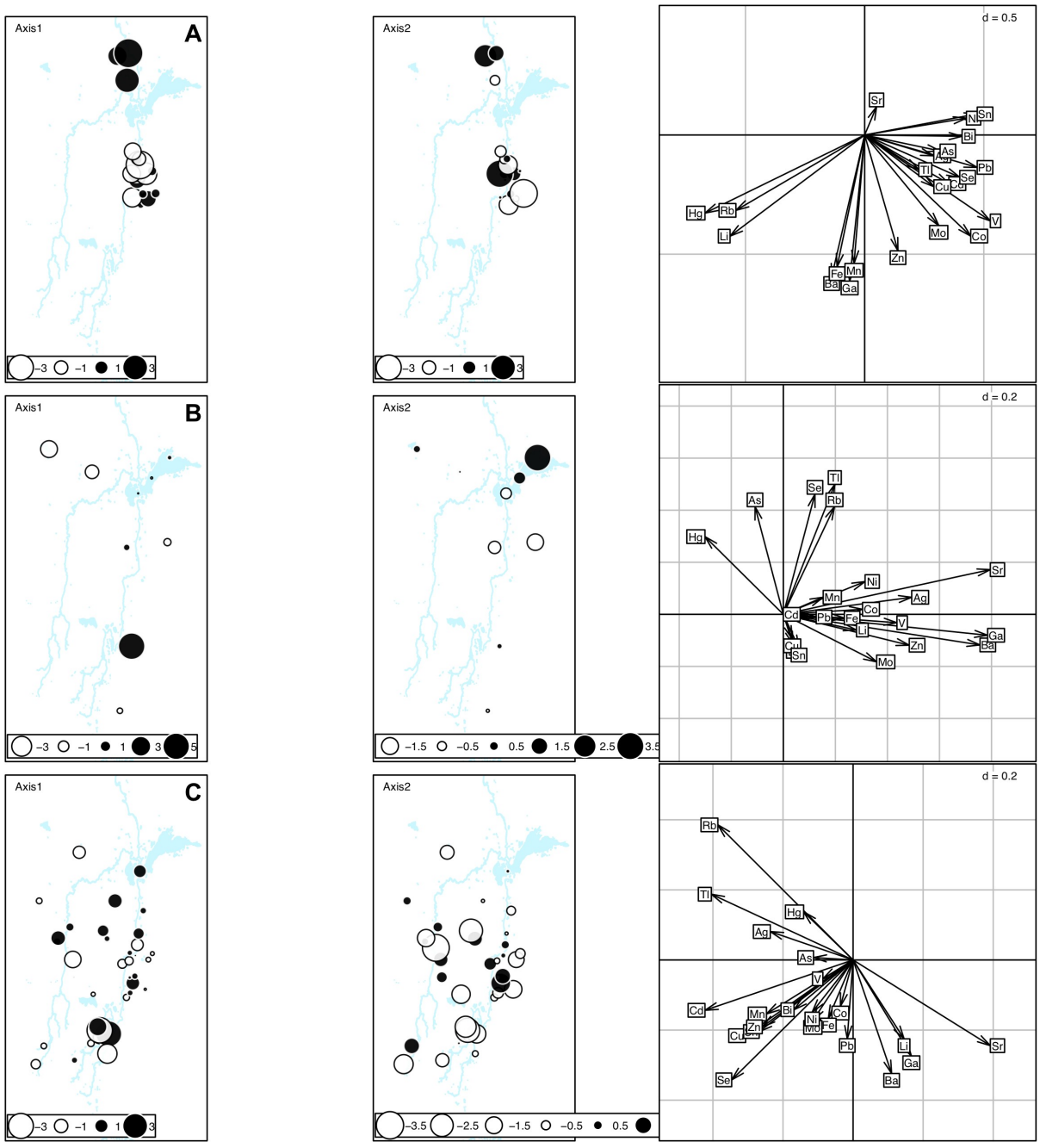

Figure E.2: Comparison of individual between components analysis (BCA) results with mapped scored for (A) amphibians, (B) gulls, and (C) mammals. These data have been square-root transformed and range normalized.

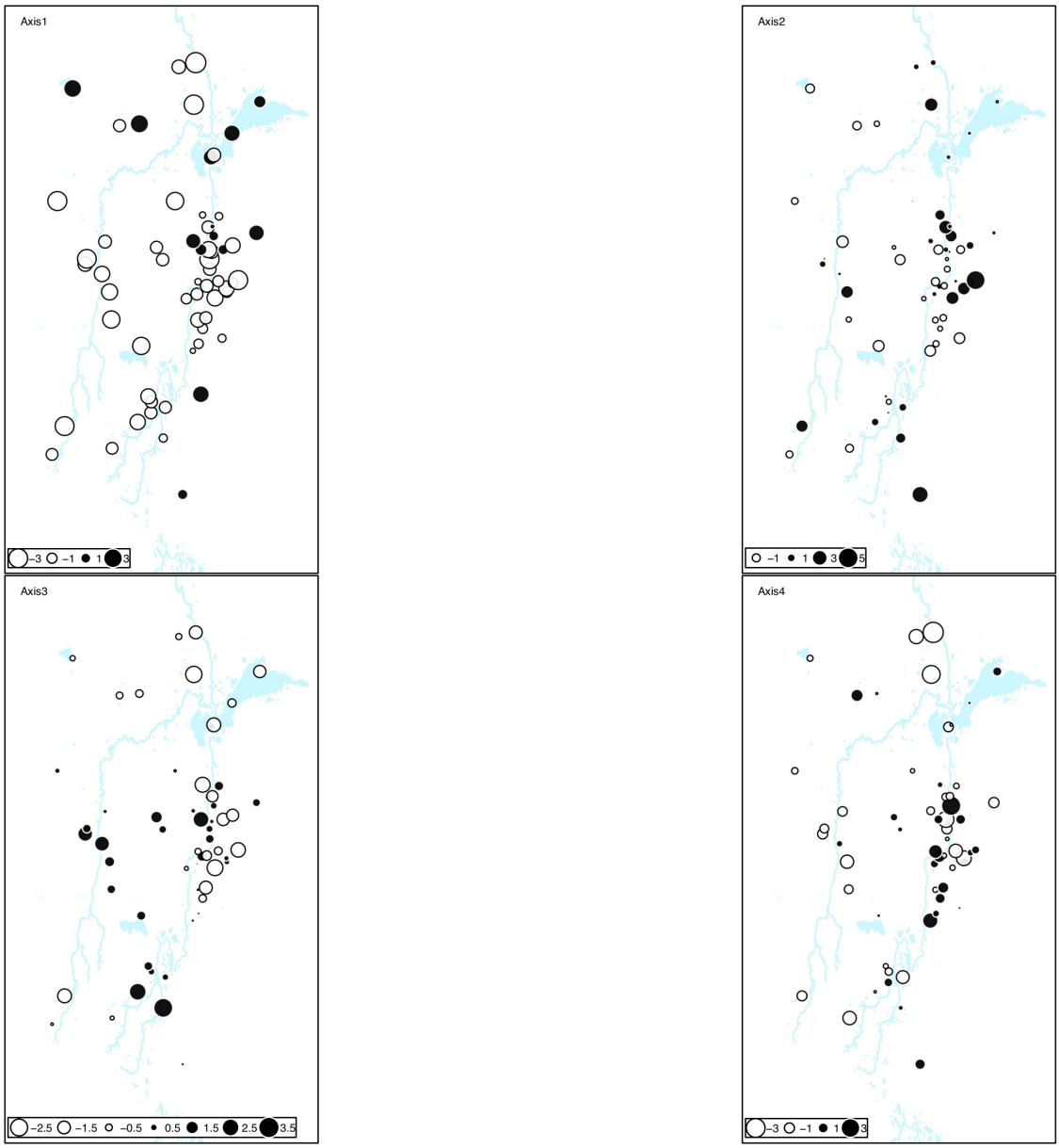

Figure E.3: Compiled BCA results with mapped scored. These data have been square-root transformed and range normalized.The figure axis number corresponds to the component number.

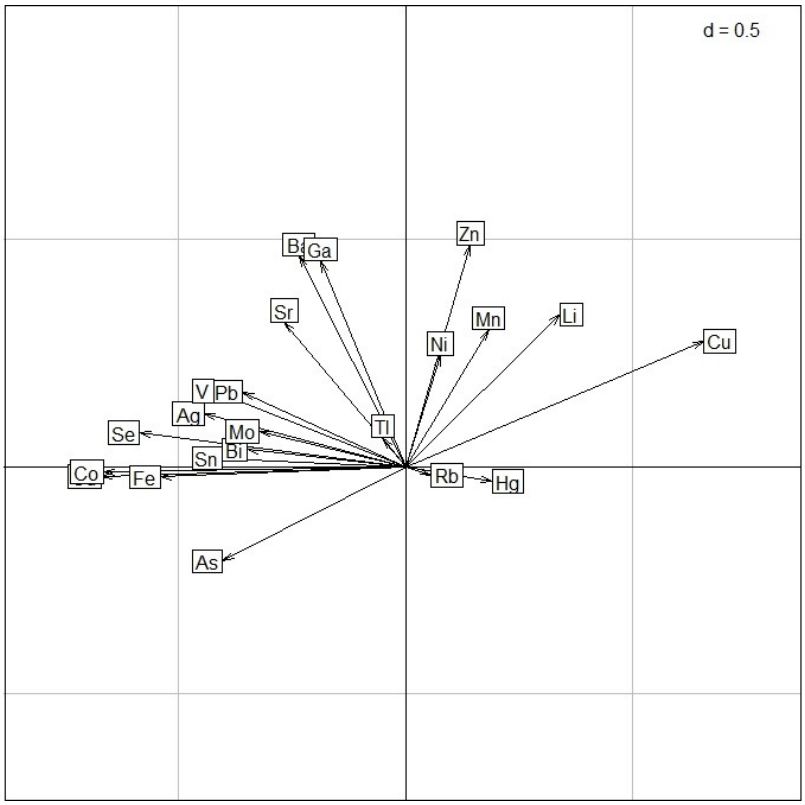

Figure E.4: Biplot for component 1 (x-axis) and component 2 (y-axis) for interpreting compiled BCA results with mapped scores from Figure E.3. The origin of this plot is (0,0).

Appendix F

Abstracts of other publications completed during PhD

Thomas, P. J., Eccles, K. M., & Mundy, L. J. (2017). Spatial modelling of non-target exposure to anticoagulant rodenticides can inform mitigation options in two boreal predators inhabiting areas with intensive oil and gas development. *Biological Conservation*, 212, 111-119.

Intensive industrial development occurs in the ecologically significant boreal forest, including oil and gas development in northern Alberta, Canada. This forest is home to many highly-valued animal species including fisher (Pekania pennanti; formerly Martes pennanti) and American marten (Martes americana). Second-generation anticoagulant rodenticides (SGARs) are commonly used near human infrastructure in developed areas to control and reduce damage from rodent pests. High body burdens of SGARs in rodent prey pose risks of secondary poisoning for fisher and marten that readily consume rodents. The objective of this research was to determine if fisher and marten living in anthropogenically-disturbed areas of northern Alberta showed evidence of SGAR exposure. Fisher and marten carcasses were collected from the region, aged, sexed, and

liver samples were analysed for rodenticides using liquid-chromatography mass spectrometry (LCMS). SGARs were found in the livers of non-target fisher and marten. As SGARs were found in the livers of fisher with sufficient frequency for complete statistical analysis, analyses including ANOVA, linear regression, and spatial cluster analyses were used to assess spatial patterns exhibited by fisher exposure frequencies against potential explanatory variables such as boreal anthropogenic disturbances and land cover classes. Additionally, companies operating in the region were surveyed to identify their current rodent control measures in an effort to verify the results of the spatial analyses. This is the first study to demonstrate non-target SGAR exposure of fisher and marten in Canada. Exposure frequency in fisher exhibited clustering, which showed the strongest relationships to factors including total boreal disturbances, number of oil sands mines, and broadleaf forest cover. The spatial methods used in this paper provide tools to develop local interventions for mitigation and conservation efforts.

Hu, X. F., Eccles, K. M., & Chan, H. M. (2017). High selenium exposure lowers the odds ratios for hypertension, stroke, and myocardial infarction associated with mercury exposure among Inuit in Canada. *Environment International*, 102, 200-206.

Background: Selenium (Se) has been reported to protect against the neurotoxicity of mercury (Hg). However, the effect of Se against Hg on cardiovascular diseases remains unclear. Inuit living in the Arctic have high exposure to both Se and Hg through their marine mammal and fish rich traditional diet. Objective: To characterize the co-exposure of Hg and Se among Inuit in Canada and to assess the associations between Hg, Se and cardiovascular health outcomes, including stroke, hypertension, and myocardial infarction (MI). Methods: Data was collected from the International Polar Year Inuit Health Survey (IHS) conducted in 2007 and 2008. Blood Se and Hg were measured, and self-report cardiovascular health outcomes were collected through a questionnaire interview from 2169 adults aged 18 and above. Results: The mean age was 42.4 years, and 38.7% of the participants were male. The geometric means (GM) of blood Se and total Hg were 319.5 µg/L and 7.0 µg/L, respectively. The crude prevalence of heart attack, stroke and hypertension were 3.55%, 2.36%, and 24.47% respectively. Participants were categorized into 4 exposure groups according to blood Hg (high: $\geq$ 7.8 µg/L; low: $<$ 7.8 µg/L), and Se (high: $\geq$ 280 µg/L; low: $<$ 280 µg/L). The odds ratio (OR) of cardiovascular outcomes were estimated using general linearized models. Results showed the low Se and high Hg group had a higher prevalence of cardiovascular disease (OR = 1.76 for hypertension, 1.57 for stroke, and 1.26 for MI. However, the prevalence was decreased in both the high Se and low Hg group (OR = 0.57 for hypertension, 0.44 for stroke, and

0.27 for MI) and the high Se and high Hg group (OR = 1.14 for hypertension, 0.31 for stroke, and 0.80 for MI). Conclusions:The high Se and low Hg group had the lowest prevalence of cardiovascular outcomes, except for stroke. These results provide evidence that Se may exhibit a protective effect against Hg on cardiovascular disease.